Université catholique de Louvain
Faculté d'Ingénierie Biologique, Agronomique et Environnementale
Département des Sciences du Milieu et de l'Aménagement du Territoire

Estimation of evapotranspiration fluxes at the field scale: parameter estimation, variability and uncertainties

François Hupet

Décembre 2003

Thèse présentée en vue de l'obtention
du grade de docteur en Sciences Agronomiques
et Ingénierie Biologique

Jury members:

President:	Prof. J. Dufey (UCL, Belgium)
Promotor:	Prof. M. Vanclooster (UCL, Belgium)
Readers:	Dr B.E. Clothier (HortResearch Center, New Zealand)
	Prof. P. Defourny (UCL, Belgium)
	Prof. J-F. Ledent (UCL, Belgium)
	Prof. E. Persoons (UCL, Belgium)
	Dr. J.C. van Dam (Wageningen UR, The Netherlands)

To my wife, Anne-Françoise
and my son, Achille

Acknowledgements

For any researcher, the weeks devoted to the finalization of a Ph.D thesis undoubtely constitute a rather particular period not only as he puts an end to a work that he generally started several years before but also as he realizes that such a work could not have been done without the contribution of many persons. Logically, I will therefore start this manuscript by thanking those who helped, supported, advised and oriented me during those five years of research.

First of all, I would like to thank warmly my promotor, Prof. M. Vanclooster, for having accepted to supervise my thesis: he really guided me through all the various phases of my doctoral research. I am particularly in his debt for two reasons: first, he has passed his passion for scientific research on to me, and second, convinced of the importance of the scientific communication, he continuously has encouraged me to present my own studies to the international scientific community. Within this framework, I am very grateful that he prompted me to write this manuscript under the form of scientific papers and that he induced me to participate to several congresses and workshops. I would like also to thank my promotor for having devoted a substantial part of his time for making numerous corrections in the successive drafts of my thesis (fortunately, there was progressively less and less red!). Once more, Marnik, thank you so much for your invaluable contribution to my work.

Then, I would like to thank Prof. E. Persoons, chief of the Agricultural Engineer Unit, who succeeded in January 1998 to convince me to start a Ph.D. thesis. At that time, I remember very well to have hesitated for a long time; at present, however, it is a choice that I absolutely do not regret: I would do it again without any hesitation. I also thank Prof. E. Persoons to have regularly insisted on two closely linked aspects of scientific research, namely "the measurement" and "the field experience": clearly, both are essential for any researcher achieving a thesis in the area of hydrology.

I am also happy to save a few lines for two of my work mates, Mathieu Javaux and Sébastien Lambot. Indeed, both of them have really contributed to this work and some chapters unquestionably are to be considered as a true team work. Beyond all our scientific discussions, their help was also very valuable for the use and the development of the Matlab version of the WAVE-model. I would like to thank more specifically Sébastien to have quickened our neverending discussions about inverse modelling that undoubtedly helped me to make things clearer in this field. Last but not least I would like to thank both of them for all the nice moments spent together, be it while eating a sandwich right in the sun at Louvain-la-Neuve or spending a sleepless night to drive back from the EGS congress in Nice.

One part of my thesis largely lies on experimental field work that could not have been performed without the help of technicians. In this respect, I particularly thank G. Rentmeesters for the making and the installation of the numerous tensiometers and A. Lannoye who helped me during the 2000 field campaign and also helped for collecting undisturbed soil cores.

As regards my scientific staying at the Sub-Department of Water Resources in Wageningen, I have firstly to thank the secretary H. Van Werven to have assumed the whole administrative part. Then, I would like to thank Prof. R.A. Feddes to have stimulated interesting discussions about root water uptake despite his very busy timetable. Finally, I have to thank warmly Dr. J.C. van Dam for his warm welcome in his laboratory, for his daily attention about my work, and for his continuous help with the use of SWAP and PEST. I also thank him to have supported me during this quite particular "lonely" period as it unfortunately coincided with my wedding. I also acknowledge him to have initiated me to Dutch bike and to have convinced me that a five minutes bike journey in the centre of Wageningen is more physically and ecologically valuable than the same ten minutes car journey. Thanks again Jos for this unforgettable staying.

Concerning my short scientific stay at ICIA (Instituto Canario de Investigaciones de Agrarias) at Tenerife, I would like to thank Prof. R. Munoz-Carpena, Dr. C. Regalado and Dr. A Ritter for their warm welcome and for the opportunity they gave me to work on the modelling of water transport in irrigated banana plantations, which appeared to be a really interesting research subject. I also thank Axel for the time that he spent to show me some remote and wild parts of the island.

The quality of several chapters of my thesis was certainly improved by numerous corrections and suggestions made by different reviewers, among which I am happy to cite M. Sivapalan and R.B. Grayson; most of these reviewers remain anonymous, but I want to associate each of them to my work, thanking them all for their important job in the reviewing process of my manuscripts.

I would like to thank also some researchers with whom I had interesting discussions about the root water uptake, namely J. Vrugt, Dr. X. Draye, Dr. B.E. Clothier and Prof. J.W Hopmans, and about pedotransfer functions, Dr. M. Schaap and Dr. J.H.M. Wösten.

I also wish to express my thanks to the persons who have accepted to read this manuscript, namely Dr. B.E. Clothier from HortResearch Center, Dr. J.C. van Dam from Wageningen UR, Prof. J-F Ledent, Prof.

E. Persoons and Prof. P. Defourny from UCL.

Different persons helped and oriented me at different levels, namely J-Y Delaveux for the determination of the soil hydraulic properties, G. Foucart from CIPF for the oven and the crusher to measure maize yield, B. Simon for solving last minute computer issues, Dr. B. Gérard from ICRISAT for discussions about kites for remote sensing "within-field" spatial variability of crop growth (a technique finally not used), Dr. D. D'Or and Prof. P. Bogaert for their judicious advices in statistics and geostatistics, and Prof. B. Delvaux for his moral support in some very particular moments.

All the experimental work carried out in the framework of my Ph.D thesis was performed within an agricultural field cultivated by the farmer N. Braibant. I whish to express him my gratitude for having trusted me and also for the few evenings that I spent at his house listening to him talking passionately about agriculture.

The secretary of the laboratory, C. De Meyer, certainly deserves to be warmly acknowledged. Indeed, she works often behind the scenes but she is continuously attentive to the researchers while being very efficient in her daily work.

I would like also to thank my parents to have always supported me and to have given me enough freedom to bring to successful conclusions the activities that I have undertaken. I would like to thank my close friends for their support even if I know that they have never really understood what I did during all those years spent at the University.

Last but not least, I would like to thank my wife Anne-Françoise wholeheartedly for all the "sacrifices" she made, whether it be to have adjusted our holidays according to the maize growing season, to have accepted that I spent a "lonely" honeymoon in Wageningen, and also for the two last months the most part of it was dedicated to the finalization of this thesis. Anne-Françoise, when you will have this manuscript in your hands, I hope you will a little bit better understand what a Ph.D. thesis consists of, even if you do not find with this one the answer to your tormenting question " What's the good to be a Ph.D? ".

Louvain-La-Neuve, 5^{th} of September 2003

François

Everything of importance has been thought of before
by someone who did not invent it.

Alfred North Whitehead, 1920.

Contents

Notation

Symbols used within the thesis are only valid for each chapter taken separately. As a matter of fact, a same symbol may be used for different variables to have a notation in correspondence with the general notation of the literature (e.g. c for the light velocity on p 160, for the extinction coefficient on p 29 and for the intercept of the TDR calibration equation on p 159). For clarity reasons, symbols are systematically explained after each equation where a new symbol for the chapter appears. Although some variables may have the same dimension, units are chosen according to "reference" units generally used in the literature as e.g. mm for evapotranspiration fluxes and cm for pressure head. Mathematical constants and operators are printed regular. Plain symbols denote scalars (e.g. c), bold symbols in lowercase denote vectors (e.g. **c**) and bold symbols in uppercase denote matrices (e.g. **C**).

Chapter 1

Introduction and objectives

During the last two decades, the public and governmental awareness for sustainable management of water resources has been increasing substantially. Nowadays, water resources are subjected to a series of unprecedented pressures exerted by the human society. The irremediable salinization and dessication of land caused by the development of new unreasonable irrigated areas; the irremediable disappearance of unique biotopes due to the construction of hydropower dams; the contamination of groundwater by agro-chemicals caused by an intensifying agriculture; or the occurrence of devastating floods caused by land use changes are just a few examples of major water problems among many others. It appears clearly that most of these issues originate from decisions performed on the basis of unreliable, unsustainable or lacking management strategies [*Peirera et al.*, 1994]. Within this context, it is now well acknowledged that there is an urgent need to develop robust and reliable water management strategies allowing the control of the impact of the continuously increasing human pressure on the world's limited water resources. In order to develop such reliable strategies, it is of paramount importance to understand in depth the functioning of the hydrologic system.

The understanding of the hydrologic system is the primary concern of the hydrological scientist and is the basis for scientifically based water resources engineering. This understanding ineluctably involves the quantification of the individual hydrological processes of the hydrologic system. Empirical observation is definitely the most sounded way for quantifying hydrologic processes within a deductionistic framework. Unfortunately, in the vast majority of cases, the space-time scales at which empirical observations are made do not comply with the space-time scales at which decision makers require answers or implement measures. Models are therefore needed allowing to predict in time and space hydrologic functioning where observations are not possible [*Bierkens et al.*, 2000; *Vanclooster et al.*, 2002]. From a scientific point of view, there is a real challenge to scale the estimations inferred from scale specific, in general local, observations to the scale of the decision making problem, in general the larger spatial scale and the longer term time scale. The solution of the "scale problem" was therefore identified by a number of recent reviews as the major unresolved problem in hydrology [*NRC*, 1991; *Kalma and Sivapalan*, 1996].

In addition to this "scale problem", a true hydrological challenge consists in characterizing the uncertainty when hydrological processes are quantified [*Beven*, 2001]. In fact, sound decision-making within a risk assessment framework needs predictions of the hydrologic functioning as well as the characterization of the uncertainties associated with these predictions. However, a thorough and accurate quantification of the uncertainties of hydrological processes is probably still much more difficult to obtain than the predictions themselves.

Among the hydrological processes which drive the hydrological cycle, the evapotranspiration process (ET) is a basic process which remains hard to estimate. In a recent review on ET estimations, *Itier and Brunet* [1996] stated that the accuracy for non punctual ET estimates is about 1.5 mm d^{-1} for daily values and 100 W m^{-2} for instantaneous values. More recently, *Kite and Droogers* [2000] showed during a comparative study between 8 different methods of estimating actual ET at a small spatial scale ($<$1 km^2) that ET estimations ranged, for two selected experimental "golden" days, from 1.5 to 6.4 mm d^{-1} and from 2.6 to 6.4 mm d^{-1} respectively according to the method used. It therefore appears clearly that the estimation of ET, even at a limited spatial scale, still remains a very challenging task, even with the assistance of extremely powerful computers, with the availability of newly developed mathematical models (more and more complex) and with the accessibility of new measurement techniques such as very small space-time resolution remote sensors. Notwithstanding all these difficulties, the accurate quantification of ET remains very important as it is a principal component of the hydrological cycle with 70% of the rainfall going back to the atmosphere under the form of ET at the global scale [*Graedel and Crutzen*, 1997] and as the ET process plays a key role across a wide range of hydrology related disciplines. For instance in meteorology, ET directly affects the quantity of water vapour going back to the atmosphere and constitutes as a matter of fact the only source of water in the process of clouds formation. In soil hydrology, ET conditions directly the groundwater recharge and the near-surface soil moisture status, controlling by this way the antecedent conditions prior to a storm event. In irrigation engineering, the quantity of transpired water, the "green water", and that of water evaporated directly from the soil, the "unproductive water", conditions the irrigation scheduling. In agronomy, the transpired water is a driving force for the crop growth and the dry matter production.

Quantification of ET and the associated uncertainties can be performed at several spatial scales such as the scale of the stomata, the plant, the field, the catchment, the region and even the continent. Nevertheless, in many environmental studies, the field is considered as the "reference" scale even if predictions or decision making strategies have to be applied at much larger scales [e.g., *Tiktak et al.*, in press]. More specifically in hydrology, the field scale is very relevant as in many cases the field size corresponds to the lateral grid size of a distributed hydrological model [*Bathurst*, 1986]. Furthermore, the field constitutes an intermediate scale between the point and the catchment scale allowing in some way to deal with the "within-field" spatial variability of soil, vegetation and climate factors, which are generally assumed uniform at the field scale in applied studies [e.g., *D'Urso and Santini*, 1996]. Within a research context, the study of the "within-field" variability of the ET process remains of paramount importance. Indeed, it has been stated recently that quantification of fine-scale heterogeneity remains a clear and high priority to improve ET estimations at a regional scale (Tucson Aggregation Workshop [*Michaud and Shutteworth*, 1997]).

The research developed within this thesis has to be situated within this context. The topic of this work was formulated under the form of the following basic question "Which strategies may be adopted to obtain accurate estimates of the field-scale ET fluxes, considering the "within-field" variation of basic soil-plant-atmosphere processes and the space-time limitations of our observational skills, and how can we quantify the associated uncertainties with these estimates?" This very broad question encompasses obviously several scientific questions that cannot be tackled thoroughly within one thesis. Consequently, only the specific issues summarized below will be addressed in this thesis.

1.1 Estimation of field-scale ET and associated uncertainties

Evapotranspiration (ET) consists in the transfer of water vapour from the Earth's surface to the atmosphere involving a diffusion process, allowing to transfer the water vapour to the atmosphere, and an energy transfer process, allowing to convert liquid or solid water into vapour.

ET includes the transpiration of the water through the crop leaves, the evaporation of soil water, and the evaporation of water intercepted by the canopies. Following *Rana and Katerji* [2000], two different methodologies can be distinguished to realise field-scale ET estimates. The first methodology consists in direct ET "measurements". Different ET measurement techniques exist, such as the soil water balance method [e.g., *Vandervaere et al.*, 1994], the lysimeter method [e.g., *Soppe and Ayars*, 2003], the energy balance method [e.g., *Bastiaanssen*, 2000], the Bowen ratio method [e.g., *Denmead*, 1993], the eddy covariance method [e.g., *Baldocchi et al.*, 1998], the scintillometer method [e.g., *Meijninger and de Bruin*, 2000], and the sap flow method [e.g., *Meiresonne et al.*, 1997]. The second methodology consists in ET modelling. The first category of ET models includes "agro-hydrological" models describing in detail the physical soil and crop growth processes. Examples of agro-hydrological models are the WAVE-model [*Vanclooster et al.*, 1996], the SWAP-model [*van Dam et al.*, 1997] and the HYDRUS-model [*Simunek et al.*, 1998]. The second category includes SVATs (soil-vegetation-atmosphere-transfer models) derived from land surface energy balances that address the exchange processes at the land surface-atmosphere interface, in particular the partitioning of net radiation into sensible and latent heat. Examples of SVATs are the SiB-model [*Sellers et al.*, 1986] and the SECHIBA-model [*Ducoudré et al.*, 1993]. All these different ET estimation methods have their inherent advantages and drawbacks in terms of spatio-temporal resolution, cost, maintenance, expertise, number of parameters and complexity. In this study both a modelling approach (i.e. the agro-hydrological modelling by means of WAVE and SWAP) and a measurement approach (i.e. the soil water balance method) are used to produce field-scale ET. This choice is justified by the fact that both methods remain probably the most commonly used within the hydrological, ecological and agronomical scientific community to estimate field-scale ET.

1.1.1 Agro-hydrological modelling

Before we can apply an agro-hydrological model to make ET predictions for a particular field, it is generally necessary that the model goes through all the stages of the modelling process, i.e. the development of a perceptual model and its translation into a conceptual model, the model calibration and the model validation [*Beven*, 2001]. Given the availability of a series of previously published conceptual models at the onset of the study, research in this thesis was primarily focused on issues relative to the agro-hydrological model calibration, i.e. the stage during which model parameter values and the associated uncertainties are obtained. This critical stage needs indeed in depth research as previous studies that have attempted to estimate model parameters a priori have generally produced unsatisfactory results [e.g., *Refsgaard and Knudsen*, 1996; *Loague and Kyriakidis*, 1997]. During the calibration stage, model parameters are estimated by fitting some observed state variables of the agro-hydrological system.

The major drawback with the direct measurement of the parameters is most likely the fact that the support of the measurement technique is generally much smaller than the field-scale for which a parameter value is needed. The most prominent example is probably the determination of the water retention curve on a 100 cm^3 soil core to make field-scale predictions using an agro-hydrological model. In fact, the measured small-scale parameters and the effective parameters needed for the prediction scale, though having the same name, are different quantities, i.e. they are incommensurate [*Beven*, 2001]. In order to bridge this scale gap, a strategy may be to measure the small-scale parameters at a large number of locations within the field in order to obtain the statistical distribution of the parameters. Then, numerous model runs can be generated e.g. through Monte Carlo simulations assuming the field soil as an ensemble of parallel and non-interacting tubes [e.g., *Booltink and Epinat*, 2001; *Vachaud and Chen*, 2002]. Subsequently, model outputs are aggregated to represent the field mean behaviour. Alternatively the parameters can be initially aggregated into one average parameter value. Then, a single model run is generated producing directly a mean output value at the field-scale. Note that both alternatives generally lead to different results which can be attributable to the nonlinear structure of agro-hydrological models [e.g., *Mallants et al.*, 1996]. In case of direct measurements, uncertainties on the field-scale estimated parameters arise as instrumental errors on the small-scale measurements are unavoidable, as the complete capture of the within-field spatial variability of the parameters is impossible to achieve, or, more generally, as both are combined. The accuracy of the ET predictions results from the combined effect of the sensitivity of ET to the model parameters and of the magnitude of the within-field variability of the parameters. Prior to the calibration process, it is therefore imperative to carry out a basic sensitivity analysis to investigate which parameters determine the predictions. In addition, the spatial variability of the small-scale parameters needs to be quantified [*Beven*, 2001].

The issue of spatial variability and its impact on the predictions has been largely investigated within the framework of soil water fluxes estimations [e.g., *Dagan and Bresler*, 1983; *Mohanty et al.*, 1994; *Mallants*, 1996]. With regard to transpiration and crop yields, the impact of the spatial variability of soil properties has been thoroughly investigated by agronomists within the context of precision farming [e.g., *Paz et al.*, 1998; *Batchelor et al.*, 2002]. Nevertheless, these latter studies were performed with crop simulation models where the soil water transport processes are often oversimplified. Additionally these studies have generally investigated the within-field variability of transpiration and crop yield considering simultaneously the complex interactions of several different stresses [e.g., *Paz et al.*, 2001]. Consequently, elucidating the impact of the variability of the soil hydraulic properties is not systematically obvious. A few studies have tackled this issue by decoupling the modelling of transpiration from that of vegetation development (i.e. making no use of a full vegetation growth module) [e.g., *Dagan and Bresler*, 1983; *Droogers*, 1997; *Kim et al.*, 1997; *Vachaud and Chen*, 2002]. Still, there is a clear feed-back between both vegetation development and transpiration. Furthermore, some of the latter studies have only considered as spatially variable the soil hydraulic properties. Yet, it is well acknowledged that the water stress parameters, actually governing the magnitude of the actual transpiration and the crop growth, depend in some way on the soil type. Consequently, in order to rigorously investigate the effect of the soil hydraulic properties within-field variability on the transpiration and the crop yield, it seems appropriate to adjust the water stress parameters according to the basic soil properties.

Estimation of model parameters by model calibration, i.e. by fitting some observed data of system state variables, is generally performed when some parameters can not be directly measured. This is the case when parameters are a conceptual representation of abstract characteristics, or when they can not be determined at the right spatial scale [*Gupta et al.*, 1998]. In case of parameter estimation by calibration, two main issues arise.

The first issue is related to the quality of the data available for field-scale model calibration. Indeed, data used to derive field-scale parameters are supposed to represent the field mean behaviour. Unfortunately data available for the calibration of agro-hydrological models are generally only constituted of small-scale (few dm^3) soil water content measurements. There is therefore a true challenge to scale-up punctual measured soil water content values to the field-scale, especially as it is well recognized that within-field variability of soil water content may be large [e.g., *Famiglietti et al.*, 1998; *Western et al.*, 1999]. In this context, different questions remain unanswered such as : "How to predict a priori the magnitude of the within-field soil water content variability? What are the main factors governing the spatio-temporal dynamics of this variability?

Does the sampling have to be more intensive during some periods to obtain the same accuracy on the field mean soil water content?" Addressing these questions is very relevant as it allows increasing the accuracy of field-scale soil water content estimations. Within the framework of calibration of agro-hydrological models, this must inevitably lead to more accurate parameter estimations and subsequently to less uncertain field-scale ET predictions.

In addition to field-scale measurements of state variables such as soil water content, the calibration process requires the specification of field-scale time-variant boundary conditions, i.e. the driving forces of the system. For agro-hydrological models, the driving forces are climatic forces induced by rainfall, insolation and temperature gradients. Accurate estimation of basic climatic parameters is important as it likely impacts both the ET predictions, when using the model in a predictive mode, and the parameter estimation through the calibration process [e.g., *Jorhar et al.*, 2002]. Errors on the estimation of meteorological variables at the field-scale, for which spatial variability can be neglected, may originate from different sources. These can be measurement errors due to the properties of the sensor [*Ritchie et al.*, 1996], errors due to the estimation of meteorological variables from other less accurate available data (e.g., *Farnsworth* [1997]), and errors caused by the temporal sampling frequency of the climatic data. This latter source of error is likely to be large as it is well acknowledged that the driving forces are highly temporally variable (e.g., *McVicar and Jupp* [1999]).

The second issue is related to the parameter estimation process itself. This one can be performed by simple trial-and-error or with automatic optimization techniques, minimizing thereby a predefined objective function which measures discrepancies between observations (e.g. soil water content) and the corresponding outputs of the model. This parameter estimation technique, referred to as inverse modelling, is attractive for parameters which cannot be directly measured. In addition, by means of this technique parameter uncertainty can be quantified. Nevertheless, the use of inverse methods has some well known limitations which are mainly related to the non-uniqueness and instability of the optimized parameter set [*Kool and Parker*, 1988]. Within the context of soil hydraulic properties estimation, these limitations have been extensively studied by means of both experimental and numerical experiments [see, e.g., *Carrera and Neuman*, 1986; *Simunek and van Genuchten*, 1996; *Lambot et al.*, 2002]. In contrast, only few studies have dealt with the identification of root water uptake parameters (RWUP) with the inverse method [*Musters and Bouten*, 1999; *Vrugt et al.*, 1999a, b]. The question "Is the estimation of RWUP by inverse modelling feasible?" remains therefore unanswered. Hence, more fundamental research is needed to identify the well-posedness and the robustness of the inverse method for identifying RWUP. That topic seems particularly relevant as root water uptake is likely to control water transport within the soil-plant system and consequently strongly influences the ET process. Additionally, analysing the properties of the RWUP inverse problem is essential as RWUP can not be measured directly and as the within-field variability of RWUP is likely to be high.

1.1.2 The soil water balance method

For field-scale estimation of ET by means of a soil water balance, two main issues can be distinguished. The first is related to the accuracy of the local ET measurement. The second is related to the transfer of information, i.e. the upscaling, from the local ET measurement(s) scale to the field scale.

Local ET estimation with a soil water balance during a drying period is quite straightforward. Indeed, it only requires estimates of soil water storage (e.g. through soil water content measurements at different depths) and an estimation of the soil water fluxes at the bottom of the soil profile. Unfortunately, assessing rigourously the accuracy of ET estimated with this approach is difficult, and if it can be assessed, turns often out to be poor. Indeed, accuracy assessment requires to develop an uncertainty propagation analysis taking into account uncertainties on individual soil water content measurements, on soil water storages (due to the integration method), on soil water storage variations, and on bottom fluxes. An example of such propagation analysis can be found in *Vandervaere et al.* [1994] for the soil water balance approach using a neutron probe and the zero flux plane method. Nowadays, the soil water balance is often used exploiting soil water content measurements performed with different types of dielectric sensors such as TDR (or TDR for soil surface and neutron probe for deeper depths). For such a case, additional investigations are needed to consider the specificity of the uncertainty associated with these "new" measuring techniques. Within this context, it is also relevant to study the temporal dynamics of the uncertainties to identify favourable periods for ET estimations with the soil water balance method. The uncertainty assessment of the soil water balance method allows quantifying the relative and absolute precisions on the ET measurement and identifying the different components contributing the total uncertainty. But it constitutes above all a preliminary and unavoidable step for studying the "within-field" spatial variability of the ET process. The accuracy of the ET measurement conditions to a large extent the feasibility of relating the apparent observed variability to the true (unknown) underlying spatial variability. The uncertainty quantification process is also necessary for the scaling of punctual ET measurements. Actually, the upscaling process inevitably introduces further uncertainty to be added to the uncertainty of the local ET measurements. In cases of inaccurate punctual ET measurements, the local scale uncertainty must be included within the upscaling process to produce field-scale ET estimation with reliable estimated uncertainty.

Accurate estimation of field-scale ET with a soil water balance and quantification of the associated uncertainties is not straightforward. The measurement support of a soil water balance based ET estimate is very limited, i.e. at most few dm^2 as compared to the few thousands m^2 of the prediction field scale. This huge scale gap is a point of concern as the within-field variability of ET is likely to be high [*Bertuzzi et al.*, 1994; *Soegaard and Boegh*, 1995; *Raghuwanshi and Wallender*, 1997]. Robust methodologies need therefore to be developed and tested for the upscaling of local ET measurements. Different approaches can be adopted such as intensifying "randomly" the number of sampling locations within the field, adopting the concept of temporal stability to select some locations within the field which exhibits a very representative ET, or appealing on the use of auxiliary variable as covariant (e.g., Leaf Area Index).

Testing all these methods requires a very good understanding of the within-field variability of the ET process. At the field-scale, this variability is likely to be of two types. The first type is the variability that may be observed at the "large" scale due to the heterogeneous vegetation growth within the field [e.g., *Paz et al.*, 2001; *Booltink and Epinat*, 2001]. The second type is the variability that may be observed at a "small" scale due to the layout of the vegetation. This type of variability is quite well acknowledged for orchards or forest ecosystems where soil water content and ET estimated with a soil water balance may vary considerably as function of the distance between the measurement point and the trunk of the tree [e.g., *Vrugt et al.*, 2001]. On the other hand, for agricultural fields, very few are known about the topic of small-scale variability. One may suspect implicitly that the presence of "small" scale variability is strongly dependent on the crop type. In any case, both types of spatial variability, if present, should be explicitly taken into account when sampling and upscaling strategies for robust estimation of field-scale ET have to be designed. Furthermore, the understanding of the small-scale variability of the processes is very relevant for improving accuracy of field-scale soil water content estimates and consequently the robustness of model calibration.

1.2 Objectives of the study

The basic question analysed in this study is "Which strategies may be adopted to obtain accurate estimates of field-scale ET and how can we quantify the uncertainties associated with these estimates?" Given the generality of this question, specific objectives are formulated to focus on issues which need a more in depth analysis. These specific objectives are:

(1) to investigate the impact of errors caused by the temporal sampling frequency of the climatic data on the estimation of ET;

(2) to analyse the temporal dynamics of the within-field spatial variability of soil water content and to quantify uncertainties on the field mean estimates;

(3) to study the impact of the within-field variability of soil hydraulic properties on the transpiration and the crop yield; and

(4) to test different approaches for the estimation of root water uptake parameters with soil water content data.

Within the context of the ET estimation with a soil water balance, the objectives are:

(1) to quantify uncertainties in a local ET estimate by developing an uncertainty propagation analysis for the case under consideration;

(2) to investigate the within-field spatial variability of the ET process and to test three different sampling strategies to scale up punctual ET measurements; and

(3) to study micro-variability of the hydrological process at the maize row scale in order to improve field-scale ET and soil water content estimations.

1.3 Outline of the thesis

The thesis is structured around the above described specific issues. Five chapters (3 to 7) are devoted to specific issues related to the estimation of ET with agro-hydrological models; three chapters (8 to 10) to the estimation of ET with a soil water balance approach. A schematic overview of the structure of the thesis is presented in Fig. 1.1 indicating the basic question, the specific questions (i.e. the main topic of each chapter) and the relations between some chapters.

In Chapter 2, we describe the experimental site and the different field campaigns that were carried out between May 1999 and August 2003. For each campaign, we describe the measurement techniques used, the number of replicates (in time and space) and the resulting data set. Climate and soil hydraulic properties of the field are also given. The last section of Chapter 2 describes the specific modules of the two agro-hydrological models that were used.

In Chapter 3, we present a methodology to investigate the impact of the sampling frequency of different climatic variables on the estimation of the reference evapotranspiration (ETo). In a first part, we study the impact of the sampling frequency on the estimation of climatic daily means. Then, a basic sensitivity analysis is carried out to identify the climatic variable that influences mostly ETo estimations. Combining these two steps, we quantify the error on ETo due to each climatic variable. Finally, we determine the effect of the temporal sampling frequency on the estimation of daily and cumulative reference ETo.

In Chapter 4, we analyse the comprehensive soil moisture data set produced during the 1999 field campaign. First, we elucidate the role of different factors controlling the spatio-temporal dynamics of soil moisture, in particular the role of the vegetation. Secondly, we identify the temporal dynamics of the spatial structure of soil moisture patterns. Finally, we investigate the relationship between the mean soil moisture and the spatial variability across time, analysing through the season the optimal sampling strategies to adopt for providing the field mean soil moisture within a given predefined error limit.

In Chapter 5, we combine measurements of soil hydraulic properties with agro-hydrological simulations in order to investigate the impact of the within-field variability of the soil hydraulic properties on the transpiration and the crop yield. We perform first a sensitivity analysis to quantify the sensitivity of the actual transpiration and the crop yield to the soil hydraulic parameters. Then, we quantify the impact of the measured within-field variability of the soil hydraulic properties on the actual transpiration and the crop yield. In a third step, all the numerical simulations are rerun considering the water stress parameters as variable and soil dependent in order to test whether different results are obtained. Finally, we study whether the water stress and the soil hydraulic parameters can be simultaneously optimized using "measurements" of transpiration and crop yield.

In Chapter 6, we analyze the identification problem of macroscopic root water uptake parameters (RWUP) from soil water content observations. We use the 1999 soil water content data set to test two different identification approaches. The first is based on a simplified water balance method considering that the whole soil water depletion is due to root water uptake.

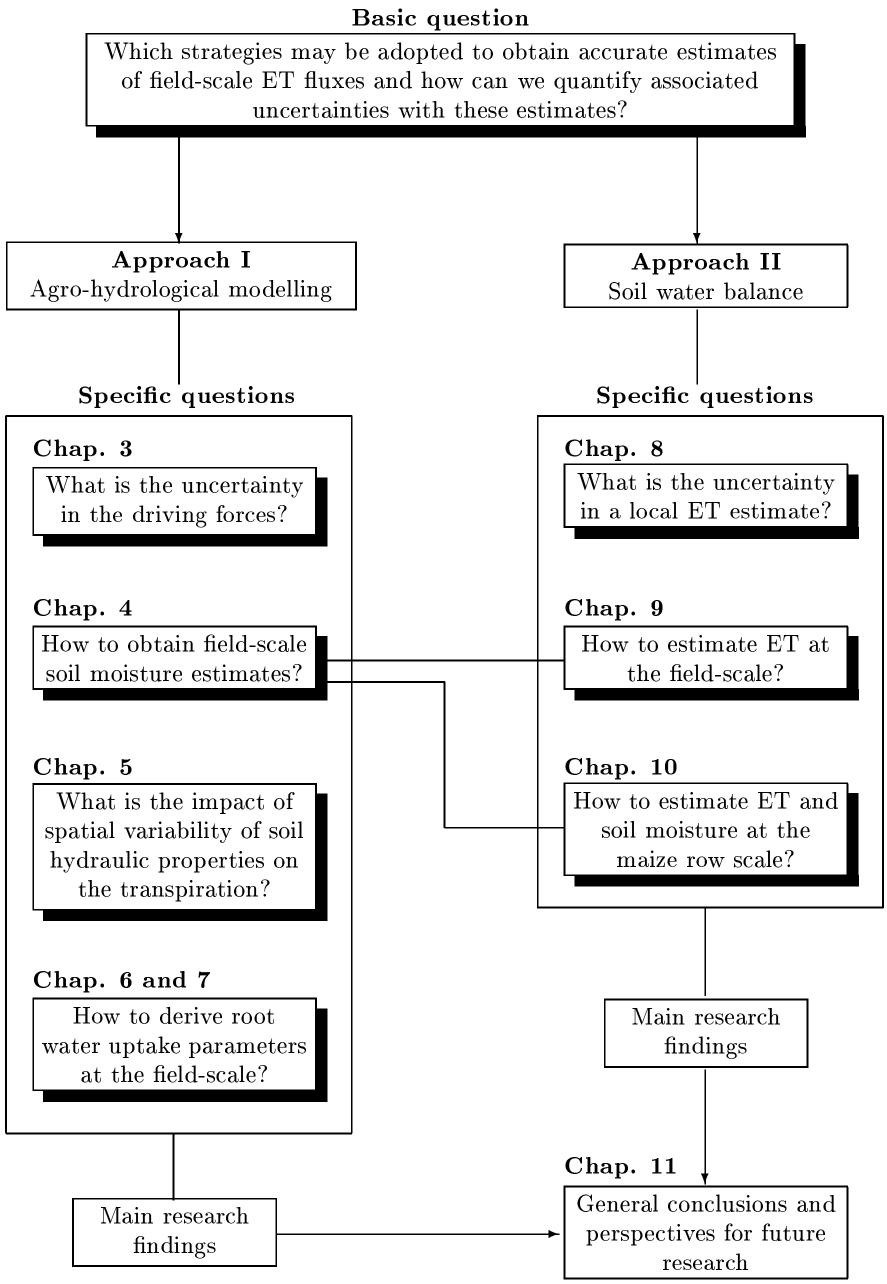

Figure 1.1. Organigram of the outline of the thesis

Accuracy of this approach is tested with numerical experiments. The second approach uses one of the agro-hydrological models in an inverse mode. In a first step we perform a thorough sensitivity analysis. Then, robustness of this approach in terms of stability and uniqueness of the optimized RWUP is investigated respectively by means of visual inspection of response surfaces and 1-D scatterplots. In this chapter, we consider that the RWU is represented by the conceptualization of *Hoogland et al.* [1981]. For both approaches, we generalise the obtained results for five differently textured soils.

In Chapter 7, we test the feasibility of the inverse modeling approach to derive root water uptake parameters (RWUP) from soil water content data using numerical experiments for three differently textured soils and for an optimal drying period. In this chapter, the RWUP of interest are the rooting depth and the bottom root length density representative of the conceptualization of *Feddes et al.* [1978]. We perform a thorough sensitivity analysis and we give a "physical" explanation for the insensitivity of the soil water dynamics to RWUP. In a second step, we analyse the well-posedness of the solution (stability and non-uniqueness) when only RWUP are optimized. Finally, we address the case where RWUP are estimated simultaneously with additional parameters of the system (i.e. with soil hydraulic parameters). In contrast to Chapter 6, full inversions of the agro-hydrological model are performed in this chapter.

In Chapter 8, we quantify the local scale uncertainty of ET estimated with a water balance approach combining two soil water content measurement techniques (TDR and neutron probe sounding) and estimating bottom soil water fluxes. The local scale uncertainty was quantified based on the 1999 data set. Uncertainty on ET was quantified by determining progressively the expected value and uncertainty on soil water content, soil water storage, soil water storage variation and on bottom flux. This latter term was quantified using two different hydraulic conductivity curves (HCC), derived from a pedotransfer function and from field measurements.

In Chapter 9, we use again the 1999 data set to analyse qualitatively and quantitatively the within-field variability of "instantaneous" and cumulated ET as measured with a soil water balance approach. Within this context, we identify the role of the spatially variable vegetation growth. Then, we test three different sampling procedures to scale up punctual ET measurements to field-scale ET estimates and to derive their associated uncertainties.

In Chapter 10, we focus on the micro-variability of the hydrological process at the maize row scale. We analyse quantitatively the micro-variability of the rainfall redistribution below the maize canopy and the micro-variability of the root water uptake and the evapotranspiration within the maize rows. Next, we investigate the spatio-temporal dynamics of the soil water content resulting from these spatially variable processes. Finally, using the measured spatial variability of the soil water content, we derive optimal sampling strategies to obtain accurate soil water content and ET estimations at the maize row scale.

In Chapter 11, we conclude by presenting the major research findings and by giving some recommendations for future research.

Chapter 2

Experimental field, measurements and models

In this chapter, details are given on the experimental site, the measurements performed between May 1999 and August 2003, and the two different agro-hydrological models used to simulate the water transport within the soil-plant-atmosphere system.

2.1 Experimental field

The experimental site consists in a 15000 m^2 agricultural field located on a plateau in Louvain-la-Neuve (Belgium), five hundred meters away from the laboratory (see Fig. 2.2 top left). The major criterion for selecting this field was its proximity to the laboratory which constitutes a significant advantage for daily experimental work. The soil of the field is classified as a well-drained silty-loam (Aba, according to the Belgian classification). Textural analysis for the superficial layer yield a loam content of 82%, a clay content of 12% and a sand content of 6%. A contour map of the field (Fig. 2.1) elucidates that the topography is rather uniform with a maximum relief of 3 m (see Fig. 2.2 top left and right). Because of its specific topographic position, the experimental field is assumed not to be influenced by the adjacent areas through the process of lateral water flow. Until March 1999, the field crop was perennial ryegrass (*Lolium perenne* L.). From 1999 onwards, this field was cropped with maize (*Zea Mays* L.). Climate at the site is moderate humid with an average annual rainfall of 780 mm [*Dupriez and Sneyers*, 1982], which is relatively well distributed over the year and with an average annual reference evapotranspiration of 528 mm [*Gellens-Meulenberghs and Gellens*, 1992].

2.2 Field campaigns

2.2.1 1999 campaign

The main objective of the 1999 field campaign was to investigate the "within-field" spatial variability of the hydrological processes with an emphasis on the actual evapotranspiration (ET). We set up an experiment within an area of 6300 m^2 centred on the field to follow intensively the different components of the water balance. The selected area is nearly flat with a maximum relief of 1.8 m and with a weak topographic convergence between sampling points 22 and 23 (see Fig. 2.1). The relief of this area and of the whole experimental field was determined by means of a Differential Global Positioning System for X-Y coordinates and a theodolite for Z coordinate on 250 points. Within the 6300 m^2 area, we adopted a regular sampling grid of 28 measurement points, each separated by a 15 m sampling interval. Note that the number of point measurement was chosen to reach a compromise between a number of points sufficiently high to investigate the spatial variability of the processes and the time required to perform all the measurements. On each sampling point, we installed vertically a triple wire home-made TDR probe to monitor the soil water content in the top 20 cm of the soil profile, an 150-cm aluminium access tube to measure with a neutron probe soil water content at 25, 50, 75, 100 and 125 cm depths and two tensiometers at 115 and 135 cm (see Fig. 2.2 bottom left). Between the 30^{th} of May and the 13^{th} of September 1999, pressure head measurements were made manually on 91 dates with a portable tensimeter (Soil Measurement Systems^{TM}), soil water content measurements were made manually on 60 dates by means of TDR (cable tester Tektronix 1502B^{TM}) and on 45 dates with a neutron probe device (Institute of Hydrology Neutron Probe System II^{TM}). All the measurement instruments are shown in Fig. 2.2 (Bottom right). The 1999 field campaign resulted in a comprehensive data set of more than 5000 pressure head measurements and nearly 8000 soil water content measurements. For this agricultural season, the field was cropped with maize (*Zea Mays* L.) which was sown on the 25^{th} of April with a density of 110,000 plants per hectare and harvested on the 10^{th} of October (DOY 283). The rows were spaced 75 cm apart and all the measurement instruments were installed in the middle of the rows (see Fig. 2.2 bottom left). On each of the 28 sampling locations, we selected 10 maize plants (5 within each row located on each side of the sampling location) which were considered as those influencing, through the process of root water uptake, the measured soil moisture profile.

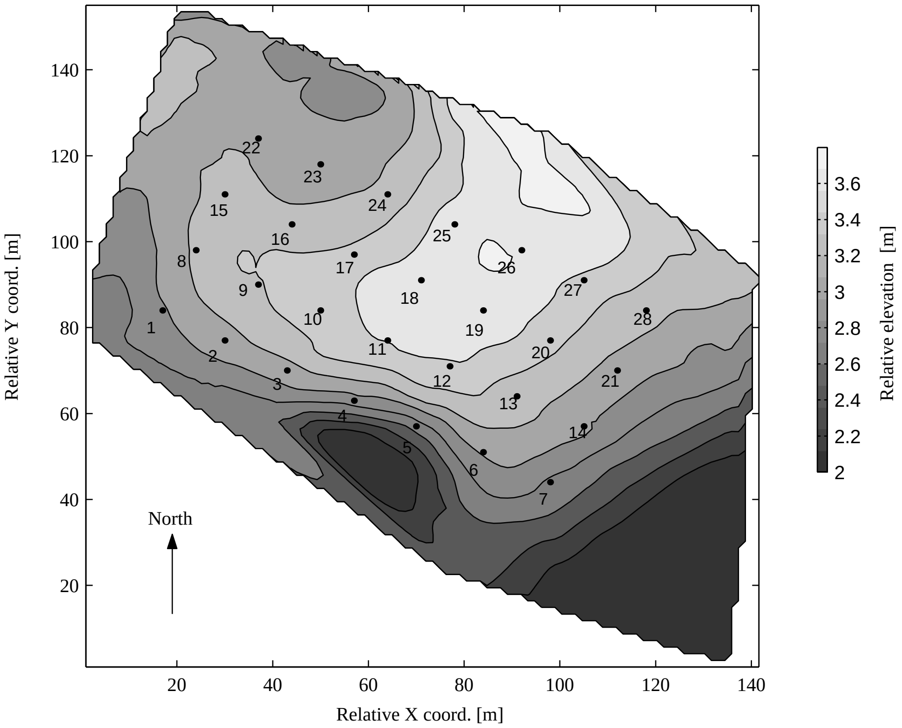

Figure 2.1. The experimental field, Louvain-la-Neuve, Belgium. Topographic features of the field are shown with the 28 sampling locations indicated with circle (studied area = 0.63 ha).

Note that these 10 maize plants are therefore situated on the border of a 75x75 cm square in the centre of which is measured the soil moisture profile. On each of the 280 selected maize plants, we measured the number of growing leaves as well as the number and size of full grown leaves (see Fig. 2.3 top left), thereby deriving the mean Leaf Area Index (LAI) on the 12^{th} of July for each 28 site according to the methodology proposed by *Ruget et al.* [1996]. The 10 maize plants on each of the 28 location were harvested on the 17^{th} September and oven dried for both total above-ground (leaves, stems, ears) and ears dry matter (see Fig. 2.3 top right). During the 1999 field campaign and the following winter, two in-situ calibration curves were established respectively for the neutron probe and TDR device (see Fig. 2.3 bottom left and right). For each calibration curve, 25 pairs of observed vs. reference soil water content were measured within the range 20 to 45% (volumetric water content).

Figure 2.2. 1999 field campaign. Top left: localization of the sampling locations within the experimental field. Top right: growing maize at the end of May. Bottom left: tensiometers, TDR probe and access tube installed mid-way between the 75 cm spaced rows. Bottom right: field measurements with neutron probe, Tektronix, tensimeter and the unavoidable field book.

The gravimetric method was considered as the reference method. Details about the calibration curves can be found in Chapter 8. Concerning the climate, the 1999 field campaign was marked by two long drying periods which obviously constitutes a significant advantage for an experiment dealing with the study of evapotranspiration fluxes. The first long drying period occurred between the 6^{th} of July and the 3^{rd} of August (DOY 187-215) with a rainfall amount of 8 mm, and the second between the 20^{th} of August and the 13^{th} of September (DOY 232-256) with a rainfall amount of 1.6 mm. These two periods were interrupted by rainy events, some of them with very high intensities (i.e. DOY 215). For details about the climate of the 1999 agricultural season, the reader is referred to Chapter 3 (see Fig. 3.1d for climatic demand) and Chapter 4 (see Fig. 4.1 for rainfall). The 1999 field campaign resulted in a comprehensive data set which was used in all the chapters further on except in Chapter 10.

2.2.2 2000 campaign

Preliminary results from the 1999 field campaign showed that both soil water content and actual ET fluxes were not spatially correlated at the considered scale, namely for the minimum considered distance between adjacent sampling points (i.e. 15m). Furthermore, soil water content measured within the deeper layers (75-100-125 cm) on some sampling locations (4 and 5) during the 1999 field campaign showed quite low values suggesting that a more "sandy" area could be present deeper in a small part of the field. Therefore, we set up an experiment to study the "micro-scale" spatial variability of the ET fluxes and to investigate more thoroughly the deeper drier area. Within this framework, we set up a linear 45 m long transect of 50 measurement points, each separated by 0.9 m sampling intervals (see Fig. 2.4 top left). The transect was installed perpendicularly to the maize rows spaced 45 cm apart about between sampling locations 4 and 25. On each point, we installed measurement instruments similar to those used in 1999, i.e. a triple wire TDR probe, an 150-cm access tube and two tensiometers at 115 and 135 cm depth. Between the 22^{th} of June and the 7^{th} of September 2000, pressure head and soil water content measurements were made manually on 10 dates. This resulted in a data set of 1000 pressure head measurements and 3000 soil water content measurements. The 2000 agricultural season, and more particularly the considered period was very humid with a rainfall amount of 168 mm quite uniformly distributed across the period 22^{th} of June to the 7^{th} of September.

Figure 2.3. 1999 field campaign. Top left: measurement of width and length of about 15 maize leaves on each 280 maize plant. Top right: manual yield of maize for dry matter estimation. Bottom left: in-situ calibration of neutron probe (second phase, i.e. measurement of volumetric soil water content at a given depth with four kopecki rings). Bottom right: TDR probes installed for in-situ calibration.

For the study of ET process, such climatic conditions are clearly unfavourable as root water uptake is permanently compensated by infiltrating rainfall meaning that the temporal evolution of the soil water content remains quite constant through the season. Furthermore, soil water fluxes are generally very large during such humid period. Quantification of ET by means of a water balance approach during such period is therefore very tricky and uncertain. For these reasons, the 2000 data set was not used further on.

2.2.3 2002 campaign

The 2002 field campaign was dedicated to the study of the "micro-scale" variability of the hydrological processes, i.e. mainly the root water uptake within the maize rows. We set up an experiment within a small area of the field. We installed 15 measurement points along a 2.25 m long transect perpendicular to the maize rows spaced 45 cm apart (see Fig. 2.4 top right). On each point, we installed a 100-cm PVC access tube to measure soil water content with a time domain probe (TRIME^{TM}). This system is a tube-probe that is lowered into a PVC tube to measure soil water content at any desired depth between the soil surface and the bottom of the tube. For this study, we chose and used this measurement instrument as it has a very small measurement support (few cm) which is an advantage to investigate micro-variability of processes. Unfortunately, this soil water content measurement instrument is also very sensitive to air gaps (only few mm) between the soil and the access tube. The installation of the access tubes is therefore critical. In our case and despite a very careful installation (bore holes with a diameter very close to the external diameter of the PVC tubes and the addition of a soil paste to ensure a good contact between the soil and the access tube) it seems that air gaps still occurred between the tube and the surrounding soil leading to unreliable soil water content profiles. For this reason, we decided not to exploit the 2002 soil water content data set including soil water content measurements performed at 8 different depths (each 10 cm between 15 and 85 cm depth) on 15 dates between early June and mid-August.

2.2.4 2003 campaign

After the 2002 field campaign "failure", we decided to set up again an experiment to study both micro-variability of root water uptake within maize rows and throughfall, i.e. the rainfall redistribution under the maize canopy. We installed 14 measurement points along a 1.5 m long transect perpendicular to three rows of maize (*Zea Mays* L. variety Fuego HS F225) spaced 75 cm apart (see Fig. 2.4 bottom left). On each measurement point, we installed a 100-cm aluminium access tube to measure with a neutron probe device (Institute of Hydrology Neutron Probe System II^{TM}) soil water content at 25, 35, 45, 55 and 65 cm depths. Soil water content was measured each two, three or four days according to the climatic conditions between the 3^{rd} of June and the 28^{th} of August, resulting in a data set of 1540 soil water content measurements. With regard to the measurements of throughfall, we installed 52 small rectangular plastic boxes (size 13.8x5.2 cm) 5 cm above the soil surface and within two interrows (see Fig. 2.4 bottom right). The containers were installed 1 m away from the access tubes, avoiding the perturbation of the soil water dynamics around the access tubes. The containers were weighted and emptied regularly after rainfall events to measure incident throughfall. In this way, the throughfall was measured on the whole soil surface except 1.5 cm on each side of the maize stems and on the stems themselves (i.e. stemflow was not measured). Leaf Area Index was estimated on 5 dates with the above-mentioned methodology. Note that this experiment was set up in a small agricultural field adjacent to the field used for the experiments of previous years. Indeed, to meet the requirements of this experiment we needed maize rows spaced 75 cm apart. The data set produced by the 2003 experiment is used exclusively in Chapter 10.

2.3 Climatic measurements

Between May 1999 and August 2003, meteorological variables were measured with an automatic weather station situated within an area consisting of a 1000 m^2 perennial ryegrass (*Lolium perenne* L.) regularly clipped to maintain a constant height of 10 centimetres. Note that this area is also equipped with a 1m^2 weighting lysimeter. The meteorological station installed and started up in April 1999 was equipped with five different sensors. The shortwave radiation and the photosynthetically active radiation (PAR) were measured respectively with a standard CM3 pyranometer and with a PAR Lite sensor (Kipp and Zonen^{TM}). The wind speed was measured at a 2 m height with a classical cup-anemometer (MDL33, GME enterprise^{TM}). Dry and wet temperatures were measured at a 1.5 m height with negative coefficient thermoresistances. From May to November 1999, all the climatic variables were measured and recorded at 1 minute interval in a data logger (EasyLog 3000, GME entreprise^{TM}).

Figure 2.4. Top left (2000 experimental setup): transect of 50 sampling points. Top right: removal of the 2002 PVC tubes. Bottom left (2003 experimental setup): small transect with 14 access tubes installed perpendicularly to three maize rows. Bottom right (2003 experimental setup): measurement of throughfall under the maize canopy.

After this date and until now, the climatic variables were measured at 1 minute interval and recorded as a mean each 5 minutes. The climatic data set collected with this meteorological station will be used in all the chapters further on except in Chapter 5. In this chapter, we use climatic variables collected by a weather station managed by the ASTR research Unit and situated 150 m away from the station described above. Climatic variables in this weather station are measured at similar height and with similar sensors, except for the wind speed which is measured at a height of 20 m.

2.4 Soil physical measurements

2.4.1 Soil water retention curve

In March 2000, 28 undisturbed 8.4-cm diameter soil columns were collected in PVC tubes from 0 to 75 cm depth and from 75 to 125 cm depth close to each 28 sampling location used during the 1999 field campaign. This was done with a hydraulic auger mounted on a four-wheel vehicle (see Fig. 2.5 top left). Afterwards, all the PVC tubes were opened (see Fig. 2.5 top right) to collect within the long soil columns three undisturbed 5.1-cm long and 5-cm diameter soil cores (kopecki ring) at respectively 45, 75 and 105 cm depth. For each of the 84 soil cores we determined the drying part of the water retention curve by means of a sand-box apparatus for soil water pressures of 1-10-100 cm. A pressure cell was used for soil water pressures of 300-1000-2500 and 15000 cm. After each applied pressure, the soil cores were systematically weighted to determine the amount of extracted water. At the end of the experiment, the bulk density and the gravimetric water content were determined allowing us to back-calculate volumetric water content at each applied pressure.

2.4.2 Saturated hydraulic conductivity

For the determination of the saturated hydraulic conductivity, K_{sat}, we used both field and laboratory methods. For the field determination of K_{sat}, we used a double-ring infiltrometer following the methodology proposed in *Reynolds et al.* [2002]. The measuring (inner) and buffer cylinders of the infiltrometer are both 25 cm long and 28 cm and 53 cm in diameter respectively. The measurements were made in October 2000 on four places chosen randomly within the experimental field at 25 cm depth.

After removing the first 25 cm of soil, both cylinders were inserted into the soil to a depth of about 10 cm with a drop-hammer apparatus. Then, we ponded a depth of water of about 10 cm inside both measuring and buffer cylinders. The rate of infiltration was regularly measured within the inner cylinder by visual observations on a graduated scale. We assumed that quasi-steady flow under the measuring cylinder was reached when the rate of infiltration becomes constant (after a minimum of six hours for the considered loamy soil). Saturated hydraulic conductivity values were obtained considering that measured quasi-steady infiltration rates are equal to the field-K_{sat}. Values of K_{sat} determined with this technique were used in Chapters 6 and 7.

Additionally to those field measurements, we determined saturated hydraulic conductivity with the constant head permeameter method. We collected in March 2002 six undisturbed soil samples at two different places and three different depths (25, 50 and 75 cm depth) within the experimental field. At each place and depth of interest, we excavated a soil pedestal slightly smaller than the rectangular "conductivity" metallic tank of 1440 cm^3 (10-cm long, section of 144 cm^2) used to collect the soil samples. After inserting the tank, melted paraffin was poured between the soil sample and the inner border of the rectangular metallic tank to avoid prefential flow. The undisturbed soil samples were brought back in the laboratory, prepared, i.e. any evidence of soil compaction at the surface was removed and a nylon cloth was fixed at the bottom of the sample, and saturated during a period of 4 days. Then, a constant head of 10 cm was applied on the top of the samples. The flow rate through the soil sample was measured by collecting at the bottom the volume of water during a set period of time. Saturated hydraulic conductivity values were obtained using Darcy's law with water flow measured at steady-state. Values of K_{sat} determined with this technique were used in Chapter 5.

2.4.3 Unsaturated hydraulic conductivity

Unsaturated hydraulic conductivity values close to saturation were determined in March 2002 at three different locations at 25 and 50 cm depth within the field (see Fig. 2.5 bottom left) with a disk permeameter (Soil Measurement Systems^{TM}). At each place and depth of interest, the soil surface was carefully levelled and a thin layer of sand was placed to ensure hydraulic contact between the soil and the permeameter. Measurements of steady-state flow rate were performed sequentially at two different imposed negative pressure heads (-4 and -7 cm) with a single

Figure 2.5. Top left: collection of the undisturbed soil columns with the hydraulic auger. Top rigth: severed undisturbed soil columns. Bottom left: infiltrometer measurement at 50 cm depth (March 2002). Bottom right (2003): visual observation of throughfall under maize canopy after a small rainfall amount of 5 mm (see the difference of soil colour within and between the rows)

disk of 30 cm in diameter. Then we used the traditional approximate solutions proposed by *Wooding* [1968] for deriving unsaturated hydraulic conductivity close to saturation. Values of unsaturated hydraulic conductivity determined with this technique were used in Chapter 8. Note that the exact location of both saturated and unsaturated soil hydraulic conductivity measurements performed within the field are not known as these measurements were not georeferenced.

2.5 Soil-Plant-Atmosphere Models

As explained in Chapter 1, estimation of water fluxes and more particularly evapotranspiraton (ET) will be performed in this study with two different approaches, i.e. the soil water balance and the agro-hydrological model. This section describes the two agro-hydrological simulation models used in this study: the WAVE-model [*Vanclooster et al.*, 1996] and the SWAP-model [*van Dam et al.*, 1997]. Both models are process-based and consist of different modules simulating different processes such as the soil water movement, the solute transport, the heat flow, and the crop growth. In this section only the soil water transport module of the WAVE-model and the soil water transport and the crop growth modules of the SWAP-model are described.

2.5.1 WAVE

For homogeneous isotropic isothermal rigid porous media, one-dimensional vertical transient water flow can be described using the Richards' equation:

$$C(h)\frac{\delta h}{\delta t} = \frac{\delta}{\delta z}\left[K(h)(\frac{\delta h}{\delta z}+1)\right] - S(z) \tag{2.1}$$

where $C(h) = \frac{\delta\theta}{\delta h}$ is the soil water capacity [L^{-1}], h is the soil water pressure head [L], t is time [T], z is the vertical coordinate [L] defined as positive upward, $K(h)$ is the hydraulic conductivity [LT^{-1}], and $S(z)$ is the sink term describing water uptake by plant roots [T^{-1}]. Eq. (2.1) is valid for both saturated and unsaturated flow conditions. Eq. (2.1) is highly non-linear and analytical solutions only exist for specific boundary conditions. To solve Eq. (2.1), the water retention (MRC=$\theta(h)$) and the hydraulic conductivity functions need to be specified. Although numerous different parametric models can be found in the literature (e.g., *Gardner* [1958]; *Brooks and Corey* [1964]; *Assouline* [2001]), we will assume in this study that the soil water functions can be described by the nonhysteretic unimodal Mualem-van Genuchten model (MVG) [*Mualem*, 1976; *van Genuchten*, 1980]. The water retention and hydraulic conductivity relationships are given respectively by:

$$\theta(h) = \theta_r + \frac{\theta_s - \theta_r}{(1+ \mid \alpha h \mid^n)^m} \tag{2.2}$$

$$K(\theta) = K_{sat}\, Se^{\lambda} \left[1 - (1 - Se^{\frac{1}{m}})^m\right]^2 \tag{2.3}$$

where θ_r and θ_s are the residual and saturated volumetric water content respectively [-], α [L^{-1}], n, $m = (1 - 1/n)$ and λ [-] are empirical parameters, K_{sat} is the saturated conductivity [L T^{-1}], and Se is the relative saturation [-]. The use of relationships presented in Eq. (2.2) and (2.3) requires the specification of four to six parameters according to value of θ_r and λ being fixed to 0 and 0.5 respectively. In order to solve Eq. (2.1) numerically, the soil profile is discretised into a number of compartments grouped in different pedological layers for which soil water retention and hydraulic conductivity curves are specified. In the WAVE-model, an implicit discretisation scheme with explicit linearization of the differential moisture capacity is used. To solve the system of linear equations, the Thomas algorithm is used combined with the Newton-Raphson solution technique [e.g., *Carnahan et al.*, 1969] to reduce mass balance errors resulting from the explicit linearization of the soil water capacity. To solve the water flow equation (Eq. (2.1)), bottom and upper boundary conditions (BBC and UBC) need to be specified. In this study we considered that the BBC is represented by a free drainage at the bottom of the soil profile (Neuman condition), i.e. we consider that the unit hydraulic gradient is present at the bottom of the profile and that the water flux equals the hydraulic conductivity. With regard to the UBC the flow situation at the soil surface is determined by the infiltration or the evaporative flux. As long as the flow conditions at the soil surface are not limiting, the flux through the soil surface Q_s equals:

$$Q_s = E_p - (R + \frac{P_d - I_c}{\Delta t}) \tag{2.4}$$

with Q_s the potential flux through the soil surface, defined as positive upward (cm d^{-1}); E_p is the potential soil evaporation rate (cm d^{-1}) as determined by the climatic conditions and the soil cover (see further on); R is the rainfall (cm d^{-1}); P_d is the ponding depth at the soil surface (cm) and I_c is the storage capacity of the canopy (cm). The potential flux Q_s is reduced when high rainfall intensities or prolonged soil evaporation without rewetting occur. In case of high rainfall intensities, potential flux Q_s can exceed the infiltration capacity of the soil (i.e. $K(h)\ \nabla H$).

In that case, and if no ponding is assumed, the excess water runs off immediately and the pressure head at the soil surface is put to zero (switch from Neuman to Dirichlet condition). In case of ponding, the soil surface pressure head can increase positively until it reaches the specified ponding value. Actual infiltration rate within the first soil compartment is then calculated using Darcy's equation multiplying the geometric mean of the hydraulic conductivities of the surface and the first nodes with the hydraulic gradients between those nodes. For prolonged soil evaporation without rewetting, a similar phenomenon is encountered. In the beginning, the soil water flux is large enough to meet the evaporative demand (E_p). At a given moment, the soil becomes so dry that the upward flux through the soil surface becomes smaller than E_p, meaning that the actual soil evaporation is smaller than the potential rate. Reduction of the potential soil evaporation is simulated by switching the flux type condition into a pressure head condition. When the pressure head at the surface tends to become more negative than a specified value (h_{sair}), corresponding to the potential of the air, the pressure head of the surface node is fixed to this value. Actual soil evaporation rate within the first soil compartment is then calculated using Darcy's equation multiplying the geometric mean of the hydraulic conductivities of the surface and the first nodes with the hydraulic gradients between those nodes. In case of cropped soils, interception and transpiration are two additional components of the water balance. Interception capacity of the crop is specified by the user. Potential transpiration rate is calculated as a fraction of the crop potential evapotranspiration (ET_p). ET_p is obtained by multiplying the reference evapotranspiration (ET_o) calculated according to *Allen et al.* [1994] (see details in Chapter 3) by an appropriate crop coefficient varying through the season as a function of the development stage. Afterwards, ET_p is partitioned between the potential soil evaporation (E_p) and potential transpiration (T_p) by:

$$E_p = ET_p \, exp^{-cLAI} \tag{2.5}$$

where LAI (-) is the Leaf Area Index and c the extinction coefficient (-) put to 0.6 in the WAVE-model. Potential transpiration (T_p) is then calculated by subtracting E_p and C_{stor} (canopy storage) from ET_p:

$$T_p = ET_p - E_p - C_{stor} \tag{2.6}$$

Afterwards, actual transpiration is derived from the potential transpiration T_p and the integration of the sink term $S(z)$ of Eq. (2.1) over the rooting depth.

The sink term is defined by *Feddes et al.* [1978] as:

$$S(z,h) = \gamma(h) S_{max}(z) \tag{2.7}$$

with $S_{max}(z)$ the maximal root water uptake as a function of depth [T^{-1}] and $\gamma(h)$ a dimensionless reduction function that simulates the effects of soil moisture stress. In the WAVE-model, the maximal root water uptake is considered to be linearly decreasing with depth as suggested by *Hoogland et al.* [1981]:

$$S_{max}(z) = A + Bz \tag{2.8}$$

with A [T^{-1}] and B [T^{-1}] [L^{-1}] parameters conditioning respectively the maximum root water uptake at the surface and the decreasing rate with depth. The reduction function $\gamma(h)$ is characterized by different pressure head values h_1, h_2, h_3 (low and high according to the climatic demand) and h_4. Above h_1, $\gamma(h)$ is zero, between h_2 and h_3(l or h) $\gamma(h)$ is 1 and between h_3 and h_4 the value of the reduction function is given by:

$$\gamma(h) = \frac{h(z) - h_4}{h_3 - h_4} \tag{2.9}$$

The shape of the water stress function is schematically illustrated in Fig. 2.6. The actual root water uptake given by Eq. (2.7) is subsequently integrated from the soil surface downwards until it reaches either the potential transpiration T_p (no water stress) or the rooting depth (water stress if the integrated root water uptake is smaller than T_p). In this study, the soil water transport module of the WAVE-model is used without the crop growth module. Consequently, Leaf Area Index and rooting depth values need to be specified for each time step of the simulations. Note that concurrently to the use of the WAVE Fortran^{TM} version, a Matlab^{TM} version of the WAVE soil water transport module was developed. Both versions were tested and produced identical results. Each version was used according to the requirements. The WAVE-model is used in Chapters 6, 8 and 9.

2.5.2 SWAP

The soil water transport module of the SWAP-model [*van Dam et al.*, 1997] is quite similar to that of the WAVE-model. Numerical schemes are slightly different with among others the soil hydraulic conductivity arithmetically averaged between the nodes in SWAP (geometrically averaged in WAVE) and the soil water capacity between two successive time steps differently evaluated.

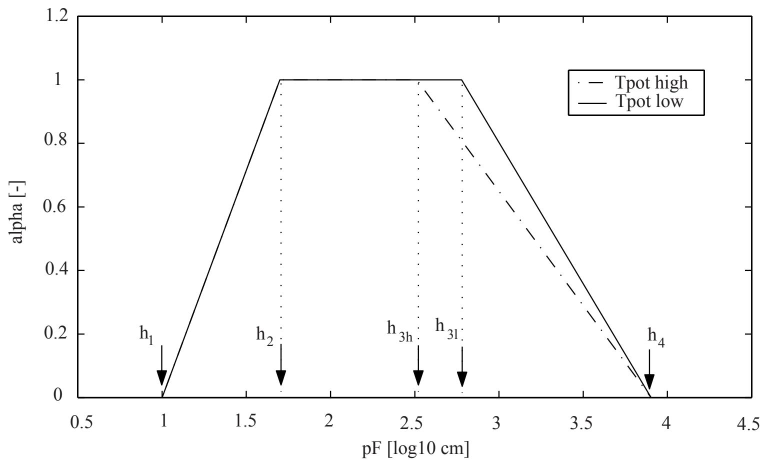

Figure 2.6. Water stress function used in WAVE and SWAP models

For the estimation of the potential soil evaporation, SWAP allows specifying the extinction coefficient (c in Eq. (2.5)) as the product of the extinction coefficient for direct and diffuse visible light (κ_{dir} and κ_{dif}). In SWAP, potential evapotranspiration can be estimated with two methods. The first method directly uses the Penman-Monteith parameterisation and calculates potential evapotranspiration for a wet canopy, for a dry canopy and for a wet bare soil considering different crop heights and surface resistances. The second method uses the "Kc ETo" approach similar to that included in WAVE. In this study, we only used the second approach to quantify potential evapotranspiration. For canopy interception, small differences exist between both models but their explanation is beyond the scope of our study. Main difference between both models is found in the used root water uptake (RWU) conceptualization. In the SWAP-model, the maximum possible RWU rate, $S_{max}(z)$, integrated over the rooting depth, is equal to the potential transpiration and is defined as follows:

$$S_{max}(z) = \frac{RLD(z)}{\int_{-RD}^{0} RLD(z)dz} T_p \tag{2.10}$$

with $RLD(z)$ the root length density at depth z [L L^{-3}]; and RD the rooting depth [L]. Note that this formulation of the S_{max} function is in fact an extension of the model by *Feddes et al.* [1978] and *Prasad* [1988] allowing a more flexible distribution of the maximum RWU according to the root density profile. In this study, only a linear root density profile will be considered requiring therefore the specification of three parameters, i.e. the top root length density ($TRLD$), the bottom root length density ($BRLD$) and the rooting depth (RD). In this study, we decided to fix $TRLD$ equal to 1 in order to characterize the linear RWU profile with only two parameters ($BRLD$ and RD). The $S_{max}(z)$ term is then adjusted according to the water stress functions of Eq. (2.9). The actual root water uptake given by Eq. (2.9) is subsequently integrated over the whole rooting depth and yields the actual transpiration rate T_a. Fig. 2.7 illustrate main differences between RWU conceptualizations of WAVE and SWAP by means of numerical simulations. These were run for a dry period of 28 days (July 1999) for a maize cropped loamy soil (see table 6.1 for hydraulic properties) starting from a soil profile at field capacity. For the simulation run generated with the WAVE-model, RWU parameter values were fixed to 100 cm for RD, 0.013 d^{-1} for A, and 0.000118 d^{-1}cm^{-1} for B (see Chapter 6 for details). For the SWAP runs, the RWU parameters were fixed to 100 cm for RD, 1 for $TRLD$ and 0.5 for $BRLD$ (see Chapter 7 for details). Fig. 2.7a shows temporal evolution of the climatic demand and Fig. 2.7b and c daily RWU patterns generated with SWAP and WAVE respectively. Bottom figures present RWU for days 2 (d-g), 6 (e-h) and 28 (f-i) simulated respectively with SWAP and WAVE. The differences between the two RWU conceptualizations can be summarized as follows:

1. In SWAP, the depth over which the RWU takes place is constant (see Fig. 2.7b) for a period when crop growth is neglected. In WAVE, the depth is variable according to the climatic conditions, i.e. the higher is T_p the deeper the RWU will take place (see Fig. 2.7c);

2. In SWAP, for a certain depth the maximum possible RWU is variable according to the climatic demand, i.e. the higher is T_p the larger the RWU will be for a given depth (see Fig. 2.7d-e). In WAVE, RWU is constant for a certain depth (fixed by Eq. (2.8)) and independent of the climatic conditions (see Fig. 2.7g-h);

3. In SWAP, a water stress occurs as soon as the pressure head drops below a critical value in any layer of the soil. In WAVE, a water stress only appears if the integration of $S(z,h)$ over the rooting depth is smaller than T_p;

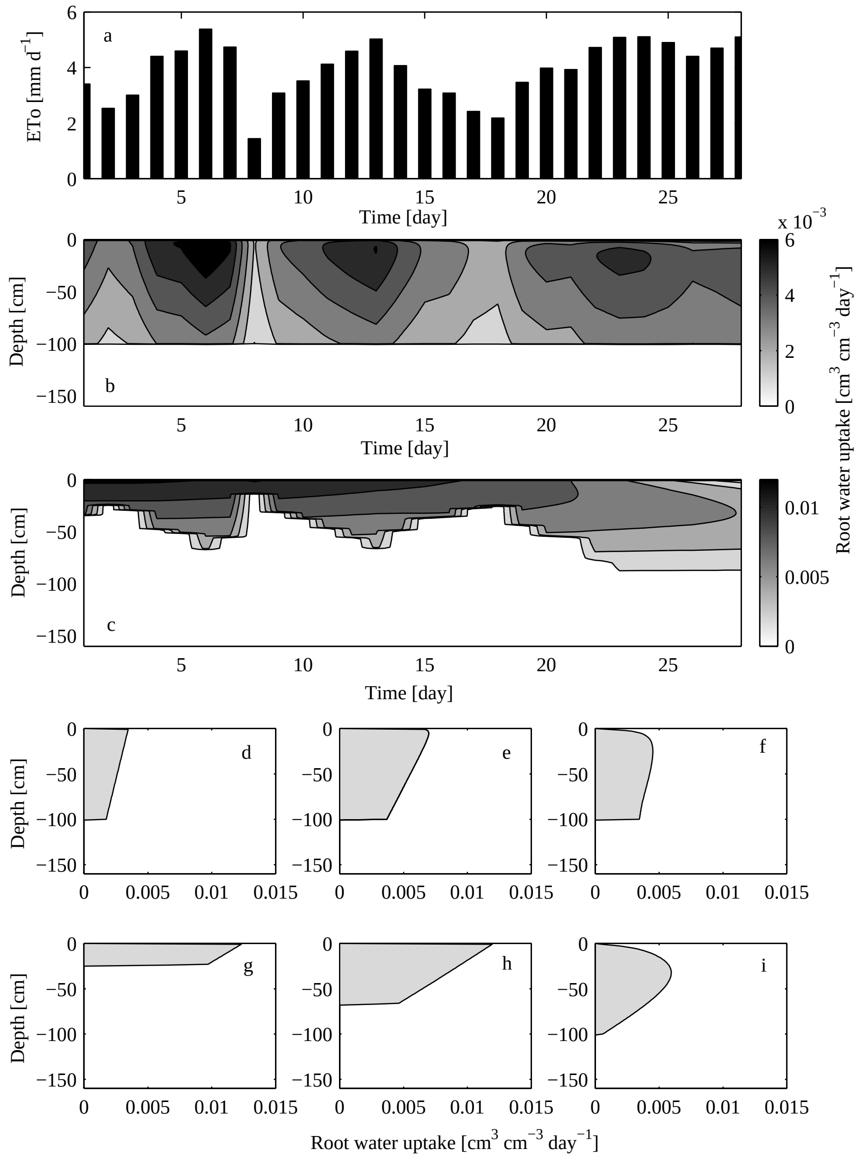

Figure 2.7. Climatic demand (a) with the corresponding root water uptake (RWU) patterns simulated with SWAP (b) and WAVE (c) for a loamy soil during a long drying period of 28 days. Bottom figures illustrates the daily RWU for days 2 (d, g), 6 (e, h) and 28 (f, i) simulated respectively with SWAP and WAVE

Note that the lastest version of the WAVE-model uses the RWU conceptualization incorporated in the SWAP-model [*Vanderborght et al.*, 2002]. With regard to the modelling of the soil water transport both with WAVE and SWAP models, the following working hypotheses were considered for the whole study:

1. Richards' equation is valid at the local and at the field-scale and can be used at these scales to simulate soil water flow ;

2. Water retention and conductivity functions are described by the model of Mualem-van Genuchten model (MVG) [*Mualem*, 1976; *van Genuchten*, 1980];

3. Water retention and hydraulic conductivity curves are nonhysteretic and unimodal (macropore flow and hysteresis can therefore not be simulated);

4. Temporal dynamics of the soil hydraulic properties, both measured and estimated, is not taken into account;

5. Ponding value is set equal to zero (runoff directly occurs when the infiltration capacity limits the infiltration rate);

6. Daily total rainfall is uniformly distributed over the day (high measured intensities of rainfall are smoothed).

Crop growth in the SWAP-model can be simulated using a detailed crop growth routine derived from WOFOST 6.0. [*Spitters et al.*, 1989]. The crop growth model calculates the radiation energy absorbed by the canopy as function of incoming photosynthetic active radiation and crop leaf area. Using the absorbed radiation and taking into account photosynthetic leaf characteristics, the potential rate is calculated. The latter is reduced due to water and/or salinity stress, as quantified by the relative transpiration rate, and yields the daily actual gross assimilation rate. This is expressed by the following equation:

$$A_{gross} = \frac{30}{44} f_{7min} \frac{T_a}{T_p} A^1_{pgross} \tag{2.11}$$

where f_{7min} is a reduction factor that is a function of the minimum temperature during the last seven days, T_a and T_p the actual and potential transpiration respectively (mm d^{-1}) and A^1_{pgross} and A_{gross} the daily potential gross assimilation rate and the daily actual gross assimilation rate respectively (kg ha^{-1} d^{-1}). Part of the carbohydrates (CH_2O) produced are used to provide energy for the maintenance of living biomass (maintenance respiration). The remaining carbohydrates are converted into structural matter. In this conversion, some of the weight is lost as growth respiration. The dry matter produced is partitioned among roots, leaves, stems and storage organs, using partitioning factors that are a function of the crop phenological development stage. The fraction partitioned to the leaves, determines leaf area development and hence the dynamics of the light interception. The dry weight of the plant organs are obtained by integrating their growth rates over time. During crop development a part of the living biomass will die due to senescence. Leaf senescence occurs due to water stress, shading, and also due to exceedance of the life span. The potential death rate of leaves due to water stress is calculated as follows:

$$\zeta_{leaf,w} = W_{leaf}(1 - \frac{T_a}{T_p})\zeta_{leaf,p} \tag{2.12}$$

where $\zeta_{leaf,w}$ is the potential death rate due to water stress (kg ha^{-1} d^{-1}); W_{leaf} is the leaf dry matter weight (kg ha^{-1}); T_a and T_p the actual and potential transpiration and $\zeta_{leaf,p}$ the maximum relative death of leaves due to water stress (kg kg^{-1} ha^{-1}). Leaf senescence due to shading is then calculated with another expression and the highest value of the combined effect of water stress and mutual shading is finally taken into account. The SWAP-model with the detailed crop growth routine has been used in Chapter 5 and with the soil water transport module only in Chapter 7.

Chapter 3

Effect of the sampling frequency of meteorological variables on the estimation of the reference evapotranspiration

Abstract*

In this Chapter, we quantify the effect of the temporal sampling frequency of commonly measured climatic variables on the estimation of the reference evapotranspiration. Using a set of data sampled on an intensive basis (i.e one measurement each minute) during a period of 6 months, we first analyse the effect of the temporal sampling frequency on the estimation of the daily means of the shortwave solar radiation, the wind speed, the dry and wet temperatures, and on the estimation of the daily maximum and minimum dry temperature. Subsequently, a sensitivity analysis of a reference evapotranspiration model is carried out to determine the most sensible meteorological variables. The sensitivity coefficients were then combined with the errors due to the temporal sampling to quantify for each variable the impact of the sampling frequency on the estimation of daily ETo. The results showed that the solar radiation and the wind speed are the most sensitive to bias induced by inadequate temporal sampling frequency. Daily errors of 5.1 MJ m^{-2} d^{-1} or 41.05% for the solar radiation, and 0.45 m s^{-1} or 18% for the wind speed

*adapted from Hupet, F. and M. Vanclooster, *Journal of Hydrology*, 243, 192-204, 2001.

may be obtained if these variables are inappropriately sampled. Moreover, the impact of inappropriate temporal sampling on the estimation of ETo can be significant with respectively maximum bias of 0.62 mm d^{-1} due to inappropriate solar radiation sampling and 0.36 mm d^{-1} due to inappropriate maximum temperature sampling. A non-intensive hourly temporal sampling schedule of all meteorological variables may induce errors on the daily ETo so high as -0.76 mm d^{-1} or -27%. Fortunately, the errors generated on the estimation of the long term integrated evapotranspiration are clearly lower (3.8%). Our study clearly demonstrates the importance of scheduling appropriately the sampling frequency of climatic variables to correctly estimate land surfaces fluxes as well in fundamental as in more practically oriented research studies.

3.1 Introduction

The transfer of water vapour through the process of evapotranspiration (ET) is a key process within the Earth's surface water and energy balance. An appropriate quantitative estimation of the evapotranspiration flux across the soil-crop continuum is further a prerequisite for irrigation scheduling, crop yield forecasting, hydrological and global circulation modelling. Considerable progress has recently been made in our understanding of the physical and the biological processes that determine evaporation rate. However, the quantitative estimation of evapotranspiration, especially at the larger regional scale remains a difficult task [*Itier and Brunet*, 1996]. Empirical [e.g., *Doorenbos and Pruitt*, 1977] as well as more physically-based approaches [e.g., *Shuttleworth and Wallace*, 1985] are currently adopted for the estimation of evapotranspiration.

The two-step or the so-called "Kc.ETo" approach [*Doorenbos and Pruitt*, 1977] was presented by the FAO as a reference methodology for calculating crop water requirements and is now largely used, mainly for practical applications in irrigation scheduling. This approach is also used within different agro-hydrological models, e.g., WAVE [*Vanclooster et al.*, 1996] and SWAP [*van Dam et al.*, 1997] for the estimation of potential crop evapotranspiration. The two-step approach calculates a reference ET for a standard surface, referred to as ETo, using reference parameters and agro-meteorological data. Then it applies appropriate empirical crop coefficients such as presented by *Doorenbos and Pruitt* [1977] and *Wright* [1981, 1982] for obtaining real crop ET. This versatile approach is widely adopted because it exploits the data available in agro-meteorological databases. However, given the recent advances in assessing crop water use, many shortcomings have been identified with the use of the original Doorenbos and Pruitt approach [*Batchelor*, 1984; *Allen et al.*, 1989; *Jensen et al.*, 1990]. To mitigate to this problem, *Allen et al.* [1994a, b] presented an update to the original, which is now adopted by FAO as the new reference methodology [*Allen et al.*, 1998]. The updated reference methodology is still based on the "Kc.ETo" principle but uses an equation based on the Penman-Monteith model with adopted parameterisation for the surface and aerodynamic resistances for obtaining reference ET from agro-meteorological data. Mainly used on a 24-hour time scale, this methodology needs the estimation of maximum and minimum daily values for dry temperature, and the mean daily values for the other climatic variables.

Daily climatic variables available in agro-meteorological data bases are subject to different sources of error. A first source of error is the error due to the properties of the sensor, to the instrument settings or to the instrument drift [*Beven*, 1979; *Meyer et al.*, 1989; *Ritchie et al.*, 1996]. A second source of error is the one due to the estimation of climatic variables from other, less accurate, available meteorological data. This was illustrated for instance by *Thompson* [1976] and *Lindsey and Farnsworth* [1997] for the estimation of solar radiation from percent sunshine hours or percent sky cover. A third source of error which influences the estimation of daily mean, and which is surprisingly rarely cited in the literature, is related to the temporal sampling frequency of the climatic data. In fact, the temporal sampling frequency which is adopted depends very much on the aim of the study. Within the framework of fundamental research studies, the adopted temporal sampling frequency is often very high with, for instance, samples collected on a time step basis of one or a few seconds, and aggregated as a mean recorded of, for example, every ten minutes or every hour [e.g., *Lascano and Van Bavel*, 1986]. Within the framework of agronomical experiments for instance, the temporal sampling frequency is often less intensive, sometimes reduced to 30 minutes, hourly or even daily time steps [e.g., *Al-Ghobari*, 2000] based on the available data logging equipment. However, climatic variables are often prone to large fluctuations at the smaller time scale. If small scale temporal variability of climatic variables is likely to be high, then the adopted temporal sampling frequency can be suspected to play an important role in the estimation error of the daily mean of the different climatic data. In addition, the dependency of temporal sampling frequency on the estimation error will be different for each different climatic variable. In order to determine this impact for each climatic variables, two different approaches can be used. The first approach compares the ETo calculated with the climatic variables intensively sampled, except the variable of interest, with the "true" ETo determined with all the climatic variables intensively sampled. The second approach, that is used in our study, combines a sensitivity analysis of the evapotranspiration model with the error of the studied variable due to the temporal sampling frequency. Various sensitivity analyses on evapotranspiration models were previously carried out [*McCuen*, 1974; *Saxton*, 1975; *Coleman and Decoursey*, 1976; *Beven*, 1979; *Rana and Katerji*, 1998; *Qui et al.*, 1998]. Nevertheless, these sensitivity analyses are generally restricted to the study of rarely measured climatic variables, such as the net radiation, and most of them are carried on a hourly step time basis. Further, in order to quantify the impact of the error on the climatic variable on the estimation of the evapotranspiration, the sensitivity analysis combines the relative sensitivity coefficients with an identical error for all of the climatic variables [*Qui et al.*, 1998]. Finally, none of the previous sensitivity analyses were carried out for the new reference methodology proposed by the FAO [*Allen et al.*, 1998].

For mitigating some of the above-mentioned problems we present, in this Chapter, a propagation analysis of the temporal sampling error on the estimate of the reference evapotranspiration. The main objectives of the study can be summarised as follows:

(1) to determine the effect of the temporal sampling on the estimation of the daily mean of the respective climatic variable. The investigated climatic variables are those available in reference agro-meteorological databases and those used in the FAO reference method;

(2) to analyse the sensitivity of the Penman-Monteith evapotranspiration model to climatic factors and to calculate daily sensitivity coefficients for the climatic data of interest;

(3) to quantify, combining (1) and (2), the ETo error due to each climatic variable; and

(4) to determine with the daily mean values calculated in (1) the effect of the temporal sampling frequency on the estimation of daily and cumulative reference evapotranspiration.

3.2 Material and methods

This chapter is based on meteorological data collected from 6^{th} of May through the 30^{th} of October 1999. The climatic variables, i.e. wet and dry temperatures, shortwave radiation and wind speed, were measured and recorded at 1 minute interval in a data logger. All climatic variables are instantaneous values except for the wind speed where the recorded values are the means for the previous minute. Further details about the

Table 3.1. Measured and estimated climatic variables.

Measured variables	Estimated variables
Shortwave radiation (R_s)	R_n
Maximum temperature (T_{max})	Δ, R_n, e_a
Minimum temperature (T_{min})	Δ, R_n, e_a
Dry temperature (T_d)	Δ, G, γ, e_d
Wet temperature (T_w)	e_d
Wind speed (U_2)	U_2

meteorological station, the sensors and the area can be found in Chapter 2 (see Section 2.3).

3.2.1 Data analysis

According to the methodology recommended by FAO [*Allen et al.*, 1994a, b], the estimation of reference evapotranspiration, defined as "ETo FAO-Penman-Monteith", can be written for 24-hour calculations as:

$$ETo = \frac{0.408\Delta(R_n - G) + \gamma_{psy}\frac{900}{T_d+273}U_2(e_a - e_d)}{\Delta + \gamma_{psy}(1 + 0.34U_2)} \tag{3.1}$$

with ETo the reference evapotranspiration (mm d^{-1}), Δ the slope of the vapour pressure curve (kPa °C^{-1}), R_n the net radiation (MJ m^{-2} d^{-1}), G the soil heat flux (MJ m^{-2} d^{-1}), γ_{psy} the psychrometric constant (kPa °C^{-1}), T_d the dry temperature (°C), U_2 the wind speed measured at 2 m height (m s^{-1}), e_a and e_d respectively the saturated and the actual vapour pressure (kPa). All these variables were calculated with the recommended procedures given by *Allen et al.* [1994b]. In particular, for R_n and G, equations (1.53) and (1.56) in *Allen et al.* [1994b] were used. The estimation of the reference ETo is driven by the measured climatic variables. The selection of the different climatic variables used in our study (see Table 3.1) was mainly dictated by the kind of measurements usually made in "non-research" meteorological stations. Indeed, net solar radiation and soil heat flux are not frequently measured in usual meteorological networks [*Lindsey and Farnsworth*, 1997]. The first step of our study focuses on the estimation of daily mean values for the different climatic variables, calculated for the different sampling intervals. As the minimum step time is one minute, a daily data set of 1440 values is available for each climatic variable. Twelve different temporal sampling intervals were then selected: 1, 2, 3, 4, 5, 6, 10, 12, 15, 20, 30 and 60 minutes. Thus, for each day twelve different daily means are calculated, with a minimum of 24 values and with a maximum of 1440 values. The maximum step time (60 min.) corresponds to the intervals usually adopted in autonomous meteorological stations. The minimum step time (1 min.) is conditioned by the minimum time resolution of the data logger. The daily means, or the minimum and maximum values for dry temperature, calculated using the minimal step time are considered as reference values and are written $< var >_{true}$ or $< var >_{1min}$. The others daily means are noted $< var >_i$ with i referring to the different sampling intervals. The error due to the temporal sampling can now be characterised by its relative error, calculated as :

$$\epsilon_{rel} = \frac{< var >_i - < var >_{true}}{< var >_{true}} 100 \tag{3.2}$$

and its absolute error, formulated as :

$$\epsilon_{abs} = < var >_i - < var >_{true} \tag{3.3}$$

The second step of the study consists of a sensitivity analysis of the FAO Penman-Monteith model as described by Eq. (3.1), using a methodology presented by *McCuen* [1974], *Beven* [1979], *Rana and Katerji* [1998], and *Qui et al.* [1998] and summarised below. The reference evapotranspiration determined by Eq. (3.1) needs different climatic variables as input, any of which is subject to error. In a more general form, we can express Eq. (3.1) as :

$$ETo = f(v_1, v_2, ..., v_n) \tag{3.4}$$

with v_1, v_2,... v_n, the n considered climatic variables. If Δ_{vi} is a perturbation of the climatic variable i, then the perturbation of ETo as a result of the perturbation on the climatic variables can be quantified by:

$$\Delta ETo = f(v_1 + \Delta v_1, v_2 + \Delta v_2, ..., v_n + \Delta v_n) \tag{3.5}$$

Expanding Eq. (3.5) in a Taylor series and ignoring second order terms, we can write:

$$\Delta ETo = \frac{\delta ETo}{\delta v_1} \Delta v_1 + \frac{\delta ETo}{\delta v_2} \Delta v_2 + ... + \frac{\delta ETo}{\delta v_n} \Delta v_n \tag{3.6}$$

This equation has an assumption built into it that the perturbations on the climatic variables are independent of each others. Although there is some correlation of the climatic variable, no correlation was found between the perturbations of the climatic variables. This can be explained by the fact that the perturbations in Eq. (3.6) have no physical meaning but are only determined by the temporal sampling frequency of the data logger. In Eq. (3.6), the derivatives $\frac{\delta ETo}{\delta v_i}$ define the sensitivity of the estimate to each climatic variables v_i. However, these sensitivity coefficients are themselves sensitive to the relative magnitudes of ETo and of v_i. Following *McCuen* [1974], a non-dimensional relative sensitivity coefficient may be defined as :

$$S_i = \frac{\delta ETo}{\delta v_i} \frac{v_i}{ETo} \tag{3.7}$$

The sensitivity coefficient described by Eq. (3.7) represents the fraction of change in v_i transmitted to the change of ETo, i.e. an S_i value of 0.1 would suggest that a 10% increase in v_i may be expected to increase ETo by 1%. On the other hand, Eq. (3.7) remains sensitive to the absolute values of ETo and v_i. In some cases, when either ETo or v_i tend to zero independently, the relative sensitivity coefficients described by Eq. (3.7) may not be a good indication of the significance of v_i [*Beven*, 1979]. In the present study, sensitivity coefficients were determined on a daily basis for the measured climatic variables summarised in Table 3.1. The partial derivatives, needed for the determination of the sensitivity coefficients, were calculated analytically by means of MATHCAD^{TM} and programmed in a MATLAB^{TM} procedure. Given the size of the analytical expressions, these are not described in this Chapter but can be obtained from the authors upon request. The third step of the study combines the two previously described steps. The error caused by each variable on the estimation of ETo can be quantified by approximating the derivatives by finite differences and rewritting Eq. (3.7) as following:

$$\Delta ETo = S_i \frac{\Delta v_i}{v_i} ETo \tag{3.8}$$

Sensitivity analyses of the evapotranspiration equation carried out in others studies were generally limited to the determination of the sensitivity coefficients. However, some of them, for instance *Qui et al.* [1998], estimated ΔETo using Eq. (3.8) and adopted an identical Δv_i for each of the climatic variables. In our study, we also use Eq. (3.8) considering, for each climatic variable and for each day of the study period, the sensitivity coefficient determined by Eq. (3.7) the daily mean error due to the temporal sampling (Δv_i) and the true value of ETo ($< ETo >_{1min}$) calculated using all the weather data. In a final step we quantify the effect of the temporal sampling on the ETo estimation. For this purpose, we simply use the different daily means determined with different temporal sampling. The calculated value $< ETo >_i$ is compared with the true value $< ETo >_{1min}$. The comparisons are made for daily and for cumulated values.

3.3 Results and discussions

3.3.1 Weather data

The time course of the observed climatic data and calculated reference evapotranspiration is given in Fig. 3.1. During the experimental study (DOY 126 to DOY 303), the daily mean shortwave solar radiation was 13.2 MJ m^{-2} d^{-1}. This value is in agreement with the commonly observed values for this period [*Malcorps*, 1999]. The maximum observed value was 27.83 MJ m^{-2} d^{-1} (DOY 170) and the minimum was 0.383 MJ m^{-2} d^{-1} (DOY 281). The daily variability is very pronounced during the summer period (June-August). The daily mean minimum temperature was 11.46 °C and the daily mean maximum temperature was 20.09 °C. The average wind speed value was moderate with a daily mean of 2.45 m s^{-1}. The daily mean vapour pressure deficit (0.55 kPa) was characteristic of the climate. The daily mean reference evapotranspiration, calculated from Eq. (3.1) was 2.75 mm d^{-1} with a maximum of 5.33 mm d^{-1} (DOY 149) and a minimum of 0.41 mm d^{-1} (DOY 282).

3.3.2 Effect of temporal sampling

The effect of temporal sampling was quantified for each climatic variable by comparing the daily mean based on a given time step with the true mean calculated with all 1440 measured values. Table 3.2 gives for five different time step (2, 5, 10, 30 and 60 min.) the mean and standard deviation of the observed relative error and the absolute value of the maximum relative error. For all the climatic variables, a consistent increased degradation of precision is observed with a decreasing temporal sampling intensity. Nevertheless, the observed errors are very different according to the different climatic variables. As an example, the absolute errors of the solar radiation and of the maximum temperature are illustrated in Figure 3.2. The error on the estimated daily shortwave solar radiation is the most sensitive to temporal sampling frequency. For a 60 minutes sampling interval, the daily relative error may reach a value as high as 41.05%, while the absolute error is 5.1 MJ m^{-2} d^{-1}. The mean daily relative error is, for each time interval, always negative, corresponding to a underestimation of the solar radiation. This has probably different interdependent causes for which different explanations could be put forward. One of them is described below. Under temperate climatic conditions where cloudless sky days are very rare, the cloud cover is intermittent, but most of part dominant with regard to the shining period, which creates very large instantaneous fluctuations of solar radiation. In some cases, the observed solar radiation can fluctuate between 850 W

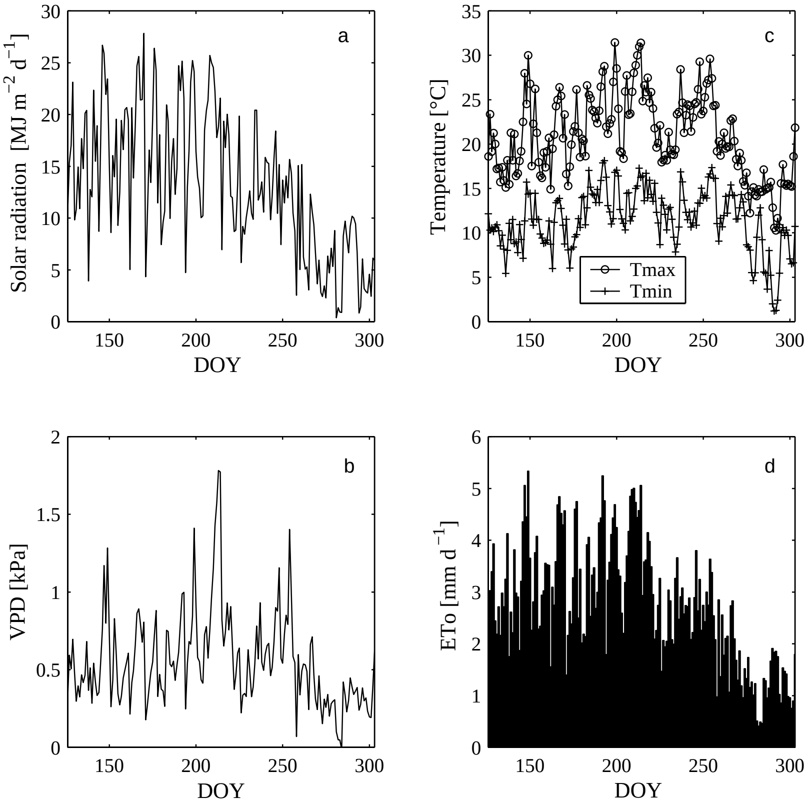

Figure 3.1. Seasonal evolution of the daily climatic variables, i.e. solar radiation (a), vapour pressure deficit (b), minimum and maximum temperatures (c), and the ETo (d) as calculated with the most intensive temporal sampling frequency.

m^{-2} to 300 W m^{-2} in only a few minutes. Nevertheless, when the cloud cover is incomplete, the sampling seems generally to occur disproportionately at times when the sky is cloudy, leading to an underestimation of the daily solar radiation. Thus for this climatic variable, the temporal sampling frequency may have a significant impact on the estimated daily mean value. Furthermore, in order to estimate the net radiation with e.g. the empirical formulae proposed by *Allen et al.* [1994], different empirical coefficients such as those given by *Brunt* [1952] and *Doorenbos and Pruitt* [1977] are generally adopted. However, these coefficients can be considered as dependent on the temporal sampling frequency of the underlying experimental database. This clearly demonstrates that the interest related to the temporal sampling intensity is not only of concern for the estimation of daily mean values but is also of interest for develop-

Table 3.2. The absolute value of the maximum daily relative error, the mean and the standard deviation of the relative daily error, for the investigated climatic variables and for 5 different sampling resolutions. The values presented in this table are expressed in %.

	Climatic variables	2	5	10	30	60
R_s	$\lvert\epsilon_{rel.max.}\rvert$	2.83	6.15	13.21	24.84	41.05
	mean	0.03	-0.06	-0.11	-0.50	-2.2
	σ	0.72	1.66	3.36	7.8	12.15
U_2	$\lvert\epsilon_{rel.max.}\rvert$	1.33	3.72	6.86	12.12	18.01
	mean	0.0072	-0.096	-0.10	0.19	0.103
	σ	0.51	1.09	1.82	3.43	5.36
T_{max}	$\lvert\epsilon_{rel.max.}\rvert$	2.67	4.08	5.91	10.79	12.71
	mean	-0.34	-0.82	-1.36	-2.29	-3.19
	σ	0.522	0.79	1.13	1.71	2.33
T_{min}	$\lvert\epsilon_{rel.max.}\rvert$	1.24	3.84	4.25	6.64	11.47
	mean	0.11	0.318	0.55	1.15	1.67
	σ	0.21	0.51	0.78	1.28	1.81
T_{dry}	$\lvert\epsilon_{rel.max.}\rvert$	0.043	0.13	0.24	0.91	1.6
	mean	-0.0016	$-4.2.10^{-4}$	$-2.6.10^{-4}$	-0.005	-0.0052
	σ	0.012	0.04	0.081	0.23	0.46
T_{wet}	$\lvert\epsilon_{rel.max.}\rvert$	0.048	0.13	0.258	1.01	1.77
	mean	-0.0015	$8.3.10^{-5}$	0.0017	-0.01	-0.019
	σ	0.014	0.043	0.094	0.257	0.51

ing more efficient parameterisation schemes in evaporation models. The wind speed, is the second most important variable in terms of the error due to the temporal sampling frequency. For a time step of 60 minutes, the maximum value of the relative error is 18%, while the maximum absolute error is 0.45 m s^{-1}. These errors are clearly smaller than those for the solar radiation errors, but are nevertheless still high especially as the wind speed measurements are not instantaneous but averaged on a per-minute basis. For the maximum and minimum temperature, the absolute value of the relative errors are, for a time step of 60 minutes, respectively 12.71% (absolute error of -2.16 °C) and 11.47% (absolute error of 0.76 °C). The differences between the maximum absolute errors of those two variables can be explained as follows. Given the fact that the daily maximum temperature varies more rapidly than the minimum temperature, a less intensive temporal sampling generates a higher error for the maximum temperature than for the minimum. For these two

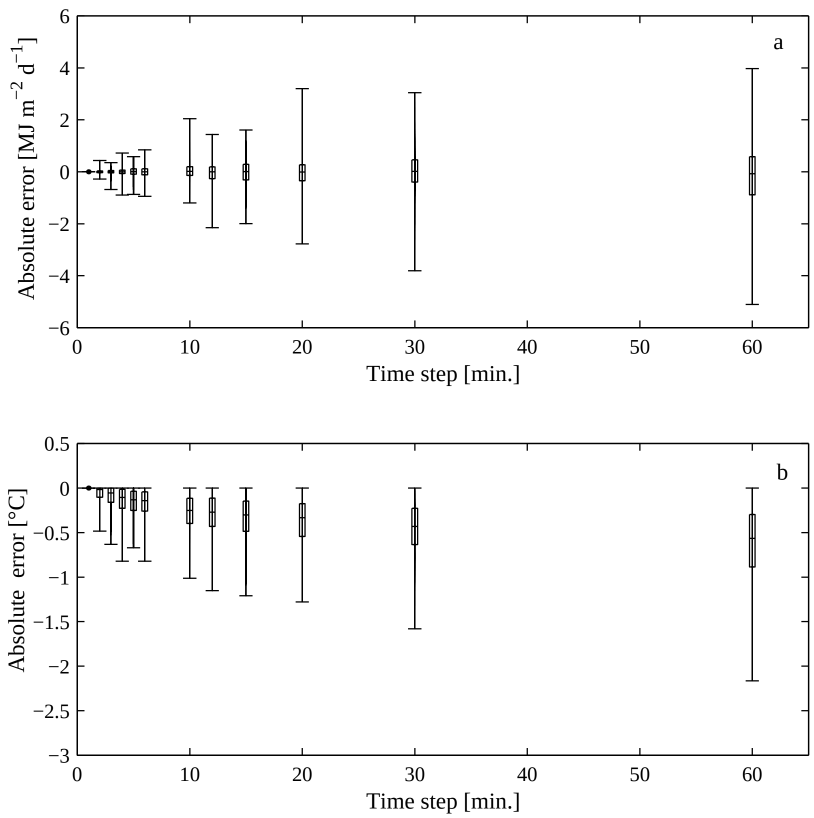

Figure 3.2. Boxplot for the distribution of the absolute errors illustrated for: (a) the shortwave radiation; and (b) the maximum temperature. Each box lies between the 0.25 and the 0.75 quartile, and the central line is the median. The whiskers indicate the range of the data within the maximum and the minimum values.

variables, the mean error is therefore different. In fact, decreasing the sampling intensity (fewer samples per day) will increase the underestimation for the maximum temperature. Similarly for minimum temperature, the decreasing sampling rate increases the overestimate of the minimum temperature. The observed errors are the lowest for the dry and the wet temperature. For a time interval of 60 minutes, the absolute value of the relative error is 1.6% for the dry temperature and 1.8% for the wet temperature. The maximum absolute errors are respectively 0.20 °C and -0.17 °C. For these two variables, increasing the temporal sampling frequency is clearly of little interest.

3.3.3 Sensitivity analysis

The sensitivity analysis was carried out on a daily basis using climatic daily means calculated from the most intensive temporal sampling frequency (1440 measurements per day). The investigated meteorological variables are those needed for the estimation of ETo calculated by Eq. (3.1). The sensitivity coefficients relative to each climatic variable are illustrated in Fig. 3.3. The daily sensitivity coefficients all exhibit large fluctuations during the study period. The mean sensitivity coefficient for the wind speed is 0.177, with a maximum value of 0.657. Nearly all the calculated values are positive. The sensitivity coefficient for the solar radiation shows a pronounced seasonal trend, similar to the trend within the measured solar radiation. The decrease of the sensitivity coefficients for the solar radiation corresponding to an increase in the sensitivity for the wind speed at the end of the season is due to a decrease of the energetic term in favour of the increase of significance of the aerodynamic term. Similar findings were reported when analysing the sensitivity of the evapotranspiration models at the temporal scale of the day and the season [*Saxton*, 1975; *Beven*, 1979; *Rana and Katerji*, 1998]. The mean sensitivity coefficient for the solar radiation is 0.404 and the maximum value is 0.734. These sensitivity coefficients are positive except during the last decade where some very small negative values were found (min. -0.07 for DOY 302). These negative coefficients, can probably be explained by the formulation of the net longwave radiation based on the use of the shortwave solar radiation. Thus, with the use of this formulation and in some rare situations, an increase of the shortwave solar radiation induces a short decrease of the net radiation. The sensitivity coefficients for the maximum and the minimum temperature show a similar trend. Nonetheless, the sensitivity coefficients for the minimum temperature are systematically below those of the maximum temperature. The mean sensitivity coefficients are 1.52 for the maximum temperature and 0.55 for the minimum temperature. These high sensitivity coefficients can be explained by the fact that they are used to estimate several relatively sensible terms within the ETo model such as the net radiation, the saturated vapour pressure and the slope of the vapour pressure curve. Furthermore, during the DOY 282-284, abnormally high sensitivity coefficients are observed with a maximum value of 5.52 for the maximum temperature and 3.65 for the minimum temperature. In this short period, high sensitivities were also observed for the other climatic variables except for the solar radiation. These high values are due to the formulation of the relative sensitivity coefficients, that may not be a good indication of the significance of the parameter sensi-

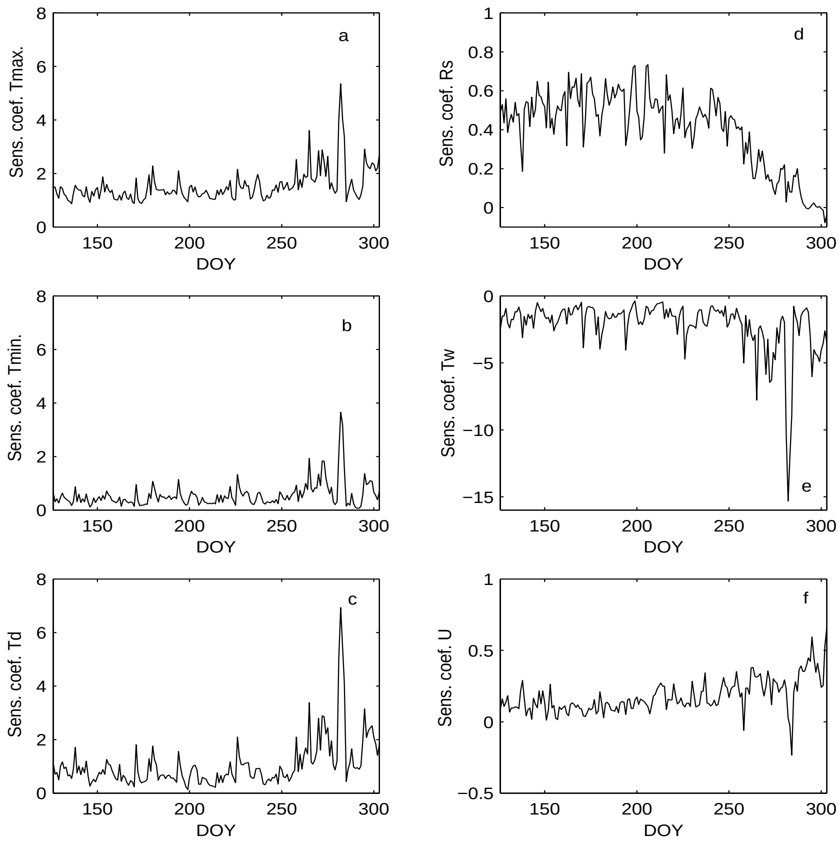

Figure 3.3. Seasonal evolution of the different relative sensitivity coefficients presented for: (a) the maximum temperature; (b) the minimum temperature; (c) the dry temperature; (d) the shortwave radiation; (e) the wet temperature; and (f) the windpseed.

tivity if ETo or v_i tend to zero independently [*Beven*, 1979]. As shown by Figure 3.1, this was typically the case for the DOY 282-284 with very small values of daily ETo ($<$ 0.5 mm). The sensitivity coefficients for the dry temperature show a similar trend to those for the maximum temperature but with a larger amplitude and with a more pronounced variation. The mean value is 1.04 and the maximum value is 6.93. The sensitivity coefficient for the wet temperature is consistently always negative. The mean coefficient is -2.15, the maximum value -0.36 and the minimum value -15.32. It is difficult to compare our results with those presented in the literature [e.g., *McCuen*, 1974; *Saxton*, 1975; *Coleman and Decoursey*, 1976; *Beven*, 1979; *Rana and Katerji* 1998; *Qui et al.*,

Table 3.3. Impact of the temporal sampling intensity of the different climatic variables on the estimation of ETo. The values presented in this table are expressed in mm d^{-1} and determined by combining the sensitiviy coefficient and the error due to inapproriate temporal sampling of the respective variable.

	Climatic variables	2	10	30	60
R_s	$\lvert\epsilon_{max.}\rvert$	0.052	0.24	0.46	0.62
	mean	$2.29.10^{-4}$	$4.9.10^{-3}$	-5.10^{-3}	-0.021
	σ	0.009	0.045	0.1	0.147
U_2	$\lvert\epsilon_{max.}\rvert$	0.018	0.054	0.135	0.162
	mean	$7.3.10^{-5}$	$-8.8.10^{-4}$	$6.3.10^{-4}$	$5.9.10^{-4}$
	σ	0.51	1.82	3.43	5.36
T_{max}	$\lvert\epsilon_{max.}\rvert$	0.095	0.18	0.255	0.36
	mean	-0.013	-0.048	-0.08	-0.114
	σ	0.0119	0.039	0.055	0.077
T_{min}	$\lvert\epsilon_{max.}\rvert$	0.012	0.038	0.06	0.065
	mean	0.0011	0.005	0.011	0.016
	σ	$2.2.10^{-3}$	$5.8.10^{-3}$	0.011	0.014
T_{dry}	$\lvert\epsilon_{max.}\rvert$	$6.1.10^{-4}$	$6.3.10^{-3}$	0.016	0.027
	mean	$-3.8.10^{-5}$	$-5.5.10^{-5}$	$-3.9.10^{-4}$	$-9.1.10^{-4}$
	σ	$2.6.10^{-4}$	$1.8.10^{-3}$	$4.9.10^{-3}$	$9.7.10^{-3}$
T_{wet}	$\lvert\epsilon_{max.}\rvert$	$2.52.10^{-3}$	0.013	0.04	0.07
	mean	$8.03.10^{-5}$	$3.61.10^{-5}$	$1.12.10^{-3}$	$2.58.10^{-3}$
	σ	$5.91.10^{-4}$	$4.09.10^{-3}$	$1.07.10^{-2}$	$2.18.10^{-2}$

1998], given the different approaches in parameterising the evapotranspiration models, the different definitions of the sensitivity coefficients and the different spatio-temporal scales for which previous studies were carried out.

3.3.4 Error propagation analysis for each climatic variable

For each climatic variables, the effect of the errors due to the temporal sampling frequency on the estimation of ETo can be quantified by means of Eq. (3.8). The absolute value of the maximum error, the mean and the standard deviation of the errors are presented in Table 3.3. The solar radiation causes the most significant error. For a sampling interval of 60 minutes, the absolute value of the absolute error reaches 0.62 mm d^{-1}. For more intensive sampling frequencies, the error remains high and only decreases significantly when the sampling interval is smaller than 10 minutes. The maximum temperature causes a maximum error of 0.36 mm d^{-1} for a time step of 60 min. Nevertheless, as for the solar radiation, the mean error is rather low with a maximum of -0.114 mm d^{-1}. The wind speed involves errors of the same order of magnitude with a maximum of 0.162 mm d^{-1} for the lowest temporal sampling frequency, but with mean errors and standard deviations which are very low. For the dry, wet and minimum temperature, a low temporal sampling frequency causes only small errors as compared to the meteorological variables described previously. For a time step of 60 minutes, the absolute values of the maximum error are respectively 0.065, 0.027 and 0.07 mm d^{-1} for the minimum, dry and wet temperature. These three meteorological variables have mean errors and standard deviations that are very small and very similar. The same results were obtained by calculating the impact of each climatic variable on the ETo calculated with the climatic variables intensively sampled, except the variable of interest, and compared with the "true" ETo determined with the climatic variables intensively sampled. The previous results illustrate clearly the relative weight of the sensitivity coefficients and the error due to the temporal sampling frequency on the calculated ETo error. Indeed, as seen for the dry temperature and for the solar radiation, the sensitivity coefficients have a very limited impact on the error of the ETo estimation. On the other hand, for the maximum temperature, the importance of the sensitivity coefficient and the error due to the temporal sampling frequency seems to be similar. In a more general way, these results emphasize the importance of connecting the sensitivity analysis with different and coherent errors relative to each variable.

3.3.5 Error analysis for daily and cumulative ETo

The error of ETo is determined on a daily basis by comparing the $< ETo >_{imin}$ (calculated with the climatic variables sampled to the time step i) with the $< ETo >_{1min}$. Figure 3.4 illustrates for each different sampling interval the relative and absolute errors of ETo. For a temporal sampling frequency of 60 min., the maximum relative error is -27% and the maximum absolute error is -0.76 mm d^{-1}. For more intensive temporal samplings (every 30 or 20 minutes), the maximum value of the absolute error is still high, respectively -0.52 mm d^{-1} and -0.4 mm d^{-1}. A relatively clear decrease of the error is observed for a time step of 6 min. For this time step, the maximum absolute value is -0.15 mm d^{-1} and the relative error is -6.96%. For the cumulative evapotranspiration, the errors are clearly lower (see Table 3.4). Indeed, for

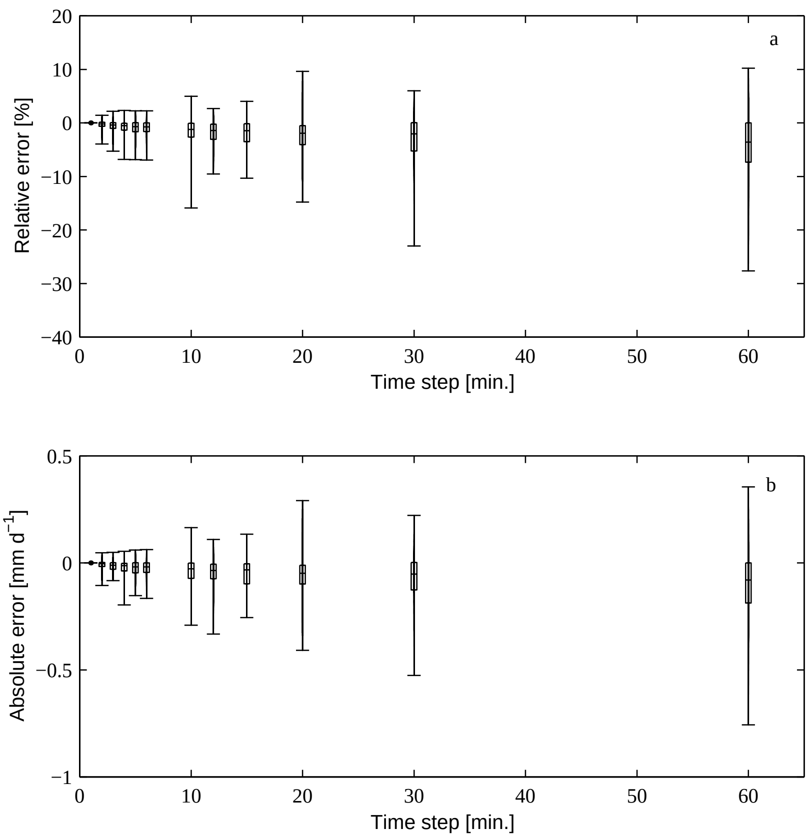

Figure 3.4. Boxplot for the distribution of the relative and absolute errors made on the daily ETo estimation. Each box lies between the 0.25 and the 0.75 quartile, and the central line is the median. The whiskers indicate the range of the data within the maximum and the minimum values.

a less intensive temporal sampling frequency, the relative error is only 3.8%, corresponding to an absolute error of 18.71 mm for a "reference" cumulative value of 491.1 mm. These low errors generated on the estimation of the cumulative evapotranspiration as compared to the large errors on the daily values can be explained by the random character of the error due to the temporal sampling. The values presented in Table 3.4 illustrate a systematic underestimation of ETo, corresponding to a "loss" of information when the sampling frequency decreases.

Table 3.4. Reference evapotranspiration cumulated for the study period and calculated with different temporal sampling frequencies.

Step time (min.)	Nb of measurements/day	Cumulative ETo (mm)	Rel. error (%)
1	1440	491.1	0
2	720	489.3	0.36
3	480	488.38	0.553
4	360	487.24	0.785
5	288	486.92	0.851
6	240	486.71	0.894
10	144	484.95	1.252
12	120	482.79	1.692
15	96	482.48	1.755
20	72	481.19	2.018
30	48	479.94	2.272
60	24	472.39	3.809

3.4 Conclusions

The reference method to estimate the reference ETo, proposed by the FAO and based on the Penman-Monteith evapotranspiration model, uses as input readily available climatic variables such as solar radiation, wind speed, and dry and wet temperature. For daily estimations of ETo, daily mean or extreme values for these climatic variables are required. In addition to the random and systematic errors which are intrinsic to meteorological measurements, the daily means and the extreme values may also be prone to errors due to inappropriate temporal sampling frequency of the measured climatic variables. In this context, one needs to define optimal sampling strategies for reduction of bias in evapotranspiration calculations. Our study showed that the climatic variables which are mostly subjected to bias due to inappropriate temporal sampling of the climatic variables are the solar radiation and the wind speed, with maximum daily relative errors of respectively 41.05% and 18%. The sensitivity analysis illustrated further that the maximum and the dry temperature are sensitive in calculating reference evapotranspiration with sensitivity coefficients of 1.52 and 1.04 respectively. By combining the sensitivity analysis with the errors due to inappropriate temporal sampling, solar radiation and maximum temperature were identified as the two meteorological variables that will have the most pronounced impact on the estimation of the daily ETo. Our study also showed that the ETo estimation error due to inappropriate temporal sampling may be as high as -0.76 mm d^{-1} corresponding to a relative error of -27%. These high values demonstrated that, beside the standard random and systematic errors, inappropriate temporal sampling causes non-negligible errors on daily estimates of ETo which may be easily reduced or even deleted by intensifying the temporal sampling frequency. However, we also showed that the estimation error due to inappropriate sampling for the cumulated ETo is relatively low, reaching 3.8% for the less intensive temporal sampling (one measurement per hour). Nevertheless, this low value would be considered as non-negligible for "reference" methods. The conclusions of this chapter are also valid for more physical ET estimation methods as climatic variables are unavoidable input data. We finally recommend more detailed analysis of the impact of inappropriate sampling on land surface fluxes also in other climatic areas.

Chapter 4

Intraseasonal dynamics of soil moisture variability within a small agricultural maize cropped field

Abstract*

The spatio-temporal dynamics of soil water content was investigated within a small agricultural maize cropped field located in Belgium. Soil moisture measurements were intensively made between 30^{th} May and 13^{th} September 1999, on 28 sampling locations at different depths (from 0 to 125 cm) with both TDR and neutron probe. The adopted sampling scheme resulted in a comprehensive data set of nearly 8 000 soil moisture measurements. Using this data set, we first probe the role of factors controlling the spatio-temporal soil moisture dynamics for the different considered soil depths. Special emphasis is thereby given to the role of the vegetation in the space-time relationships of soil moisture. Secondly, we identify the temporal dynamics of the spatial structure of soil moisture patterns at different soil depths. Thirdly, we investigate the relationship between the mean soil moisture and the spatial variability across time, analysing through the season the optimal sampling strategies to adopt for providing the field areal soil moisture within a given predefined error limit. The results showed that the vegetation, spatially variable within the field, and subsequently through the process of evapotranspiration and the root water uptake, plays a non-negligible role in

*adapted from Hupet, F. and M. Vanclooster, *Journal of Hydrology*, 261, 86-101, 2002.

the temporal dynamics of the observed soil moisture patterns for the superficial layers. The spatial structure of these soil moisture patterns was non-existent or only weakly marked. The study finally indicated that a negative correlation exists between the spatial variability and the mean soil moisture, implicitly suggesting that the sampling has to be more intensive for the drier conditions. Besides these results, this study reemphasises the importance of conducting soil moisture spatial variability studies with measurements performed on the entire hydrological active zone and to adopt temporally unchanged sampling locations in order to progress in the thorough understanding of the physical processes generating the soil moisture spatial variability.

4.1 Introduction

Soil moisture is a key state variable for a wide variety of hydrological processes acting over a range of spatial and temporal scales. For example, soil moisture is one of the factors influencing the partitioning of rainfall into infiltration and runoff and the partitioning of net radiation into sensible and latent heat. In addition, it controls the subsurface drainage of water and thereby the leaching of chemicals to the groundwater. It is therefore evident that a thorough understanding of the soil moisture behaviour is of primary importance for soil hydrological research and engineering applications in areas such as irrigation scheduling, soil based precision farming, hydrological modelling, flood forecasting, and estimating the groundwater recharge. Accurate estimation of soil moisture is also extremely important for the calibration of models simulating the water transport within the soil-plant-atmosphere continuum (e.g. agro-hydrological models). Indeed, soil moisture is one of the few "easily" measurable state variables that can be used in this aim. As the prediction scale of agro-hydrological models is generally the field scale, the calibration must be performed with field areal soil moisture values which are very difficult to obtain.

During the last decade an increasing number of studies have been published focusing on the areal estimation of soil moisture, considering explicitly the spatio-temporal variations of this property [e.g., *Crave and Gascuel-Odoux*, 1997; *Grayson and Western*, 1998; *Famiglietti et al.*, 1999]. These studies, often based on the near-surface soil moisture (0-5 cm), were conducted at different spatial scales (1m^2 to a few km^2), at different temporal scales (few days to few years), with different measurement techniques (e.g., gravimetric sampling, TDR, remote sensing), in a variety of hydrologic and climatic conditions. Within all these studies, the important spatio-temporal dynamics of soil moisture have been put forward. This spatio-temporal variability is influenced by topographic features such as the soil surface slope angle [*Hills and Reynolds*, 1969; *Moore et al.*, 1996; *Nyberg*, 1996] and slope orientation [*Reid*, 1973; *Western et al.*, 1999a], by the soil (hydrodynamics) properties [*Henninger et al.*, 1976; *Crave and Gascuel-Odoux*, 1997], by the vegetation distribution [*Bouten et al.*, 1992; *Mohanty et al.*, 2000a], by land use and in particular the agricultural practices [*Famiglietti et al.*, 1999], by the climatic variability and by the combined effects of some of those factors [e.g., *Hawley et al.*, 1983]. However, until now the environmental controlling factors have been investigated rather unequally. For example, topographical control of soil moisture has been studied far more extensively than that of vegetation. This research bias can mainly be explained by the current availability of detailed digital elevation models, which can be used to derive statistical distributions of terrain indices related to the spatial patterns of soil moisture. The vegetation factor on the other hand is, in numerous studies conducted at the field-scale, explicitly considered as uniform across the studied area [e.g., *Famiglietti et al.*, 1998; *Mohanty et al.*, 2000b]. However, everyone examining carefully an agricultural field or forest stand can easily discern a variable vegetation growth. This variable crop growth is a result of genetics, plant population, management, weather and the temporal integration of stresses that the plant population experiences during the season. Furthermore, it is generally well accepted that the vegetation growth is in one way or another related to the transpired fluxes [e.g., *Doorenbos and Kassam*, 1987]. In this context, we can suspect that during the vegetative period, the vegetation through the process of evapotranspiration plays a non-negligible role in the development of spatial soil moisture patterns within fields. This role of the evapotranspiration process was already implicitly suggested by *Grayson et al.* [1997] within its concepts of preferred states and local control in the development of spatial soil moisture patterns and by *Western et al.* [1999a] with the very small-scale variations contributing significantly to the poor performance of the terrain indices within the Tarrawarra catchment.

The observed soil moisture variability within a field is likely to reflect the combined influences of the above-mentioned factors acting at different spatial scales. In order to quantify and describe spatial variability of soil moisture, the geostatistical correlation structure needs to be identified. Indeed, quantitative estimations of this structure are required for a number of purposes such as, for example at the field-scale, the interpolation of spatial patterns from point measurements and the subsequent estimation of the average field soil moisture, and for example the determination of the optimal spacing between sampling points. Nevertheless, rigorous quantitative estimations of the geostatistical structure of soil moisture are prone to various difficulties as described by *Western et al.* [1998] and by *Western and Blöschl* [1999] as the observed geostatistical structure is directly a function of the soil moisture measurement scale defined by the spacing, extent and support.

Besides the challenge of determining the relative roles of the different factors governing the spatio-temporal dynamics of soil moisture and of deriving the geostatistical structure of the soil moisture patterns, more in depth knowledge on the relationship between the field-scale means and standard deviations of soil moisture across time is needed. Whereas some authors have found a positive correlation between the standard deviation and the mean soil moisture [*Hills and Reynolds*, 1969; *Reynolds*, 1970; *Bell et al.*, 1980; *Robinson and Dean*, 1993; *Famiglietti et al.*, 1998] other investigations found no good predictive relationship [*Hawley et al.*, 1983; *Charpentier and Groffman*, 1992]. Some others studies [e.g., *Famiglietti et al.*, 1999] showed relationships where the variance is negatively correlated to the mean soil moisture. Until now, and in the light of the diversity of previous results, there is no well-established consensus about this relationship whereas a sound knowledge of this is of a primary importance for a number of purposes. For example, such relationship can be interesting to pronounce about the underlying soil moisture spatial variability within remote sensing pixels or to determine strategic sampling periods which minimise the errors for a given sample size. Although there have been a series of studies which have improved our understanding of the dynamics of the soil moisture variability, additional studies for different spatial and temporal scales and for various hydroclimatic and geographic settings are needed [*Georgakakos and Baumer*, 1996]. Keeping in mind that for many hydrologic applications the whole soil moisture profile is of important significance [*Western et al.*, 1998], soil moisture variability should be studied for the whole soil profile (or at least over a depth of several decimeters) rather than just over a thin layer at the soil surface [*Blöschl and Sivapalan*, 1995]. In this framework, we conducted an experiment at the field-scale, initially designed to investigate the in-situ spatial variability of evapotranspiration, providing a comprehensive set of soil moisture data, allowing us to tackle some of the above-discussed issues. The main objectives of this chapter are:

(1) to analyze the temporal dynamics of the soil moisture spatial variability and to probe the role of governing factors for the different

considered soil depths. Special emphasis will be given to the role of the vegetation in the space-time relationships of soil moisture;

(2) to identify the temporal dynamics of the spatial structure of soil moisture patterns at different soil depths; and

(3) to investigate the relationship between the mean soil moisture and the spatial variability across time, analyzing through the season the optimal sampling strategies (in terms of number of samples) to adopt for providing the field areal soil moisture within a given predefined error limit.

4.2 Material and methods

This chapter is based on the 1999 experimental setup. It makes use of the comprehensive data set of nearly 8 000 soil water content measurements coming from the 28 sampling locations. Data relative to the crop growth, i.e. the dry matter yield and the Leaf Area Index are also used.

4.2.1 Data analysis

First of all, we investigated systematically for each depth and each sampling day if the soil moisture data were normally distributed both with the visual inspection of normal probability plots and with the Shapiro-Wilk statistic [*Shapiro and Wilk*, 1965]. The degree of spatial dependence was then investigated by using standard geostatistical techniques [*Isaaks and Srivastava*, 1989] such as the visual examination of sample semivariograms. The sample semivariogram, at a given lag, h, is given by:

$$\gamma_s(h) = \frac{1}{2N(h)} \sum_{i,j} (\theta_i - \theta_j)^2 \tag{4.1}$$

with N the number of pairs of observations for a specified lag, θ_i and θ_j the soil moisture at sampling locations respectively i and j and the summation performed for all the i, j pairs of observations of the selected lag. In order to ensure a minimum number of pairs of observations within each lag, only omni-directional semivariograms were used with a minimum and maximum lag of respectively 15 m and 58 m. This resulted in a minimum of 33 soil moisture data pairs for each selected lag interval, except 20 and 23 pairs for the 42.5 and 45 m lags. The semivariograms were only plotted for the normally or close to normally distributed soil moisture values. Geostatistical analysis was done by means of a geostatistical toolbox programmed in a MATLAB^{TM} environment. For quantifying the number of samples necessary to estimate the mean with a given accuracy for a given probability level, we applied the central limit theorem

$$n = \frac{t_\alpha^2 s^2}{d} \tag{4.2}$$

where n is the number of samples, s^2 is the estimated sample variance, t_α^2 the Student's parameter corresponding to the confidence level $(1-\alpha)$ and d the relative accuracy. For the soil moisture values which were not normally distributed, the results obtained by the central limit theorem were checked by applying the bootstrapping technique as used by *Dane et al.* [1986] with 1000 bootstrap replicates.

4.3 Results and discussion

4.3.1 Spatio-temporal dynamics of the soil moisture

Space-time fields of volumetric soil moisture content for the different depths are given in Fig. 4.1. In this figure, the Y-axis numbering is referring to the sampling locations indicated in Fig. 2.1. Also shown are the daily precipitation depths. A thorough inspection of Fig. 4.1 allows details of the spatio-temporal behavior of soil moisture within the field to be addressed. First of all, the soil moisture temporal dynamics is obviously depth dependent. The temporal dynamics is more pronounced closer to the soil surface, where soil is subjected to the root water uptake and rainfall events. The two long low rainfall periods are relatively well identified for the superficial soil layers, especially for the first drying period (DOY 187-215). Indeed, as a result of the important transpiration from the well developed maize crop combined with a high climatic demand, the water depletion of the superficial layers (0-20, 25 cm) is abundant during the first drying period. For the second period, the climatic demand is quite similar, yet the maize crop much more senescent, resulting in a less depletion. The temporal dynamics in the intermediate layers (50, 75 and 100 cm) is clearly more attenuated. Nevertheless, these layers become progressively drier in response to the root water uptake combined with the upward flux. Fig. 4.1 also shows that, within the deeper layers (75, 100 and 125 cm), the temporal persistence of some dry (sampling locations 4, 5 and 16) and wet zones (location 23) within the field remains high. The persistence of drier zones can be explained by the sandy material underlying the loamy soil. Indeed, it is well known that the thickness of the loamy layer is quite variable within the region but also within fields [*Dudal*, 1953]. It is therefore assumed that the "dry" sampling locations (4, 5 and 16) are situated where the loamy soil is shallow, leading to measuring the soil moisture within the transition

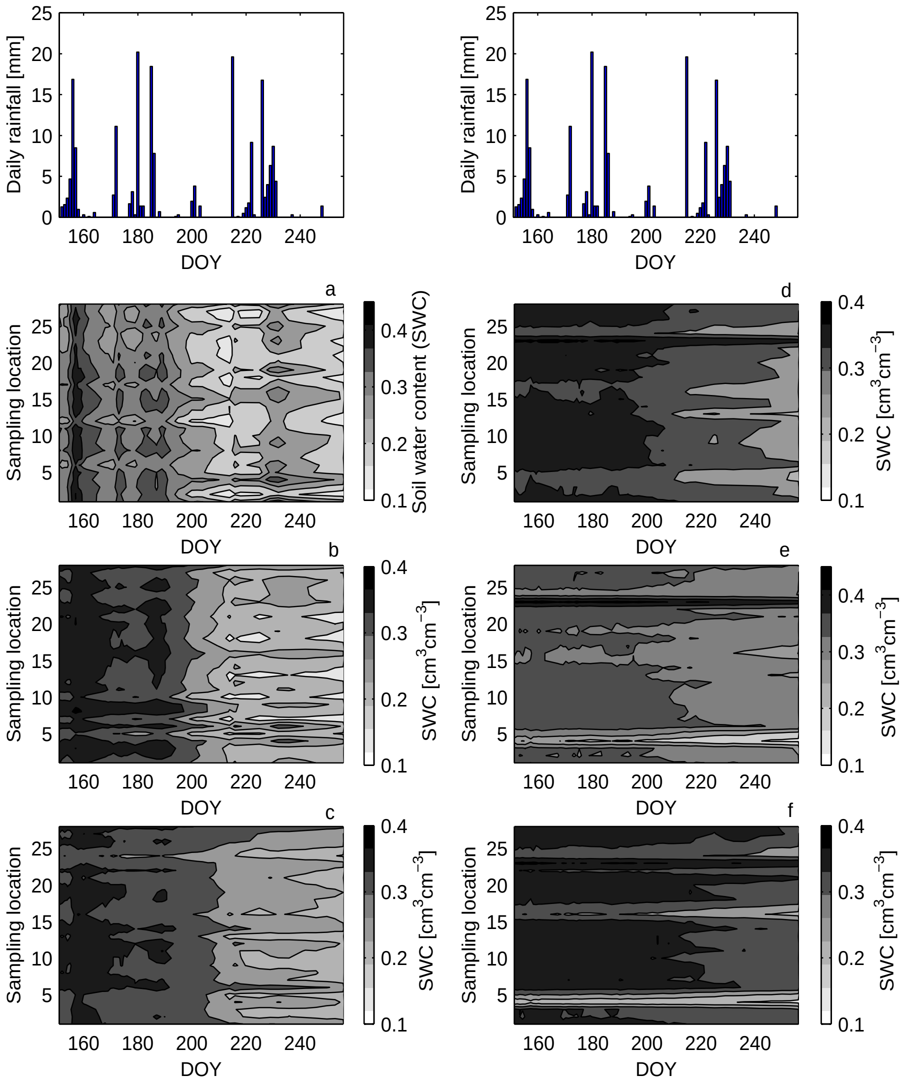

Figure 4.1. Daily precipitation and space-time fields of volumetric soil moisture content for the different depths (a 0-20 cm, b 25 cm, c 50 cm, d 75 cm, e 100 cm, f 125 cm)

zone between the loamy soil and the sandy material. Visual observations of the soil profile on the sampling locations 4 and 5 and some field values for these locations confirm this hypothesis. The sampling location 23 on the other hand is very wet at 75, 100 and 125 cm depth. It is hypothesised that a fine textured layer at this location leads locally to a perched water table. The qualititative information on the spatial variability of soil moisture within the field from Fig. 4.1 is quantitatively summarised in Fig. 4.2. This figure shows the temporal evolution of the observed spatial variances expressed in terms of standard deviation and the mean soil moisture for the different depths. Also shown are the daily precipitation depths for a better insight of the temporal dynamics of the spatial variability. First of all, Fig. 4.2 reveals that the temporal variations of the mean daily soil moisture is depth dependent, and less pronounced deeper in the profile. Indeed, the observed range for the 0-20 cm layer is between 0.4 to 0.21 cm^3 cm^{-3}, for the 25 cm 0.38 to 0.22, for the 50 cm 0.36 to 0.24, for the 75 cm 0.37 to 0.28, for the 100 cm 0.36 to 0.31 and for the 125 cm 0.35 to 0.31 cm^3 cm^{-3}. Similar results, but for longer time periods, were already observed by *Loague* [1992]. The observed spatial variability is also depth dependent. For the 0-75 cm layer which can be considered as the active root-zone, the spatial variability tends to decrease with depth with a maximum standard deviation of 0.038 for the 0-20 cm, 0.035 for the 25 cm depth, 0.031 for the 50 cm depth and 0.03 for the 75 cm depth. In this context, one should remember that two different techniques, TDR and neutron probe, were used to measure soil water content, each with specific sampling volumes estimated respectively at approximately 1000 cm^3 and 15 000 cm^3. Although it is virtually impossible to quantify the direct impact of the two different sampling volumes on the observed variability, this might explain in some extent the larger variability of the first 20 cm (with TDR) compared to that measured at other depths (with neutron probe). Nevertheless, as observed variability increases gradually from 75 cm to 25 cm for neutron probe measurements, there is no reasons to believe that the larger variability observed for the first 20 cm is due to the smaller sampling volume of TDR. For the deeper layers (100 and 125 cm depth), the observed spatial variability increases again with a value for the maximum standard deviation of respectively 0.04 and 0.042. This high variability observed at these depths is almost exclusively explained by some singular wet and dry spots deeper in the profile. As explained above, those spots can probably be related to areas of different texture, i.e. different hydraulic properties, leading to a variable observed soil moisture. Note that those observed values of soil moisture spatial variability are in the range of those found in other fields and small catchment-scale experiments [e.g.,

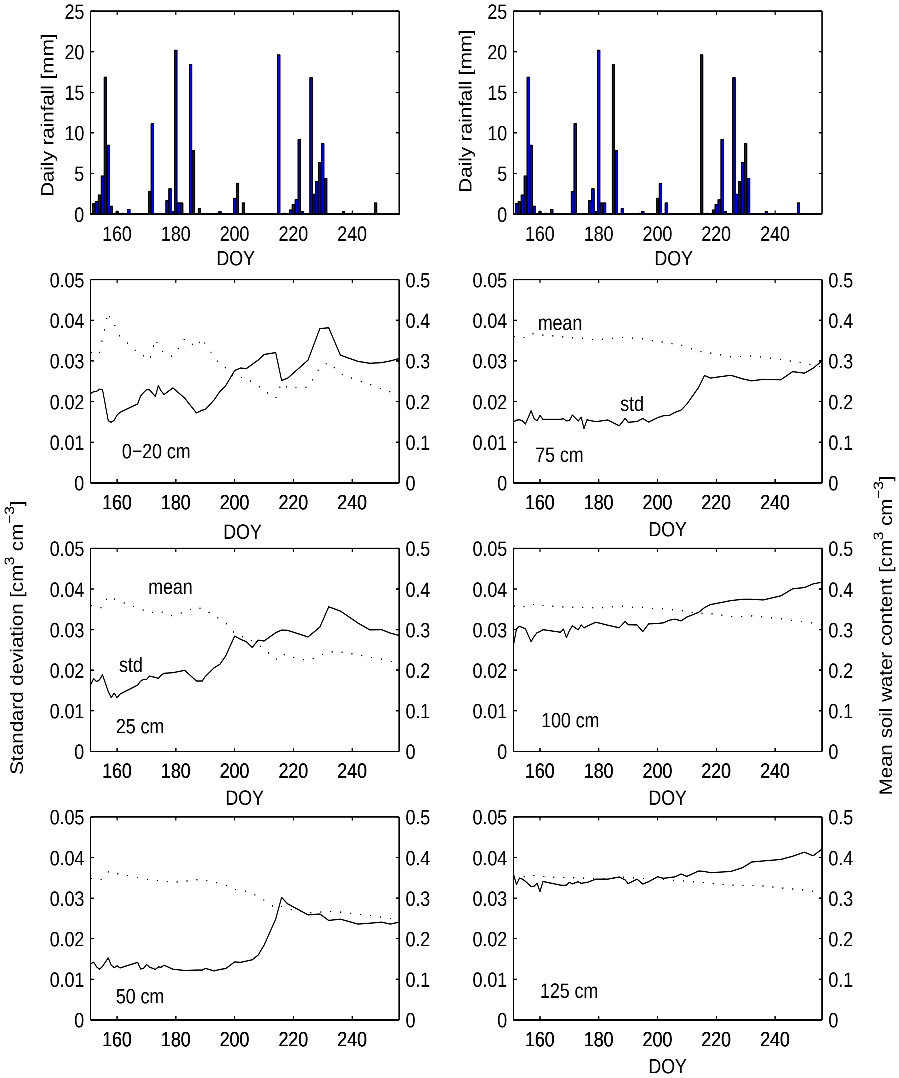

Figure 4.2. Daily precipitation and intraseasonal evolution of the spatial variability and the mean soil moisture content for the differents soil depths.

Charpentier and Groffman, 1992; *Western et al.*, 1999b]. Note also that it was considered in our study that all the observed soil moisture variance is explained by the spatial variability within the field. In the following paragraphs we explain the observed temporal dynamics of the spatial soil moisture patterns. Firstly, it can be easily observed in Fig. 4.2 that the temporal stability of the spatial variability is more pronounced for the deeper soil layers, whereas for the active root-zone (0-75 cm depth) the spatial variability is much more time variant. For example, a sharp increase of the soil moisture spatial variability is observed during the first dry period (DOY 187-215). This increase is well marked for the 0-20 and 25 cm depths and also with a time lag for the 50 and 75 cm depths. As during such a dry period the temporal dynamics of the soil moisture is mainly governed by the root water uptake and as the Leaf Area Index (LAI) measured on DOY 193 on each sampling location is indeed very variable (see Table 4.1) we can suspect that this increase in the spatial variability is mainly driven by a variable root water uptake within the field. To test this hypothesis, the root water uptake, here assimilated to the soil water depletion, between DOY 192 and 215 was determined on each sampling location by means of a simplified water balance (θ_{DOY192}-θ_{DOY215}) for the different depths. As shown in Fig. 4.3, the calculated root water uptake was then correlated with the measured LAI. Although these correlations are not well defined (linear regression with maximum r^2 of 0.31 for 25 and 50 cm depths), there is a trend between the root water uptake and the LAI especially for the 25, 50 and 75 cm depths. That tends to confirm that the root water uptake is spatially variable within the field at a given depth, partially due to the variable areal crop growth, and that it partially controls the temporal dynamics of the spatial soil moisture variability. Furthermore, as shown in Fig. 4.2, the increasing spatial variability is delayed for the deeper layer as the root water uptake firstly affects the surface soil layers. Indeed, the spatial variability increases substantially from DOY 190 onwards for the 25 cm depth, DOY 205 for the 50 cm depth and only from DOY 210 for the 75 cm depth. All these observations confirm the important role of the vegetation in explaining soil moisture variability, as was already suggested by *Grayson et al.* [1997] and *Western et al.* [1999a]. We showed that vegetation is spatially variable within the field, inducing variable evapotranspiration rates (not yet quantified) and consequently variable root water uptake rates. It is often put forward that the variable radiation influx is the main factor controlling the spatial variability of evapotranspiration. Yet, it is not relevant to consider this source of variation as explanatory factor, given the scale of our field study and the nearly flat topography. After the long low rainfall period (DOY 187-215), the rain-

Table 4.1. Mean Leaf Area Index (LAI) of 10 plants measured on each sampling location (Sl.) on DOY 193. Also shown are the yields (dry matter production in kg) measured on DOY 260.

Sl.	LAI	Yield	Sl.	LAI	Yield	Sl.	LAI	Yield	Sl.	LAI	Yield
1	2.81	1.69	8	3.41	1.68	15	3.97	1.92	22	3.58	1.75
2	3.34	2.02	9	4.32	2.42	16	3.82	2.08	23	3.94	2.08
3	3.44	1.77	10	3.85	2.20	17	3.47	1.64	24	3.25	1.75
4	3.26	1.95	11	3.65	2.13	18	3.35	1.88	25	3.67	2.22
5	4.26	2.75	12	4.05	2.45	19	3.99	2.26	26	3.74	2.20
6	3.3	1.54	13	4.12	2.39	20	4.09	2.26	27	3.71	2.26
7	4.21	2.04	14	3.77	2.16	21	3.71	2.04	28	2.55	1.55

fall event of DOY 215 tends to slightly decrease the spatial variability of the 0-20 cm layer. This decrease can probably be explained by the high intensity of this rainfall event (20 mm in less than 20 min.) combined with some variable hydraulic soil properties leading to some differential infiltration in the topsoil. After this rainfall event, the spatial variability increases again for the 0-20 and 25 cm layers until DOY 232 from which it slightly decreases. If we consider that the increasing soil moisture spatial variability during the period DOY 160-230 is mainly explained by the variable root water uptake, vegetation can explain about 6.7 $(\%\text{vol/vol})^2$ of the variance for the 0-20 cm depth and 6.2 $(\%\text{vol/vol})^2$ of the variance for the 25 cm depth. In light of such results, it is not surprising that terrain indices will in some cases perform poorly in explaining soil moisture variability as was already suggested by *Western et al.* [1999a]. It is important to note that, despite the lack of quantitative information about the spatial variability of soil hydraulic properties of the surface layers, these properties must probably also contribute partially to the soil moisture variability. For the two deepest depths (100 and 125 cm), we observe that the high spatial variability is very temporally stable and slightly increasing during the experiment. As a matter of fact, it is not so surprising because the main factors controlling the temporal dynamics of the soil moisture variability at this scale are acting mainly on the superficial layers.

4.3.2 Spatial structure

In a first step, we investigated the normality of the soil moisture data for each day and depth. The Shapiro-Wilk statistic and the visual inspection

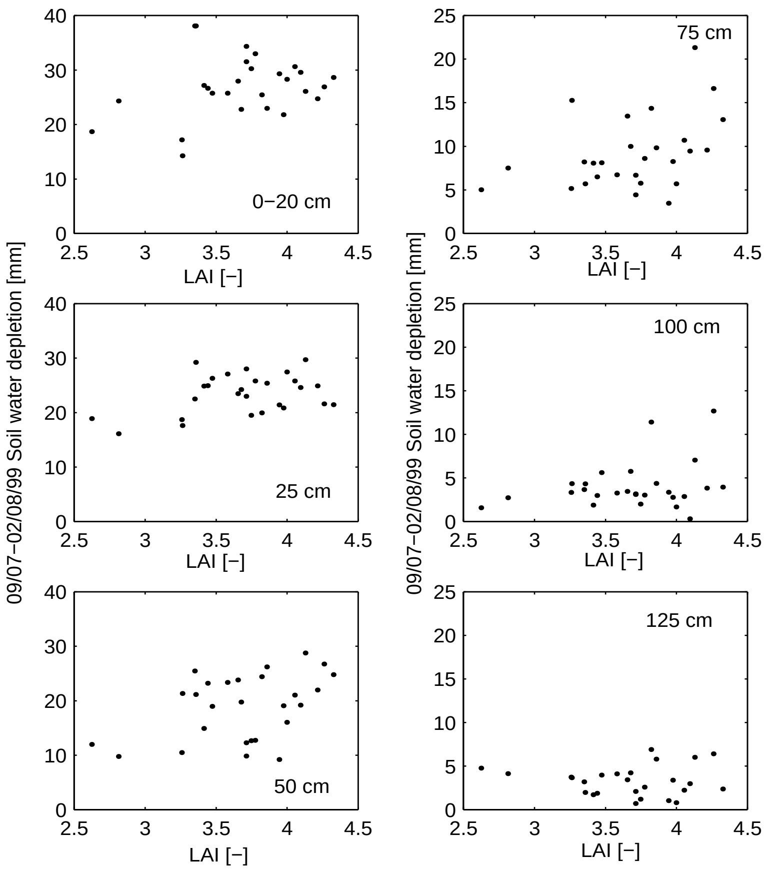

Figure 4.3. Relation between the Leaf area index (LAI) and the soil water depletion (mm) for the different soil depths for the period between 09/07-02/08 (DOY 192-215).

of the probability plots showed that the data are normally or approximately normally distributed for the surface soil layers (0-20, 25, 50 and 75 cm). For the two deepest soil depths (100 and 125 cm), the data are non-normal but tending towards normality. Omnidirectional sample semivariograms were then calculated systematically for each depth but only for the sampling days where the data were normal or close to normality. Fig. 4.4 shows the sample semivariograms calculated for each depth for one representative run (DOY 214). Also shown in Fig. 4.4f is the number of pairs of observations for the different lags. No apparent spatial structure was found for that day (DOY 214) and semivariograms calculated for other days showed similar behaviour. Nevertheless, for the two deeper depths, there is a general increasing trend in semi-variance

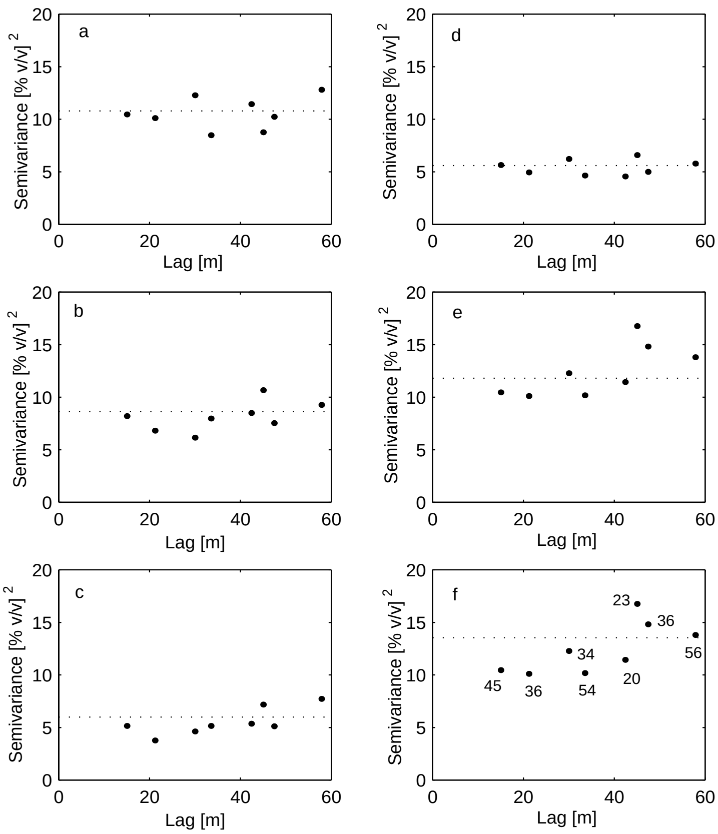

Figure 4.4. Sample omnidirectional semivariograms calculated for DOY 214 for the six different depths (a 0-20 cm, b 25 cm, c 50 cm, d 75 cm, e 100 cm, f 125 cm). Also shown are the observed total variances (dotted line).

with increasing lag, suggesting that the sill is not reached for the maximum lag. In fact, results (not shown here) of a more recent experiment within the same field with 50 sampling locations at 0.9 m intervals (2000 field campaign) suggest that there is a well-defined anisotropic spatial correlation of 40 m for the 100 and 125 cm depths. Unfortunately, the experimental set-up of 1999 did not allow us to investigate this anisotropy. For the surface layers (0-75 cm) no spatial structure can be discerned considering the adopted sampling scheme. These results are in agreement with the findings of *Charpentier and Groffman* [1992] who carried out a similar experiment in terms of measurement extent and spacing. The observed lack of spatial structure for the superficial soil layers is not so surprising if we consider that the vegetation is effectively the main

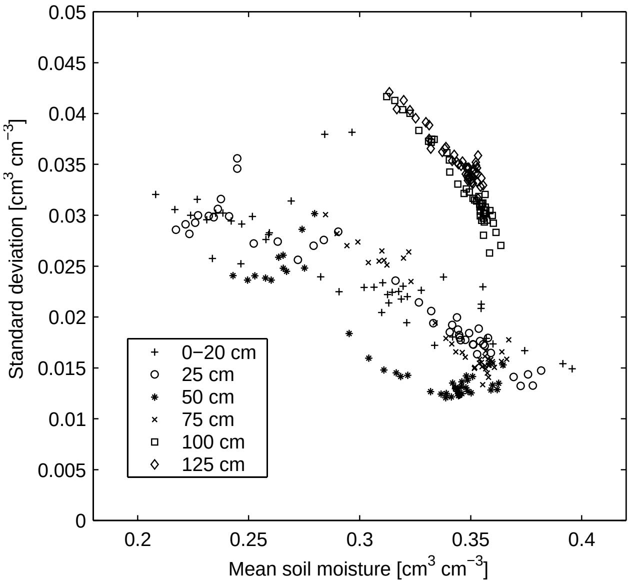

Figure 4.5. Standard deviation of soil moisture content (cm^3 cm^{-3}) versus mean soil moisture content (cm^3 cm^{-3}) for the different soil depths.

factor controlling the development of the soil moisture patterns. Indeed as the vegetation growth is variable at short distance (few meters), we can suspect that spatial correlations are existent but for smaller lags than those investigated. Furthermore, our results are consistent with the findings of *Musters and Bouten* [1999] showing a range of 14 m in a forest stand.

4.3.3 Sampling analysis

The soil moisture data set collected in this study allows investigation of the relationship between the field-scale means and variances of soil moisture content across time. If such relationships exist, they can be of great significance, for example, to optimize the number of samples required to estimate the mean value within a specified limit of error. Figure 4.5 shows the standard deviation of soil moisture within the field versus its mean value for the different depths. We can observe that the absolute variability, i.e. the standard deviation, increases quite linearly with decreasing mean soil moisture. Furthermore, Fig. 4.5 illustrates that this relationship is depth dependent, with important differences between the superficial depths (0-75 cm) and more profound depths (100 and

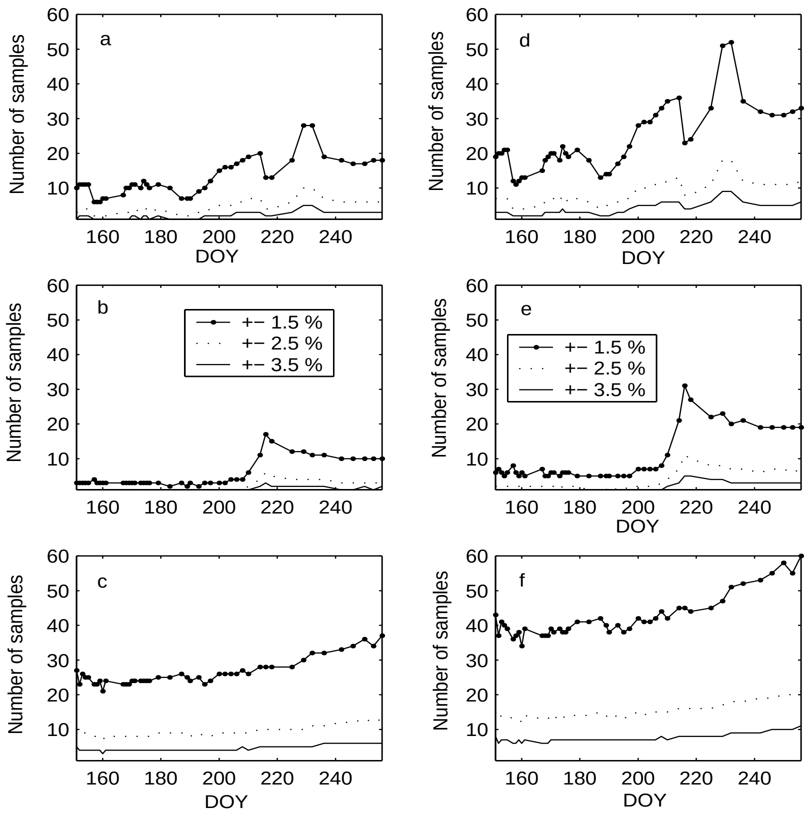

Figure 4.6. Intraseasonal evolution of the number of samples for three selected soil depths (0-20 cm a-d, 50 cm b-e and 125 cm depth c-f) for 95 and 99% probability level for different levels of absolute error (1.5% - 2.5% - 3.5% volumetric soil moisture content).

125 cm). This negative correlation is consistent with the previous findings of *Famiglietti et al.* [1999], who analysed the surface soil moisture within six different cultivated relatively flat remote sensing pixels (0.64 km^2). Nevertheless, they are in contrast with other previous investigations [e.g., *Hills and Reynolds*, 1969; *Henninger et al.*, 1976; *Famiglietti et al.*, 1998]. Note most of these studies, in contrast with our results, were conducted on experimental sites with quite well pronounced topographic features. The observed relationship between the field-scale means and standard deviations of soil moisture directly affects the number of samples required to reach a same level of accuracy on the field-scale mean soil moisture. The time series of the number of required samples was calculated for each depths with the central limit theorem. As the W

Table 4.2. Summary of the number of samples (minimum and maximum) needed to reach a given absolute precision for the different depths for two given probability levels. Results (*) are also presented for 100 cm depth without "outliers" (sampling points 4, 5 and 23) and 125 cm depth (sampling points 4, 5, 16 and 23).

Depth (cm)	95% Probability level			99% Probability level		
	±1,5%	±2,5%	±3,5%	±1,5%	±2,5%	±3,5%
0-20 cm	2-33	1-12	1-6	5-60	1-22	1-113
25 cm	5-23	1-8	1-4	6-43	3-15	1-7
50 cm	2-17	1-6	1-3	5-31	1-11	1-5
75 cm	4-17	1-6	1-3	7-30	2-11	1-5
100 cm	13-32	4-11	2-5	23-59	8-21	5-10
100 cm*	1-7	1-2	1-2	1-14	1-5	1-2
125 cm	20-33	7-11	3-6	34-60	12-21	6-11
125 cm*	1-8	1-2	1-2	3-13	1-4	1-2

statistic [*Shapiro and Wilk*, 1965] showed that the soil moisture content was not systematically normally distributed over the field, especially for the deeper layers (100 and 125 cm), we confirmed the results obtained by means of the central limit theorem with those of the bootstrapping method. Comparisons showed very small differences between the two techniques. Fig. 4.6 shows the intraseasonal evolution of the number of samples for three selected depths (0-20 cm a-b, 50 cm c-d and 125 cm depth e-f) for two probability levels (95 and 99 %) and for three absolute errors (1.5% - 2.5% - 3.5% volumetric soil moisture). Firstly, we can observe in Fig. 4.6 that the number of samples used in our experiment was sufficient to estimate the mean within an absolute error of 1.5% for a probability level of 95%. A striking feature is the temporal variations of the number of samples which is depth dependent. This is a corollary of the temporal behaviour of the soil moisture spatial variability presented in Fig. 4.2. For the 99% probability level, we show that the number of samples drastically increases. This figure also illustrates quite clearly that optimal sampling strategies have to be adjusted across the season. Optimising the sampling design could also be investigated by the use of some techniques such as the one based on the time stability concept [e.g., *Vachaud et al.*, 1985; *Grayson and Western*, 1998]. Although this technique has not yet been investigated in our study, Fig. 4.2 suggests that this kind of technique could be appealing mainly for the deeper layers for which a strong time stability is observed. Table 4.2 summarizes the minimum and maximum number of samples for the

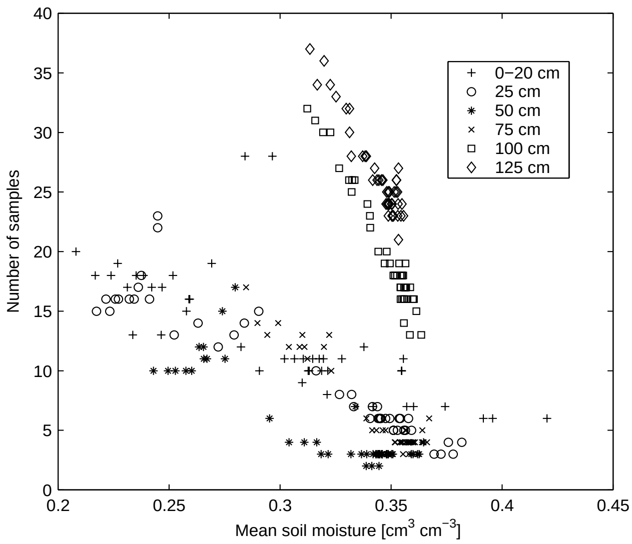

Figure 4.7. Relation between the mean soil moisture content and the number of samples required to reach the mean +-1.5% at the 95% probability level.

course of our experiment. These are relatively low for the estimations of the mean soil moisture within an absolute error of 3.5%, slightly increasing for an absolute error of 2.5% and becoming large, considering the small sampled area, for the 1.5% error. It is also clear in Table 4.2 that the number of required samples decreases from the soil surface to the 75 cm depth to increase again for the deeper layer. Nevertheless, if the same exercice is done for 100 and 125 cm depths without "outliers" (sampling locations 4, 5, 16 and 23), the number of samples is strongly reduced (cfr Table 4.2). The increasing soil moisture spatial variability between 75 cm depth and the soil surface also suggests that the number of samples required for estimating appropriately the mean of the 0-5 cm soil moisture content, which is of interest for remote sensing purposes, could increase even further. Finally, Fig. 4.7 shows the relationship between the mean field soil moisture and the number of samples needed to reach the mean ±1.5% at the 95% probability level. Such relationships, which have to be confirmed in the next few years with other investigations, could be of the greatest interest for the hydrological community dealing with ground truthing of remote sensing data, estimation of mean soil moisture in hydrological modelling, irrigation scheduling and other soil hydrological applications.

4.4 Conclusions

In this Chapter, we addressed three basic questions related to the spatial (field-scale) and temporal (intraseasonal) dynamics of the soil moisture content. These questions were addressed by means of a comprehensive data set of nearly 8 000 soil moisture measurements, collected on 28 locations at different depths (from 0 to 125 cm) within a small cropped field.

The first question deals with the factors controlling the spatial soil moisture patterns. We observed during the vegetative growth period that the soil moisture spatial variability tends to strongly increase in the superficial soil layers (0-50 cm). In order to elucidate this behaviour, we quantified the root water uptake based on a simplified water balance. We showed that the calculated root water uptake variability, like the measured vegetation size, was important. Furthermore, significant correlations between the vegetation size (LAI) and root water uptake was observed. In view of these observations, we conclude that the vegetation growth, and subsequently the evapotranspiration and the root water uptake play a non-negligible role in the temporal dynamics of the observed soil moisture patterns. Considering that the spatial variability is due to the root water uptake, variable vegetation growth could explain spatial variance of 6.2 to 6.7 $(\%\text{vol/vol})^2$ for the superficial layers. Such high values can also explain the poor performance of the terrain indices as shown, among others, by *Western et al.* [1999a]. To the authors' knowledge, there have been no previous detailed studies conducted at the field-scale investigating the role of the vegetation in the spatio-temporal dynamics of the soil moisture. In this context, this study aimed to bring new insights into the role of the vegetation until now often put forward but never quantified.

The second question was related to the soil moisture spatial structure. We showed that for the adopted sampling scheme, the observed spatial structure was non-existent or only weakly marked. For this kind of small fields, without significant relief, and during the vegetative period where vegetation would act as the main controlling factor, it is quite logical to observe absence of significant spatial structure for the superficial soil layers.

The third question addresses the sampling problem for estimating mean soil moisture. The study indicated that a negative correlation exists between the spatial variability and mean soil moisture. This relationship implicitly suggests that the sampling has to be more intensive for the drier conditions. For an absolute error of 2.5% (v/v) and for a probability level of 95%, the number of samples required is quite low varying between 1 and 12 according to the depth and time. On the other hand, this number increases to a maximum of 33 for an absolute error of 1.5% (v/v). One should realize that all these above-presented conclusions are based on data from just one season and one location, further from a small field, so their generality will need to be tested with results from other locations.

Finally, the authors stress again the importance to conduct soil moisture spatial variability studies with measurements performed on the entire hydrologically active zone and not only on the first few centimeters of the soil. As the small-scale variability is often important, we also recommend adoption of temporally unchanged sampling locations. Following these two basic recommendations, we believe progress in the thorough understanding of the physical processes generating the soil moisture spatial variability can be made. Future studies focusing on the soil moisture controlling factors (e.g., topographic features) must explicitly and rigorously take into account the within field spatial variability of the vegetation. Finally, the study presented in this chapter reinforces the fact that accurate field areal soil moisture estimation is far from being easy although it is essential for the robust field-scale calibration of agro-hydrological models.

Chapter 5

Impact of within-field variability of soil hydraulic properties on transpiration and crop yields: a numerical study

Abstract*

In this Chapter, we investigate for three contrasted climatic scenarios the impact of the within-field variability of the soil hydraulic properties on the actual transpiration and the dry matter yield by means of numerical modelling. For this, we perform first a sensitivity analysis of the variability of the soil hydraulic properties by means of an agro-hydrological model. The sensitivity analysis firstly shows that the sensitivity of the simulated actual transpiration and dry matter yield differs according to the soil hydraulic parameters and is more pronounced for drier climatic conditions. The numerical simulations with soil independent stress factors further demonstrate that the impact of the within-field variability of the soil hydraulic properties on the simulated transpiration and dry matter yield can be very large. The generated spatial variability of transpiration and of dry matter yield increases systematically with the dryness of the climate, with coefficients of variation increasing from 7 to 14.6% and from 6.7 to 16% for the actual transpiration and the dry matter yield respectively. In a subsequent analysis, all agro-hydrological

*adapted from Hupet, F., J.C. van Dam, and M. Vanclooster, to be submitted to *Agricultural and Forest Meteorology*, December 2003.

simulations are rerun considering that the water stress parameters are spatially variable and soil dependent. The results obtained with the adjusted water stress parameters are quite different though the spatial variability of simulated transpiration and dry matter yield still increases for drier conditions. The different results obtained, though not validated experimentally, illustrate that the use of an agro-hydrological simulation model in a stochastic mode requires an accurate estimation of the water stress parameters which should further be considered as soil dependent. Finally, we show that the simultaneous estimation of the water stress and the soil hydraulic parameters can not be robustly performed using measurements of transpiration or dry matter yield alone. Consequently, the use of an agro-hydrological model in a stochastic mode for a vegetated surface requires alternative strategies for the specification of reliable water stress parameters. The one presented in this study, that is the adjustment of the water stress parameters from some reference unsaturated hydraulic conductivity values seems attractive but needs more in depth research.

5.1 Introduction

The accurate estimation of transpiration and growth of crops is of the greatest importance as well for hydrological and agricultural scientists as for agriculture system managers. Indeed, transpiration is a major component of the hydrological cycle, while the yield of crops and their optimization undoubtedly constitute the main centre of interest of any agricultural enterprise. Transpiration and crop yields can be directly measured within the fields but measurements are often expensive, time consuming, very punctual in space and time, and further generally destructive. Consequently, the use of simulation models is becoming very widespread as it allows making predictions in space (where measurements are not available) and forecasts into the future (where measurements are not possible) [e.g. *Vanclooster et al.*, 2002]. These models are also very relevant tools to evaluate alternative management strategies for tactical or strategic decisions within an agronomical and environmental context [e.g., *Otegui et al.*, 1996]. The first category of models allowing the simultaneous estimation of transpiration and crop growth includes "agro-hydrological" models like e.g. WAVE [*Vanclooster et al.*, 1996] and SWAP [*van Dam et al.*, 1997]. These models describe in detail the physical soil processes while the crop growth is quite simply represented and generally only limited by climatic factors, physiological characteristics and water stress. The second category includes crop simulation models like e.g. CERES-maize [*Jones and Kiniry*, 1986] and MACROS [*Penning de Vries*, 1989] which are mainly focused on the crop development. This latter category of models generally allows the simulation of yields at several production levels considering, e.g. nitrogen balance, phosphorus and potassium uptake, weeds and pests. As well agro-hydrological as crop simulation models are very powerful tools although their use may be subject to some limitations due to the high number of parameters to be specified [*Boote et al.*, 1996]. Among these ones, the soil hydraulic properties are key parameters as they govern the soil water movement and thereby influence the soil water available for transpiration and crop growth.

Besides issues related to the soil hydraulic properties estimation, additional problems arise due to the variability of these characteristics. Indeed, these ones are known to be highly variable in space even for small agricultural fields lying within one soil class [e.g., *Rawls et al.*, 1983; *Shouse et al.*, 1995; *Logdson and Jaynes*, 1996]. As the spatial scale at which soil hydraulic properties are estimated is generally very punctual and as the number of replicates is often limited, field-scale estimates of these parameters and the subsequent predictions of transpiration and crop yield may be erroneous. Nevertheless, the magnitude of the errors in the field-scale predictions is strongly dependent both on the spatial variability of the soil hydraulic properties and on the sensitivity of the model outputs to the hydraulic properties. The sensitivity depends further on the climatic conditions. As a matter of fact, the sensitivity is assumed to be low in humid climates where transpiration is mainly controlled by the evaporating demand of the atmosphere. Conversely, the sensitivity is assumed to be high in very dry climates where transpiration is more controlled by the soil. In this case, the within-field variability of the soil hydraulic properties is likely to generate spatially variable transpiration and crop growth.

The impact of the soil hydraulic properties "small-scale" variability (i.e. field, small catchment) on water fluxes has been quite extensively studied for infiltration and runoff [e.g., *Merze and Plate*, 1997; *Kim et al.*, 1997], drainage [e.g., *Mallants*, 1996; *Vachaud and Chen*, 2002] and soil evaporation [e.g., *Lewan and Jansson*, 1996; *Zhu and Mohanty*, 2003]. With regard to transpiration and crop yields, the impact of the spatial variability of soil properties has been thoroughly investigated by agronomists within the context of precision farming [e.g., *Paz et al.*, 1998; *Batchelor et al.*, 2002]. Nevertheless, these latter studies were performed with crop simulation models where the soil water transport processes are often oversimplified. Additionally these studies have generally investigated the within-field variability of transpiration and crop yield, considering simultaneously the complex interactions of several different stresses [e.g., *Paz et al.*, 2001]. Consequently, elucidating the impact of the variability of the soil hydraulic properties is not systematically obvious. A few studies have tackled this issue by decoupling the modelling of transpiration from that of vegetation development (i.e. making no use of a full vegetation growth module) [e.g., *Dagan and Bresler*, 1983; *Droogers*, 1997; *Kim et al.*, 1997; *Vachaud and Chen*, 2002]. Still, there is a clear feed-back between both vegetation development and transpiration. Furthermore, some of the latter studies have only considered as spatially variable the soil hydraulic properties. Yet, it is well acknowledged that the water stress parameters, actually governing the magnitude of the actual transpiration and the crop growth, depend in some way on the soil type. Indeed, the reduction of the potential root water uptake and subsequently of the potential transpiration within agro-hydrological models is tacitly assumed to be controlled by the water flow within the soil surrounding the root rather than within the root tissue [e.g., *Molz*, 1981]. Actual root water uptake and transpiration are therefore made dependent through a water stress function on soil water content [*Feddes et al.*, 1976], on soil water pressure head [*Feddes et al.*, 1978] or soil hydraulic conductivity [*Selim and Iskandar*, 1978]. Consequently, in order to rigorously investigate the effect of the soil hydraulic properties within-field variability on the transpiration and the crop yield, it seems appropriate to adjust the water stress parameters according to the basic soil properties. Yet, such an adjustment is not at all straightforward as the water stress parameters can not be directly measured and as the indirect estimation is very tricky to perform [e.g., *Musters et al.*, 2000]. The main objective of this study is to investigate, using numerical agro-hydrological simulations, the impact of the within-field variability of soil hydraulic properties on the transpiration and the crop yield. For this we used a comprehensive data set of soil hydraulic properties measured within a small agricultural field. The combined use of the measured hydraulic properties with the numerical simulations allows tackling some of the above-mentioned issues. The specific objectives of the study can be summarized as follows:

(1) To perform a sensitivity analysis to investigate the sensitivity of cumulative actual transpiration and crop yield to the measured soil hydraulic properties;

(2) To study the impact of the variability of soil hydraulic properties on the transpiration and the crop yield for the case where water stress parameters are either soil dependent or not;

(3) To investigate the feasibility of estimating spatially variable soil hydraulic and water stress parameters from actual transpiration and crop yield measurements.

5.2 Material and methods

This Chapter uses the soil hydraulic properties measured within the experimental field in 2000 and 2002. The hydraulic properties include water retention curves and saturated conductivity measured at three different depths (45, 75 and 105 cm) on 28 and on 2 different locations respectively (see section 2.2.1 and 2.2.2 for further details). For the transpiration and the crop yield modelling, we use both the soil water transport and the crop growth modules of the agro-hydrological SWAP-model [*van Dam et al.*, 1997] such as described in Chapter 2. In this model, the soil hydraulic properties may affect the potential transpiration through a water stress function depending on soil water pressure head. Numerical runs are generated for three contrasted climatic scenarios, namely a very wet (1998), a normal (1999) and a very dry (1990) crop season. Table 5.1 summarizes the climatic conditions encountered during the agricultural season (from 5^{th} May till 30^{th} October) of these three years in terms of rainfall, evaporating demand (ETo) and ratio between the two. Maize is chosen as the crop of interest for all numerical scenarios. All the crop related parameters are derived from literature and are provided in Table 5.2. The numerical simulations systematically start at maize emergence on 5^{th} May of each year, i.e. 10 days after sowing, and stop when maize reaches maturity, i.e. at development stage equal to 2. The simulations are generated for a soil profile of 160 cm depth with free drainage as the lower boundary condition. The flow domain is discretized into 40 compartments using a nodal distance of 1 cm for the first ten compartments and a nodal distance of 5 cm for the remaining soil profile. In this study, we assume that the soil water relations can be described by the closed-form *van Genuchten* [1980] relations requiring the specification of 4 parameters (θ_r and λ are fixed to 0 and 0.5 respectively, and $m = 1 - 1/n$).

In a first step, we carry out a sensitivity analysis. A reference run is generated for the three different climatic scenarios with soil hydraulic properties averaged for the three investigated depths and for the 28 sampling locations. The three depths are treated together as the soil properties are very similar for the three investigated depths (see hereafter Table 5.4). Then, the averaged soil hydraulic parameters are successively and independently perturbed by 5% in order to quantify the sensitivity

Table 5.1. Rainfall, ETo and ratio "ETo/rainfall" for the three considered climatic scenarios. The presented values are the cumulative total for the period from 5^{th} of May till 30^{th} of October.

Years	Rainfall (mm)	ETo (mm)	Ratio ETo/Rainfall
1990 (dry)	270.2	435.3	1.68
1998 (wet)	532.7	369.5	0.69
1999 (normal)	339.5	374.29	1.10

of the cumulative actual transpiration and the final dry matter yield to the perturbed parameter. Sensitivity coefficients are calculated with the following expressions:

$$\Omega_{Ta}(p_j) = \frac{(Ta(p_j + \Delta p_j) - Ta(p_j))}{Ta(p_j)}100 \tag{5.1}$$

$$\Omega_{DMY}(p_j) = \frac{(DMY(p_j + \Delta p_j) - DMY(p_j))}{DMY(p_j)}100 \tag{5.2}$$

with $\Omega_{Ta}(p_j)$ and $\Omega_{DMY}(p_j)$ the relative change of cumulative actual transpiration and dry matter yield corresponding to a 5% change in parameter pj ($\Delta p = 0.05p$). Sensitivity coefficients are multiplied by 100 in Eqs. (5.1) and (5.2) to express the relative change in percentage. This formulation of the sensitivity coefficients allows a comparison of the sensitivities to different parameters, independent of the invoked units or their absolute values, and a comparison between the sensitivity of different outputs. It is worth noting that the parameters are systematically changed by +5 % of the nominal value but additional changes between -10 and +10 % are performed for some cases to check linearity of the model outputs to the perturbed parameters. In this sensitivity analysis, we choose to modify all the soil hydraulic parameters, plus the water stress parameters and the time series of the driving forces (i.e. ETo and rainfall).

In a second step, we investigate the influence of the soil hydraulic properties spatial variability on the simulated transpiration and the crop yield. We run numerical simulations for each 28 sampling location with depth averaged soil hydraulic parameters. As saturated hydraulic conductivity values are not available for each location we generate for each 28 location 40 stochastic simulations with K_{sat} randomly sampled within a uniform distribution bounded by the extreme values, i.e. 13.39 and 48.96 cm d^{-1} measured with the constant head permeameter (see section 2.4). That results in 1120 (28x40) simulations for each climatic scenario.

Table 5.2. Maize crop parameters used for the numerical simulations. All the parameter values are derived from *Boons-Prins et al.* [1993] and from *Wesseling* [1991].

Parameter	Values
Crop parameter Kc	1 (0) - 1.1 (1) - 1.1 (1.5) - 0.7 (2)
Temp. sum from emerg. to anthesis, from anth. to mat. (°C)	693 - 786
Initial total crop dry weight (kg ha^{-1})	5
Leaf Area Index at emergence (-)	0.0074
Maximum relative increase in LAI (-)	0.0294
Specific leaf area (ha kg^{-1})	0.0035 (0)- 0.0016 (0.78) - 0.0016 (2)
Life span of leaves under opt. conditions (d)	31
Lower threshold temp. for ageing of leaves (°C)	10
Extinction coef. for diffuse and direct visible light (-)	0.65 - 0.75
Light use eff. for real leaf (kg CO_2 ha^{-1}hr^{-1} J^{-1}m^{-2}s^{-1})	0.45
Max. CO_2 assimilation rate(kg CO_2 ha^{-1}h^{-1})	70(0)-70(1.25)-63(1.5)
	49(1.75)-21(2)
Eff. of conversion into leaves and stor. organs (kg kg^{-1})	0.68 - 0.671
Eff. of conversion into roots and stems (kg kg^{-1})	0.69 - 0.658
Rel. increase in respiration rate with temperature	2
Rel. maint. resp. rate of leaves (kgCH_2O kg^{-1}d^{-1})	0.03
Rel. maint. resp. rate of st. org. (kgCH_2O kg^{-1}d^{-1})	0.01
Rel. maint. resp. rate of roots and stems (kgCH_2O kg^{-1}d^{-1})	0.015
Reduction factor of senescence (-)	1(0)-1-(1.5)-0.75-(1.75)-0.25 (2)
Fract. of total DM increase partitioned to roots (kg kg^{-1})	0.4(0)-0.37(0.1)-0.34(0.2)-0.31(0.3)
	0.27(0.4)-0.23(0.5)-0.19(0.6)-0.15(0.7)
	0.1(0.8)-0.06(0.9)-0(1)-0(2)
Fract. of total DM increase partitioned to leaves(kg kg^{-1})	0.7(0)-0.7(0.33)-0.15(0.88)-0(0.95)-0(2)
Fract. of total DM increase partitioned to stems (kg kg^{-1})	0.3(0)-0.3(0.33)-0.85(0.88)
	1(0.95)-0(1.05)-0(2)
Fract. of total DM increase partitioned to st. organs (kg kg^{-1})	0(0)-0(0.95)-1(1.05)-1(2)
Max. rel. death rate of leaves due to water stress (d^{-1})	0.03
Rel. death rates of roots and stem (kg kg^{-1}d^{-1})	0(0)-0(1.5)-0.02(1.51)-0.02(2)
h_1, h_2, h_{3l}, h_{3h}, h_4 (cm)	-15 -30 -325 -600 -8000
Interception coefficient (cm)	0.25
Top and bottom relative root length density (-)	1 and 0
Initial rooting depth	10
Maximum daily increase in rooting depth (cm)	1.5
Maximum rooting depth crop/cultivar (cm)	150

All these simulations are performed assuming that the parameters of the water stress function are constant (see reference values derived from literature in Table 5.2).

In a third step, all the simulations are rerun considering now dependence between the spatially variable soil hydraulic parameters and the water stress parameters. Before rerunning each simulation, the water stress parameters (i.e. the critical pressure heads h_{3l}, h_{3h}, and h_4) are adjusted according to three "reference" unsaturated hydraulic conductivity values. Indeed, though the water stress function by Feddes [*Feddes et al.*, 1978] explicitly assumes that the reduction of the potential root water uptake occurs from some critical pressure head, the function also implicitly assumes that the unsaturated soil hydraulic conductivity governs this reduction. As a matter of fact, it is well acknowledged that the critical pressure heads are different according to the soil type and that the reduction occurs much earlier in a sandy than in a loamy soil, i.e. that $\mid h_{crit} \mid_{sand} < \mid h_{crit} \mid_{loam}$ [e.g., *Musters et al.*, 2000] as the unsaturated hydraulic conductivity curve drops much faster. This concept is used here to adjust the critical pressure heads according to our spatially variable measured hydraulic properties. We consider that the critical pressure head values used during the simulations of the previous step (i.e. h_{3l}=-600cm, h_{3h}=-325cm and h_4=-8000cm) are effectively valid for the run of 1998 for which the soil hydraulic properties have generated the most limited water stress (i.e. θ_s=0.403 cm^{3}cm^{-3}, α=0.0051 cm^{-1}, n= 1.275 and K_{sat}=14.1 cm d^{-1}). This assumption seems very realistic as the 1998 climate is wet (see Table 5.1) and a pronounced water stress is very unlikely to be encountered for the considered loamy soil. Then, we determine the three "reference" unsaturated hydraulic conductivity values corresponding to the above-mentioned critical pressure head values derived from literature. These reference values are K_{3l}= 0.0156 cm d^{-1} (for h_{3l} -600 cm), K_{3h}= 0.0791 cm d^{-1} (for h_{3h} -325 cm) and K_4= 2.15 10^{-5} cm d^{-1} (for h_4 -8000 cm). The reduction of the potential root water uptake is subsequently assumed to be activated from these three "reference" hydraulic conductivity values for all the numerical simulations. Before launching each run, critical pressure heads are adjusted with the "reference" hydraulic conductivity values. According to *Feddes et al.* [1974] and *Nimah and Hanks* [1973], we decide that the critical pressure value for h_4 can not be less than -15000 cm. Fig. 5.1 schematically illustrates the adjustment procedure of the reference critical pressure head h_{3h} (i.e. -325 cm) from the "reference" hydraulic conductivity value K_{3h}. It is worth mentioning that the adopted adjustment procedure explicitly considers that the reduction of the potential root water uptake occurs from certain threshold unsaturated hydraulic conductivity values.

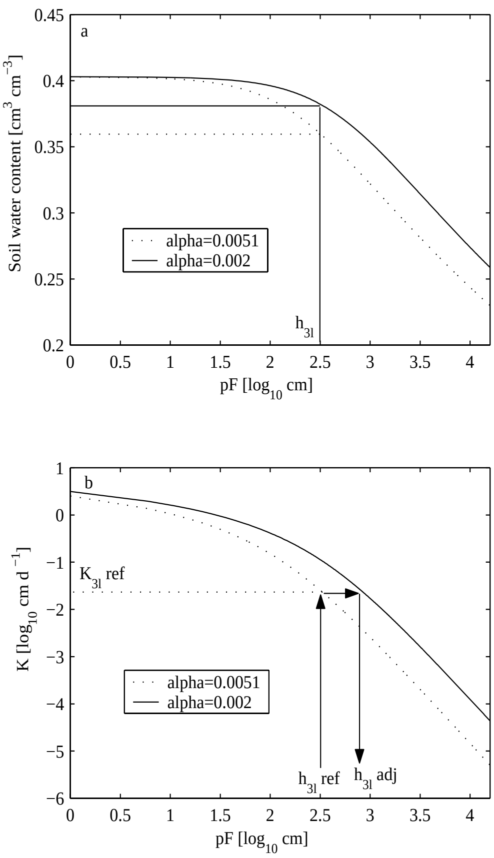

Figure 5.1. Schematic representation of the adjustment procedure of the critical pressure head h_{3l}. Fig. 5.1a shows the "reference" moisture retention curve (α= 0.0051) and that of a similar soil with α= 0.002. Fig. 5.1b presents the two corresponding hydraulic conductivity curves and the K_{3ref} value used for the adjustment.

In a fourth step, we investigate whether "measurements" of transpiration and crop yields can be used in order to simultaneously estimate the spatially variable hydraulic parameters and the water stress parameters. Within this context, it is considered that the parameter identification process is performed by minimizing one of the two following objective functions (OF):

$$OF_{Ta}(\boldsymbol{b}) = \sqrt{(Ta^* - Ta(b))^2} \tag{5.3}$$

$$OF_{DMY}(\boldsymbol{b}) = \sqrt{(DMY^* - DMY(b))^2} \tag{5.4}$$

with **b** the model parameter vector; Ta^* and $Ta(\mathbf{b})$ the "measured" (in our case generated with a reference run) and the simulated cumulative transpiration; and DMY^* and $DMY(\mathbf{b})$ the "measured" and simulated final dry matter yield. After generating a reference run for the averaged hydraulic properties of the experimental field (similar to the reference run of the sensitivity analysis with reference water stress parameters derived from literature), the simulations are rerun for every combination of two parameter values (including systematically a water stress and a hydraulic parameter) within a predefined parameter space discretized into 50 discrete increments. For each of the 2500 (50x50) runs, values of the OF are calculated with Eqs. 5.3 and 5.4. The feasibility of the identification process is subsequently tackled by visual observation of two-dimensional surface responses of OF for different combinations of parameters.

5.3 Results and discussions

5.3.1 Sensitiviy analysis

Results of the sensitivity analysis are summarized in Table 5.3a and b in terms of absolute values and sensitivity coefficients (SC) respectively for the three different climatic scenarios. It is clear in Table 5.3 that the sensitivity of the cumulative actual transpiration and the final dry matter yield is very variable according to the hydraulic parameters. For the three climatic scenarios, the sensitivity is maximum to the saturated water content parameter (θ_s) and to the shape parameter (n). The increase of these two parameters leads to increase both the actual transpiration and the final dry matter yield. As a matter of fact, the increase of θ_s results in an upward shifting of the moisture retention curve (MRC) leading to an increase of the available water between saturation and the critical pressure heads at which the reduction of the potential root water uptake start. The effect is similar for n as an increase of this parameter induces a steeper slope for the MRC and consequently an increase of the available water. In terms of absolute values, the impact of the modified hydraulic parameters on the actual transpiration is not very pronounced with a maximum of 5 mm for the n parameter. On the contrary, the increase of 5% of the n parameter induces an increase of more than 500 kg of the final dry matter yield for the very dry 1990 agricultural season. It is worth noting that such an effect on the final yield is quite important especially considering the magnitude of the uncertainty generally associated to the field-scale soil hydraulic parameter estimates. Yet, this effect is much more attenuated for the wetter years, i.e. for 1998 and 1999.

Table 5.3. Results of the sensitivity analysis presented for the three considered climatic scenarios. Table 5.3a shows absolute values of both cumulative transpiration (mm) and final dry matter yield (kg ha^{-1}) for the reference run and for the runs with modified parameters. Table 5.3b shows corresponding sensitivity coefficients calculated with Eqs. (5.1) and (5.2).

a

Parameter	1990		1998		1999	
	Ta	DMY	Ta	DMY	Ta	DMY
Reference run	173.1	15415	188.1	21000	194.2	20534
θ_s	176.4	15751	189.4	21130	195.4	20668
α	175	15603	189	21089	195.5	20672
n	178.1	15948	189.7	21158	194.7	20622
K_{sat}	172.2	15323	187.7	20597	193.6	20470
λ	173.2	15421	188.2	21004	194.2	20535
h_{3h}	173.4	15434	188.3	21017	194.5	20556
h_{3l}	173.5	15451	188.4	21026	194.6	20577
h_4	174.9	15588	188.9	21071	195.1	20627
ETo	177.5	14921	196.7	20743	201.9	20207
$Rainfall$	175.6	15708	188.8	21121	195.9	20757

b

Parameter	Ref. and perturbed values	1990		1998		1999	
		Ta	DMY	Ta	DMY	Ta	DMY
θ_s	0.3894- 0.4088	1.9	2 .17	0.69	0.61	0.61	0.65
α	0.00408-0.004284	1.09	1.21	0.47	0.42	0.67	0.67
n	1.204 - 1.2642	2.88	3.45	0.85	0.75	0.25	0.42
K_{sat}	30 - 31.5	-0.5	-0.59	-0.21	-0.2	-0.3	-0.31
λ	0.5 - 0.525	0.057	0.038	0.05	0.02	0	0.004
h_{3h}	325-341	0.17	0.12	0.1	0.12	0.15	0.1
h_{3l}	600 - 630	0.23	0.23	0.15	0.12	0.2	0.2
h_4	8000 - 8400	1.03	1.12	0.42	0.33	0.46	0.452
ETo	Time series*1.05	2.54	-3.2	4.57	-1.22	3.96	-1.59
$Rainfall$	Time series*1.05	1.44	1.9	0.37	0.57	0.87	1.08

Generally speaking, the transpiration and the dry matter yield are much less affected by the soil hydraulic parameters for those two years than for the dry 1990 year. This stems obviously from the fact that transpiration and crop production are much more controlled by the soil than by the atmosphere in these very dry conditions. The differences between the dry year and the wetter ones are well illustrated in Table 5.3b with SC for n decreasing from 2.88 to 0.85 and from 3.45 to 0.75 for transpiration and yields respectively. Note that such differences of sensitivity were already observed by *St'astna and Zalud* [1999] using two different crop simulation models but in this case the sensitivity was also markedly different according to the model used. In our study, the transpiration and the crop yield are not very sensitive to the saturated hydraulic conductivity (K_{sat}) with SC ranging between -0.59 and -0.2. These small negative values mean that an increase of K_{sat} leads to a small decrease of both transpiration and crop yields. The increase of K_{sat} reduces the soil control on the potential soil water evaporation leaving by this way a smaller quantity of water for transpiration. This is coherent with the results obtained by *Diels* [1994]. Note that in our study all the rainfall reaching the ground infiltrates into the soil (no runoff occurs) as the daily rainfall values are evenly distributed over the whole day (i.e. instantaneous intensities are systematically low). Consequently, the perturbation of the K_{sat} parameter does not affect the quantity of water infiltrating into the soil. In Tables 5.3, it may seem surprising that the perturbation of the soil hydraulic properties has a perceptible effect on the transpiration and the crop yields for the 1998 year as this one is very wet (ratio ETo/rainfall=0.69). These possibly biased results could be explained by the fact that potential correlations between soil hydraulic parameters and water stress parameters are not taken into account (see next section). Finally, it is worth noting that the effects of the soil hydraulic properties on the transpiration and the crop yield are very similar (see sensitivity coefficients in Table 5.3b). This is inherent to the conceptualization used by the agro-hydrological model linking the actual transpiration to the dry matter production.

Compared with the soil hydraulic parameters, the perturbation of the critical pressure heads has quite a limited impact on the cumulative actual transpiration and the final dry matter yields. However, the range of uncertainty related to the critical pressure head parameters may be much larger than that related to the soil hydraulic parameters [*Homaee*, 1999]. This however does not mean that the water stress parameters do not need further attention within the calibration process.

Transpiration and crop yield are both sensitive to the driving forces (ETo and rainfall) but very differently according to the climatic scenar-

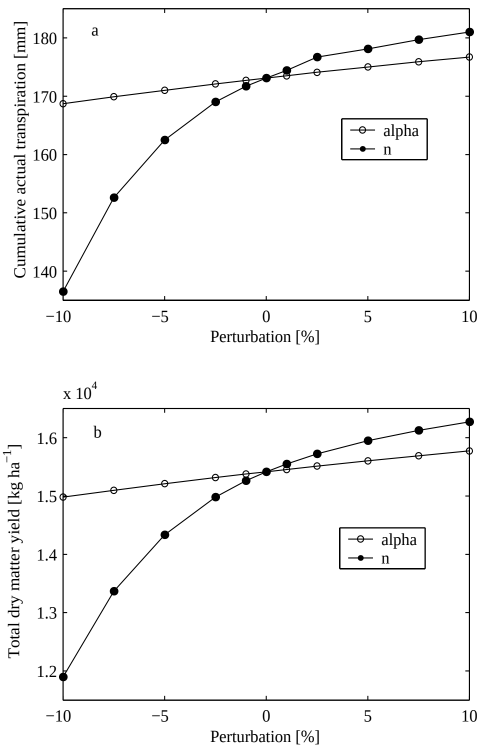

Figure 5.2. Impact of the perturbation of α and n on the actual cumulative transpiration (Fig. 2a) and on the crop yield (Fig. 2b) for the dry 1990 climatic scenario.

ios. For the very dry year (1990), the increase of ETo only leads to a slight increase of the cumulative transpiration (+4.4 mm) but strongly affects the crop yield (-494 kg). Such a yield decrease is due to the fact that an increase of ETo involves a proportional increase of the potential crop transpiration and therefore, in case of a dry year, an exacerbated water stress. Note that the selected perturbation for ETo is similar to the magnitude of the error in ETo caused by a poor temporal sampling frequency of meteorological variables [*Hupet and Vanclooster*, 2001]. On the other hand, for the 1998 and 1999 agricultural seasons, the effect of the modification is more marked for the actual transpiration than for the crop yields. Indeed, for wet years, the actual transpiration is more controlled by the evaporating demand than by the soil. However the increase of ETo for both years leads to a slight decrease of the crop yield revealing that a water stress occurs. Concerning the rainfall, its impact on the transpiration is more limited and the sensitivity is more and more pronounced for drier years with SC equal to 0.37, 0.87 and 1.44 for 1998, 1999 and 1990 respectively (for absolute values see Table 5.3a). Investigating the sensitivity of transpiration and crop yield to the driving forces is rarely performed in classical sensitivity analysis. Results obtained in this sensitivity analysis could be compared to those obtained in other studies. Nevertheless, the model structure, more particularly, the soil water transport module included in crop growth simulation models is so different that such comparisons seem not very relevant (see results of *St'astna and Zalud* [1999]). Finally, we present the results obtained for the case where the model parameters (α and n) are perturbed around their nominal values from -10 to +10%. Results for the very dry scenario (1990) for cumulative actual transpiration and crop yield are illustrated in Figs. 5.2a and b respectively. These figures show that the model response can be very linear to some parameters (e.g. for α) while in some cases is highly nonlinear (e.g. for n). These results, though not surprising (see e.g. results of *Brooks et al.* [2001]), suggest that a classical sensitivity analysis in which no correlation between the perturbed parameters and a quite arbitrary modification of the parameters is assumed, only gives a limited view of the model response within the parameter space. Furthermore, in order to quantify the true impact of the spatially variable soil hydraulic properties on the variables of interest, the sensitivity coefficients should be combined with measured spatial variability of each soil hydraulic parameters. For this, the agro-hydrological model can be run in a stochastic mode using measured spatial variability of soil hydraulic properties.

5.3.2 Impact of within-field variability of soil hydraulic properties

Table 5.4 summarizes the spatial variability of the soil hydraulic properties measured within the experimental field. The presented values are typical for a medium-fine textured soil (loam) with values close to 0.4 cm^3 cm^{-3} and with small values for both n and α parameters. The magnitude of the observed variability is very similar to that found in other studies, e.g. *Shouse et al.* [1995], *Mallants* [1996] except for K_{sat}. For this parameter, the observed spatial variability is smaller which can be explained by the limited number of replicates (i.e. 6) and by the relatively "large" support volume of the measurement technique used [*Mallants et al.*, 1997]. The variability observed for the α parameter is more than one order of magnitude larger than that observed for n and θ_s. It is worth mentioning that taking into account of such a difference of variability within the sensitivity analysis might obviously strongly

Table 5.4. Variability of the soil hydraulic properties measured within the experimental field (mean, max, min, CV). The presented values are the averaged of the three investigated depths.

	θ_s (cm^3 cm^{-3})	α (cm^{-1})	n (-)	K_{sat} (cm d^{-1})
Mean	0.3894	0.004084	1.204	29.74
Min.	0.3682	0.0014	1.1441	13.39
Max.	0.4135	0.0078	1.2753	48.96
CV	2.85	40	2.67	57.7

modify the results obtained by perturbing each parameter of a similar value. Figs. 5.3a-b-c illustrate the variability of the moisture retention curves (MRC) for the first (45 cm), the second (75 cm) and the third investigated depth (105 cm) respectively. Fig. 5.3d shows the 28 MRC averaged for the three depths. These latter are used in the subsequent agro-hydrological simulations.

Figs. 5.4 a-c-e and b-d-f present the results obtained by means of the numerical simulations for the very dry 1990 and the very wet 1998 agricultural campaign respectively. Figs. 5.4c-d and e-f show the cumulative actual transpiration and the dry matter yield respectively, with the whiskers indicating the minimum and the maximum values of the 1120 runs. The period needed by maize to reach maturity is 163 days for 1990 and 147 days for 1998 due to differences of temperature. Concerning the cumulative actual transpiration and the dry matter yields, we can firstly observe that the values are markedly different for the two climatic scenarios. For the 1990 and 1998 agricultural campaigns, the simulated cumulative actual transpiration range between 92.8 and 202.9 mm and between 132.8 and 198.3 mm with mean values of 166.9 and 182.68 mm respectively. For the dry matter yields, the differences are also very pronounced with mean values of 14.76 and 20.39 T ha^{-1} for 1990 and 1998 respectively. The 1999 agricultural season presents an intermediate behaviour both for yields and transpiration (see Table 5.5). In Table 5.5, we note that the spatial variability of the simulated transpiration and crop yield progressively increases with the dryness of the agricultural season. Indeed, from the wet 1998 to the very dry 1990 agricultural season, CV values increase from 7 to 14.6% and from 6.7 to 16% for the transpiration and the dry matter yield respectively. That clearly means that the dryness of the climate does not only affect the mean values but also govern the magnitude of the effect of the spatial variability of the

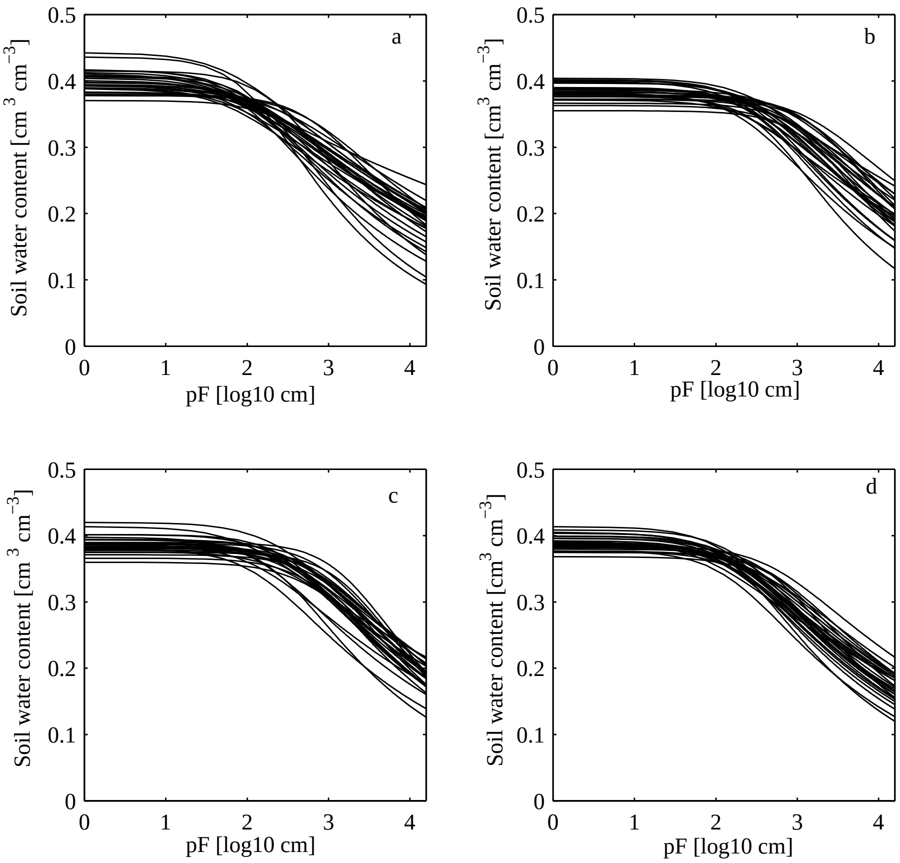

Figure 5.3. Fig. 5.3 a-b-c shows the measured spatial variability of the moisture retention curves (MRC) for the first depth (45 cm), the second (75 cm) and the third (105 cm) respectively. Fig. 5.3d presents the 28 MRC with soil hydraulic properties averaged for the three investigated depths.

Table 5.5. Numerical simulation results for the three different climatic scenarios. Cumulative transpiration and dry matter yields are expressed in mm and T ha^{-1} respectively.

	1990	1998	1999		1990	1998	1999
	Transpiration				Dry matter yield		
Mean	166.9	182.68	188.46	Mean	14.76	20.39	19.92
Max.	202.9	198.3	209	Max.	18.45	22.01	22.22
Min.	92.8	132.8	124.1	Min.	7.8	14.79	12.89
CV	14.6	7	9.5	CV	16	6.7	9.7

soil hydraulic properties on the transpiration and the crop yield variability. The effect of the climate on the magnitude of the transpiration variability is similar to the results obtained by *Braud et al.* [2003] at a larger scale. A corollary of these results is that the incomplete capture of the within-field variability of the soil hydraulic properties likely bias the field-scale estimations of the transpiration and the crop yields during dry years. The results obtained by means of our numerical simulations also corroborate the fact that the use of information about measured spatially variable crop growth or transpiration to retrieve the structure of the underlying soil spatial variability is likely to perform successfully only in dry climates [see *Jhorar*, 2002].

The results obtained with the agro-hydrological simulations presented in Figs. 5.4 and in Table 5.5 cannot easily be validated experimentally. Nevertheless, some results, especially those generated for the wet 1998 agricultural season, may be strongly questionable for three reasons. Firstly, we can observe that some locations within the field experience a severe water stress($T_{a,min}/T_{a,max}$= 0.66) although a water stress is very unlikely to occur for a maize crop growing in such wet conditions (ratio ETo/rainfall=0.69 with only one "long" 16 days dry spell without any rainfall) [*Otegui et al.*, 1995; *G. Foucart*, 2002, personal communication]. Secondly, the results presented in Fig. 5.4d show that the water stress is highly variable within the loamy field for which the measured soil hydraulic properties variability is rather small (see Table 5.4). This is further surprising as this soil type is generally considered as optimal in terms of soil water availability. Thirdly, the minimum cumulative actual transpiration values obtained during the dry 1999 season (92.8 mm) seem much too low as it corresponds to a daily mean transpiration value of hardly 0.66 mm d^{-1}. Consequently, all this allows us to suspect that the water stress parameters are not correctly specified (although

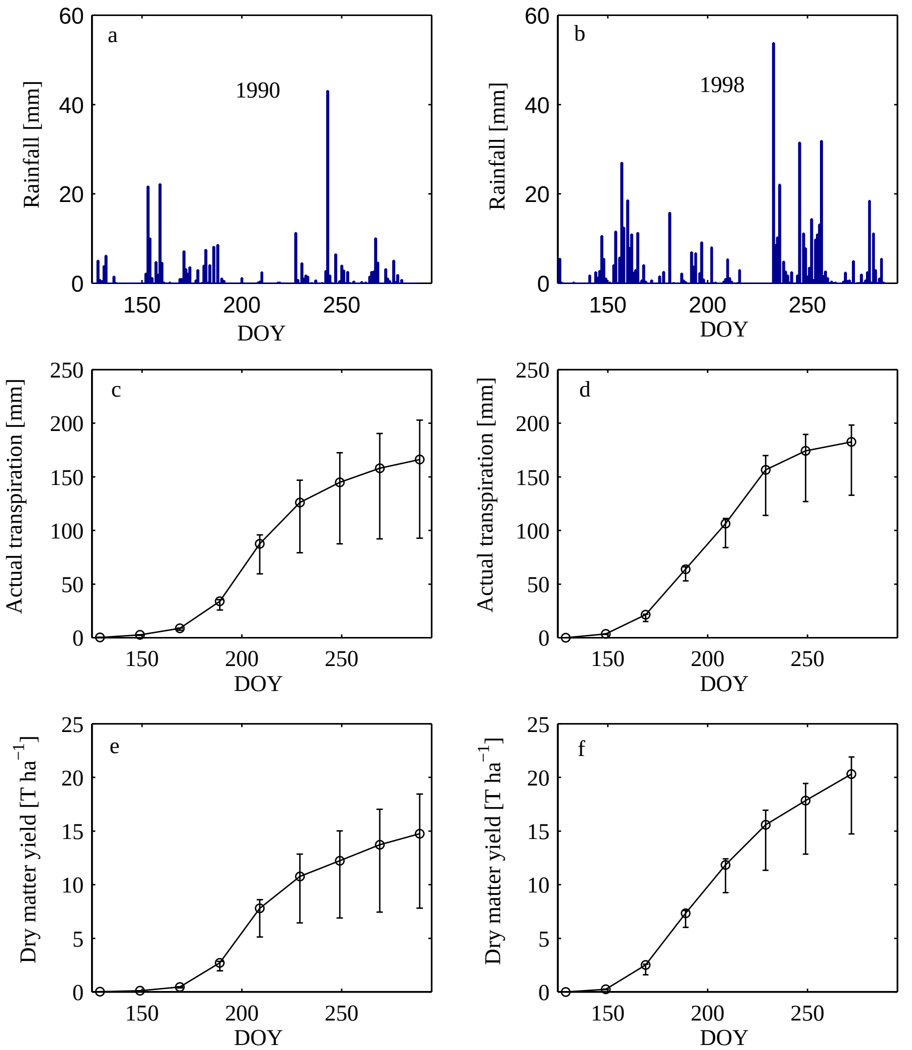

Figure 5.4. Impact of the within-field variability of the soil hydraulic properties on the actual transpiration (c-d) and the dry matter yield (e-f) for the dry 1990 (a-c-e) and the 1998 climatic scenarios. Whiskers indicate the maximum and minimum simulated values. Top figures show the rainfall encountered during the two respective climatic scenarios.

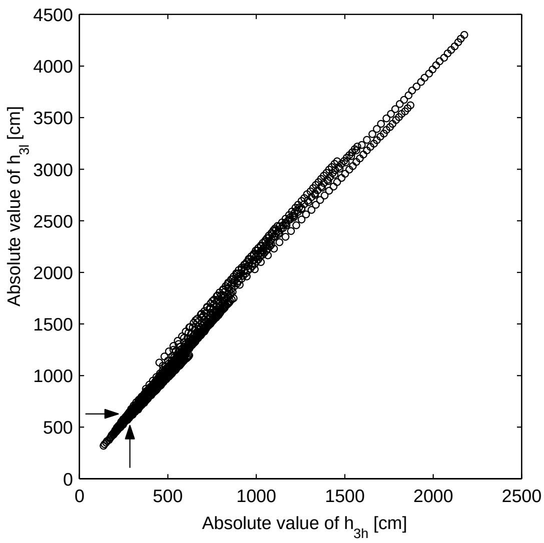

Figure 5.5. Scatter plots of the adjusted critical pressure heads h_{3l} and h_{3h}. Arrows indicate the reference values, i.e. -300 and -625cm for h_{3h} and h_{3l} respectively.

derived from reference literature values for this crop, see Table 5.2) at least for some locations for which the "erroneous" parameters exacerbate the water stress. On the contrary, some sampling locations (i.e. some combinations of hydraulic parameters) present a normal behaviour with a very limited water stress.

As a consequence, we decided to rerun all the numerical simulations, adjusting the water stress parameters as explained in section 2. This was performed according to the three "reference" unsaturated hydraulic conductivity values (K_{3l}= 0.0156 cm d^{-1} for h_{3l}, K_{3h}= 0.0791 cm d^{-1} for h_{3h} and K_4= 2.15 10^{-5} cm d^{-1} for h_4) derived from the less stressed 1998 run. Fig. 5.5 presents the 1120 combinations of h_{3h} and h_{3l} (arrows in this figure indicate the original values, i.e. -325 and -600 cm) obtained with this strategy. The adjusted water stress parameters range for h_{3h} between -136 and - 2176 cm (the vast majority between -220 and -840 cm), for h_{3l} between -431 and - 4301 cm (the vast majority between -580 and -1460 cm) and for h_4 between -5626 and -24996 cm (the vast majority between -7500 and -14600 cm). Table 5.6 shows the agro-hydrological simulation results rerun with the modified water stress parametrization procedure. In Table 5.6, we can observe both for transpiration and dry matter yields that the simulated values are higher than those obtained previously (for comparison see values in Table 5.5). With regard to the

Table 5.6. Results of the numerical simulations for the three different climatic scenarios rerun with the modified critical pressure heads. Cumulative transpiration and dry matter yields are expressed in mm and T ha^{-1} respectively.

	1990	1998	1999		1990	1998	1999
	Transpiration				Dry matter yield		
Mean	191.8	195.6	206.55	Mean	17.27	21.75	21.02
Max.	203.8	199.8	209.9	Max.	18.54	22.19	22.35
Min.	164.7	174.4	198.5	Min.	14.48	19.28	21.01
CV	4.6	1.6	2.5	CV	5.4	1.55	1.75

mean actual transpiration, values increase by +13, +18 and +25% for 1998, 1999 and 1990 respectively. Such increases, progressively larger with the dryness of the year are also observed for the simulated dry matter yields. These increases both for transpiration and crop yields are revealing of less accurate water stresses which is obviously a consequence of the adjustment of the water stress parameterization. Concerning the simulated spatial variability, this one is now more limited (CV values range between 1.55 and 5.4%) but still increases systematically with the dryness of the considered climatic scenario. For the 1990 dry year, we also observe that the minimum values obtained for the actual transpiration are much realistic (i.e. 164.7 instead of 92.1 mm). Results of these simulations rerun with the modified water stress parameters can not easily be validated experimentally. Indeed, a comparison exercise should require accurate measurements of transpiration and dry matter yield within the field. Dry matter yield measurements are only available for the 1999 agricultural season, although these measurements were not performed exactly on the same 28 locations where soil hydraulic properties were determined (+-50 cm). Additionally the agro-hydrological model used was not previously calibrated and does not consider various stresses inevitably occurring within the field. Trying to mimic the measured within-field variability of transpiration and crop yield under these conditions seems irrelevant and the comparison exercise is therefore not performed.

The results obtained with the numerical simulations, though not validated, illustrate that the use of water stress parameters derived from literature may be very problematic. Indeed, our results show that these parameters can strongly affect the simulated transpiration and the crop yield even during a wet year. Furthermore, the results show that the adjustment of the water stress parameters does not only influence the mean simulated transpiration and crop yield but also the spatial variability of these latter variables. The results produced by the sensitivity analysis might therefore be shaded as the perturbation of the hydraulic parameters was performed independently of the water stress parameters which might be considered physically inconsistent. Within this context, it is likely that introducing some correlations between the soil hydraulic and the water stress parameters during the perturbation process could lead to different results. Our results reinforce also the fact that it is very important to develop water stress parameterization procedures which consider appropriately the hydraulic function of the soil in terms of retention and conductivity.

5.3.3 Estimation of water stress and hydraulic parameters

Estimation of water stress parameters can be performed by fitting simulated actual transpiration and/or dry matter yield to measured values. As the within-field variability of the soil hydraulic parameters is generally high and as the water stress parameters are soil dependent, we firstly investigate the feasibility of the simultaneous estimation of both types of parameters. The parameters considered during the calibration process are the soil hydraulic parameters n and α, and the critical pressure head h_4. Fig. 5.6 shows 2D Object Functions (OF) obtained when h_4 is simultaneously optimized with n (a-b-e-f) and α (c-d-g-h) for the 1990 (a-b-c-d) and 1998 agricultural season (e-f-g-h). The left (a-c-e-g) and the right figures (b-d-f-h) illustrate the response surfaces of OF calculated using actual cumulative transpiration and final dry matter yield respectively. True values, i.e. n =1.204, α=0.00405 and h_4=-8000cm, are marked with a star. Fig. 5.6 reveals in all cases a strong parameter interaction between h_4 and n or α. Indeed, we can observe that many pairs of parameter values give very similar goodness of fit both for OF calculated with actual transpiration and dry matter yield. For example in Fig. 5.6a, perfect fits can be obtained for some combinations of parameter across the whole selected parameter space (i.e. -15000 $<h_4<$-5000 and 1.05$<n<$1.8). Similar results are obtained for each combinations of parameter and for both climatic scenarios. Note, however, that the response surfaces are much flatter for the wet 1998 scenario compared with the dry one. Fig. 5.6e and f show quite extreme cases where very good fits are obtained almost everywhere in the parameter space (Fig. 5.6e-f) for the simultaneous optimization of and h_4. This is a consequence of the low sensitivity of actual transpiration and dry matter yield to the water stress and the soil hydraulic parameters compared to a dry year. All these results clearly point out that the simultaneous estimation of a water stress and a soil hydraulic parameter is not sound. Indeed, although very good fits can be obtained in terms of transpiration or actual dry matter yield, the derived parameter values may not be representative for the physical "unknown" parameters. Such a calibration exercise is further very problematic as the derived hydraulic parameters can be strongly biased leading possibly to a very abnormal model response in terms of e.g. drainage or runoff predicted during wetter periods. Furthermore, the use of this calibration procedure to estimate simultaneously spatially variable water stress and soil hydraulic parameters (using e.g. spatially measured crop yields) could exaggerate or underestimate the variability of the parameters. The feasibility of the simultaneous estimation of water stress and soil hydraulic parameters is not tested for h_{3h}, h_{3l}, and K_{sat} but similar results are very likely to occur. The estimation of the parameters of interest is only shown for the case where the final actual cumulative transpiration and dry matter yield are used. Yet, identical results are obtained if the whole time series of the daily variables is incorporated in the OF of Eqs.(5.3) and (5.4)(results not shown).

From this we can conclude that alternative strategies are needed to estimate both the hydraulic and water stress parameters. The soil hydraulic parameters can be estimated alternatively by means of a series of direct or indirect measurement techniques [*Dane and Topp*, 2002]. Then, water stress parameters only can be estimated fixing the soil hydraulic parameters at these estimated values. This strategy is certainly more robust as the OF minimum should be more easily found (at least in case of a dry year, see Fig. 5.6 a-b-c-d) and the uncertainty related the water stress parameters should be smaller. Note that in this study, we do not test the possibility of the simultaneous estimation of several water stress parameters (e.g. h_{3l} and h_4) although one may suspect that additional correlations occur for this kind of parameter combinations.

The results presented in this section of our study show that very good fits can be obtained by adjusting water stress and hydraulic parameters on actual transpiration and dry matter yield measured within a given experimental site. Notwithstanding such apparent good results, the derived parameters may not at all be physical. Therefore, it is extremely problematic to consider such derived water stress parameters as reference values for a given crop and to use them as such in a modelling exercise for other sites where soil hydraulic parameters may only slightly differ. However, such a methodology is often the only alternative that can be used and many examples can often be found in the literature [e.g. *Droogers*, 1997; *Meiresonne et al.*, 1999; *Droogers*, 2000; *Ritter et al.*, 2003]. In front of the "disappointing" results presented in Fig. 5.6, a

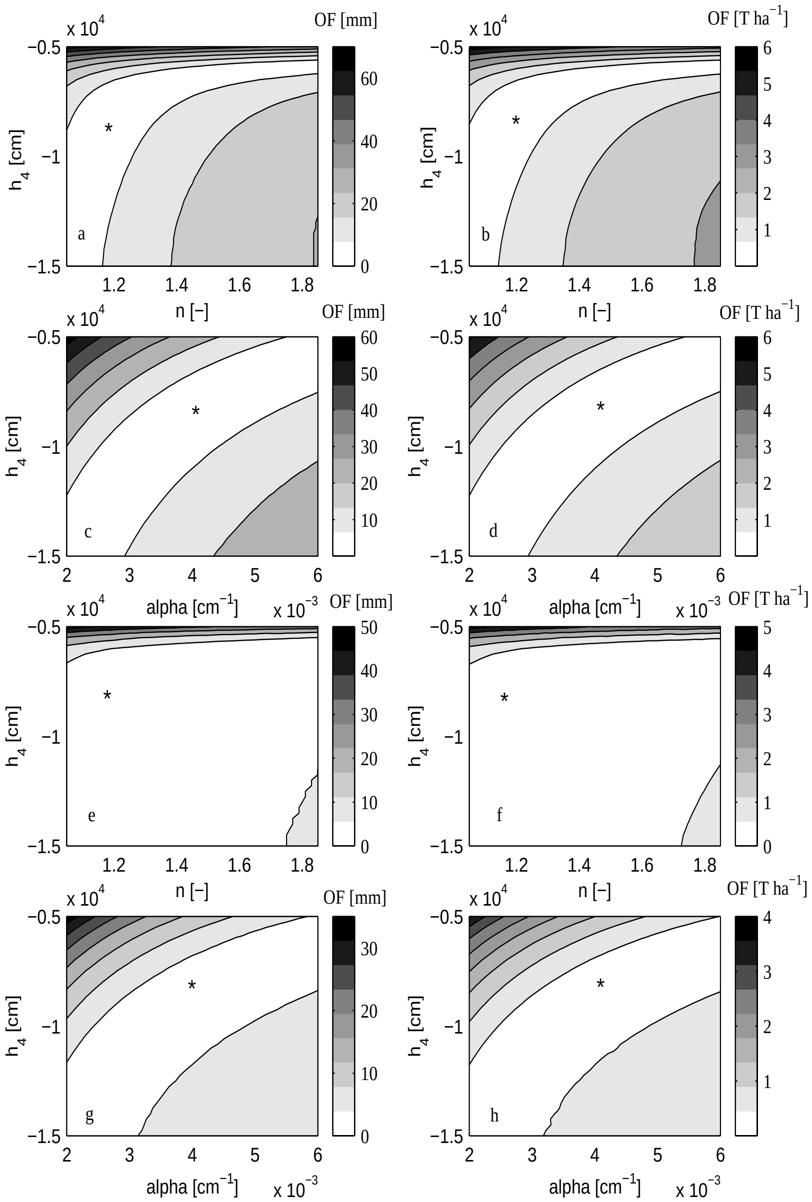

Figure 5.6. 2D response surfaces of OF obtained when h_4 is simultaneously optimized with n (a-b-e-f) and α (c-d-g-h) for the 1990 (a-b-c-d) and 1998 agricultural season (e-f-g-h). The left (a-c-e-g) and the right figures (b-d-f-h) illustrate the response surfaces of OF calculated using actual cumulative transpiration and final dry matter yield respectively.

plea is made for developing alternative strategies for the specification of reliable water stress parameters within agro-hydrological models.

5.4 Conclusions

In this Chapter, we investigate the impact of the within-field variability of the soil hydraulic properties on cumulative actual transpiration and dry matter yield for three contrasted climatic scenarios combining measurements and agro-hydrological simulations.

In a first step, a sensitivity analysis is carried out to quantify the sensitivity of the actual transpiration and the dry matter yield to the soil hydraulic properties. The results show that the sensitivity is very variable. Some parameters have a marked effect, e.g. θ_s and n, while others, e.g. K_{sat}, have only a weak effect. In a general way, the actual transpiration and the dry matter yield are progressively more and more affected by the soil hydraulic properties when dryness increases. This corresponds to the increase of the soil control on the water fluxes and on the dry matter production in dry conditions. The sensitivity of the actual transpiration and the dry matter yield to the soil hydraulic parameters is often very similar, which is a direct consequence of the conceptualization used by the agro-hydrological model to reduce the daily potential gross CO_2 assimilation rate.

In a second step, we investigate the impact of the within-field variability of the soil hydraulic properties on the simulated actual transpiration and dry matter yield, considering the water stress parameters as constant for all the simulations. The measured variability of the soil hydraulic parameters is typical of what is generally observed within agricultural fields, with coefficients of variation ranging between 2.67 and 57.7%. The results of the agro-hydrological simulations are very different according to the climatic scenarios. For the dry 1990 and the wet 1998 agricultural seasons, the simulated cumulative actual transpiration range between 92.8 and 202.9 mm and between 132.8 and 198.3 with mean values of 166.9 mm and 182.68 respectively. The results show that the spatial variability of the simulated transpiration and crop yield increases progressively with the dryness of the agricultural season. From the wet 1998 to the very dry 1990 agricultural season, CV values increase from 7 to 14.6% and from 6.7 to 16% for the transpiration and the dry matter yield respectively. This means that the incomplete capture of the within-field variability of the soil hydraulic properties likely bias the field-scale estimations of the transpiration and the crop yields during dry years.

In a third step, all the simulations are rerun adjusting beforehand the water stress parameters according to three reference soil hydraulic conductivity values. Compared to the previous results, the "updated" mean actual transpiration values increase with +13%, +18% and +25% for 1998, 1999 and 1990 respectively. Such increases, progressively larger with the dryness of the year are also observed for the simulated dry matter yield alone. Concerning the simulated spatial variability, this one is now more limited (CV values range between 1.55 and 5.4%) but still increases systematically with the dryness of the considered climatic scenario. These results point out that the accurate estimation of water stress parameters is important for studies dealing with the impact of the soil hydraulic properties variability on the estimation of transpiration and dry matter yield. Furthermore, that emphasizes the importance of developing specific procedures allowing the estimation of soil specific water stress parameters.

Finally, we study using numerical simulations whether the simultaneous estimation of the soil hydraulic and the water stress parameters can be performed using measurements of transpiration and dry matter yield. By visual observations of 2D response surfaces, we show in all cases that there are strong interactions between the soil hydraulic and the water stress parameters. This clearly illustrates that the simultaneous estimation of a water stress and a soil hydraulic parameter is not sound. Such a calibration exercise, may lead to physical inconsistent water stress parameters. Consequently, the use of an agro-hydrological model in a stochastic mode for a vegetated surface requires alternative strategies for the specification of reliable water stress parameters.

Chapter 6

On the identification of macroscopic root water uptake parameters from soil water content observations

Abstract*

In this chapter, we analyze the identification problem of macroscopic root water uptake parameters from soil water content observations. For this study, the macroscopic root water uptake is considered to be linearly decreasing with depth with A and B parameters conditioning respectively the maximum root water uptake at the surface and the decreasing rate with depth. For identification of parameter A and B, two different identification approaches are tested using a detailed soil moisture data set consisting of vertical profiles measured with TDR and neutron probe on 28 locations within a small maize cropped field during a dry period of 24 days. The first approach is based on a simplified water balance while the second one uses an integrated soil water balance model in an inverse mode. Results of the simplified water balance show firstly that the root water uptake measured within the field is quite variable with CV ranging from 22 to 34% for respectively the root uptake parameters A and B. Furthermore, positive correlation between A and B suggests that low superficial root water uptake could be compensated by high deep root water uptake. Secondly, numerical simulations used to test the validity of this simplified approach show that the method is quite robust at least for a certain range of A parameter values ($0.008 < A < 0.013$), for B and for all

*adapted from Hupet, F., S. Lambot, M. Javaux, and M. Vanclooster, *Water Resources Research*, 38(12), 1300, doi:10.1029/2002WRR001556, 2002.

investigated differently textured soils, except the coarse sand. To investigate the feasibility and the robustness of the second approach, we address the problems of insensitivity, instability and non-uniqueness by means of numerical simulations. Results show, for soils with different textures, that the soil water content and in a lesser extent the time derivative of soil water content are quite insensitive to root water uptake parameters, at least compared to soil hydraulic parameters. Furthermore, instability analysis clearly illustrates that root water uptake parameters are quite and even very unstable with respect to small uncertainties on the apparently known parameters (e.g., soil parameters). Finally, results show that if root water uptake plus additional other parameters (e.g., soil parameters) are simultaneously optimized, non-uniqueness of parameter sets must be expected. Therefore a robust identification of root water uptake parameters by means of a full soil water balance model inversion is unlikely to be achieved during a dry period with soil water content observations at least when some other parameters driving the system, like soil hydraulic properties, are not error-free. In this context, further in depth research is needed to investigate if the use of longer periods characterized by both drying and redistribution events may increase the success of a full inversion. Finally, to extend the results of this study, we recommend to apply a similar analysis to other macroscopic conceptual root water uptake models.

6.1 Introduction

Modeling water fluxes through the soil-plant-atmosphere continuum at different scales is of paramount importance in hydrological sciences and engineering. A wide variety of models, varying in degree of sophistication and complexity, are presently available and applied in as well a research as an engineering context [*Dolman et al.*, 2001]. These models generally contain numerous distinct parameters characterizing different physical processes such as the flow of soil water, the crop growth and the transfer of water through the root-canopy system to the atmosphere. As the uptake of water in the root zone largely controls the fluxes in the soil-crop-atmosphere continuum [*Canadell et al.*, 1996], robust root water uptake models and parameterization schemes are definitely needed.

Root water uptake in a soil water balance model can be conceptualized by different approaches. Probably the most popular modeling approach in this context appeals on a macroscopic root water uptake model [*Whisler et al.*, 1968; *Feddes et al.*, 1978; *Molz*, 1981]. Using this approach, a depth dependent soil water sink term is defined which then is added to the soil water mass conservation equation. Examples of this approach are included in models like SWAP [*van Dam et al.*, 1997], HYDRUS [*Simunek et al.*, 1998a] or WAVE [*Vanclooster et al.*, 1996]. The depth dependent sink term may be represented by different root water uptake functions ranging from linear to nonlinear [see, e.g., *Raats*, 1974; *Hoogland et al.*, 1981; *Prasad*, 1988] and from 1-D to 3-D according to the considered dimensionality of the system [*Vrugt et al.*, 2001a].

The identification of the depth dependent macroscopic water uptake can be achieved in different ways. Adopting a direct approach, root water uptake can be obtained using sap flow measurements in local roots [see, e.g., *Green and Clothier*, 1999]. Unfortunately, direct methods are extremely laborious and only applicable at the local scale. The upscaling of the local model parameters to the scale of interest (e.g., the field scale, or the scale of a hydrological unit) is further complicated by the important spatial variability of the local system parameters. Therefore, the adoption of direct identification methods of root water parameters in larger scale assessments will contribute significantly to the modeling uncertainty.

As an alternative, root water uptake parameters can be indirectly inferred from soil water balance studies. Recently, quite some progress has been made in the experimental characterization of the soil water balance as new technologies for characterizing the soil water content at different spatial and temporal scales such as TDR, GPR or SAR becomes available [see, e.g., *Ulaby et al.*, 1996; *Huisman et al.*, 2001]. Given these advanced technologies, the quality of the soil water balance studies can now considerably be improved. Therefore, scope exists to improve also the estimates of the root water uptake parameters from soil water balance studies, hereby exploiting high spatial and temporal resolution soil water content observations.

Following the indirect approach, different levels of complexity can be adopted to establish the soil water balance and infer the root water uptake parameters. *Green and Clothier* [1995] and *Coelho and Or* [1996] for instance, used a simplified water balance approach, thereby neglecting the vertical soil water fluxes. With this approach the soil water depletion is only considered to be due to root water uptake, and measured soil water depletion curves allows the inference of macroscopic uptake parameters. This simplified water balance approach is attractive as it appeals only on the "direct available" soil water content observations. Unfortunately, this approach can only be applied during optimal periods characterized by a fully developed crop and by a dry period with high climatic demand long enough to avoid large vertical soil water fluxes to occur. Although this simplified procedure has been previously used, no attempt was done so far to test limitations of this approach and thereby characterizing the resulting errors on the estimated model parameters.

In a more elaborated way, a detailed integrated soil water balance model can be used in an inverse mode for identifying the unknown root water uptake parameters. This second approach is generally combined with an optimization algorithm allowing a more efficient identification of the unknown parameters. *Rasiah et al.* [1992] for instance optimized root water uptake functions (continuous vs. discontinuous) with two parameter estimation methods (linear vs. nonlinear). *Musters and Bouten* [1999] calibrated rooting depths of a forested stand; while *Vrugt et al.* [2001b] optimized simultaneously seven root water uptake and two soil hydraulic parameters. Notwithstanding these successful applications of the inverse method, some recent studies also illustrated the shortcomings of this approach. *Musters et al.* [2000] and *Musters and Bouten* [2000] presented results showing with the same data set that the soil water content dynamics was hardly affected by root water uptake parameters and that identifiability problems might arise for those parameters. The lack of identifiability using the more elaborated modeling procedure may have different quite interrelated causes. A first cause is the sensitivity of the soil water content to calibrated parameters. It is well known that the efficiency of parameter calibration can clearly be enhanced if the efforts are concentrated on those parameters to which the model simulation results are most sensitive [*Beven*, 2001]. In some cases, soil water content dynamics are not sensitive to root water uptake parameters as illustrated, e.g., by *Vogeler et al.* [2001] who showed that three different root water uptake functions did not significantly affect the soil water content profiles. A second cause of lack of identifiability is the stability of the calibrated parameters, in particular the change in the estimated parameters due to small errors in other model inputs. Indeed, the calibration of root water uptake parameters will depend on the other system parameters (e.g., the soil hydraulic functions). Small errors on these "known" parameters may result in large changes in the inferences of root water uptake parameters. A third cause situates in the non-uniqueness of calibrated parameters. Non-uniqueness is used here in the sense that similar fitting errors can be obtained with different parameters sets each within a physically reasonable range.

In order to elucidate some of these issues more in detail, we investigate in this chapter the robustness of different indirect root water uptake parameter identification procedures. For answering the central question if root water uptake parameters can be obtained in a robust indirect way from detailed soil water balance studies, and in particular from

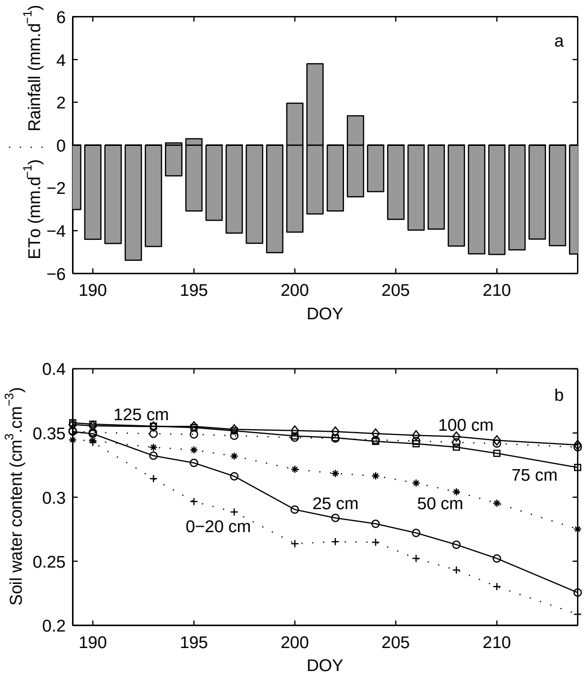

Figure 6.1. Time evolution of measured daily ETo (mm) and rainfall (mm) for the considered dry period (a) and of the mean soil water content measured within the field both with TDR (0-20 cm) and neutron probe for deeper depths (b).

direct soil water content observations obtained during a dry period, we apply the simplified water balance and the more elaborated inverse modeling approach on an available field data set to estimate the root water uptake parameters and associated uncertainty ranges. In this analysis, we address problems related to parameter insensitivity, instability and non-uniqueness. To generalize the results of this analysis beyond those obtained for the experimental field, numerical experiments were also run for five differently textured soils.

6.2 Material and methods

This chapter is based on the 1999 experimental setup and is focused more specifically on the first long dry period (July 1999, DOY 190-DOY 214) during which the two estimation methods are tested. In this chapter, we use the soil water content data set presented in Chapter 2. Fig. 6.1a shows the time evolution of measured daily ETo (mm) and rainfall (mm) for the considered dry period (DOY 190-214). Fig. 6.1b presents for the same period the mean soil water content measured within the field both with TDR (0-20 cm) and neutron probe (25, 50, 75, 100 and 125 cm depth). To investigate the instability and non-uniqueness problems, we used the WAVE model with the RWU conceptualization of *Hoogland et al.* [1981].

6.2.1 Parameter estimation methods

The simplified water balance method

This method consists in determining the root water extraction at different depths on the basis of a simplified water balance neglecting the vertical soil water fluxes, considering therefore that all soil water depletion is due to water uptake by plant roots [see, e.g., *Rasiah et al.*, 1992; *Musters et al.*, 2000]. This approach was adopted for our field data set for the period between the 9^{th} of July and the 2^{nd} of August as this period matches exactly all the conditions previously specified maximizing the success of this method. A simplified water balance was applied on each of the 28 points for the 6 depths (0-20, 25, 50, 75, 100 and 125-cm) for 8 different 3 days periods corresponding to the frequency of soil water content measurements. The integrated soil water depletion measured between 0 and 20 cm depth was considered to be representative of the root water uptake at 10 cm. Afterwards, as in the study of *Elhers et al.* [1991], the maximum value for each depth and each point was taken as the maximum root water extraction. A linear regression was then applied on these measured maximum root water extraction values resulting in 28 sets of A and B parameters conditioning the S_{max} function of the RWU parameterization of *Hoogland et al.* [1981]. Note that the fitting used only the first 4 depths (0-20, 25, 50, 75-cm) as different numerical simulations run with various root water uptake parameters showed that root water extraction was non-existent or negligible below 85 cm for the period under consideration. This is furthermore confirmed by literature on maize root activity [e.g., *Girardin*, 1999].

To derive the parameter uncertainty errors associated with the simplified water balance approach, Monte Carlo simulations were carried out with the detailed WAVE model parameterized with a set of "true" root water uptake parameters, generating plausible sets of soil water content, which subsequently were analyzed with the simplified water balance approach to identify "back-calculated" root uptake parameters. The Monte Carlo runs with WAVE were executed for similar boundary conditions as those encountered within the field, i.e., initial profile at field capacity; measured ETo and rainfall as upper boundary conditions; and free drainage at 135 cm depth as lower boundary condition. Measured crop size (LAI) and measured soil hydraulic properties averaged for the whole field and parameters derived from literature used for these numerical simulations are summarized in Table 6.1. Hundred simulations were run for different linear root water extraction functions randomly generated between the range of those obtained with the simplified water balance method within the field ($0.008 < \mathrm{A} < 0.019$ d^{-1}, $0.000043 < \mathrm{B} < 0.00022$ d^{-1}cm^{-1}). To avoid some bias, correlation between A and B parameters was neglected and A and B distributions were considered uniform in the random procedure generating the root water extraction functions. Then, on the basis of the soil water content simulated in each run, we used the above-described methodology based on the simplified water balance to determine A and B parameter values. This resulted therefore in a set of 100 "true" and "back-calculated" A and B parameters. For the simplified water balance applied on the simulated soil water content, we also used a time lag of three days (as the time lag used for the field measurements) and depths 0-20, 25, 50 and 75 cm (as the measurement depths for the field measurements), so as to correspond closely to the methodology adopted for the field data set. Subsequently, we quantified the error on the root water uptake function associated to the use of the simplified water balance methodology by comparing "true" and "back-calculated" A and B parameter values. Error ranges for A and B were calculated as follows [*Janssen and Heuberger*, 1995]:

$$RMSE = \sqrt{\frac{\sum_{i=1}^{N}(O_i - P_i)^2}{N}} \tag{6.1}$$

$$NRMSE = \frac{RMSE}{\overline{O}} \tag{6.2}$$

with $RMSE$ the root mean squared error; O_i and P_i respectively the observations ("true" values used for the simulations) and the predictions ("back-calculated" values); N the number of observations; $NRMSE$ the normalized $RMSE$; $\overline{O}$ the mean of the observations. Furthermore, to extend the results of the study, numerical experiments were run also for similar conditions for five differently textured soils with contrasting hydraulic properties (see Table 6.2) [*Wösten et al.*, 1998]. Finally, some additional simulations were run for more intensive spatial sampling strategies of soil water contents (e.g., each 5 cm between the soil surface and 75 cm depth) to explore if better results might be obtained for these conditions.

Table 6.1. Plant and soil parameters required for a Wave simulation run during the selected period. Parameter values (*) are mean measured for the experimental field. Other parameter values are derived from literature

	Reference value		Reference value
Plant parameters		Soil parameters	
A^* (d^{-1})	0.0123	θ_r^* (cm^3 cm^{-3})	0.000
B^* ($d^{-1}cm^{-1}$)	0.000118	θ_s^* (cm^3 cm^{-3})	0.392
RD (cm) rooting depth	100^a	α^* (cm^{-1})	0.003
c (-)	0.6^b	$n^*(-)$	1.22
LAI^* (-)	3.67	λ (-)	0.5^d
K_c crop factor (-)	1.1^a	K_{sat}^* (cm d^{-1})	5
h_1(cm)	-15^c		
h_2(cm)	-30^c		
h_{3l}(cm)	-600^c		
h_{3h}(cm)	-325^c		
h_4(cm)	-8000^c		
a *Girardin* [1999]	b *Belmans et al.* [1983]	c *Wesseling* [1991]	d *Mualem* [1976]

The inverse method

The inverse method consists of combining the detailed soil water balance model with an appropriate optimization algorithm to identify directly the unknown root water uptake parameters from soil water content data. To address the insensitivity, instability and non-uniqueness problems associated with this approach we performed in a first step a thorough sensitivity analysis for all plant and soil parameters involved in the model simulations for the very dry period 9 July through 2 August. For the sensitivity analysis, simulations were run with the "field" boundary conditions (measured ETo and rainfall as upper and free drainage at 135 cm depth as lower) and with the soil and plant parameters summarized in Table 6.1. We analyzed the sensitivity of both the soil water content and the time derivative of soil water content to all parameters. The analysis on the time derivative of the soil water content was performed to be consistent with the simplified water balance approach. In this latter method, soil moisture storage changes are used to infer the root water uptake parameters.

Table 6.2. Hydraulic properties for the 5 different European soils [*Wösten et al.*, 1998] used for the numerical experiments.

	θ_r	θ_s	α	n	λ	K_{sat}
coarse	0.025	0.366	0.043	1.5206	1.2500	70.00
medium	0.010	0.392	0.0249	1.1689	-0.743	10.75
medium-fine	0.010	0.412	0.0082	1.2179	0.5000	4.000
fine	0.010	0.481	0.0198	1.0861	-3.712	8.500
very fine	0.010	0.538	0.0168	1.073	0.0001	8.235

Sensitivity coefficients $\Omega(z,t,p)$ were determined for each day (09/07-02/08) and each depth (0 to -135 cm) according to *Simunek et al.* [1998b]:

$$\Omega_\theta(z,t,p_j) = (\theta(p + \Delta p\boldsymbol{e}_j) - \theta(p))100 \tag{6.3}$$

$$\Omega_{\Delta\theta}(z,t,p_j) = (\Delta\theta(p + \Delta p\boldsymbol{e}_j) - \Delta\theta(p))100 \tag{6.4}$$

with $\Omega_\theta(z,t,p_j)$ and $\Omega_{\Delta\theta}(z,t,p_j)$ the change of the variable θ and $\Delta\theta$ corresponding to a 1% change in parameter p_j; $\mathbf{e}_j$ the j^{th} unit vector; Δp=0.01p. Sensitivity coefficients are multiplied in Eq. (6.3) and (6.4) by 100 to avoid too small numbers. This formulation of the sensitivity coefficients allows a comparison of the sensitivities to different parameters, independent of the invoked units or their absolute values. Note that in Eq. (6.4) $\Delta\theta$ values are calculated by difference of soil water contents "measured" with a time lag of one day. To extend the results of this study, the sensitivity analysis was performed also for the 5 differently textured soils as described in Table 6.2. In addition, we investigated the instability of the identified parameters (A and B) due to uncertainties on other parameters required for the soil water balance simulations (e.g., soil parameters). To identify the two target parameters A and B, modelers can either fix all other parameters to measured values and optimize the only two desired parameters (first case) or optimize the same two but considering uncertainties on the fixed parameters (second case). For stable solutions, both cases must lead to similar results. For the first case, a first numerical experiment generating time series of daily "measured" soil water content with depth increments of 5 cm was run for the period between the 9^{th} of July and the 2^{nd} of August with the previously described boundary conditions and specified parameters (see Table 6.1). The parameters A and B were subsequently perturbed around their true values (respectively 0.0123 d^{-1} and 0.000118 $d^{-1}cm^{-1}$) keeping all the other parameters constant, and the following objective function in the

A, B parameter space was calculated :

$$OF_\theta = \left[\frac{1}{ij} \sum_i \sum_j \left[\theta^*(z_i, t_i) - \theta(z_i, t_i, p) \right]^2 \right]^{0.5} \tag{6.5}$$

with $\theta^*(z_i, t_i)$ the "measured" soil water content at depth z_j and time t_i; $\theta(z_i, t_i, p)$ the simulated soil water content at depth z_j and time t_i given the parameter vector p. The objective function was calculated for 2500 points, each two parameter domain being discretized into 50 discrete points. For the second case, we applied the same procedure but instead of considering all other parameters constant at the value used in the first numerical run, a small random error on the 4 distinct parameters (K_c, θ_s, n, K_{sat}) was added on each of the 2500 simulations. The range of assigned random error was chosen to correspond closely to typical values occurring in laboratory or in-situ field experiments (Table 6.3). Two-dimensional response surfaces for A and B parameters were generated for randomly generated parameters. Afterwards, the instability problem was investigated by visual inspection of the response surfaces as done by *Russo et al.* [1991]. To be consistent with the simplified water balance approach, the stability analysis was also performed on the time derivative of the soil water content. In this case the objective function for the parameter estimation yields:

$$OF_{\Delta\theta} = \left[\frac{1}{ij} \sum_i \sum_j \left[\Delta\theta^*(z_i, t_i) - \Delta\theta(z_i, t_i, p) \right]^2 \right]^{0.5} \tag{6.6}$$

with $\Delta\theta^*(z_i, t_i)$ the 'measured' soil water content difference between t_i and t_{i-1} at depth z_j; $\Delta\theta(z_i, t_i, p)$ the simulated soil water content difference between t_i and t_{i-1} at depth z_j given the parameter vector p. Note that instability of identified A and B parameters due to measurement errors on soil water content was not investigated in this study. Finally, we investigated the problem of non-uniqueness by means of a MonteCarlo analysis. A first reference numerical experiment (similar to the first one used in the instability analysis) generated time series of daily soil water content with a 5 cm depth increment. Subsequently, we ran 20.000 simulations with different parameter sets chosen randomly by uniform sampling across the ranges of each parameter space (Table 6.3). For each run, we calculated the value of the objective function given by Eq. (6.5) with respect to the reference run. Subsequently, uniqueness of the identification problem was evaluated as in *Franks et al.* [1997] in terms of 2-D scatter plots showing the range of calculated OF values produced

Table 6.3. Parameter ranges for Monte Carlo simulations used to address the problem of instability and non-uniqueness.

Parameter	Range
A (d^{-1})	0.00088 - 0.019
B ($d^{-1}cm^{-1}$)	0.000044 - 0.000143
K_c (-)	1-1.2
n (-)	1.15-1.25
K_{sat} (cm d^{-1})	1-10
θ_s (cm^3 cm^{-3})	0.382 - 0.402

across model parameter ranges. Five additional Monte Carlo analysis were also performed for the 5 different soils listed in Table 6.2. These were run for similar boundary conditions with the same 6 unknown parameters and with the range of uncertainties for soil parameters (θ_s, n, K_{sat}) similar as those presented in Table 6.3. As for the sensitivity and instability analysis, non-uniqueness problem was also investigated with $OF_{\Delta\theta}$ expressed as of function of the time derivative of the soil water content (Eq. (6.6)).

6.3 Results and discussions

6.3.1 Simplified water balance method

The maximum soil water depletion measured at each depth on each of the 28 sites is illustrated in Fig. 6.2a. Considering that these measured soil water depletions are representative for the maximum root water extraction, at least for the superficial layers, we observe a relatively large spatial variability with coefficient of variation (CV) ranging between 27 and 33%. This root water uptake variability within the field may probably be explained by a variable root growth linked to some extent to the variable growth of the areal parts of the plant (measured LAI ranging between 2.55 and 4.32). Indeed, as it can be seen from Fig. 6.3, there is a correlation (though poorly defined, r^2=0.38) between the measured LAI and the soil water depletion (i.e. the root water uptake) for the considered dry period. As explained previously, only the values from the 4 most superficial depths (10-25-50-75 cm in Fig. 6.2a) were used to derive the A and B parameter values. The adopted linear relation seemed in most cases very well adapted for the 28 locations with r^2 ranging from 0.55 to 0.99 but with most of them being superior to 0.8. The 28 mea-

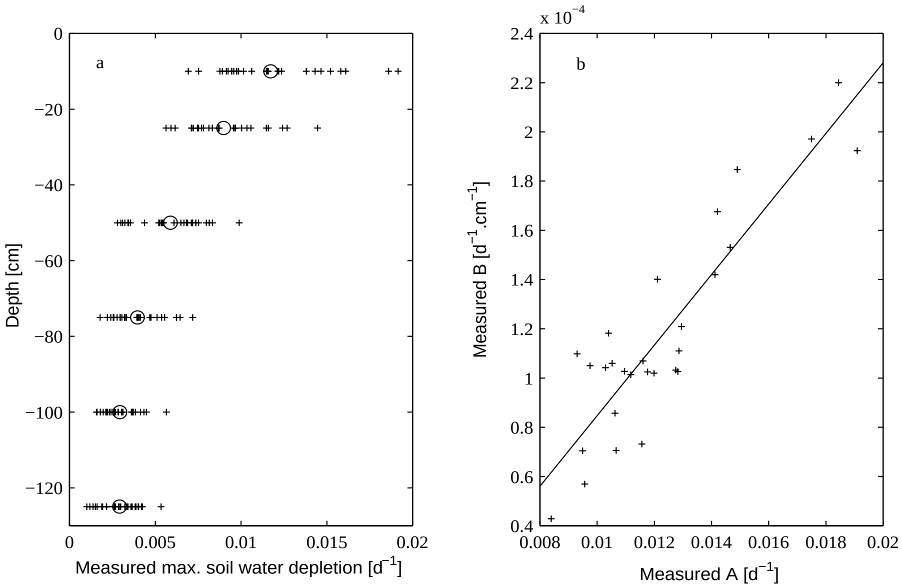

Figure 6.2. This figure shows maximum measured soil water depletion for each of the 28 points for six depths (10-25-50-75-100 and 125 cm). Circles indicate the mean for each depth. Fig. b illustrates correlation between A and B coefficients (r^2=0.81).

sured sets of A and B parameter values are shown in Fig. 6.2b. Mean values and CV are respectively 0.0123 d^{-1} and 0.000118 d^{-1}cm^{-1} and 22 and 34%. The A parameter mean value is very similar to the 0.013 d^{-1} value measured by *Allmaras et al.* [1975] but, unlike our observations, these authors found also root water extraction of 0.013 d^{-1} at 100 cm depth. In addition to the spatial variability, Fig. 6.2b reveals a good positive correlation ($r^2 = 0.81$) between A and B suggesting that low superficial root water uptakes was compensated by a higher uptake deeper in the profile. The above mentioned observations are subjected to the validity of the simplified water balance methodology to derive A and B. Table 6.4 presents results of the validity test. The root mean square error ($RMSE$) and normalized $RMSE$ ($NRMSE$) characterize the difference between the "true" and the back-calculated A and B values for two different measurement strategies. The first strategy corresponds to that used during the field experiment, while the second considers theoretical sampling on a 5 cm depth distance grid. Results obtained for the soil of the experimental field are not shown in this table as they are very similar to those of the medium-fine textured soil. We observe in Table 6.4 that the $RMSE$ and $NRMSE$ are relatively similar for all

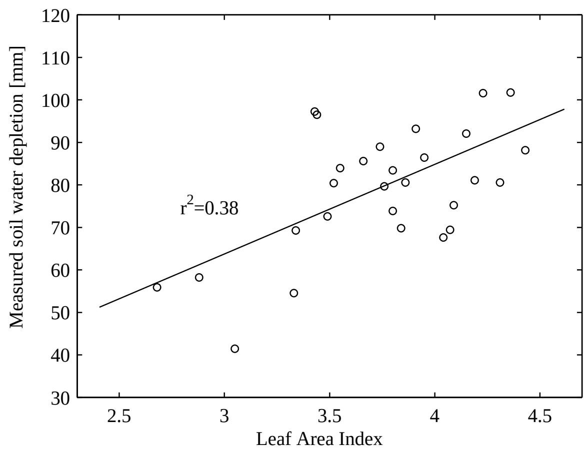

Figure 6.3. Relationship between measured Leaf Area Index and soil water depletion measured for the considered dry period. Each dot represents one of the 28 sampling locations.

soils except for the coarse textured soil for which very large errors on the B parameter are observed with $NRMSE$ values for the two measurement strategies of respectively 0.85 and 0.76. It is worth to note that in general B parameters were well estimated except for S_{max} functions with large A values combined with small B values (or the opposite). For our experimental field conditions (i.e. medium-fine textured soil and soil water content measured at 4 depths), the B parameter is very well estimated with a $NRMSE$ of 0.061. On the other hand, the $NRMSE$ of A is much larger with a value of 0.32. Nevertheless, Fig. 6.4a shows clearly that the magnitude of the error depends strongly on the value of the A parameter. Indeed, adopting the simplified water balance method leads only to slight underestimations ($\pm$ 0.002 d^{-1}) of A for "true" parameter values smaller than 0.013 d^{-1}, and somewhat larger underestimations ($\pm$ 0.005 d^{-1}) for larger values. As in this study most of the measured A parameters are smaller than 0.013, we accept the simplified water balance approach as quite reliable. Note that the back-calculated values for A are systematically lower than the true values because our method does not compensate for capillary rise. Fig. 6.4b illustrates typical results obtained for a numerical run carried out for the medium-fine textured soil for a mean root water extraction function (A=0.013 d^{-1}, B=0.000118 d^{-1}cm^{-1}) with the measurement strategy used in the experimental field. We observe the close agreements between the "true" and the estimated root water uptake function. This figure shows also the back-calculated

Table 6.4. Root mean squared error (RMSE) and normalized RMSE (NRMSE) between "true" and back-calculated A and B parameters for two different measurement strategies. Bold values characterize errors for the adopted measurement strategy and soil of the experimental field.

Measurement strategy	coarse	medium	medium-fine	fine	very fine
Field					
(0-20, 25, 50, 75 cm)					
RMSE A	$3.62\ 10^{-3}$	$2.35\ 10^{-3}$	$\mathbf{3.2\ 10^{-3}}$	$2.95\ 10^{-3}$	$3.5\ 10^{-3}$
NRMSE A	0.3511	0.209	**0.32**	0.278	0.355
RMSE B	$6.9\ 10^{-5}$	$6\ 10^{-6}$	$\mathbf{6\ 10^{-6}}$	$5\ 10^{-6}$	$6\ 10^{-6}$
NRMSE B	0.85	0.054	**0.061**	0.052	0.064
Each 5 cm					
RMSE A	$2.88\ 10^{-3}$	$2.2\ 10^{-3}$	$3.1\ 10^{-3}$	$2.9\ 10^{-3}$	$3.1\ 10^{-3}$
NRMSE A	0.2766	0.203	0.309	0.279	0.321
RMSE B	$6.7\ 10^{-5}$	$8\ 10^{-6}$	$6\ 10^{-6}$	$5\ 10^{-6}$	$3.9\ 10^{-5}$
NRMSE B	0.76	0.067	0.0609	0.057	0.3388

S_{max} values below the maximum depth at which root water extraction takes place (80 cm). The origin of these apparent extraction values is the capillary rise or drainage component considered in the full model which is not considered in the simplified approach. The very good correspondence between Fig. 6.4b and Fig. 6.2a confirms further the choice of taking only the first 4 depths for fitting A and B parameter values. The results of the more intensive measurement strategy (e.g., available soil water measurement for each 5 cm depth increment) do not show significant improvements (Table 6.4). A and B parameter estimations are quite similar except for the very fine textured soil for which a better estimation of A and worse estimation of B are obtained.

6.3.2 The inverse method

Some results of the sensitivity analysis are illustrated in Fig. 6.5. This figure shows the space and time distribution of the absolute sensitivity of three plant parameters (K_c (graphs a-d), A (b-e) and B (c-f)) for the medium-fine textured soil corresponding very closely to our experimental field soil. Left graphs (a-b-c) correspond to sensitivity coefficients (SC) calculated with Eq. (6.3), i.e. $\Omega_\theta(z,t,p_j)$, while the right graphs evaluates Eq. (6.4), i.e. $\Omega_{\Delta\theta}(z,t,p_j)$. On the left graphs (a-b-c) of this figure, we observe that the sensitivity of soil water content to the crop

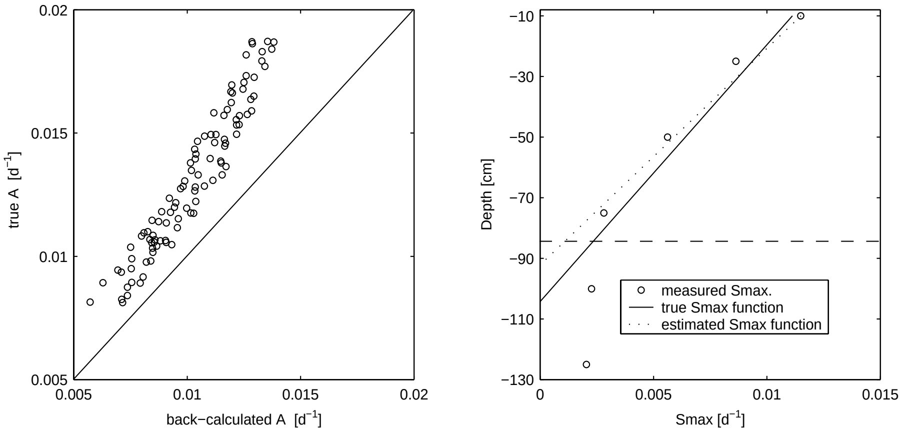

Figure 6.4. Relation between "true" and back-calculated A parameter values derived for medium-fine textured soil are displayed on the left graph. Right graph shows true root water extraction function used for the numerical run (A=0.0123 d^{-1}, B=0.000118 d^{-1}cm^{-1}), "measured" S_{max} for the different depths and estimated S_{max} function with the simplified water balance method.

parameters is much higher in the topsoil (>-0.6 m) than in the deeper layers which is clearly not surprising as the parameters controlling root water uptake act mainly on the superficial soil layers. At intermediate depths sensitivity coefficients increase substantially with time as the superficial soil layers dry out. Sensitivity coefficients of other plant parameters exhibit a similar temporal behavior (results not shown). These results suggest that soil water contents of the superficial layers contain obviously the most valuable information to identify crop parameters. Similar findings were already presented by *Musters and Bouten* [2000] showing that the optimal location of only one soil water content sensor to calibrate a root water uptake model lies within the active root zone. The soil parameters have a much more pronounced effect on the soil water content than the crop (see Table 6.5) and they affect also water content deeper in the soil profile. On the right graphs of Fig. 6.5 (d-e-f), we observe spatio-temporal patterns of $\Omega_{\Delta\theta}$ values which are quite different than those obtained for Ω_{θ}. Indeed, these patterns are characterized by some very high values generally situated at the bottom of the maximum root water uptake depth. Note that this is a direct consequence of the chosen conceptualization for root water uptake. The $\Omega_{\Delta\theta}$ values calculated within the root zone generally range between one or even two orders of magnitude which is completely different to what was observed for Ω_{θ}. The patterns for $\Omega_{\Delta\theta}$ implicitly suggest that some spe-

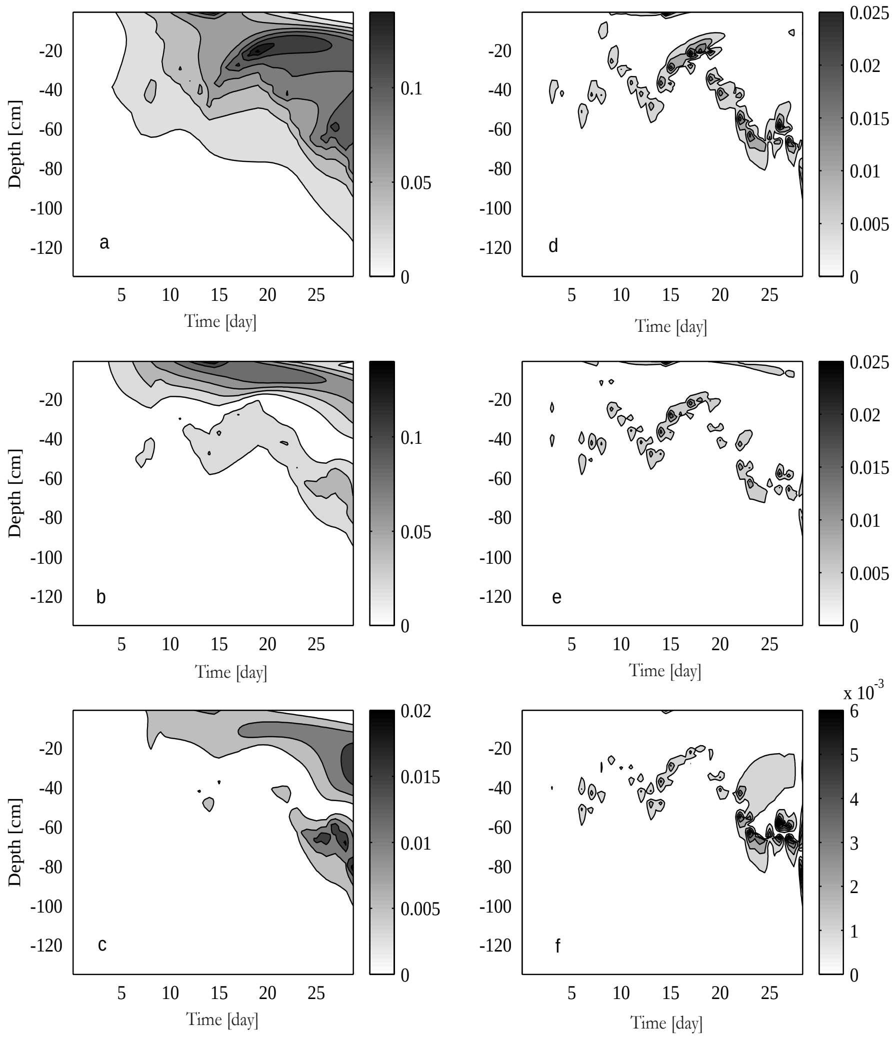

Figure 6.5. Space and time evolution of the absolute value of the sensitivity coefficients calculated with Eq. (6.3) (left graphs) and Eq. (6.4) (right graphs) illustrated for three crop parameters, i.e. K_c (a-d), A (b-e) and B (c-f). Note that shadings are different across figures a through f and that white zones in each graph are representative of small but non zero values.

cific depths contain much more information than other depths at least for the identification of root water uptake parameters. Relatively similar spatio-temporal patterns of SC (not shown) were also obtained for the numerical simulations for the 5 other evaluated soils. Table 6.5 summarizes time and depth-averaged absolute sensitivity coefficients calculated with both approach ($\Omega_{\Delta\theta}$ and Ω_{θ}) for soil and selected plant parameters calculated for the dry period between the 9^{th} of July and the 2^{nd} of August. Results are presented for the coarse, medium-fine and very fine textured soils. Sensitivity coefficients for the experimental field soil are not shown as they are very similar to those obtained for the medium-fine textured soil. This table shows that time and depth-averaged absolute sensitivity of soil water content (Ω_{θ}) to some soil parameters, i.e. θ_s and n is much larger (an order of magnitude) than to the root water uptake parameters. These results suggest therefore that even during a very dry period for which sensitivity for root water uptake is intuitively assumed to be at a maximum, soil water content dynamics is still much controlled by some soil parameters. Such a finding, yet not quantified by a classical sensitivity analysis, is similar to that presented by *Gardner* [1991] suggesting that the dominant factor in the uptake calculations is the non-linear water retention curve, and by *Musters et al.* [2000] showing that the uncertainties in plant uptake parameters and those in root distribution hardly affect simulated soil water content dynamics. Other soil parameters (α, K_{sat}, θ_r, λ) have a similar or smaller influence on the soil water content than root water uptake parameters. Note the increasing and decreasing importance of respectively θ_s and n and θ_r, λ and K_{sat} when moving from a coarse to a very fine textured soil. Table 6.5 also shows that compared to other textured soils, medium fine textured soils (as the experimental field soil) are relatively unfavourable for the determination of A and B parameters as the sensitivity is at its minimum. Sensitivity coefficients of other crop parameters (e.g., h_2, h_4, c) are not presented in Table 6.5 since these are lower than those obtained for K_c, A and B parameters. Table 6.5 also presents the time and depth-averaged absolute sensitivity of the time derivative of soil water content $\Omega_{\Delta\theta}$ to soil and selected plant parameters. Notice in Table 6.5 that $\Omega_{\Delta\theta}$ for soil hydraulic parameters is still larger than those for crop parameters but that the sensitivity of the time derivative of soil water content to crop parameters is a little bit exacerbated. To underline this, we calculated the ratio between the two different SC ($\Omega_{\theta}/\Omega_{\Delta\theta}$) allowing us to investigate the relative sensitivity to the different parameters within the two approaches. We observed for all soils that the ratio for A and B parameter is around 10 whereas this ratio equals 20, 30 or even 40 for some soils and for soil hydraulic parameters.

Table 6.5. Time and depth-averaged absolute sensitivity coefficients of the soil water content (Ω_θ) and of the time derivative of soil water content ($\Omega_{\Delta\theta}$) to soil and plant parameters. The ratios between the two sensitivity coefficients ($\Omega_\theta/\Omega_{\Delta\theta}$) are also presented to compare the relative sensitivity to the different parameters within the two approaches.

	Coarse			Medium fine			Very fine		
	Ω_θ	$\Omega_{\Delta\theta}$	$\Omega_\theta/\Omega_{\Delta\theta}$	Ω_θ	$\Omega_{\Delta\theta}$	$\Omega_\theta/\Omega_{\Delta\theta}$	Ω_θ	$\Omega_{\Delta\theta}$	$\Omega_\theta/\Omega_{\Delta\theta}$
Soil parameters									
θ_r	0.0067	$3.1\ 10^{-4}$	21.61	$4\ 10^{-4}$	$3\ 10^{-5}$	13.33	$4.9\ 10^{-4}$	$4.8\ 10^{-5}$	10.20
θ_s	0.095	0.003	31.66	0.155	0.005	31	0.394	0.018	21.88
α	0.022	0.0013	16.92	0.0095	$4.2\ 10^{-4}$	22.619	0.021	0.0014	15
n	0.107	0.0047	22.76	0.137	0.0065	21.077	0.304	0.026	11.69
λ	0.011	$3\ 10^{-4}$	36.66	$8\ 10^{-4}$	$4.4\ 10^{-5}$	18.182	$4.5\ 10^{-9}$	$2.4\ 10^{-9}$	1.87
K_{sat}	0.016	$4\ 10^{-4}$	40	0.011	$3.9\ 10^{-4}$	28.205	0.0064	$2.6\ 10^{-4}$	24.61
Plant parameters									
K_c	0.015	0.0011	13.63	0.0301	0.0017	17.706	0.0104	0.001	10.4
A	0.022	0.0021	10.47	0.0169	0.0015	11.267	0.0214	0.0018	11.88
B	0.0067	$6.2\ 10^{-4}$	10.80	0.0047	$3.6\ 10^{-4}$	13.056	0.00729	$6.8\ 10^{-4}$	10.72

This clearly put forward that compared to the sensitivity of the soil water content to root water uptake parameters the sensitivity of the time derivative of soil water content is exacerbated and the sensitivity to the soil hydraulic parameters is attenuated. We should note however that those coefficients are depth and time averaged what can be very misleading. Indeed, it has been shown above that $\Omega_{\Delta\theta}$ calculated for root water uptake parameters may take very large values at some very specific depths. It is therefore obvious that ignoring those depths in the calculation of the SC can have a large impact on the resulting calculated $\Omega_{\Delta\theta}$. As a conclusion, this sensitivity analysis shows that soil water content is quite insensitive to crop parameters, in particular root water uptake parameters, at least as compared to other parameters (i.e. soil hydraulic parameters) even during an optimal dry period. This analysis also shows that the time derivative of the soil water content is, as compared to the soil water content itself, more sensitive to root water uptake parameters, although the sensitivity coefficients for soil hydraulic parameters are still larger than those for root water uptake parameters. This suggests implicitly that for identifying root water uptake parameters during a dry period by means of an inverse modeling approach, it is probably more judicious to define the objective function in terms of the time derivative of soil water content instead of the soil water content itself at least if depths rich in information are taken into account.

As mentioned before, instability of the identification problem was investigated by visual inspection of two-dimensional response surfaces of OF_θ and $OF_{\Delta\theta}$, calculated respectively with Eq. (6.5) and (6.6) for different A and B parameter values. Surface responses are drawn as the OF logarithm for a better visualization of the surface topography. Six different response surfaces are displayed, two for the reference case (K_{sat}=5, n=1.2, θ_s=0.392, K_c=1.1) and four for randomly selected generated parameters. Fig. 6.6a and b shows the response surfaces for the reference case for respectively OF_θ and $OF_{\Delta\theta}$ We observe in both cases that the minimum is well located around the true parameter values (A= 0.0123 d^{-1} and B= 0.000118 d^{-1}cm^{-1}). Note in Fig. 6.6b that the surface response is steeper than that of Fig. 6.6a which is a direct consequence of the larger sensitivity of the time derivative of soil water content to root water uptake parameters. Fig. 6.6c to f illustrate response surfaces for cases where a small randomly generated error was added on K_{sat}, n, θ_s and K_c. In Fig. 6.6b and e (K_{sat}=9, n=1.17, θ_s=0.402, K_c=1.18), we observe that the minimum remains well defined but situates no longer in the neighborhood of the true A and B parameters. Fig. 6.6c and f illustrate an other case for which small perturbations were generated on some apparently known parameters (K_{sat}=2, n=1.25,

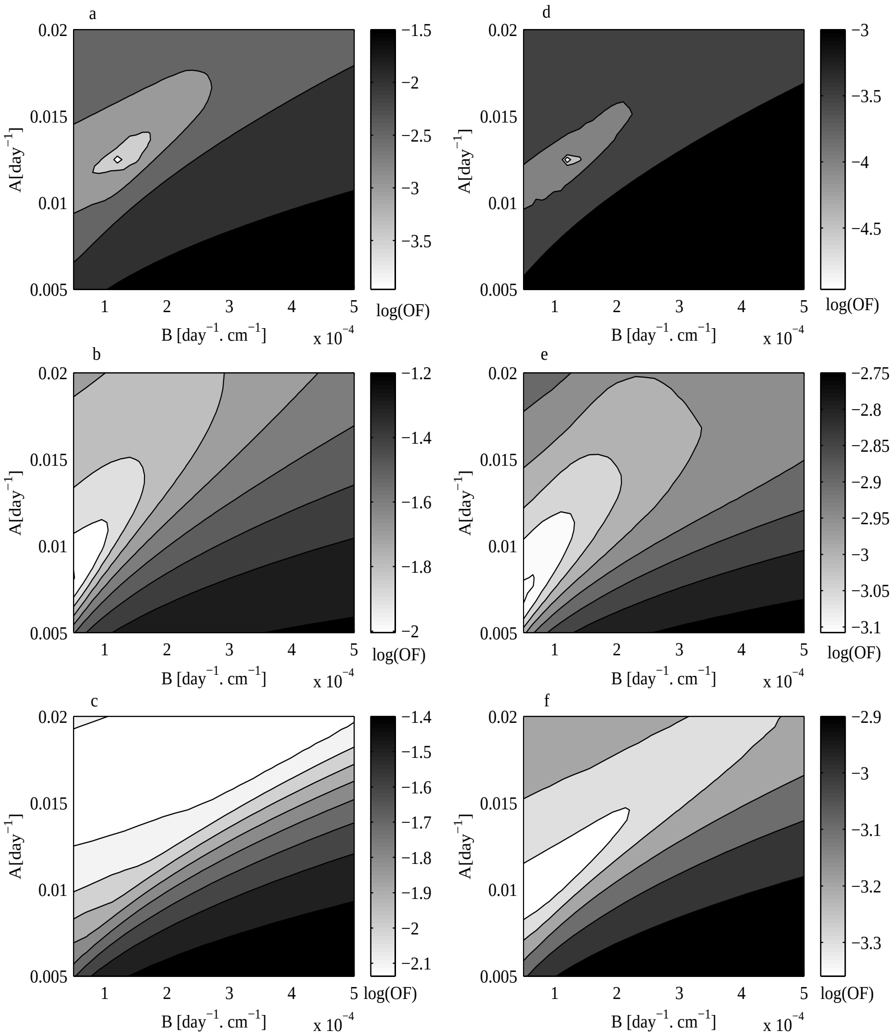

Figure 6.6. Response surfaces of the objective function logarithm as a function of A and B parameter values (true values are respectively 0.0123 d^{-1} and 0.000118 $d^{-1}cm^{-1}$). Left graphs (a-b-c) show response surfaces of OF_θ , right graphs those of $OF_{\Delta\theta}$. Instability problems are displayed in Fig 6b and e (K_{sat}=9, n=1.17, θ_s= 0.402, K_c=1.18) and in Fig. 6c and f (K_{sat}=2, n=1.25, θ_s= 0.384, K_c=1.03) with respect to the reference run illustrated in Fig. 6a and d (K_{sat}=5, n=1.2, θ_s= 0.392, K_c=1.1).

θ_s=0.384, K_c=1.03). Fig. 6.6c represents a quite extreme situation for which the response surface becomes markedly different compared to the reference case (Fig. 6.6a). In this case, the minimum is no longer situated in the neighborhood of the true parameter values. Moreover, the shape of the response surface suggests that a well-defined minimum is probably not existent. In Fig. 6.6f, we observe that the response surface is less sensitive to the perturbation of the apparently known parameters, though the flat response surface around the minimum suggests that identification problems persist. Note that similar results (not shown here) were obtained with different textured soils. This analysis shows that optimized root water uptake parameters are very unstable with respect to small uncertainties on the apparently known parameters (e.g., soil parameters). However, this instability seems to be less marked for OF calculated using the time derivative of the soil water content. The instability arises directly from the relative insensitivity of root water uptake parameters compared to other parameters. Therefore optimizing root water uptake parameters during a dry period is not commendable. Indeed, irrespective of the optimization algorithm used, the inversion will lead to significant different estimates of A and B parameter values even if small errors on some other system parameters are explicitly accounted for. It should be worth noting here that the instability problem clearly depends on the magnitude of the error on some "fixed" parameters. In this context, more in depth research is needed to assess the range of error on e.g. soil hydraulic parameters that can be accepted to obtain a robust estimation of root water uptake parameters through inversion.

The unicity of the identification problem was examined as done by *Franks et al.* [1997] by means of a visual inspection of scatter plots showing objective function values (OF) obtained across model parameter ranges. Notice that OF function values were obtained with a Monte Carlo analysis with respect to a reference numerical run; each dot represents one run of the model. Fig. 6.7 shows the range of OF_θ obtained across the range of three parameters (A, B and θ_s). From this figure, it can be seen that very small OF_θ values are produced in all areas of the parameter space. Same behavior (not shown here) was observed for the three other free parameters (K_c, K_{sat}, n). These results suggest that a global minimum is probably not well defined as very good fits can be achieved in the whole parameter space. As the OF is expressed as a root mean square error, it is quite simple to select "acceptable" parameter sets corresponding to OF_θ values smaller than a fixed threshold value. If this threshold value is fixed to 0.005, corresponding for example to small measurement errors, accepted parameter sets will still range across the whole specified parameter space explored during Monte Carlo analysis.

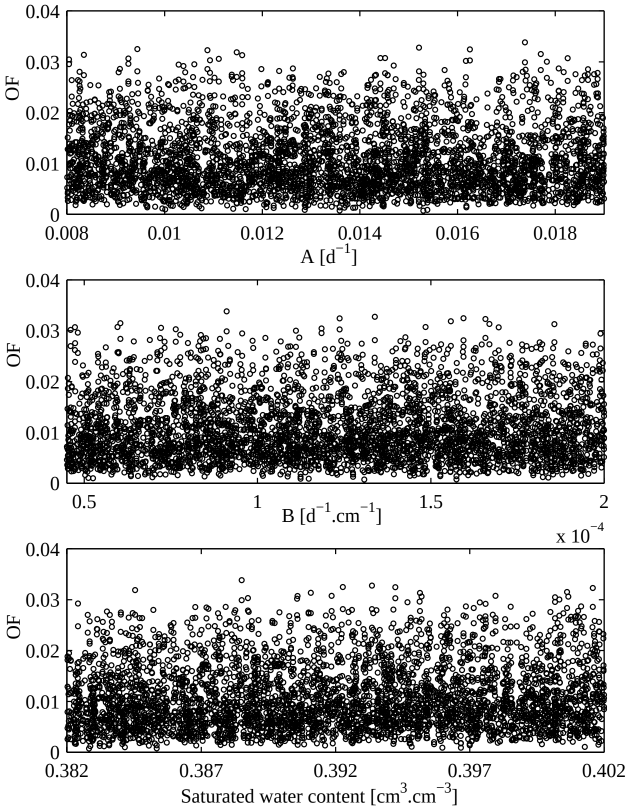

Figure 6.7. Scatter plot showing the range of objective function values (OF_θ) calculated by Eq. (6.5) across three model parameter space (A, B and θ_s). Similar results were obtained for the three other parameters (n, K_c, K_{sat}). Note that all these results are derived from numerical experiments.

Similar results were previously presented by *Musters et al.* [2000] for identification of five parameters of a forested ecosystem. Furthermore, it is also worth noting that increasing the threshold value to 0.01 will even not result into a large range of plausible parameter values. Additional Monte Carlo analysis performed for other different textured soil present exactly the same results (not shown here). This approach was also tested for $OF_{\Delta\theta}$ calculated with Eq. (6.6) and similar results were obtained. In summary, the results derived from numerical experiments strongly suggest that identification of root water uptake parameters plus some other parameters (e.g., soil parameters) will lead significant uniqueness problems. Indeed, very good fits may be achieved in the whole parameter space. This is in fact not so surprising as a dry period, such as the one considered in our study, characterized by a gradually decreasing water content time series (see Fig. 6.1b), does not contain sufficient information to identify too many parameters through model inversion. Note that all the results presented for the instability and non-uniqueness analysis were obtained considering that soil water content was measured daily with a depth increment of 5 cm between the surface and 135 cm depth. This is in fact a very optimal case in terms of experimental design.

6.4 Conclusions

The technology for monitoring soil water content with a high temporal and spatial resolution measurement frequency is now available and is adopted to identify macroscopic root water uptake parameters within integrated soil water balance models. Although recent studies clearly put forward the limitations of optimizing the root water uptake parameters from soil water content measurements by inverse modeling [see, e.g., *Musters et al.*, 2000 ; *Musters and Bouten*, 2000] some authors succeeded in this task [e.g., *Vrugt et al.*, 2001]. In front of these contrasting results and for elucidating whether the macroscopic root water uptake parameters can be derived from soil water contents only, we analyzed in detail the inference properties of two different approaches to derive the macroscopic root water uptake parameters. The first approach appeals on a simplified water balance method, the second fully inverses an integrated soil-crop water balance model. These two approaches were tested using a case study where soil water content data were collected during a dry period of 24 days.

Results of this study show that the root water uptake measured within our field is quite variable. Coefficients of variation range from 22 to 34% for the two considered macroscopic root uptake parameters A and B respectively. Next, numerical experiments for a dry period show that the simplified water balance approach gives quite good estimates of the A and B parameters. Though very simple, this approach is robust. Similar results are obtained for all other soils except for the coarse textured soil. For the simplified water balance approach, future research should focus on the impact of soil water content measurement errors on estimated root water uptake parameters and on the development of some procedures allowing the improvement of the predictions of these parameters. For example, a procedure that could be performed is to identify optimal soil water content sampling strategies both in space and time as done, e.g., by *Musters and Bouten* [2000]. The simplified water balance method should also be tested for other macroscopic root water extraction conceptualizations. Note that the adoption of the presented simplified water balance approach required specific climatic conditions namely a long dry period (about 15 days) with insignificant rainfall and with high evaporative demand. As in temperate climate (e.g., Belgium) such periods generally occur during the growing season, this seems not to be a limitation for the application of the method.

The study shows further that soil water content is quite insensitive to crop parameters and in particular to root water uptake parameters, at least compared to soil hydraulic parameters, even for an optimal dry period where sensitivity is assumed to be at maximum. Similar results are obtained when the time derivative of the water content is considered.

Furthermore, instability analysis clearly illustrates that root water uptake parameters are very unstable with respect to small uncertainties on the apparently known parameters (e.g., soil parameters). Though apparently less marked for OF defined in terms of the time derivative of the soil water content, this arises directly from the relative insensitivity of root water uptake parameters compared to other parameters. Therefore optimizing root water uptake parameters during a long dry period should not be recommended when other soil and plant parameters are prone to error.

Finally, the results show that if root water uptake plus additional other parameters (e.g., soil parameters) are simultaneously optimized, non-uniqueness of parameter sets must be expected. Indeed, a lot of good model fits may be achieved across the whole parameter space because the information content of such a dry period characterized by a decreasing water content time series is clearly not sufficient to correctly determine so many parameters. It should be noted that in all the numerical cases considered in the analysis, water content measurement strategy was very intensive both in space and time. Worse results should be expected for less intensive soil water content monitoring strategies.

To conclude, results of this study show that a robust identification of root water uptake parameters by means of a full soil water balance model inversion during a dry period is unlikely to be achieved with soil water content observations at least when some fixed parameters are not error-free. The range of these errors will clearly condition the results of the soil water balance model inversion and the optimized root water uptake parameter values. On the contrary, identification of root water uptake parameters with a simplified water balance approach seems feasible and much more robust, at least for some soils (all except the coarse sand) and for a certain range of parameter (e.g., $0.008<A<0.013$). This approach is furthermore very easy to apply and requires only soil water content measurements. Moreover, as soil water content is very insensitive to root water uptake parameters, these might be fixed at values obtained with the simplified water balance approach before being used in soil water balance model simulations. In this way, robustness of subsequent calibrations of these soil water balance models will certainly be improved. Finally, to extend the results of this study we recommend applying the same methodology as developed in our study (or alternatively a full inversion of the model) to other macroscopic conceptualizations of root water uptake.

Chapter 7

Estimation of root water uptake parameters by inverse modelling with soil water content data

Abstract*

In this chapter, we have tested the feasibility of the inverse modeling approach to derive root water uptake parameters (RWUP) from soil water content data using numerical experiments for three differently textured soils and for an optimal drying period. The RWUP of interest are the rooting depth and the bottom root length density. In a first step, a thorough sensitivity analysis was performed. This one showed that soil water content dynamics is relatively insensitive to RWUP and that the sensitivity depends on the texture of the considered soil. For medium-fine textured soil, the sensitivity is particularly low due to a "compensating effect", i.e. vertical unsaturated water flows overshadowing in some way the root water uptake. In a second step, we analyzed the well-posedness of the solution (stability and non-uniqueness) when only RWUP are optimized. For this case, the inverse problem is clearly ill-posed except for the estimation of the rooting depth parameter for coarse and the very-fine textured soils. In a third step, we addressed the case where RWUP are estimated simultaneously with additional parameters of the system (i.e. with soil hydraulic parameters). For this case, our study showed that the inverse problem is well-posed for coarse and very-fine textured soils allowing the estimation of both RWUP of interest provided that a

*adapted from Hupet, F., S. Lambot, R.A. Feddes, J.C. van Dam, and M. Vanclooster, *Water Resources Research*, 39(11), 1312, doi:10.1029/2003WR002046, 2003.

powerful global optimization algorithm is used. On the contrary, the estimation of RWUP is unfeasible for medium-fine textured soil due to the "compensating effect" of the vertical unsaturated water flows. In conclusion, we can state that the inverse modeling approach can be applied to derive RWUP for some soils (coarse and very-fine textured) and that the feasibility is strongly improved if the RWUP are simultaneously optimized with additional parameters. Nevertheless, more detailed research is needed to apply the inverse modeling approach to real cases for which additional issues are likely to be encountered such as soil heterogeneity and root dynamics.

7.1 Introduction

The correct modeling of evapotranspiration fluxes at different spatio-temporal scales remains an important challenge for hydrologists. Numerous evapotranspiration models have been developed such as those derived from land surface energy balances [e.g., *Dickinson et al.*, 1993; *Ducoudré et al.*, 1993] or found in agro-hydrological simulation models describing more in detail the soil water, the soil vapour and energy balance in the soil-crop-atmosphere continuum [e.g., *Jarvis et al.*, 1994; *van Dam et al.*, 1997]. This latter type of model generally contains various components representing different physical processes such as e.g., soil water flow and root water uptake (RWU). The RWU process is of paramount importance as in relatively moist systems most water leaves the soil through root water uptake and plant transpiration, rather than by direct evaporation at the soil surface [*Chahine*, 1992]. For modeling purposes, RWU in agro-hydrological models is often conceptualized by a macroscopic approach in which a depth dependent soil water sink term is defined, which is then added to the soil water mass conservation equation for a representative elementary soil volume [*Whisler et al.*, 1968; *Molz*, 1981]. Actual RWU is calculated as the product of a maximum possible RWU and a reduction function taking into account water stress, salinity stress or both [*Homaee*, 1999]. Maximum RWU is time and depth dependent and is generally defined by some parameters characterizing the rooting depth and the root density distribution. These root water uptake parameters (RWUP) have to be identified before using the agro-physical hydrological model in predictive mode. A straightforward method to generate RWUP is to combine a soil water and energy transport model of the soil-plant-atmosphere system with a vegetation growth model [see, e.g., *Van den Broek and Kabat*, 1995]. However, this approach is uncommon in the field of surface hydrology as it relies on elaborate crop-specific parameterization schemes which depend on species, genotypes and genotype environment. Hence, there is a need to evaluate the robustness of alternative RWUP identification strategies such as the method based on hydrological tracers [e.g., *Brunel et al.*, 1995], or the method based on a simplified water balance [e.g., *Hupet et al.*, 2002], or the use of an inverse modeling procedure [e.g., *Vrugt et al.*, 2001a]. This latter approach is an estimation method in which parameters are optimized by minimizing a predefined objective function which measures discrepancies between observations, i.e. measurements of a state variable (e.g., soil water contents) and the corresponding outputs of the model. Inverse procedures for parameter estimation have been widely used in the field of vadose zone hydrology [see *Hopmans and Simunek*, 1999] but have almost exclusively been confined to the estimation of soil hydraulic properties from outflow experiments [e.g., *van Dam et al.*, 1994], evaporation experiments [e.g., *Romano and Santini*, 1999] or infiltration and redistribution experiments [e.g., *Si and Kachanoski*, 2000]. Quite recently, the inverse procedure was also applied to the whole soil-plant-atmosphere system to infer RWUP from soil water content observations by coupling appropriate numerical models with a parameter optimization algorithm [*Musters and Bouten*, 1999; *Vrugt et al.*, 2001a,b; *Zuo and Zang*, 2002]. This inverse approach is becoming more popular because only a few restrictions are imposed on the experimental conditions. In addition, it results in effective parameter estimates for which the uncertainty ranges can be quantified. Nevertheless, the use of inverse techniques has some well known limitations which are mainly related to the nonuniqueness and instability of the optimized parameter set. Nonuniqueness leads to several parameter sets describing the data, each yielding equivalent minimum values for the objective function [*Gupta and Sorooshian*, 1985; *Duan et al.*, 1992]. Non-unique parameter estimates may occur when the parameter sensitivity is low or when the parameters are mutually dependent. Instability is related to the fact that errors on measurements, fixed parameters, or boundary conditions may result in considerable changes in optimized parameter sets. Instability generally occurs when high measurement noise characterizes the data for the inversion and/or when the sensitivity of the parameters to the input data is too low. The well-posedness, the uniqueness and the stability of the identification of soil hydraulic properties have been extensively studied by means of both experimental and numerical experiments [see, e.g., *Kool et al.*, 1985; *Carrera and Neuman*, 1986; *Simunek and van Genuchten*, 1996]. In contrast, only a few studies have dealt with the identification properties of RWUP parameters. *Musters and Bouten* [1999] and *Vrugt et al.*, [2001a, b] identified RWUP for a field experiment, but did not investigate the feasibility of the procedure by means of numerical experiments. Yet this preliminary 'testing' step is necessary to claim that the inverse problem is well-posed and that the approach can be robustly applied for identification of RWUP. Using a combined numerical and experimental approach, *Hupet et al.* [2002] identified non-uniqueness and stability problems in the estimation of RWUP through inversion.

The general purpose of this study was to investigate numerically the feasibility of estimating RWU parameters from soil water content observations by an inverse modeling approach. We chose a numerical analysis since in such an analysis everything is known, i.e. the chosen model is correct, and all parameters and measurement errors are known beforehand [*Simunek et al.*, 1998]. This is obviously an optimal situation for testing the potential and the limitations of the inverse procedure. In this study, preference is given to the use of soil water content data in the objective function since advanced soil moisture probing technology such as Time Domain Reflectometry (TDR) is now readily available to monitor this state variable with a high spatio-temporal resolution. Furthermore, to be able to compare our results we chose the same state variable, i.e. soil water content, as that used in the previous studies dealing with the inverse estimation of RWUP [*Musters and Bouten*, 1999; *Vrugt et al.*, 2001a,b]. Numerical experiments were generated for a long dry period in three differently textured soils. The two target RWUP of interest are the rooting depth (RD) and the bottom relative root length density (BRLD), which together fully characterize the maximum RWU profile. Firstly, we analyze the sensitivity of RD and BRLD as instability and nonuniqueness may be strongly related to the sensitivity of the optimized parameters. Secondly, we address the uniqueness and stability of the solution when only RWUP are optimized. In this case, Monte Carlo simulations are performed to test the stability of the solution to errors in input data, to errors in some fixed parameters, and to errors in both. Finally, we investigate uniqueness and stability of the solution when RWUP and some additional parameters are optimized simultaneously.

7.2 Material and methods

7.2.1 The forward problem

In this chapter, all the numerical simulations were performed with the soil water transport module of the SWAP-model [*Van Dam et al.*, 1997] including an extension of the root water uptake conceptualization proposed by *Feddes et al.* [1978] and *Prasad* [1988]. For the identification

Table 7.1. Mualem-van Genuchten parameters corresponding to the loamy soil of the experimental field (hereafter called medium-fine) and to the two other considered soils, i.e., a coarse and a very-fine textured soil [*Wösten et al.*, 1998]

	θ_r	θ_s	α	n	λ	K_{sat}
coarse	0.025	0.366	0.043	1.5206	1.2500	70.00
medium-fine	0.0	0.392	0.003	1.22	0.5000	5.000
very fine	0.010	0.538	0.0168	1.073	0.0001	8.235

of RWUP, a reference run was generated for a long dry period of 28 days (without any significant rainfall) corresponding to actual climatic conditions in Belgium encountered between 6^{th} July and 2^{nd} August 1999 in the field experiment described in Chapter 2. This period was characterized by a moderate potential evapotranspiration with a mean value of 3.93 mm d^{-1}. The reference run and subsequent numerical simulations were generated for a homogeneous soil profile, 160 cm deep with free drainage as the lower boundary condition. The flow domain was discretized into 40 compartments using, as suggested by *van Dam and Feddes* [2000], a nodal distance of 1 cm for the first ten compartments and a nodal distance of 5 cm for the remaining soil profile. The initial condition was selected as a pressure head profile corresponding to field capacity, considered here as the state of "equilibrium" reached after 3 days of water redistribution within a saturated soil profile with zero flux as top boundary condition. We used soil hydraulic properties corresponding to the average of those measured within a small loamy experimental field at 28 different locations (see section 2.4). The soil was assumed to be covered with a fully developed and non-growing maize crop characterized by a LAI of 4, a crop coefficient of 1.1 and a rooting depth of 100 cm [*Girardin*, 1999], a top root length density of 1 and a bottom root length density of 0.5. Note that the value of this latter parameter was selected quite arbitrarily, although it is located just in the middle of the defined parameter space (i.e. 0-1, see further), which is an advantage for the study under consideration. The critical pressure heads of the water stress function were assigned to values listed by *Wesseling* [1991] for maize, i.e. h_1=15 cm , h_2=50 cm, h_{3l}=600 cm, h_{3h}= 325 cm and h_4=8000 cm. To extend the results of this study, two additional reference runs were also generated for two differently textured soils corresponding to a coarse and a very-fine soil whose respective soil hydraulic properties were derived from *Wösten et al.* [1998] (see Table 7.1 and Fig. 7.1).

7.2.2 The inverse problem

Objective function

Identification of RWUP by an inverse procedure is a nonlinear optimization problem which consists in finding the parameter vector **b** (containing the RWUP to be optimized) by minimizing an objective function OF(**b**). Considering incorporation of only soil water content observations in the OF (thereafter called OF), and assuming that residuals, i.e. errors between "measured" and simulated soil water contents are normally distributed, independent and homoscedastic, the unweighted Maximum Likelihood OF yields:

$$OF(\boldsymbol{b}) = (\boldsymbol{\theta}^* - \boldsymbol{\theta})^T(\boldsymbol{\theta}^* - \boldsymbol{\theta}) = \mathbf{e}^T\mathbf{e} \tag{7.1}$$

with **b** the model parameter vector; $\boldsymbol{\theta}^*$=$\boldsymbol{\theta}^*(z_j, t_i)$ and $\boldsymbol{\theta}$=$\boldsymbol{\theta}(z_j, t_i, b)$ the vectors containing, respectively, the "measured" and the simulated soil water content data relative to depth z_j and time t_i; and **e**= $\boldsymbol{\theta}^*$- $\boldsymbol{\theta}$ the vector of residuals. In the present study, we considered a hypothetical intensive sampling scheme where soil water content is measured with a daily time step (n=28) each 10 cm between 0 and 160 cm, i.e. at 10, 20,...,150 cm depth (n=14) resulting in 420 soil water content data points in the OF.

Optimization algorithms

For the minimization of Eq. (7.1), we used two different optimization algorithms. The first one is derived from the Gauss-Marquardt-Levenberg (GML) method which starts by searching mainly along the steepest gradient of the OF surface and gradually switches to a direction based on a first order approximation of the OF surface. This optimization algorithm is included in PEST [*Doherty et al.*, 1995] which is a non-linear parameter estimation program which can be linked via templates to any model. As the GML algorithm is very efficient in terms of the number of model calls to find the global minimum [e.g., *Finsterle and Pruess*, 1995], we used it when the number of parameters to be optimized was small, typically in our case for one or two RWUP. Nevertheless, it is well known that efficiency of local optimization algorithms to find the global minimum becomes very limited when the number of parameters increases, e.g., in our case when RWUP are simultaneously optimized with some soil hydraulic parameters. In this case, we used a second optimization algorithm based on a global search procedure. This is the Global Multilevel Coordinate Search (GMCS) algorithm [*Huyer and Neumaier*, 1999] combined sequentially with the classical Nelder-Mead Simplex (NMS)

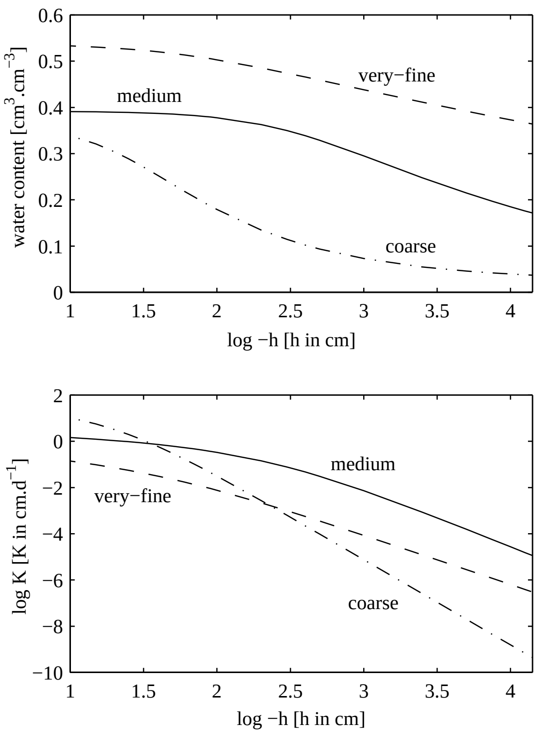

Figure 7.1. Water retention and hydraulic conductivity curves of the three differently textured soils.

algorithm. This global optimization algorithm introduced in the area of unsaturated zone hydrology by *Lambot et al.* [2002] is very efficient for the complex topography of nonlinear objective functions containing many local minima and compares favourably with other existing global search algorithms [*Huyer and Neumaier*, 1999; *Lambot et al.*, 2002]. The GMCS-NMS algorithm used in this study is entirely programmed in MATLAB^{TM} routines (version 5.3 [*The MathWorks*, 1999]) and directly linked to the SWAP model (fortran executable). Details of the programming procedure can be obtained upon request.

Parameter uncertainty

Besides the optimized parameter values, it is also desirable to determine the precision of those estimates, i.e. the optimized parameter uncertainty. In this study, this was derived by two different methods. The first is used exclusively when only RWUP are optimized and is based on Monte Carlo simulations. This method generates many optimized parameter sets from model fitting of data (in our case produced by the reference run) corrupted with measurement errors. Uncertainty of the optimized parameters in terms of standard deviations and confidence intervals is subsequently derived from the optimized parameter distributions obtained [*Press et al.*, 1992; e.g., *Clausnitzer et al.*, 1998]. As this first method requires quite high computing resources, we used a second method when the number of parameters was larger. This method approximated parameter confidence intervals using classical linear regression analysis, i.e. by assuming local-linearity around the minimum of the OF. Uncertainty of the optimized parameters is derived from the parameter variance-covariance matrix **C** [*Kool and Parker*, 1988] calculated as follows:

$$\boldsymbol{C} = \frac{\boldsymbol{e}^T \boldsymbol{e}}{n-p} \boldsymbol{H}^{-1} \tag{7.2}$$

with n the number of observations, p the number of parameters and $\boldsymbol{H}$ the Hessian matrix whose elements are defined by:

$$H_{i,j} = \frac{\delta OF(\boldsymbol{b})}{\delta b_j \delta b_i} \tag{7.3}$$

Approximate individual confidence intervals of the estimated parameters are finally calculated as follows:

$$b_i - t^{n-p}_{1-\alpha/2} \sqrt{C_{j,j}} \leq b_i \leq b_i + t^{n-p}_{1-\alpha/2} \sqrt{C_{j,j}} \tag{7.4}$$

with $C_{j,j}$ the diagonal elements of the variance-covariance matrix, $t^{n-p}_{1-\alpha/2}$ the value of the Student distribution with $(n-p)$ degrees of freedom; and $(1-\alpha)$ the confidence level, i.e. in our case 0.95 for the 95% confidence interval.

Parameter sensitivity

Assessment of parameter sensitivity prior to any model calibration is of paramount importance as efforts must normally be concentrated on parameters to which the model simulation results are most sensitive [*Beven*, 2001]. In the present work, sensitivity coefficients are calculated for each day and each depth as follows:

$$\Omega_{i,j} = b_j J_{i,j} \tag{7.5}$$

with $\Omega_{i,j}$ the ij elements of the sensitivity matrix $\boldsymbol{\Omega}$ (size n x p); and $\boldsymbol{J}$ the Jacobian matrix (size n x p) whose elements $J_{i,j}$ are defined as the partial derivatives $\frac{\delta e_i}{\delta b_j}$ and obtained by forward difference approximation with $\delta b_j = 0.01 b_j$. Note that such an expression for the sensitivity coefficients allows a direct comparison between different parameters whatever the invoked units. We also calculated for each parameter a mean absolute space and time sensitivity coefficient defined as:

$$\bar{\Omega_j} = \frac{1}{n} \sum_{i=1}^{n} \mid \Omega_{i,j} \mid \tag{7.6}$$

7.2.3 The identification strategy

Sensitivity analysis

In a preliminary step, we performed a thorough sensitivity analysis for all parameters governing the transport of water within the soil-plant-atmosphere system, i.e. RWUP (RD, TRLD, BRLD), parameters of the water stress function (h_1, h_2, h_{3l}, h_{3h}, h_4), parameters expressing the crop development (LAI, K_c) and hydraulic parameters (θ_r, θ_s, α, n, K_{sat}, λ). For the three differently textured soils, mean absolute space and time sensitivity coefficients were calculated with Eq. (7.6) for a perturbation of 1% of the parameters with respect to the true parameters (i.e. the reference run). Further, as sensitivity coefficients represent quite abstract values, we generated the water content dynamics for each soil in four additional runs corresponding to the bounds of the RWUP space (RD =50 and 150 cm; BRLD= 0 and 1).

Optimization of RWUP only

Where only RWUP parameters are optimized (i.e. one or two parameters), we investigated first the uniqueness of the solution by visually checking the behavior (in 1-D or 2-D) of the objective function calculated with Eq. (7.1). The parameter space of the optimized parameters was divided into 100 discrete values while all the other parameters were fixed at their true values. Subsequently, we investigated instability with respect to measurement errors on soil water content data, to measurement errors on some fixed parameters, and to both combined. For water contents, we chose five different levels of measurement errors (normally distributed with zero mean), i.e. 0.005, 0.01, 0.015, 0.02 and 0.025 in terms of standard deviation (std), corresponding typically to TDR calibration equations of different quality. The 0.01 error level will be considered in the following as the most realistic although many studies have found larger values (e.g., 0.02 [*Vrugt et al.*, 2001a]). Subsequently, for each level of error and for the three soil types, we performed

250 Monte Carlo simulations optimizing with PEST separately RD and BRLD and both parameters simultaneously. This resulted in 250 (x 3 x 3 x 5) optimized parameter sets. After visually checking for normality of the distributions obtained, confidence intervals were constructed with the true distribution of the 250 parameters. Note that in our study we assumed that the confidence intervals were well approximated with quite a low number (i.e. 250) of Monte Carlo simulations. Therefore, we checked the validity of this assumption for some cases by generating confidence intervals with 5000 Monte Carlo simulations. In all analyzed cases, confidence intervals derived with 250 and 5000 Monte Carlo simulations were very similar validating our assumption of constructing confidence intervals with "only" 250 Monte Carlo simulations. When RD and BRLD were simultaneously optimized, the correlation coefficient between the two parameters was also determined. Next, instability analysis was performed considering measurement errors on some fixed parameters. Other system parameters such as soil hydraulic parameters and crop coefficients are intrinsically uncertain since the scale of the modeled soil-plant-atmosphere system is inevitably quite large, i.e. at least that of the pedon or the lysimeter (1 to a few m^3). In this study, we considered 5 different error levels on 5 "fixed" system parameters i.e. θ_s, α, n, K_{sat} and K_c. The error level expressed in terms of CV was specified considering the likely uncertainty resulting from the use of different methods for the determination of these "fixed" parameters (see Table 7.2). Note that uncertainty levels reported for K_c were chosen quite arbitrarily although the selected values seem quite small and plausible for the case of a field experiment. For the measurement error on fixed parameters, the third level of error will be considered in the following as the most realistic. Again 250 Monte Carlo simulations were performed with error (normally distributed and with zero mean) added simultaneously to the 5 "fixed" parameters, considering first that the water content data are error-free. Subsequently confidence intervals were derived from the obtained distribution of optimized RWUP. These confidence intervals represent in fact the range of variation of the optimized RWUP due to uncertainty on some fixed parameters. Finally, Monte Carlo simulations were performed combining both corrupted soil water content data and "fixed" parameters corresponding to a practical case. To avoid too many simulations, we combined the second level of error for soil water content data, i.e. that considered as the most realistic (std=0.01), with the 5 different levels of error for "fixed" parameters.

Table 7.2. Considered levels of uncertainty on the "fixed" parameters in terms of coefficients of variation (CV=$(\sigma/\mu)100$).

Level of error	θ_s	α	n	K_{sat}	K_c
	Coefficient of variation				
1	1.25	3.33	0.4	10	0.9
2	1.9	6.66	0.8	15	1.8
3	**2.5**	**10**	**2**	**20**	**2.7**
4	3.8	13.33	3.2	30	3.6
5	5.1	16.66	4.0	40	4.5

Optimization of RWUP plus additional parameters

We finally addressed the case where RWUP plus additional parameters are simultaneously optimized. Uniqueness was investigated by launching the inverse procedure on error-free data for the identification of a gradually increasing number of unknown parameters, systematically including RD or RD and BRLD and some additional normally "fixed" parameters among θ_s, α, n, K_{sat} and K_c. In a first step, the optimization was performed with PEST, i.e. with the Gauss-Marquardt-Levenberg (GML) algorithm. As suggested by e.g., *Simunek and van Genuchten* [1996], each optimization case was repeated with three different initial estimates of the unknown parameters to assess the uniqueness of the inverse problem. The different initial estimates were selected randomly at the bounds of the parameter space which was deliberately small for the normally "fixed" parameters (true value ± 2 std for level of error 5 in Table 7.2) as if prior information about these parameters were available. For RD and BRLD, the initial estimates were chosen randomly between the bounds of the parameter space namely 50 or 150 cm for RD and 0 or 1 for BRLD. Note that we also used the GMCS-NMS [*Lambot et al.*, 2002] algorithm to make sure that any nonuniqueness problems encountered were not simply related to the use of the local optimization algorithm (GML). This strategy to tackle nonuniqueness problems was chosen rather than the traditional approach consisting of a visual inspection of 2D response surfaces of the OF as this method is not totally reliable for multi-dimensional parameter space [*Simunek and van Genuchten*, 1996]. Finally, we investigated instability problems by launching the inverse procedure as for the non-uniqueness analysis but with a noise of 0.01 added to soil water content data. For that case, we used only the GMCS-NMS algorithm and instability problems were derived from the width of the confidence intervals of the parameter estimates quantified with Eqs. (7.2) and (7.4).

7.3 Results and discussion

7.3.1 Sensitivity analysis

Results of the sensitivity analysis are presented in Table 7.3 in which mean absolute space and time sensitivity coefficients ($\bar{\Omega}$) are shown for the three differently textured soils. In this table we also indicated the ranking of the sensitivity coefficients for all parameters with the values 1 and 16 assigned respectively to parameters affecting the most and the least the soil water content dynamics. The results show that soil water content dynamics are much more sensitive (one to two orders of magnitude) to some hydraulic parameters, i.e., θ_s and n, than to RWUP. Similar results were found by *Hupet et al.* [2002] for the RWU conceptualization proposed by *Hoogland et al.* [1981]. Yet soil water content dynamics in the study of *Hupet et al.* [2002] was completely insensitive to the rooting depth showing clearly that the impact of RWUP on soil water content dynamics also depends on the model concept adopted. Similar results showing insensitivity of soil water content dynamics to RWUP although this was not quantified in a classical sensitivity analysis were also found by *Musters and Bouten* [2000]. Additionally, the results of our study show that the two parameters that influence the gradually drying soil profile the most are θ_s and n which are also the main governing parameters during evaporation experiments [see *Simunek et al.*, 1998]. Visual inspection of the space and time patterns of sensitivity coefficients (not shown here) shows that perturbing RWUP affects soil water dynamics over the whole soil profile, though generally this is more apparent close, to the soil surface. It also shows that sensitivity coefficients of RWUP increase gradually as the experiment progresses, i.e. when the soil profile becomes drier. The relative sensitivity of the soil water content dynamics to moisture retention curve (MRC) parameters and RWUP may seem quite surprising for a dry period. The sensitivity of MRC parameters suggests that a small error in e.g., θ_s will directly affect simulated soil water content even for the case where the temporal dynamics of soil water content are mainly driven by RWU and where vertical water fluxes are negligible. Note that in this case soil water content variation ($\frac{\delta\theta}{\delta t}$) is much less sensitive to MRC parameters than soil water content itself as noted by *Hupet et al.* [2002]. The relative insensitivity of soil water content to RWUP suggests that a small perturbation of RWUP results in almost all cases in a proportional modification of

Table 7.3. Mean absolute space and time sensitivity coefficients ($\bar{\Omega}$) calculated for the different textured soils (coarse, medium-fine and very-fine).

	medium-fine		coarse		very-fine	
parameter						
θ_s	1	0.364	2	0.134	2	0.48
n	2	0.149	1	0.309	1	0.75
K_c	3	0.038	4	0.0315	4	0.029
α	4	0.019	3	0.051	5	0.021
RD	**5**	**0.01488**	**5**	**0.0308**	**3**	**0.0296**
K_{sat}	6	$7.6\ 10^{-3}$	11	$2.3\ 10^{-3}$	10	$2.8\ 10^{-3}$
LAI	7	$6.2\ 10^{-3}$	7	$8.1\ 10^{-3}$	6	$7.9\ 10^{-3}$
TRLD	**8**	$\mathbf{2.7\ 10^{-3}}$	**8**	$\mathbf{5.8\ 10^{-3}}$	**7**	$\mathbf{5.5\ 10^{-3}}$
BRLD	**9**	$\mathbf{2.7\ 10^{-3}}$	**9**	$\mathbf{5.8\ 10^{-3}}$	**8**	$\mathbf{5.5\ 10^{-3}}$
h_{3l}	10	$8.5\ 10^{-4}$	13	$2.6\ 10^{-4}$	12	$5.8\ 10^{-4}$
h_4	11	$7.4\ 10^{-4}$	12	$9.8\ 10^{-4}$	9	$2.38\ 10^{-3}$
λ	12	$7.2\ 10^{-4}$	10	$3.9\ 10^{-3}$	14	$1.2\ 10^{-6}$
θ_r	13	$3.7\ 10^{-4}$	6	0.0158	11	$1.1\ 10^{-3}$
h_{3h}	14	$1.1\ 10^{-4}$	14	$1\ 10\ 10^{-4}$	13	$7.4\ 10^{-5}$
h_1	15	0	15	0	15	0
h_2	16	0	16	0	16	0

the sink term. This modifies indirectly vertical soil water fluxes which compensate and mask in some way the perturbation effect of RWUP on soil moisture. To illustrate this "compensating effect", we generated numerical runs for the loamy soil described in Table 7.1 and for the same soil with hypothetical saturated conductivities of 100 cm d^{-1} and 0.01 cm d^{-1} and with RD set to 50, 100 and 150 cm. Results presented in Fig. 7.2 show the temporal dynamics of soil water content at 25 cm depth (a, b and c graphs) and the accumulated RWU at the same depth (d, e and f graphs). We notice that for the most conductive loamy soil, the perturbation of the RD does not have a significant effect on the soil water content dynamics at 25 cm depth (Fig. 7.2a) in contrast to accumulated RWU (Fig. 7.2d). Hence, vertical water fluxes are able to mask RWU differences in the soil moisture observations. For the other two loamy soils (Fig. 7.2b and c), the "compensating effect" is less marked and the impact of the different RD on the soil water content dynamics is more pronounced as the soil becomes less conductive. Hence, the "compensating effect" of the soil plays a certain role in the insensitivity of the soil water content dynamics to RWUP but this insensitivity is soil

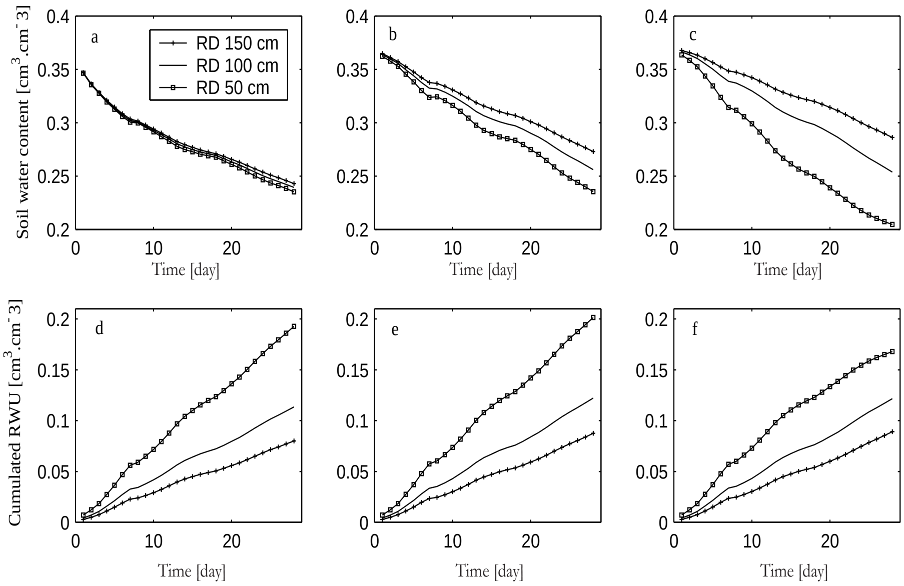

Figure 7.2. "Compensating" effect of the soil according to different conductivity characteristics. Fig. 7.2 a-b-c shows the temporal dynamics of soil water content at 25 cm depth for a medium fine soil with a Ksat of respectively 100, 5 and 0.01 cm d-1. Fig. 7.2 d-e-f show for the same depth and for the same three different Ksat cumulated root water uptake (cm3 cm-3).

specific. In particular, for coarse and the very-fine textured soils values of the unsaturated conductivity are smaller than those of the medium-fine (for h<-100 cm) preventing therefore that vertical unsaturated flow overshadows the root water uptake "signal". We also generated four additional runs for each soil, selecting RD and BRLD at the bounds of the parameter space (RD =50 and 150; BRLD =0 and 1). Fig. 7.3 shows for the whole soil profile the maximum difference in terms of soil water content between the reference run (RD = 100 and BRLD =0.5) and these other four runs. Note that maximum differences between the reference run and the other 4 runs were systematically encountered at the end of the 28-day simulation period. For the loamy soil (Fig. 7.3b), maximum differences are very small (max. 0.02 cm^3 cm^{-3}) except for the first 20 cm and the order of magnitude of this maximum difference corresponds to the standard deviation of a "poor" quality calibration curve of a soil water measurement device. Furthermore, we note that for the two runs with RD equal to 50 cm, the shape of the root length density distribution has virtually no effect on the magnitude of the maximum difference.

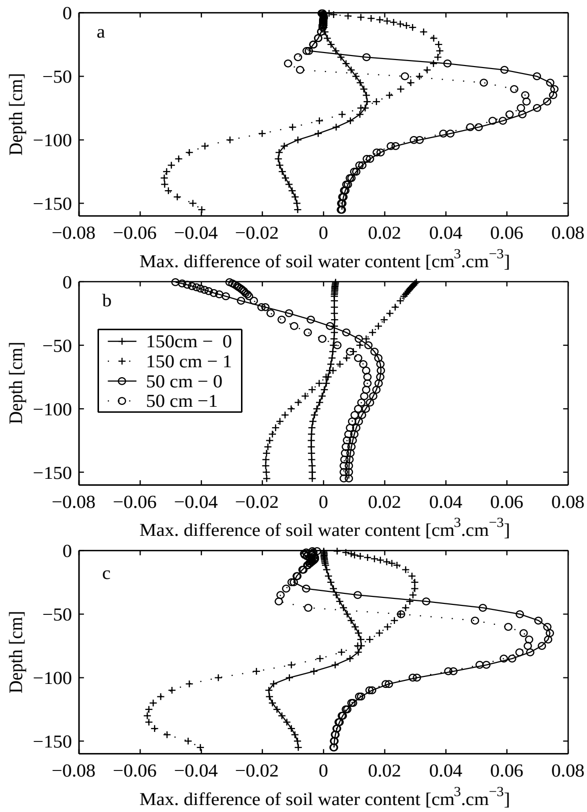

Figure 7.3. Maximum difference between soil water content of the reference run an that of the other four simulations run for the bounds of the parameter space. Fig. 7.3 a-b-c are respectively given for the coarse, medium-fine and very-fine textured soils.

Coarse and the very-fine textured soil behave quite similarly with larger maximum differences ranging between -0.06 and 0.07 cm^3 cm^{-3}. Again, in this case, the two simulation runs with RD equal to 50 cm are very similar whatever the shape of the root length density distribution. We also note that nearly all the depths are informative. The largest values of the maximum difference are observed at various depths for the selected cases. This may seem in contradiction to the results obtained in the sensitivity analysis where information content was generally larger close to the soil surface. This may be explained by the fact that during the sensitivity analysis, in contrast to the additional runs, small perturbations were induced in the close vicinity of the true parameters. We further looked at the impact of the four different runs, on the accumulated actual transpiration fluxes as this kind of information might be

Table 7.4. Differences (expressed in mm) between cumulated actual transpiration fluxes of the reference run and of the four other runs.

	RD=150 cm BRLD=1	RD=150 cm BRLD=0	RD=50 cm BRLD=1	RD=50 cm BRLD=0
coarse	8.76	1.35	-32.2	-44.8
medium-fine	2.18	0.56	-4.8	-10.1
very fine	12.32	2.56	-28.5	-39.5

additionally used for the inverse procedure. Results of Table 7.4 suggest that for medium fine textured soil, RWUP have no significant impact on the accumulated transpiration which is obviously consistent with the small impact of RWUP on soil water content dynamics. For the two other soils, the impact is much larger and particularly well pronounced when the RD is reduced. To conclude, we can state that the results of this sensitivity analysis are clearly not favorable for the identification of RWUP parameters from soil water content observations alone. Soil water content dynamics are relatively insensitive to RWUP, i.e. to RD and BRLD, at least compared to other parameters of the system. This suggests implicitly that small errors on the time series of soil water content will have quite a large effect on the uncertainty associated with optimized RWUP. Furthermore, small errors on some parameters for which soil water content dynamics are much more sensitive may well result in very different RWUP estimates.

7.3.2 RWU parameters

Results obtained for the uniqueness analysis are illustrated in Fig. 7.4 for coarse textured soil. The response of the logarithm of OF is presented in Fig. 7.4a and b for two different cases, i.e. for the optimization of respectively RD alone and RD and BRLD simultaneously. In each figure, we can see a well-defined global minimum corresponding to the true parameter values (RD=100 cm and BRLD=0.5). Note that these results were obtained from error free soil water content data for a coarse textured soil but that similar results were obtained from corrupted soil water content data and for the two other textured soils. Results of the stability analysis generated with the five levels of error on soil water content "measurements" are presented in Table 7.5 (a and b) for the medium and coarse textured soil. Means and individual parameter confidence intervals at 95% (CI) are presented separately for the optimization of RD,

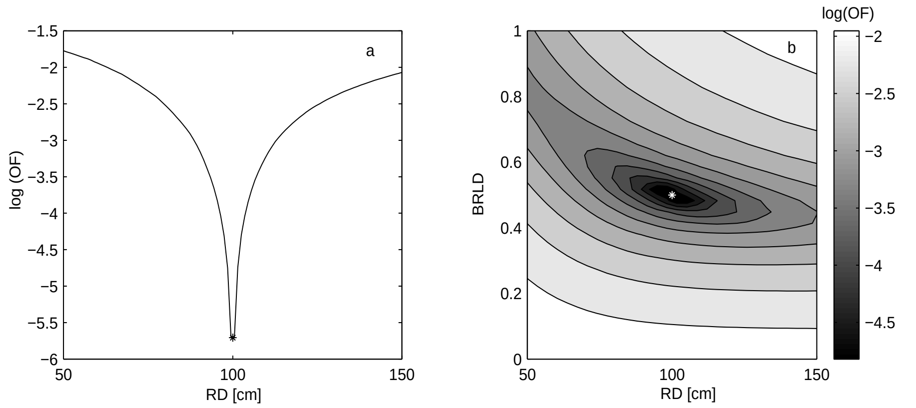

Figure 7.4. Uniqueness illustrated for the estimation of RD alone (a), and for RD and BRLD together (b). The true minimum is indicated with a marker.

BRLD and both simultaneously. For the RD, we observe that the range of the confidence intervals are quite small (6.5<CI<32 cm) and that the ranges increase as the magnitude of the "measurement" error increases. Confidence intervals for BRLD are much larger with values covering a large proportion of the predefined parameter space already when considering the second level of error. This means that small errors in soil water content measurements have a very large effect on the stability of optimized BRLD. Note that the difference in stability of identifying RD and BRLD is a direct consequence of the difference of sensitivity for these two parameters (see Table 7.3). When RD and BRLD are optimized simultaneously, results are markedly worse. Indeed, for the second error level, the confidence interval of BRLD (0.08-0.92) is almost the same as the size of the initial parameter space (0-1) meaning that uncertainty on BRLD generated by the parameter estimation method is virtually equivalent to the original uncertainty. Given these results, Monte Carlo simulations for the next three error levels were not run. Note that optimizing both parameters simultaneously substantially increases the confidence intervals as compared to the case when the parameters are optimized separately. Indeed, the parameters RD and BRLD are strongly negatively correlated (see correlation coefficients in Table 7.5a) meaning that a small increase of RD can be compensated by a small decrease of BRLD and can lead to very similar soil water content dynamics. The high correlation between RD and BRLD is clearly not optimal in terms of parameter estimation as it could substantially contribute to the non-uniqueness of the problem. For coarse textured soil (see Table 7.5b), the generated

Table 7.5. Impact of measurement errors on soil water content on the optimized RWUP for the medium-fine (a) and coarse textured soils (b); CI=95% confidence interval, r=correlation coefficient.

a

level of error	1 parameter				2 parameters simultaneously				
	RD		BRLD		RD		BRLD		
(std)	mean	CI	mean	CI	mean	CI	mean	CI	r
0.005	99.89	96.6-103.1	0.498	0.35-0.64	99.6	87.7-111.4	0.52	0.24-0.86	-0.86
0.01	100.04	93.5-106.6	0.509	0.19-0.83	99.5	79-119.9	0.505	0.08-0.92	-0.9
0.015	99.98	89.8-110.1	0.517	0.15-0.88	-	-	-	-	-
0.02	100.05	87.4-112.6	0.5305	0.1-0.97	-	-	-	-	-
0.025	99.61	83.5-115.6	0.541	0.03-1.03	-	-	-	-	-

b

level of error	1 parameter				2 parameters simultaneously				
	RD		BRLD		RD		BRLD		
(std)	mean	CI	mean	CI	mean	CI	mean	CI	r
0.005	100.95	100-101.8	0.521	0.49-0.55	100.97	99.4-102.4	0.5	0.45-0.55	-0.63
0.01	100.98	99.2-102.7	0.517	0.46-0.57	100.89	98.3-103.3	0.5	0.42-0.58	-0.66
0.015	101.08	98.4-103.7	0.519	0.42-0.61	101.02	97.1-104.9	0.505	0.39-0.61	-0.6
0.02	100.83	97.1-104.4	0.529	0.41-0.65	100.82	95.5-106.1	0.508	0.36-0.65	-0.65
0.025	101.02	96.1-105.9	0.517	0.38-0.64	100.95	95.2-106.6	0.512	0.31-0.7	-0.6

confidence intervals are much smaller. For the optimization of RD or BRLD alone, the confidence intervals are acceptable for all considered error levels with maximum values of 9.8 cm and 0.26 respectively for level 5. The smaller confidence interval for the coarse soil is obviously a direct consequence of the higher sensitivity of the soil water content dynamics to RWUP. For the simultaneous optimization of both RWUP, confidence intervals hardly increase while the correlation between the two estimated parameters is also smaller ($-0.66 < r < -0.6$). Results for very-fine textured soil are very similar to those obtained for coarse soil and are therefore not presented here. This similar behavior can probably be explained by the fact that, although less sensitive to RWUP, the range of soil water content "measurements" for very-fine textured soil is about 0.2 cm^3 cm^{-3} larger than for coarse textured soil giving less weight to the added noise (similar in terms of standard deviation for the

Table 7.6. Impact of measurement error on some "fixed" parameters on the optimized RWUP for the medium-fine (a) and coarse textured soils (b).

a

level of error	RD		BRLD	
	mean	CI	mean	CI
1	100.24	89.5-110.9	0.498	0.35-0.64
2	98.63	77.1-120.1	0.56	0.13-0.99
3	101.64	65.2-138	0.492	0.002-0.982
4	101.05	59-143	-	-
5	101.5	54-149	-	-

b

level of error	1 parameter				2 parameters simultaneously				
	RD		BRLD		RD		BRLD		
	mean	CI	mean	CI	mean	CI	mean	CI	r
1	100.17	96.9-103.4	0.5	0.42-0.57	101.7	82.3-121.1	0.495	0.2-0.79	-0.91
2	100.1	93.8-106.4	0.5	0.37-0.63	106.1	73.3-128.8	0.5	0.08-0.85	-0.96
3	100.44	91.3-109.6	0.51	0.32-0.7	107.5	66.6-148.3	0.498	0.03-0.97	-0.9
4	101.22	83.3-119.1	0.51	0.2-0.82	-	-	-	-	-
5	101.17	78.9-123.4	0.51	0.14-0.88	-	-	-	-	-

two soils). Before constructing the aforementioned confidence intervals, we checked for normality of the parameter distribution by visual inspection of the histogram. In the vast majority of cases, distributions of the 250 optimized parameters were close to normal. Furthermore, we also compared true confidence intervals produced by Monte Carlo simulations and those calculated with Eq. (7.4). In the few cases investigated, the confidence intervals were very similar (not presented) thus validating the local-linearity assumption for constructing confidence intervals. At this stage of the analysis, we can state that measurement errors have a markedly different impact on the stability of the optimized RWUP for different soil types. For medium textured soil, even if all 14 other parameters are known, the small noise added to the soil water content data will produce large uncertainties that preclude simultaneous inverse modeling of RD and BRLD. In contrast, solutions are much more stable with respect to soil water content measurement errors for the other two soils. The effect of "measurement" errors on some "fixed" parameters of the modeled system is presented in Tables 7.6 a and b for medium-fine and coarse textured soils respectively. For medium-fine textured soil, the confidence interval of the optimized RD parameters increases with the increase of the magnitude of the error. For the fifth error level, the confidence interval is as large as the predefined parameter space (50-150). For the third error level, considered the most realistic, uncertainty in the optimized RD parameter ranges from 65 to 138 cm. This is of the same order of magnitude of uncertainties associated with "expert" judgement. The results are even worse for BRLD. Indeed, at the third level of error, the uncertainty corresponds to the size of the original parameter space (0-1). These results suggest that, irrespective of the optimization algorithm used, the inversion will lead to completely different estimates of BRLD parameter values if small errors on some other system parameters are explicitly accounted for. Such a large instability arises directly from the relative insensitivity of the BRLD parameter compared to other parameters (see Table 7.3). Given the results at the third level of error, Monte Carlo simulations were not generated for the fourth and fifth error levels. The impact of error in "fixed" parameters was not investigated for the simultaneous optimization of both parameters. Indeed, previous results showed for medium fine textured soil that the simultaneous optimization is not feasible due to instability problems with respect to errors in soil water content "measurements". For coarse textured soil, results (see Table 7.6b) are substantially different. Indeed, for RD and BRLD parameters optimized separately, confidence intervals produced at the third error level seem acceptable with ranges of 18 cm and 0.38 respectively. We suspect that the difference of sensitivity for the different parameters (both RWUP and "fixed") explains this success. For the simultaneous optimization of RD and BRLD, however, the results are very poor in that the estimated confidence intervals are very large at the third error level. A high correlation between the two optimized parameters ($-0.96 < r < -0.9$) exists in this case. Consequently, these results suggest that simultaneous optimization of RD and BRLD parameters, while fixing other parameters of the system at measured values, is not recommended. Small perturbations on fixed parameters will lead to completely different RD and BRLD parameter estimates. Results for very-fine soil (not shown) are very similar although the estimated confidence intervals are generally a little larger. In conclusion, the effect of instability arising from measurement errors on some "fixed" parameters is soil specific. For medium-fine textured soil, only the optimization of the RD parameter tolerates some uncertainty on the "fixed parameters". For the other two soils, separate optimization of RD or BRLD seems feasible, although its performance deteriorates for BRLD at the fourth and fifth error level. Within this context, one can speculate whether the

Table 7.7. Combined impact of measurement errors on soil water content data (level of error 2, i.e., std=0.01) and on some fixed parameters on the optimized RWUP for the medium-fine (a) and very-fine textured soils (b).

a

Level of error	Rooting depth	
	mean	CI
1	99.37	86.32-112.4
2	101.21	75.21-127.32
3	98.33	60.54-136.54
4	103.47	55.85-151.11
5	102.34	47.01-157.02

b

Level of error	Rooting depth		BRLD	
	mean	CI	mean	CI
1	100.16	95.8-104.5	0.503	0.39-0.61
2	100.07	92.91-107.22	0.503	0.34-0.66
3	100.02	89.88-110.15	0.510	0.28-0.71
4	100.75	84.6-116.88	0.516	0.19-0.83
5	100.33	77.16-123.57	0.507	0.11-0.88

third error level for "fixed" parameters chosen as the most realistic one in this study is underestimated. Indeed, for field experiments where soil layering is generally more the rule than the exception, it is really difficult (if not impossible) to obtain at the considered scale (1 to a few m^3) such accurate parameter estimates. The combined effect of errors on some "fixed" parameters of the modeled system and on soil water content data (std=0.01) is presented in Tables 7.7a and b for medium and coarse textured soils respectively. Note that this corresponds to a realistic case for which errors are encountered at all levels. Results for very-fine textured soil are very similar to coarse textured soil and are therefore not presented here. Results are quite similar to those obtained in the previous step, but increased confidence intervals are found. Nonetheless, they are slightly smaller than if we had simply added the confidence intervals produced in the two previous steps. For medium-fine textured soil, we observe that at the third error level the estimated confidence intervals are quite large (60.5-136.4) illustrating the limitations of the inverse procedure for the identification of the RD parameter. The same reasoning holds for the identification of the BRLD parameter for coarse textured soil as the confidence interval ranges between 0.23 and 0.76 (compared to the original 0-1). Only the inverse modeling of the RD parameter for very-fine and coarse textured soil seems robust to both errors in soil water contents and on the other fixed parameters of the system. Note that these results are consistent with the study of *Musters and Bouten* [1999] who assessed the spatial variability of rooting depths of an Austrian pine stand on a sandy soil by inverse modeling and using soil water content data. In their study, more than one third of the optimized rooting depths were outside the physically reasonable range (i.e. 0.5-3 m). As stated by *Musters and Bouten* [1999] and confirmed by our results, this can be explained by errors in the other fixed parameters of the system (e.g., soil hydraulic properties). On the other hand, our results question the study of *Vrugt et al.* [2001a and b] who optimized up to 9 parameters related to the maximum RWU while fixing 4 other parameters of the system at measured values (i.e. θ_s, θ_r, α and K_c). Even though the RWUP obtained were well correlated with root observations and soil water dynamics were quite well reproduced, our results suggest that there is great chance that slightly perturbing some of the fixed parameters would have led to quite different estimated RWUP. Nevertheless, it is worth noting that in the study of *Vrugt et al.* [2001a] two hydraulic parameters are simultaneously optimized with the RWUP and that the parameters fixed at "measured" values (θ_s, θ_r, α and K_c) are not exactly similar to those of our study which could explain the different results that were obtained.

7.3.3 RWU and additional parameters

Results of the uniqueness analysis are presented in Tables 7.8 a, b and c. Note that only six different combinations of parameters are reported here, though all the 29 possible combinations were tested. Table 7.8a shows that for medium textured soil the GML algorithm reaches the true minimum when the number of parameters is less than or equal to four. Indeed, the three different runs launched with different initial estimates (GML1- GML2- GML3) all led to exactly the same true minimum. For the case where five different parameters are optimized, identification of the true minimum is no longer guaranteed and depends strongly on the initial values. Generally, only one of the three runs was successful in finding the true minimum.

Table 7.8. Results of the uniqueness and instability analysis ($*$ =unique, - = nonunique). Table a presents the results for the case where RD is optimized with additional parameters for the medium-fine textured soil. Tables b and c show the results for the coarse textured soil for the estimation of respectively only RD and both RD and BRLD with additional parameters.

a

Nb param.	parameters	GML_1	GML_2	GML_3	GMCS	CI for RD (cm)
1	RD	$*$	$*$	$*$	$*$	12.9
2	RD-n	$*$	$*$	$*$	$*$	14.16
3	RD-n-K_c	$*$	$*$	$*$	$*$	26.54
4	RD-n-K_{sat}-α	$*$	$*$	$*$	$*$	42.85
5	RD-θ_s-n-K_c-α	$*$	-	-	$*$	47.05
6	RD-θ_s-n-K_{sat}-K_c-α	-	-	-	$*$	44-58-73

b

Nb param.	parameters	GML_1	GML_2	GML_3	GMCS	CI for RD (cm)
1	RD	$*$	$*$	$*$	$*$	3.64
2	RD-n	$*$	$*$	$*$	$*$	3.77
3	RD-n-K_c	$*$	$*$	$*$	$*$	4.12
4	RD-n-K_{sat}-α	$*$	$*$	$*$	$*$	4.36
5	RD-θ_s-n-K_c-α	-	-	$*$	$*$	4.5
6	RD-θ_s-n-K_{sat}-K_c-α	-	-	-	$*$	4.82 -6.25 -8.1

c

Nb param.	parameters	GML_1	GML_2	GML_3	GMCS	CI RD-BRLD
2	RD	$*$	$*$	$*$	$*$	4.57- 0.14
3	RD-BRLD-n	$*$	$*$	$*$	$*$	6.02-0.165
4	RD-BRLD-n-K_c	$*$	$*$	$*$	$*$	5.32 - 0.164
5	RD-BRLD-n-K_{sat}-α	-	$*$	-	$*$	5.2 - 0.21
6	RD-BRLD-θ_s-n-K_c-α	-	-	-	$*$	5.24 - 0.1845
7	RD-BRLD-θ_s-n-K_{sat}-K_c-α	-	-	-	$*$	6.66 - 0.196
						9.4 - 0.254
						12.5 - 0.34

When all six parameters are optimized, the optimization algorithm was not able to find the correct minimum irrespective of the initial estimate. Results obtained with the GMCS-NMS algorithm are markedly different. This algorithm succeeds in retrieving the true minimum for all tested combinations of parameters even when the number of optimized parameters is large (i.e. 5 or 6). For this optimization algorithm, only one run was launched for each combination of parameters as the global search procedure uses the bounds of the parameter space instead of specified initial estimates. Similar results are obtained for coarse textured soil (Tables 7.8b and c) for the optimization of only RD or RD and BRLD together. Again, the success of the GML algorithm is limited to four parameters, or sometimes five depending on the chosen initial estimates. Furthermore, for a larger number of parameters (6 or 7), this algorithm is not able the find the true minimum which seems quite logical as such a demanding exercise is clearly beyond the capabilities of a local search optimization algorithm.

In contrast, the GMCS-NMS algorithm is powerful enough to retrieve the correct minimum for all the tested combinations of parameters, and even for the cases where six and seven parameters are simultaneously optimized. These results were systematically obtained with a number of optimization runs smaller than 2500. Similar good results were also obtained for very-fine textured soil (not presented). Therefore, the results of this uniqueness analysis show that the chosen optimization algorithm strongly conditions the success of the optimization when the number of parameters increases. In such a context, the use of a powerful global search algorithm such as GMCS-NMS allows finding of the global minimum and simultaneous optimization of RWUP and up to five additional parameters. Note that such results may seem contradictory to the results obtained in the study of *Hupet et al.* [2002]. Nevertheless, the conclusions of this latter study concerning non-uniqueness problems were only derived from visual inspection of scatter plots which is probably not totally robust. Note additionally that in the study of *Hupet et al.* [2002] the RWUP of interest (A and B) were different from those considered in this study which might also partially explain the different results that are obtained.

Results of the instability analysis are presented in the last column of Tables 7.8 a, b and c, in terms of confidence intervals calculated with Eq. (7.4) after the optimization run was finished. For medium-fine textured soil, the confidence intervals increase progressively with the number of optimized parameters. This is a logical consequence of the increasing degree of freedom caused by an increasing number of "free" parameters. By increasing the number of parameters, correlations between parameters may be activated leading to a widening of the individual confidence intervals. The width of the confidence interval produced for the case when only RD is optimized, i.e. 12.9 cm, is very similar to the value of the true confidence interval presented in Table 5a for the second error level. For the case where all six parameters are simultaneously optimized, the range of the confidence interval estimated for RD is much larger, i.e. 44 cm, implying that the solution is unstable. We also tested the adopted methodology by slightly increasing the error added to the soil water content data for the most difficult case (optimization of RD plus 5 additional parameters). Two additional errors were considered, i.e. 0.015 and 0.02 in terms of standard deviation. For these cases, the range of the confidence intervals increase up to 58 and 73 cm respectively. Such high values mean that the solution is highly unstable. For coarse textured soil, the results are completely different. Indeed, Table 8b shows for the case where RD is optimized with additional parameters that the range of the confidence intervals are very small (3.74<C.I.<4.82) and only increase slightly with the increasing number of parameters. This is obvioulsy the result of a highly stable solution, due to the higher sensitivity of soil water dynamics to RWUP for coarse textured soil and to weaker correlations between RWUP and the additional optimized parameters. In addition, the range of the confidence intervals produced at the larger error level are only slightly larger with values of 6.25 and 8.1 cm for the 0.015 and 0.02 error level respectively. For the case where both RD and BRLD and additional parameters are optimized, the range of the confidence intervals still remain small with values for RD ranging between 4.57 and 6.6 cm and for BRLD between 0.14 and 0.196. Such small values mean that the solution (RD and BRLD) is stable and that it is appropriate to use the inverse procedure. These results are consistent with the study of *Vrugt et al.* [2001a] who estimated RWUP of an almond tree on a sandy soil by inverse modeling using soil water content data. The confidence intervals obtained in their study for RWUP are similar to the values presented in Table 7.8c. By increasing the error in the soil water content data, the performance deteriorates only slightly. The range of the confidence interval reaches maximum values of 12.5 cm for RD and 0.34 for BRLD for the 0.02 error level. We do not present in Tables 8 the confidence intervals of the other optimized parameters (i.e. the soil hydraulic parameters) as we are mainly interested in the optimization of RWUP. Nevertheless, some of the obtained confidence intervals especially those of K_{sat} are very large. More detailed information for K_{sat} should be obtained by alternative techniques for an accurate prediction of soil water movement during periods when K_{sat} plays an important role (e.g., infiltration-redistribution events). In this framework, we could suggest using a re-wetting event during or at the end of the drying period which could help to improve the estimation of the simultaneously optimized hydraulic parameters. Nevertheless, the use of such a re-wetting event at the end of the drying period will inevitably need to consider hysteresis issues. Consequently, there is a risk of making the inverse problem more complex and the optimized parameters more uncertain. The results obtained for very-fine textured soil are not presented as they are very similar to those obtained for coarse textured soil, with the confidence intervals broadening only a little.

7.4 Conclusions

In this chapter, we have tested the feasibility of the inverse modeling approach to derive root water uptake parameters (RWUP) with only soil water content data. This was performed with numerical experiments for three different textured soils and for a long dry period during which crop growth was considered negligible.

The sensitivity analysis showed that soil water content dynamics are relatively insensitive to the RWUP though the sensitivity is higher for very-fine and coarse textured soils. The insensitivity of soil water dynamics to RWUP for medium-fine textured soil compared to the other two textured soils can be explained by a "compensating effect", i.e. by vertical unsaturated water flows overshadowing in some way the root water uptake "signal". Visual inspection of response surfaces (in 1-D and 2-D) showed that the solution is unique when only RD, BRLD or both are optimized. The instability analysis showed, for medium textured soils, that the inverse modeling approach is only feasible for estimating RD, although the estimated confidence interval is very large (60.5-136.4cm). For coarse and very-fine textured soil, the optimization of RD is robust to both errors in soil water contents and in the other 'fixed' parameters of the system. These results suggest that the inversion of soil water content data for RWUP identification is ill-posed except for the estimation of RD for coarse and very-fine textured soil. These results are consistent with the study of *Hupet et al.* [2002] and *Musters and Bouten* [1999].

Finally, the well-possedness of the inversion was studied for the case where RWUP are simultaneously optimized with additional system parameters. For the three differently textured soils, the solution is unique if a powerful global optimization algorithm is used. For coarse and very-fine textured soils, the solution is quite stable which allows the simultaneous identification of RD and BRLD. These results clarify some of the conclusions presented in *Hupet et al.* [2002] concerning the unfeasibility of the simultaneous estimation of RWUP with additional soil hydraulic parameters.

In conclusion, our study showed that the inverse modeling approach to estimate RWUP is feasible subject to two cautionary notes. First, the texture of the soil strongly influences the success of the inversion. Coarse and very-fine textured soils are much more suitable for the identification of RWUP than medium-fine soils. Indeed, for these soils the "compensating effect" of vertical unsaturated water flows overshadowing the RWU is only slightly marked because the unsaturated conductivity of these soils decreases rapidly beyond a certain suction range. Secondly, the success depends on the choice of the parameters to optimize. Indeed, this study showed that the estimation of RWUP by fixing all the other parameters of the system is unreliable.

We further recommend studying the impact of the sampling frequency (both temporal and spatial) of soil water content data on the results of the inverse procedure. Indeed, the sampling strategy adopted in this study was very intensive both in time and space, which is hard to implement in real experiments. Similar studies should also be tested for more pessimistic error levels both for soil water content measurements and for fixed parameters. Indeed, some presented results are probably dependent on the selection of the error levels which remains in some way subjective. In addition, we recommend investigating the possibility of incorporating additional information such as measured transpiration fluxes or the time derivative of the soil water content in the inverse problem. Indeed, this study showed that the RWU parameterization has a pronounced impact on the transpiration fluxes for some soils and the study of *Hupet et al.* [2002] suggested that the use of the time derivative of soil water content could be valuable. The use of periods including a re-wetting event during or at the end of the monotonic drying period should also be tested as the use of shorter periods (e.g., a week) for which the assumption of no root growth is certainly more realistic. We also recommend extending the methodology adopted in this paper to multi-dimensional (2-D and 3-D) root water uptake parameterizations. Indeed, such parameterizations raise additional problems as they contain many more RWUP and the domain over which the soil water dynamics is simulated is larger, which necessitates dealing with the lateral spatial variability of the soil hydraulic properties. We finally suggest, before applying the inverse approach for real cases, studying the feasibility of the inverse estimation of RWUP for multi-layered soils.

Chapter 8

Quantifying the local scale uncertainty of actual evapotranspiration estimated with a soil water balance approach

Abstract*

In this chapter, we quantified the local scale uncertainty of the actual evapotranspiration estimated from a water balance approach combining two soil water content measurement techniques (TDR and neutron probe sounding). The local scale uncertainty was quantified for 28 sampling points located within a small maize cropped field. This was done by determining progressively the expected value and uncertainty in soil water content, soil water storage, soil water storage variation and in bottom flux. This latter term was quantified using two different hydraulic conductivity curves (HCC), derived from a pedotransfer function and from field measurements. Results show that uncertainty in a soil water storage estimate for the considered experimental measurements in terms of standard deviation range between 9.72 and 10.37 mm. This uncertainty is mainly due to the calibration of the soil water content measurement instruments. For a soil water storage variation estimate, the uncertainty is smaller with values ranging between 3.48 and 5.42 mm. In this case, the main component of the total variance is the instrumental variance

---

*adapted from Hupet, F., P. Bogaert, and M. Vanclooster, accepted for publication in *Hydrological Processes*.

and the variance resulting from the technique used to integrate soil water content measurements. The expected values and uncertainties for the bottom fluxes were significantly different for the two different HCC characterisation techniques in some places in the field. For estimated ET fluxes with in-situ estimated HCC results show that the uncertainty range in terms of standard deviation between 3.82-5.97 mm and between 2.6 and 2.8 mm if errors due to the integration method are considered as negligible. It should be stressed that these values can be considered as very low and that a better precision is probably very difficult to obtain as all sensitive factors contributing to the ET variance have been determined in a consistent and optimal way. Finally, it is shown that the uncertainties in estimated HCC with PTF's may result in large uncertainties in estimated ET, questioning thereby the use of PTF's in characterising the field water balance.

8.1 Introduction

Estimating accurate evapotranspiration fluxes (ET) at different spatial and temporal scales remains an important challenge for a wide range of disciplines, such as irrigation management, surface hydrology and meteorology. ET fluxes or components of these (evaporation and transpiration) can be estimated by different methodologies, including sap flow, weighing lysimeter, soil water balance, SVAT modelling, eddy correlation and catchment water balance. Each of those methodologies produce ET estimates at a particular scale [*Wilson et al.*, 2001] and the choice of one or another method depends on both the spatio-temporal scale of interest and the working context for which ET estimations are needed, such as a fundamental research context [e.g, *Jhorar et al.*, 2002], an applied research context [*Howell et al.*, 1998], or for engineering purposes [e.g., *Lascano et al.*, 1996].

At the field scale, the soil water balance approach remains one of the most commonly used method for different reasons. Firstly, it implies quite simple instrumentation and calculations; secondly it does not impose restrictions to the analysed field size; and thirdly it provides some insight on soil water processes within the soil profile. Nonetheless, the soil water balance has well known weaknesses which are mainly a low spatio-temporal resolution and a degree of accuracy which is often poor. Indeed, uncertainty on a field ET estimate can be large due to e.g. spatial variability of processes within the field, uncertainty on drainage estimate and uncertainty on soil water content measurements [*Rana and Katerji*, 2000; *Wilson et al.*, 2001]. A thorough understanding of the contribution of these partial uncertainties in the total uncertainty of the ET estimates is important to improve the efficiency of ET characterisation methods and for being more performant in hydrological studies appealing on ET assessments.

Somewhat paradoxically, although the soil water balance approach is well established and has been extensively used, rigorous quantification of associated uncertainties in the soil water balance terms is rarely done. In this context, the study of *Sinclair and Williams* [1979], and that of *Haverkamp et al.* [1984] and of *Vauclin et al.* [1984] can be considered as precursors. These authors quantified uncertainties in soil water content, soil water content variation and soil water storage. Later, *Poss* [1991] and *Vandervaere et al.* [1994a,b] extended the proposed methodology for quantifying uncertainties in ET fluxes estimated at the local and field scale. Although these latter studies can clearly be seen as a step forward compared to former ones, they have some limitations. Firstly, soil water content measurements in these studies were performed with a neutron probe. The interpretation of neutron probe measurements for characterising soil water content in the superficial soil layers may be problematic. Alternative soil water content measurement techniques such as gravimetric soil water content determination or one or more vertically installed TDR probes [e.g., *Leuning et al.*, 1994; *Abrisqueta et al.*, 2001] are often used to complement at the soil surface the neutron probe readings. Secondly, uncertainties on the fluxes at the bottom of the soil profile were not considered in the study of *Vandervaere et al.* [1994a, b] as the zero flux plane method was used by these authors. It is well known that the zero flux plane method can be a limitation for adopting the soil water balance during some periods such as during redistribution events. Furthermore, in general, large uncertainties are associated with the bottom fluxes in the water balances [*Katerji et al.*, 1984]. Thirdly, the number of sampling points, i.e. the number of access tubes were quite low in these studies (3 or 4 tubes per plot) limiting the validity of the studies in terms of spatial variability and spatial dependence between the sampling locations. Finally, in the study of *Vandervaere et al.* [1994a,b], the considered time period is quite short (22 days) limiting the assessment of the temporal dynamics of the uncertainties. The present study has been designed to avoid some of these limitations and to proceed in analysing uncertainty components in ET estimates. The study is based on the results of a field experiment initially designed to study the spatio-temporal variability of the hydrological processes at the field scale. For this field experiment, a large data set of soil water content observations, pressure head observations, and soil hydraulic properties are available. With respect to the limitations of aforementioned studies, the present field experiment can be characterised by an improvement of the experimental design for measuring soil water content (i.e. the combination of TDR and neutron probe technique), by an improved spatial resolution of sampling (i.e. 28 sampling points), by a longer analysis period (4 months), and by considering the fluxes at the bottom of the soil profile in the analysis. As the uncertainty quantification of an ET estimate is a really gradual and stepwise process, this requires quantification of uncertainties for soil water content, soil water storage, soil water storage variation and flux at the bottom of the profile. Quantification of those uncertainties is in fact also of paramount importance as soil water contents is used e.g. for calibrating soil-water transport models, soil water storage variations e.g. for scheduling irrigation and fluxes at the bottom of the profile for estimating groundwater recharge. In this study, uncertainty quantification will be performed at the local scale, i.e. at the scale of the measurement instrument corresponding to a specific sampling location within the field. The objectives of this chpater can be summarised as follows :

(1) to quantify uncertainties both for a soil water content estimate performed with TDR and neutron probe; a specific methodology is proposed for TDR, and for neutron probe we used existing statistical developments;

(2) to quantify uncertainties related to a soil water storage estimate combining two measurement techniques, and to a soil water storage variation estimate. Estimation of fluxes at the bottom of the profile and associated uncertainty are investigated with two different approaches. The first one uses hydraulic conductivity curves predicted with pedotransfer functions while the second uses field measurements;

(3) to quantify uncertainty on a local ET estimate by combining all the previously quantified uncertainties and investigate the temporal evolution of the magnitude of those uncertainties. Note that for estimated variations of soil water storage and estimated ET, we will only focus on two long dry periods which are normally optimum periods for accurate estimates of the aforementioned variables.

8.2 Material and methods

This chapter is based on the 1999 experimental setup. It makes use of the comprehensive data set collected on the 28 sampling locations including nearly 8 000 soil water content and 2500 pressure head measurements.

Soil hydraulic parameters describing the water retention curve and the hydraulic conductivity curve are also used.

8.2.1 Uncertainty analysis

Volumetric soil water content

For soil water content measurements performed with a neutron probe, *Sinclair and Williams* [1979] and *Haverkamp et al.* [1984] showed, considering that calibration curve can be represented by a linear equation, that total variance of an individual predicted soil water content is expressed as the sum of both instrument and calibration components expressed as:

$$s^2_{inst}(\widehat{\theta}) = \{\widehat{b}^2 - s^2(\widehat{b})\}\left[\frac{\widehat{n}}{pT_c} + \frac{\widehat{n}^2}{qT_s}\right]\frac{1}{\widehat{N_s}} \tag{8.1}$$

$$s^2_{calib}(\widehat{\theta}) = s^2(\widehat{a}) + \widehat{n}^2 s^2(\widehat{b}) + 2\widehat{n}s(\widehat{a},\widehat{b}) + s^2(e_{neut}) \tag{8.2}$$

with $\widehat{a}$ and $\widehat{b}$ estimates of the intercept (a) and the slope (b) of the regression line, $s^2(\widehat{a})$ and $s^2(\widehat{b})$ their respective estimates, $s(\widehat{a},\widehat{b})$ the estimated covariance between $\widehat{a}$ and $\widehat{b}$, $s^2(e_{neut})$ the estimated variance of e_{neut}; $\widehat{N_s}$ the estimate of N_s the mean count rate of q replicates recorded in water during a counting time of T_s sec, and $\widehat{n}$ the estimate of n the ratio between the mean count rate of p replicates recorded in the soil at the same depth during a counting time of T_c sec and the mean count rate N_s. Note that e_{neut} in Eq. (8.2) is a stochastic disturbance term of zero mean caused both by deviation of the exact linear model, as only one linear model is considered for the whole field though some spatial variability is present, and by errors involved during the calibration process on soil water content and count rate ratio. All parameters associated to the calibration curve are directly derived from an unbiased regression analysis and are detailed in *Haverkamp et al.* [1984].

For soil water content measurements performed with Time Domain Reflectometry (TDR), the calibration curve, i.e. the relation between the apparent dielectric constant (K_a) and the soil water content (θ_{TDR}), can be expressed by different empirical relationships or by different mixing models [e.g., *Topp et al.*, 1980; *Herkelrath et al.*, 1991; *Dirksen and Dasberg*, 1993]. For this study, we opted for a linear relationship between the root of the apparent dielectric constant and the soil water content as proposed by *Ledieu et al.* [1986]. This calibration equation can be expressed as:

$$\theta_{TDR} = c + d\sqrt{K_a} + e_{TDR} \tag{8.3}$$

As for the neutron probe, the measurement errors mask more or less the true values θ_{TDR} and $\sqrt{K_a}$, so that only the following equation can be established :

$$\widehat{\theta}_{TDR} = \widehat{c} + \widehat{d}\sqrt{\widehat{K}_a} \tag{8.4}$$

Extending the statistical developments proposed by *Haverkamp et al.* [1984] for the neutron probe for the TDR leads to the total variance of an individual predicted estimation of $\widehat{\theta}_{TDR}$:

$$s^2\widehat{\theta}_{TDR} = \left[\widehat{d}^2 - s^2(\widehat{d})\right] s^2(\sqrt{\widehat{K}_a}) + s^2(\widehat{c}) + \widehat{K}_a s^2(\widehat{d}) + 2\sqrt{\widehat{K}_a} s(\widehat{c}, \widehat{d}) + s^2(e_{TDR}) \tag{8.5}$$

with $\widehat{c}$ and $\widehat{d}$ estimates of the regression coefficients c and d, $s^2(\widehat{c})$ and $s^2(\widehat{d})$ their respective estimated variance, $s(\widehat{c}, \widehat{d})$ the estimated covariance between $\widehat{c}$ and $\widehat{d}$ and $s^2(e_{TDR})$ the estimated variance of e_{TDR}. In Eq. (8.5), all parameters can be derived from the regression analysis except $s^2(\widehat{K_a})$. In order to estimate this term, we must restart from the original expression of the apparent dielectric constant expressed as :

$$K_a = \left[\frac{c\Delta t}{2L}\right]^2 \tag{8.6}$$

with c the velocity of light in vacuum (3.10^8 m s^{-1}), Δt the travel time (s) of the TDR signal in the soil and L the physical length of the waveguides (0.2 m in the present study). After converting Δt into ΔL_a, and as we use a relative velocity propagation equal to 0.66 c, we can rewrite Eq. (8.6) as the root of the apparent dielectric constant:

$$\sqrt{K_a} = \frac{\Delta L_a}{0.66L} = \frac{(L_2 - L_1)}{0.66L} \tag{8.7}$$

with L_2 and L_1 the apparent lengths at which occur respectively the first and the second reflection and ΔL_a the difference between these two lengths. As the interpretation of the TDR trace was done manually on the screen, it was assumed that the major source of uncertainty induced on $\sqrt{K_a}$ results from the determination of the apparent length at which the second reflection occurs [as in *Topp et al.*, 1980]. In this framework, numerous comparisons between manual determinations of the point of the second reflection and those determined with the WinTDR 98 software [*Or et al.*, 1998], considered here as giving the true value of L_2, showed that $\widehat{L_2}$ can be approximated by L_2 and $s^2(\widehat{L_2})$ by 1.10^{-4} m. As the length of the probes used are 0.2 m, we can rewrite Eq. (8.7) and quantify the variance of $\sqrt{\widehat{K_a}}$ as:

$$s^2(\sqrt{\widehat{K}_a}) = 7.58^2 s^2(\widehat{L}_2) \tag{8.8}$$

Replacing this in Eq. (8.5) and decomposing the total variance into its two components gives :

$$s^2_{instr}(\widehat{\theta}_{TDR}) = \left[\widehat{c}^2 - s^2(\widehat{c})\right] 7.58^2 s^2(\widehat{L}_2) \tag{8.9}$$

$$s^2_{calib}(\widehat{\theta}_{TDR}) = s^2(\widehat{c}) + \widehat{K}_a s^2(\widehat{d}) + 2\sqrt{\widehat{K}_a} s(\widehat{c},\widehat{d}) + s^2(e_{TDR}) \tag{8.10}$$

Soil water storage

The soil water storage held within the soil profile between the soil surface and a given depth z can be calculated as follows :

$$S = \int_o^z \theta(z) dz \tag{8.11}$$

As soil water contents at different depths are estimated and as there is generally no analytical integrable form of Eq. (8.11), only an estimate of the true storage S can be obtained. The total variance of the soil water storage is therefore composed of two terms [*Haverkamp et al.*, 1984; *Vandervaere et al.*, 1994a]:

$$s^2(\widehat{S}) = s_1^2(\widehat{S}) + s_2^2(\widehat{S}) \tag{8.12}$$

with $s_1^2(\widehat{S})$ the storage variance due to uncertainties on soil water content measurements and $s_2^2(\widehat{S})$ the storage variance caused by the numerical technique used to integrate Eq. (8.11). In this study, soil water storage was estimated between 0 and 125 cm depth which corresponds to the deepest depth at which soil water content measurements were done. Note that as the measured soil profiles between 110 and 125 cm depth (and even slightly deeper) were generally very uniform, we considered here that soil water content measurements performed at 125 cm were representative of soil water content between 100 and 125 cm depth. Four different integration techniques, trapezoidal method and Simpson's $\frac{1}{3}$ rule with two different integration methods between 20 and 25 cm depth, were firstly tested (see Fig. (8.1)). Although some theoretical formulae are available to quantify variance of integration [see e.g., *Poss et al.*, 1991 and *Ould Mohamed et al.*, 1997], we adopted in the present study a methodology using a numerical soil water balance model

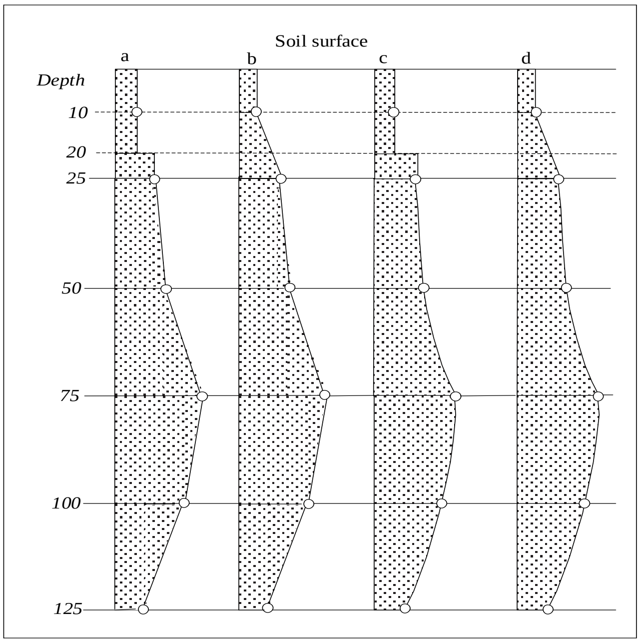

Figure 8.1. Four different integration techniques, trapezoidal method (a-b) and Simpson rule (c-d) with two different integration methods between 20 and 25 cm depth.

to generate quasi continuous soil water content profiles which were then integrated to yield the reference soil water content storage. In this context, we run for the period of interest the WAVE-model [*Vanclooster et al.*, 1996] roughly parameterised (soil and crop parameters) for the field under consideration. For each centimetre down to 125 cm depth, the numerical run produced daily soil water contents which were then integrated to generate daily 'true' soil water content storage. Subsequently, with the numerically generated soil water contents corresponding to the field depths of measurement (0-20, 25, 50, 75, 100 and 125 cm depth), we tested the four different integration techniques against the 'true' storage and quantified the errors and the variance $s_2^2(\widehat{S})$ caused by the integration method. As it will be shown in the results, Simpson's $\frac{1}{3}$ rule with a linear interpolation between 20 and 25 cm depth yielded the best results leading therefore to the following expression for the estimated soil water storage:

$$\widehat{S} = 200\widehat{\theta}_1 + 50\widehat{\theta}_2 + \frac{250}{3}(\widehat{\theta}_2 + 4\widehat{\theta}_3 + 2\widehat{\theta}_4 + 4\widehat{\theta}_5 + \widehat{\theta}_6) \tag{8.13}$$

with $\widehat{S}$, the estimated soil water storage and $\widehat{\theta}_1, \widehat{\theta}_2, \widehat{\theta}_3, \widehat{\theta}_4, \widehat{\theta}_5$, and $\widehat{\theta}_6$ the estimated soil water content measured respectively at the aforementioned depths.

In order to develop the term $s_1^2(\widehat{S})$ of Eq. (8.12) it was considered as in the study of *Vandervaere et al.* [1994 a] that neutron probe soil water content measurements were not independent of one another as the same calibration equation was used for soil water content measurements between 25 and 125 cm depth. Taking into account this dependence and considering the TDR measurements as independent of the neutron probe measurements, can be expressed as :

$$s_1^2(\widehat{S}) = 200^2 s^2(\widehat{\theta_1}) + 133^2 s^2(\widehat{\theta_2}) + 333^2 s^2(\widehat{\theta_3}) + 166^2 s^2(\widehat{\theta_4}) + 333^2 s^2(\widehat{\theta_5}) + 83^2 s^2(\widehat{\theta_6}) + fh \sum_{i=2}^{6} \sum_{j=2_{j \neq i}}^{6} s(\widehat{\theta}_i, \widehat{\theta}_j) \quad (8.14)$$

with f and h equal to 133, 333, 166 or 83, and the covariance terms $s(\widehat{\theta}_i, \widehat{\theta}_j)$ quantified by Eq. (8.25) given in Appendix 1.

Soil water storage variation

The difference between two soil water storages estimated at days t_1 and t_2 can be written as follows :

$$\Delta\widehat{S}_{t1,t2} = \widehat{S}_{t1} - \widehat{S}_{t2} \quad (8.15)$$

with $\Delta\widehat{S}_{t1,t2}$ the estimated difference, and $\widehat{S}_{t1}$ and $\widehat{S}_{t2}$ the estimated soil water storage at days t_1 and t_2. Considering that the two estimated soil water storages $\widehat{S}_{t1}$ and $\widehat{S}_{t2}$ are dependent, we can express the variance of a soil water storage variation as:

$$s^2(\Delta\widehat{S}_{t1,t2}) = s^2(\widehat{S}_{t1}) + s^2(\widehat{S}_{t2}) - 2s(\widehat{S}_{t1}, \widehat{S}_{t2}) \quad (8.16)$$

with $s^2(\Delta\widehat{S}_{t1,t2})$, $s^2(\widehat{S}_{t1})$ and $s^2(\widehat{S}_{t2})$ respectively the estimated variance of the difference $\Delta\widehat{S}_{t1,t2}$, of $\widehat{S}_{t1}$ and $\widehat{S}_{t2}$ and $s(\widehat{S}_{t1}, \widehat{S}_{t2})$ the estimated covariance between $\widehat{S}_{t1}$ and $\widehat{S}_{t2}$. The first two terms of Eq. (8.16) are estimated with Eq. (8.12) and the covariance term $s(\widehat{S}_{t1}, \widehat{S}_{t2})$ with the expression developed in Appendix 2 (see Eq. (8.28)).

Bottom flux

The downward and upward fluxes at the bottom of the soil profile (125 cm) can be estimated from Darcy's law :

$$\widehat{q} = -\widehat{K}(h)\widehat{\nabla}(H) \quad (8.17)$$

with $\widehat{q}$ the estimated daily fluxes at the bottom of the profile (mm d^{-1}) taken as positive and negative for respectively upward and downward fluxes, $\widehat{K}(h)$ the estimated unsaturated hydraulic conductivity (mm d^{-1}) and $\widehat{\nabla}(H)$ the estimated total hydraulic gradient. In this study, uncertainty on $\widehat{\nabla}(h)$ is considered as negligible. Indeed, the only uncertainty robustly quantifiable for $\widehat{\nabla}(H)$ is due to errors on measured pressure heads. The variance of the measurement error on H is, according the manufacturer, estimated to be 0.01 cm^2, which is similar to the value given by *Dirksen* [1999], and which is very small compared to uncertainties generally presented on hydraulic conductivity curve (HCC). Therefore, the estimated variance of $\widehat{q}$ can be written as follows:

$$s^2(\widehat{q}) = \widehat{\nabla}H^2 s^2(\widehat{K}(h)) \tag{8.18}$$

with $s^2(\widehat{q})$ and $s^2(\widehat{K}(h))$ respectively the estimated variance of $\widehat{q}$ and $\widehat{K}(h)$. For deriving $\widehat{K}(h)$ and $s^2(\widehat{K}(h))$, two different approaches are used and tested. The first is an indirect approach (I) which uses pedotransfer functions (PTFs), in this case the hierarchically structured PTFs presented by *Schaap et al.* [2001], which provides estimates of HCCs and associated uncertainties. As moisture retention curves are available for each sampling location at 105 cm depth, we use moisture retention curve information to predict the HCC. Uncertainty and confidence intervals of HCCs are calculated with uncertainty of estimated parameters (K_o and λ) provided by the Rosetta software [*Schaap et al.*, 2001]. This approach produces therefore 28 different HCCs with their own associated uncertainty, each one corresponding to one sampling location. Note that special care is taken when defining confidence intervals of hydraulic conductivity curves and estimated bottom fluxes as uncertainty on hydraulic conductivity parameter K_o provided by Rosetta is normally distributed in a log_{10} basis. In the second approach (II), HCCs are "in-situ" determined by combining two kinds of measurements. The first consists of tension disc infiltrometer measurements providing estimates of the HCC for pressure heads larger than -11 cm. The second consists of a simplified water balance applied during the dry period occurring between the 8^{th} and the 19^{th} of June. For this period, five measured soil water storages, pressure heads and hydraulic gradients at the bottom of the profile are available allowing an estimation for each 28 location of 10 points of the HCC. Note that adopting this methodology, we explicitly took into account uncertainties on the water storage variations due to uncertainties mentioned in Section 1.2 but also to uncertainties on surface fluxes. Therefore, a confidence interval is associated to each of the 10 points of the HCC produced with the simplified water balance. Subsequently, HCCs are estimated for each location with 21 "in-situ" determined K-h pairs (11 pairs from tension infiltrometer and 10 from simplified water balance) using the Mualem-van Genuchten $K(h)$ relation [*van Genuchten*, 1980] with fitted K_{sat} and parameters. The fitting operation was repeated 100 times for each location, each run corresponding to 10 points (generated with the simplified water balance) selected within their confidence interval and 11 points selected among the observed variability of the tension infitrometer measurements. Indeed, as places and depths of measurements for tension infitrometer are not exactly those of interest and as it is well known that microvariability of soil hydraulic properties is very large [e.g., *Mallants*, 1995], all tension infitrometer measurements were considered valid for each sampling location. As the first approach, the second one (II) produces therefore 28 HCC with their own uncertainties, each one for each sampling location.

Actual evapotranspiration

The actual evapotranspiration flux between t_1 and t_2 for a dry period during which no or negligible rainfall, irrigation and runoff occurred can be estimated as:

$$\widehat{ET}_{t1,t2} = \widehat{\Delta} S_{t1,t2} + \widehat{q}_{t1,t2} \tag{8.19}$$

with $\widehat{ET}_{t1,t2}$ the estimated evapotranspiration flux (mm), $\widehat{\Delta} S_{t1,t2}$ the estimated difference of soil water storage between t_1 and t_2 (mm), and $\widehat{q}_{t1,t2}$ the estimated water flux at the bottom of the profile (mm). Assuming that uncertainties on $\widehat{\Delta} S_{t1,t2}$ and $\widehat{q}_{t1,t2}$ are independent, we can express actual evapotranspiration uncertainties as follows:

$$s^2(\widehat{ET}_{t1,t2}) = s^2(\widehat{\Delta} S_{t1,t2}) + s^2(\widehat{q}_{t1,t2}) \tag{8.20}$$

with $s^2(\widehat{\Delta} S_{t1,t2})$ and $s^2(\widehat{q}_{t1,t2})$ quantified by respectively Eq. (8.16) and (8.18). A relative error was also calculated for each considered variable, i.e. $\widehat{\theta}$, $\widehat{S}$, $\widehat{\Delta} S$, $\widehat{q}$ and $\widehat{ET}$. This relative error was expressed as the ratio between the standard deviation of the variable of interest and the estimated value of this same variable.

8.3 Results and discussions

8.3.1 Volumetric soil water content

The physical soil water content values were obtained by using the in-situ established calibration equations presented in Figs. 8.2a and b respectively for neutron probe and TDR. This figure shows the regression lines and the associated prediction intervals at 95%. Note that in this study,

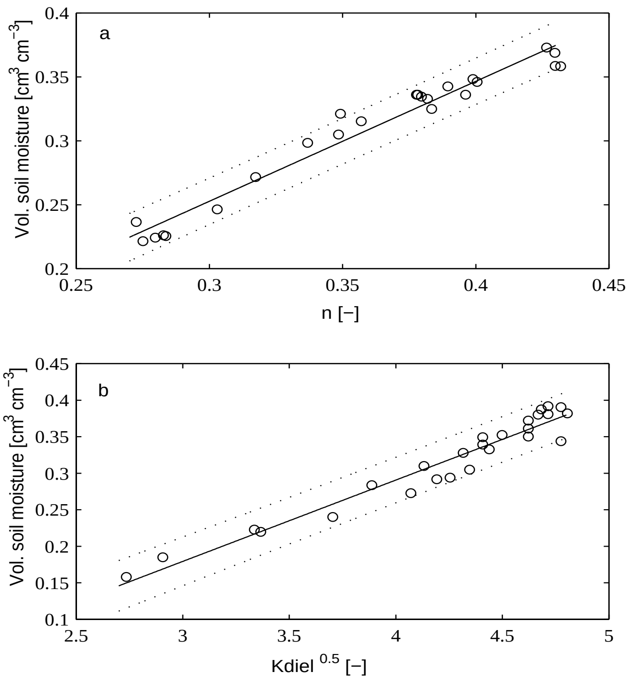

Figure 8.2. Calibration curves of neutron probe (a) and TDR (b). Circles indicate experimental observations. Also shown are the regression lines and the prediction intervals at 95%.

we adopted an unbiased statistical treatment (i.e. taking into account uncertainties on θ and n) so as to minimise uncertainties on the predicted variables although a biased treatment produced quite similar results (not shown here). This can be explained by the fact that the two calibration curves were carefully established taking e.g. several replicates for the volumetric water content determination and replicating measurements with a long counting time for neutron probe measurements minimising therefore errors on each 25 pairs of measurements. Table 8.1 summarises the different components of the variance associated to a soil water content estimate. Note that for clarity reasons the variance of estimates in this study is expressed in terms of standard deviation. Yet, variance is used when the relative contribution of the different components to the total variance is quantified. In Table 8.1 and in all tables further on, presented values correspond to minimum and maximum observed for the whole field, i.e. for each 28 sampling location. On the other hand, all figures will be drawn either for sampling locations 2 or 8 or both, as they are particularly different and illustrative for the considered vari-

Table 8.1. Components of total variance (i.e. calibration and instrument component) for a volumetric water content estimate. Results are expressed in terms of standard deviation (cm^3 cm^{-3}). Also shown are intercept and slope values of the regression lines.

	Neutron probe	TDR
intercept ($\widehat{a}$ and $\widehat{c}$)	-0.02864	-0.1547
slope ($\widehat{b}$ and $\widehat{d}$)	0.93801	0.11135
$s_{inst}(\widehat{\theta})$($cm^3$ cm^{-3})	0.0021-0.0028	0.005801
$s_{calib}(\widehat{\theta})$ (cm^3 cm^{-3})	0.0087-0.0092	0.0147-0.0166
$s_{tot}(\widehat{\theta})$($cm^3$ cm^{-3})	0.0091-0.0095	0.0158-0.0176
relative error	2.2-5.7 %	3.7-11.7 %

ables and their associated uncertainty. From Table 8.1, it emerges that the instrument component is quite small compared to the calibration component. As a matter of fact, the relative contribution of the instrument variance to the total variance is less than 10%, a value quite similar for the two measurement techniques. Table 8.1 also shows that the total standard deviation of a soil water content estimate is larger for TDR (0.0158-0.0176) than for neutron probe (0.0091-0.0095). Nevertheless, these values can be considered as low, especially for neutron probe, and representative of a very good calibration process. Figure 8.3 illustrates the intraseasonal dynamics of soil water content measured on sampling location 2 with TDR (b) and neutron probe at a depth of 25 cm (c), with shaded areas corresponding to the one standard deviation confidence interval. Note that uncertainty of soil water content measurements can be considered as constant through the season. This results directly from the fact that pairs of observations used for the calibration process explore a large range of soil water content values and are further well distributed within this range. Figure 8.3 illustrates also the temporal evolution of the relative error of a soil water content estimate (line with cross markers) bounded for the selected sampling location between 2.5 and 10.5%.

8.3.2 Water storage

In a preliminary analysis, we tested different integration techniques. Fig. 8.4 illustrates the temporal evolution of the absolute error on a soil water storage estimate for the four tested integration methods. These are trapezoidal method (a and b) and Simpson's $\frac{1}{3}$ rule (c and d) with two

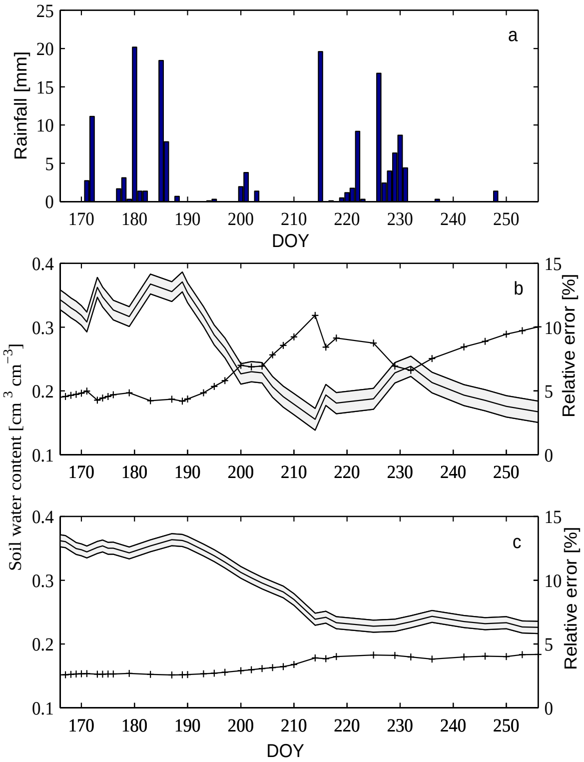

Figure 8.3. Temporal dynamics of volumetric soil moisture illustrated for sampling point 2 for TDR (a) and neutron probe at 25 cm depth (b). Shaded area indicated ± one standard deviation. Dynamics of the relative error is also presented in these figures with daily rainfall for the corresponding period in the upper graph.

different techniques for interpolating between 20 and 25 cm depths. In Fig. 8.4 are also shown simulated soil water content profiles at days identified with an arrow within the daily rainfall figure. Circles indicated on the soil water content profiles are simulated soil water content values corresponding to the depths of interest in our study. Fig. 8.4 shows clearly that the method of integration has a direct impact on the magnitude of the absolute error and that error is larger during rainfall events or during redistribution periods when soil water content profile is likely to be irregular. In our case, Simpson's $\frac{1}{3}$ rule yields better results than trapezoidal method especially when the soil water content profile is nonhomogeneous which is coherent with the results obtained by *Haverkamp et al.* [1984]. As the Simpson's $\frac{1}{3}$ rule with a linear interpolation between 20 and 25 cm depth is the one minimising errors on a soil water stor-

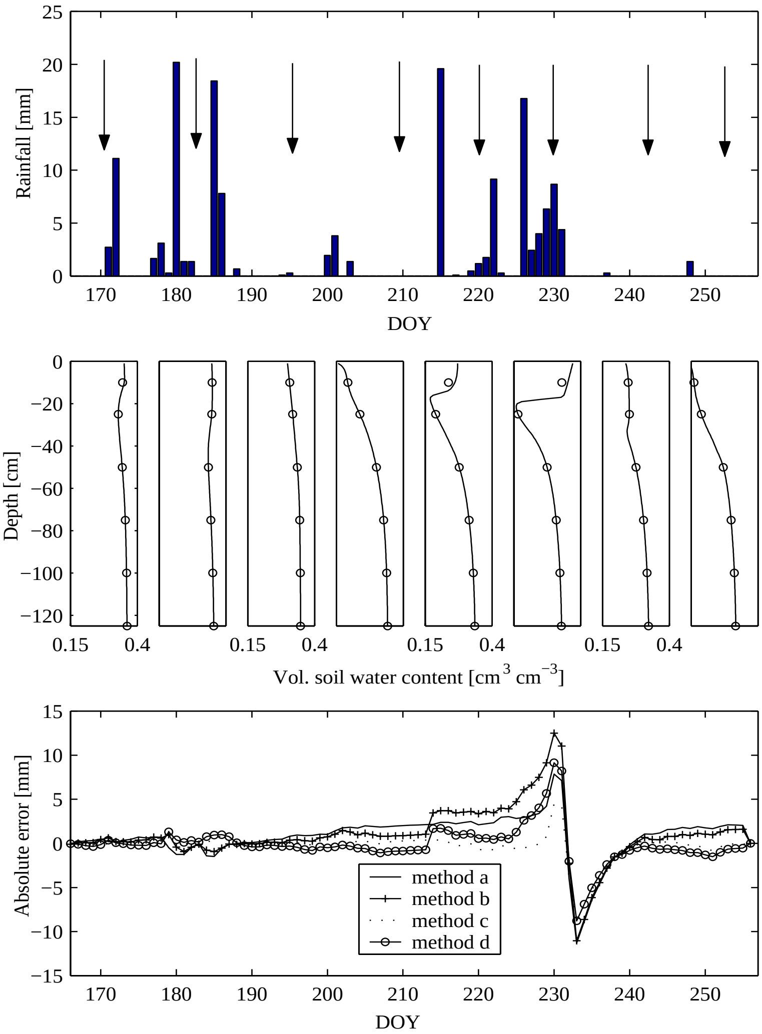

Figure 8.4. Impact of the method of integration on the soil water storage estimate. Bottom figure illustrates the temporal dynamics of the absolute error (mm) for the four tested methods (a-b trapezoidal method; c-d Simpson's $\frac{1}{3}$ rule). Middle figure shows some simulated soil moisture profiles corresponding to days indicated with an arrow in the upper figure.

Table 8.2. Components of total variance (i.e. calibration, instrument and integration component) expressed in terms of standard deviation (mm) for a soil water storage estimate held within 0-125 cm. Presented data are minimum and maximum values of soil water storage for all sampling locations.

$s_{inst}(\widehat{S})$	1.59- 1.93 mm
$s_{calib}(\widehat{S})$	9.42- 10.06 mm
$s_{integ}(\widehat{S})$	1.62 mm
$s_{tot}(\widehat{S})$	9.72-10.37 mm
relative error	2.09-3.62 %

age estimate, only this method will be afterwards considered. In order to quantify the variance associated to this selected integration method ($s_2^2(\widehat{S})$ in Eq. (8.12)), we used the statistical distribution of the absolute errors of soil water storage (method c) which can be approximated by a normal distribution with a mean of zero and a standard deviation of 1.62 mm. It is worth to note that this constitutes probably an overestimation of the variance as in our case the estimate of the uncertainties on ET is only focused on dry periods when the selected integration method produces very good results. Table 8.2 shows the different components of the errors in terms of standard deviation (mm). The obtained values for the total standard deviation for a soil water storage estimate bound between 9.72 and 10.37 mm which is similar to values obtained by *Poss* [1991] for a soil water storage held within 0-150 cm (std=8.9mm) and by taking into account the smaller profile (70 cm) by *Vandervaere et al.* [1994] with values between 5.7 and 6.9 mm. In contrast with those results, *Haverkamp et al.* [1984] obtained values as small as 4.02 mm for a soil water storage held within 0-105 cm but they did not consider the dependence between the different depths neglecting therefore the covariance terms of Eq. (8.14). If we had neglected covariance terms in this study we would have reduced the standard deviation of the soil water storage estimate of 60% leading to values bound between 5.96 and 6.41 mm. Such an increase of the precision for a soil water storage estimate can be performed for instance if separate good quality calibration curves are obtained for each investigated depth [e.g., *Ould Mohamed et al.*, 1997] as in this case covariance terms of Eq. (8.14) are missing. In our study, the main component of the total variance for a soil water storage estimate is the calibration variance with a relative contribution of 93.1%. On the other hand, the components relative to the instrumental and integration errors are very small with values of respectively 2.6% and 4.4%.

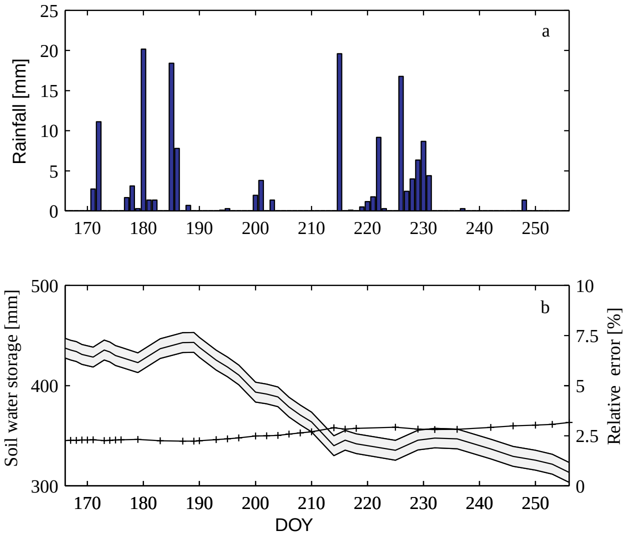

Figure 8.5. Temporal dynamics of soil water storage illustrated for sampling point 8. Shaded area indicated ± one standard deviation. Dynamics of the relative error is also presented in these figures with daily rainfall for the corresponding period in the upper graph.

Intraseasonal dynamics of soil water storage estimated on sampling location 8 is illustrated in Fig. 8.5b with shaded areas corresponding to one standard deviation confidence interval. Similar to the water content measurements we observed that the standard deviation is very constant through the season. Nevertheless, although the integration component is only a small component of the total variance, a small artefact associated to the chosen methodology for quantifying uncertainties exists as Fig. 8.4 clearly shows that absolute error varies quite well through the period of interest. We like to note that the relative error on a soil water storage estimate is very small and lies between 2.09 and 3.6%.

8.3.3 Water storage variation

Quantification of uncertainty associated to soil water storage variations is performed for two selected long dry periods (DOY 190-214, DOY 232-256) during which no or negligible rainfall occurred. Soil water storage variations are systematically calculated both between each day for which measurements are available (10 variations for period 1 and 6 for period 2) and with respect to the first day of each dry period with an increasing time step ($1 < \Delta_{day} < 24$) corresponding to days for which measure-

Table 8.3. Components of total variance (i.e., calibration, instrument and integration component) expressed in terms of standard deviation (mm) for an estimated soil water storage variation. Presented data are minimum and maximum values of cumulative and "instantaneous" soil water storage variation obtained for all sampling locations.

$s_{inst}(\widehat{\Delta S})$	2.6 - 2.71 mm
$s_{calib}(\widehat{\Delta S})$	0.41 - 0.5 mm
$s_{integ}(\widehat{\Delta S})$	2.29 mm
$s_{tot}(\widehat{\Delta S})$	3.48 - 5.4 mm
relative error	3.2-1084 %

ments are available. Table 8.3 presents the components of the variance expressed in terms of standard deviation. The minimum and maximum standard deviation of a local soil water storage variation estimate is respectively 3.48 and 5.42 mm which is similar to values obtained by *Poss* [1991] for a soil water storage held within 0-150 cm (std values of about 4 mm). Note that in our case it clearly constitutes an overestimation of the total variance of a soil water storage variation as during dry periods the selected integration results give very good results (see Fig. 8.4) and as we neglected the integration variance in the covariance term of Eq. (8.28). Unlike what we obtained for the variance of a soil water storage estimate, the calibration component is very small with values smaller than 0.5 mm corresponding to a contribution of less than 1% to the total variance. Note that the integration and the instrumental errors are of similar order of magnitude with values ranging between 2.29 and 2.71 mm. It corresponds to respectively 43% and 56% of the total variance. Hence, it is obvious that the use of an appropriate integration technique is of paramount importance to obtain accurate soil water storage variation estimates. In addition, it is important to use a soil water content measurement instrument with small instrumental errors or to replicate measurements to limit the extent of this error. Concerning relative errors, these are very variable (3.2-1084%) and their magnitude is directly related to the magnitude of the time dependent soil water depletion value. Figure 8.6 illustrates for sampling location 8 the temporal dynamics of the "instantaneous" (8.6a) and cumulated (8.6b) soil water storage variations, the associated one standard deviation confidence intervals and the relative errors (8.6c with circles for "instantaneous" and with squares for cumulated soil water storage variations). Fig. 8.6a and b show that uncertainty on soil water storage variations varies slightly

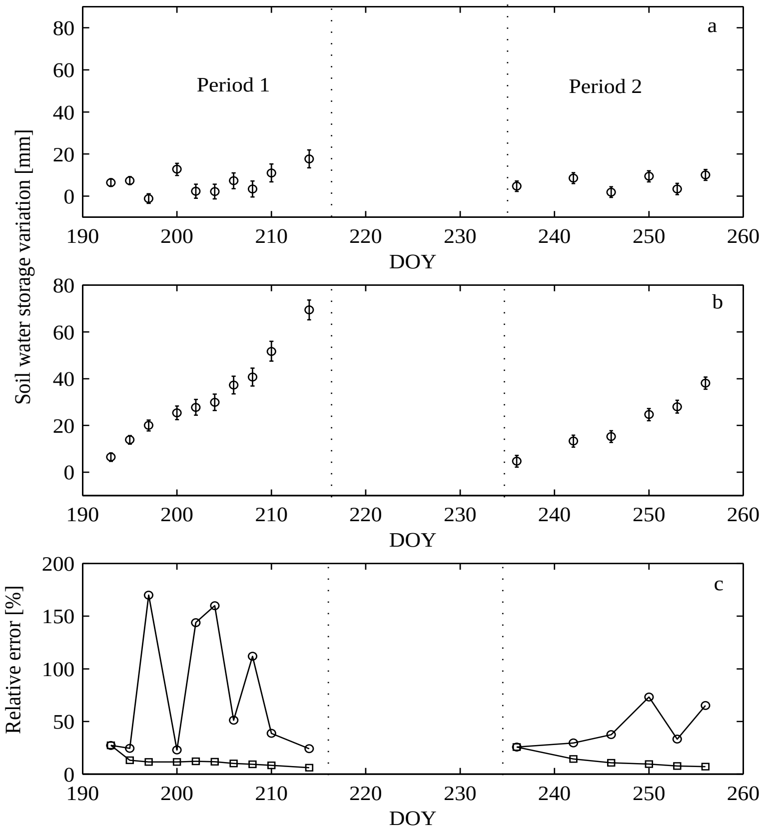

Figure 8.6. Instantaneous (a) and cumulated (b) soil water storage variations (mm) with the one standard deviation confidence interval for two selected dry periods for sampling point 8. Fig. c illustrates the corresponding relative errors.

during the season with values a little bit higher when the soil water storage is low.

8.3.4 Bottom flux

Estimation of bottom fluxes within the framework of water balance studies requires accurate knowledge of HCC at place and depth of interest. Fig. 8.7a shows the 28 different HCC predicted with PTFs, each one corresponding to one of the 28 sampling locations within the field. Also presented are field measurements, i.e. those obtained with tension infiltrometer (0< h <-10 cm) and with a simplified water balance (-100< h <-300 cm). As can be seen in Fig. 8.7a, the spatial variability of the HCC predicted with PTFs is quite pronounced which is a direct conse-

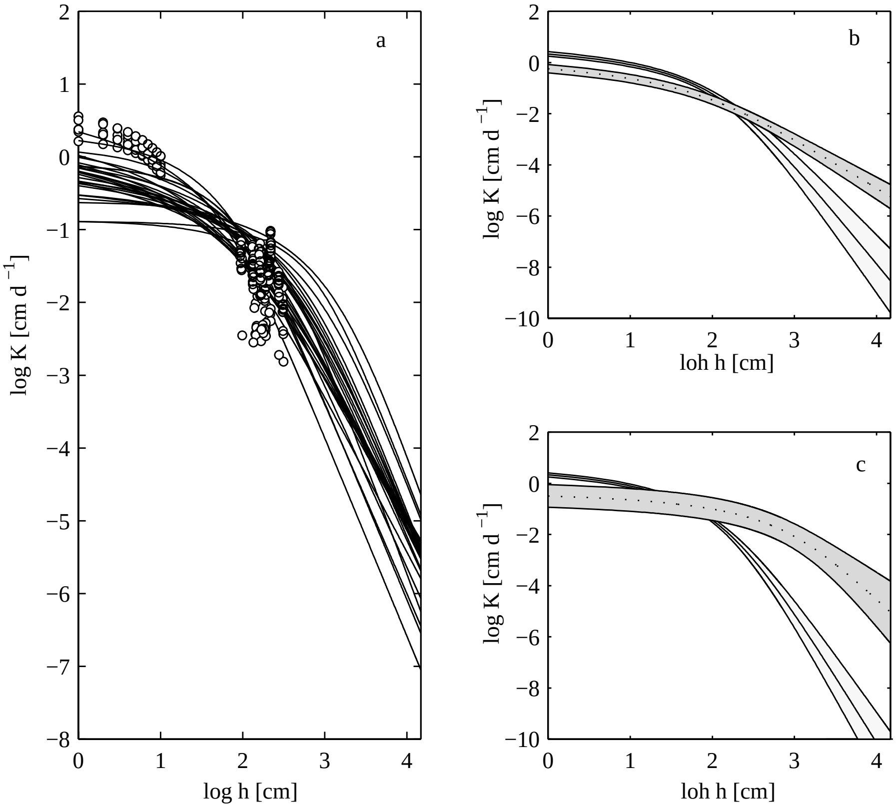

Figure 8.7. Fig.a illustrates both 28 hydraulic conductivity curves estimated with PTFs and field measurements. Fig. b and c show hydraulic conductivity curves and the one standard deviation confidence interval estimated with field measurement (light grey) and predicted with PTFs (dark grey) for respectively sampling locations 2 and 8.

quence of the measured spatial variability of moisture retention curves (not shown). Note that such a variability for HCC is not really surprising as this has already been observed for similar soils at the field scale by among others *Mallants et al.* [1995] and *Jacques* [2000]. Compared to HCC predicted with PTFs, field measurements produce higher unsaturated hydraulic conductivity values in the low suction range and similar to lower values in the range -100 to -300 cm. Spatial variability within the low suction range seems rather low. Nevertheless this may be an artefact due to the lower number of tension infiltrometer measurements although different depths and locations within the field were explored. Fig. 8.7b and 8.7c present HCC estimates and their associated uncertainty (one standard deviation confidence interval) for respectively sampling locations 2 and 8. HCC obtained with both methods are presented (light grey for predicted PTFs and dark grey for field measured). These two figures illustrate that compared to field measured HCC obtained with PTFs generally tend to underestimate unsaturated hydraulic conductivity for suction >-100 cm and to overestimate beyond this value. Note that uncertainties (illustrated here in terms of one standard deviation confidence interval) produced with PTFs are quite different for the two selected sampling locations and depend as a matter of fact on the MRC parameter inputs. One can also observe for sampling location 8 that discrepancies between HCC predicted with both methods are very large for h values <-200 cm.

Figure 8.8 present for the whole considered period (DOY 141-256) and for the two selected sampling locations estimated fluxes at the bottom of the profile with their associated uncertainty. Fig. 8.8a (sampling location 2) show that daily fluxes produced with both methods are very similar over the whole period. Furthermore, Fig. 8.8c (PTFs estimated) and e (field measured) illustrate that their associated uncertainties are also of the same order of magnitude. In contrast with these good results, Fig. 8.8b-d-f show what we obtained for sampling location 8. Daily fluxes obtained with both methods are very different. Indeed, daily fluxes estimated with HCC predicted with PTFs seem to be considerably overestimated at least compared to those produced with HCC predicted with field measurements. Such a difference is a direct consequence of high hydraulic conductivity values predicted with PTFs (one order of magnitude above that predicted with field measurements) within the range of observed pressure heads. Furthermore, uncertainties associated to daily flux estimates are very large which is obviously related to the uncertainties on the predicted HCC (see Fig. 8.7c). It must be said that such large uncertainties and such divergences between daily fluxes predicted with both methods were observed for 8 different sampling locations within the field. These results show therefore that uncertainties associated to estimated fluxes are not only dependent on the methodology chosen for estimating HCC but also that these uncertainties unlike other investigated variables are strongly time and space dependent.

8.3.5 Actual evapotranspiration

Uncertainties associated to actual evapotranspiration estimates are calculated with all above quantified uncertainties (Eq.(8.20)). Figure 8.9 shows for the two dry periods of interest "instantaneous" (a-b) and cu-

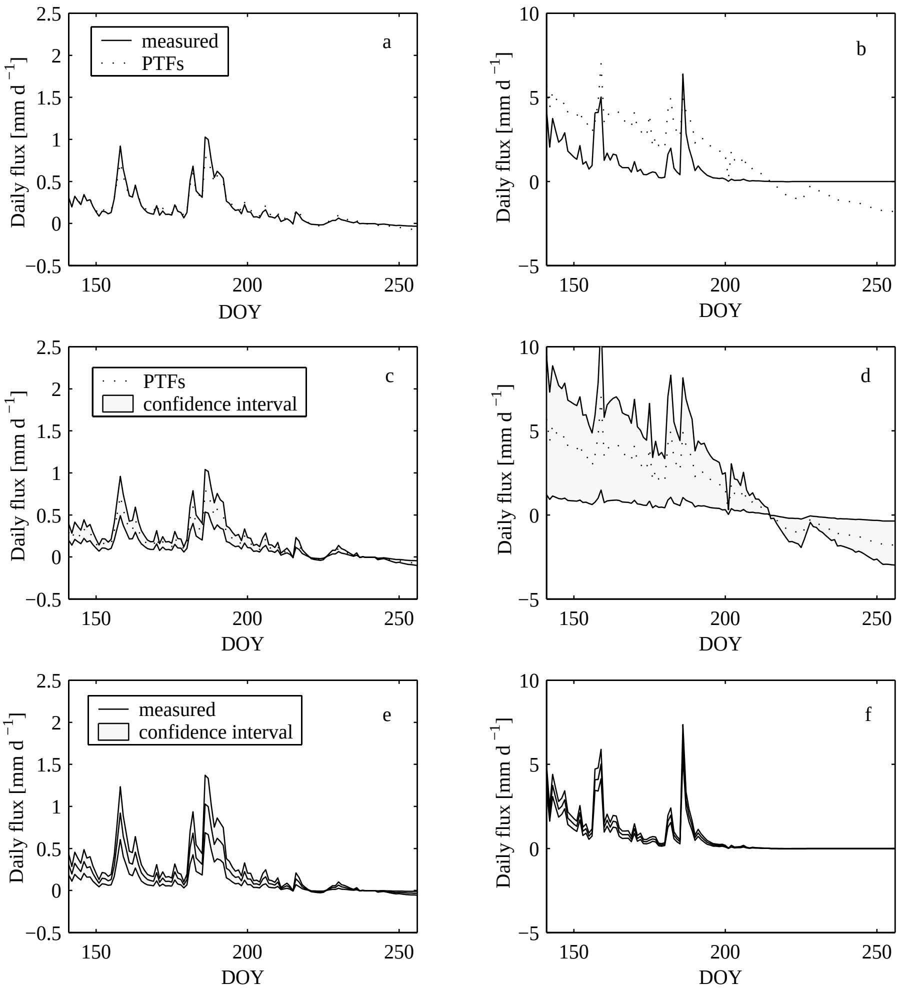

Figure 8.8. Temporal evolution of estimated daily fluxes at the bottom of the profile and associated uncertainties for sampling locations 2 (a-c-e) and 8 (b-d-f). Fig. c-d and e-f illustrate daily fluxes and associated uncertainties estimated respectively with HC predicted with PTFs and with HC field measured.

mulated (c-d) estimated evapotranspiration fluxes with the one standard deviation confidence interval for sampling locations 2 (a-c) and 8 (b-d). In Fig. 8.9, circles correspond to ET fluxes calculated with field measured HCC and squares to ET fluxes calculated with HCC predicted with PTFs. As a direct result of similar HCC obtained with the two methods, "instantaneous" and cumulated ET fluxes and uncertainty estimated on sampling location 2 are very similar for both periods. On the other hand, estimated ET fluxes for sampling location 8 with both methods are completely different. For the first period, ET fluxes calculated with HCC predicted with PTFs are largely underestimated. Further, those ET fluxes are negative at the beginning of the period as drainage is strongly overestimated as a consequence of an overestimated HCC. For the second period, the trend is inverse with ET fluxes calculated with HCC predicted with PTFs being largely overestimated. Indeed, capillary rise occur during this period. Uncertainties are within the same order of magnitude as during period 1. It must be said that, although it has been shown that uncertainty associated to HCC predicted with PTFs could be large (see e.g., Fig. 8.7c), this drops rapidly below pressure head values of -300 cm. As during the two periods selected for estimating ET fluxes, pressure head values at the bottom of the profile are in this range or even smaller, uncertainties on cumulated bottom fluxes and ET fluxes are quite small and very temporally constant. Table 8.4 summarises the different components of the total variance expressed in terms of standard deviation for evapotranspiration fluxes estimated with HCC field determined. The presented values are valid for cumulative and instantaneous ET fluxes. The total standard deviation ranges between 3.82 and 5.9 mm which is a little bit larger than for a soil water storage variation due to the contribution of the bottom fluxes uncertainties. In contrast to those results, *Vandervaere et al.* [1994] obtained values one order of magnitude smaller, namely ranging between 0.36 and 0.42 mm for the standard deviation of an ET estimate. Two reasons allow us to explain such a difference. The first is that they neglected uncertainty on the bottom fluxes as they used the zero flux plane method by considering no errors in the position of the zero flux plane. The second is that they neglected covariance terms between measured soil water content variations at the different depths. It is worth noting that the uncertainty in ET fluxes can be reduced in our case to 2.6-2.8 mm (in terms of standard deviation) if we consider that the uncertainty due to the method of integration ($s_2^2(\widehat{S})$) is equal to zero. This assumption is valid if the shape of the soil water profile is relatively similar at t_1 and t_2 which is likely to be the case for short drying periods. For our study, the relative error on a ET estimate ranges between 3.8 and 1180 % depending on mag-

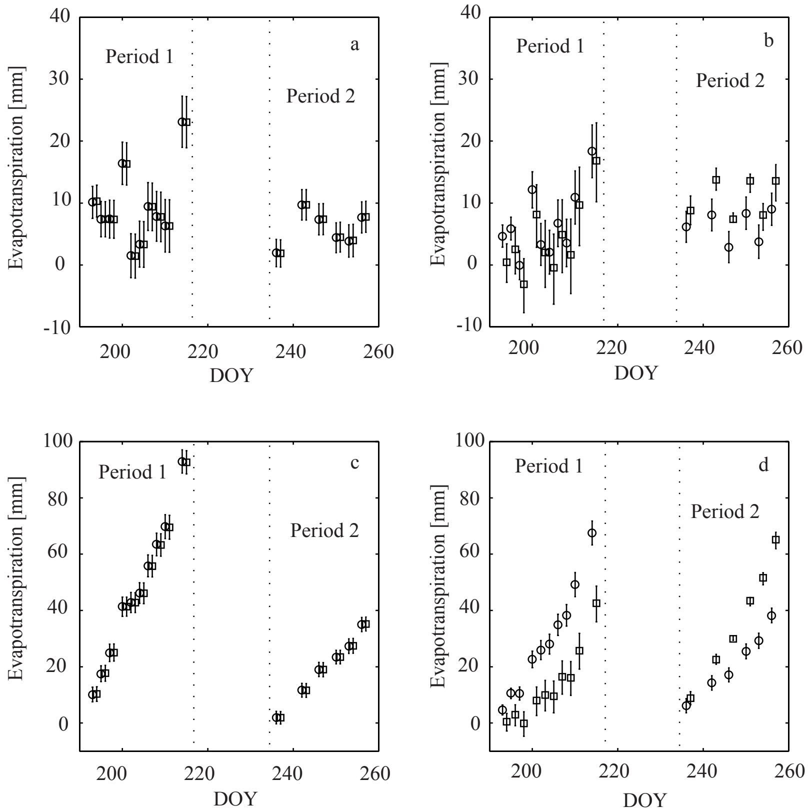

Figure 8.9. "Instantaneous" (a-b) and cumulated (c-d) ET fluxes for period 1 and 2 for sampling point 2 (a-c) and 8 (b-d). Vertical bars indicate ± one standard deviation. Circles correspond to ET fluxes calculated with field measured HCC and squares to ET fluxes calculated with HCC predicted with PTFs.

nitude of the estimated ET fluxes and therefore on the considered time step. The contribution of the different components to the total variance is very similar to what we obtained for a soil water storage variation estimate with a relative contribution of the integration and instrumental components together larger than 90%.

The results obtained for sampling location 8 (and on some other locations) show that the estimation of HCC's with PTF may introduce serious bias in the estimation of ET fluxes by means of a water balance approach. Indeed, the use of the water balance typically requires accurate knowledge of HCC at a specific depth and at a specific location within the field which can obviously be considered as far beyond the predicting power of any existing PTFs. Furthermore, as uncertainties

Table 8.4. Components of total variance (i.e. calibration, instrument, integration component and bottom fluxes component) expressed in terms of standard deviation (mm) for estimated ET fluxes. Presented data are minimum and maximum values of cumulative and "instantaneous" estimated ET fluxes obtained for all sampling locations.

$s_{inst}(\widehat{ET})$	2.6 - 2.71 mm
$s_{calib}(\widehat{ET})$	0.41 - 0.5 mm
$s_{integ}(\widehat{ET})$	2.29 mm
s($\widehat{q}$)	0.08 - 0.61 mm
$s_{tot}(\widehat{ET})$	3.82 - 5.9 mm
relative error %	3.4 - 1180 %

associated to HCC predicted with PTFs are easily quantifiable (outputs of Rosetta program according to MRC parameters), one can check a priori if the accuracy of HCC within the pressure range of interest is in accordance with the desired accuracy for ET fluxes predictions, or if additional costly soil physical measurements are justified.

8.4 Conclusions

In this chapter we addressed problems related to quantification of uncertainties associated to actual evapotranspiration fluxes estimated with the field water balance approach at the local scale. As the ET uncertainty quantification reflects the propagation of the uncertainty on the different terms of the water balance, this requires a rigorous estimation of uncertainties associated to soil water content measured both with TDR and neutron probe, to soil water storage, to soil water storage variation and to bottom fluxes. This analysis was done for a maize cropped field experiment carried out in 1999 in Belgium.

For soil water content, results show that associated uncertainties are quite low for the experimental conditions with standard deviations of 0.0158-0.0176 cm^3 cm^{-3} and 0.091-0.096 cm^3 cm^{-3} for respectively TDR and neutron probe with corresponding relative errors ranging between 2.5 and 10.5%.

For soil water storages within a 125 cm deep soil profile, we show, by means of numerical experiments, that Simpson's $\frac{1}{3}$ rule provides the best results to estimate profile water storages. Uncertainties associated to a soil water storage estimate range, in terms of standard deviation, between 9.72 and 10.37 mm with corresponding relative errors of 2.09

and 3.62%.

For soil water storage variations, standard deviations range between 3.48 and 5.42 mm with corresponding relative errors of 3.2-1084%. Note that as the variable of interest represents a variation, relative errors are strongly dependent of the considered time step. For the three above-mentioned variables, it is relevant to note that standard deviations are very constant through the season. For the soil water content and the soil water storage estimates, the main component of the total variance is the calibration variance (>90%) whereas the contribution of this component is very small for a soil water storage variation estimate (<1%).

For estimating HCC, bottom fluxes and associated uncertainties, we investigated two different approaches. This first one uses HCCs predicted with PTF while the second one uses field measurements. The two approaches produce on some sampling locations consistent results in terms of estimated HCC and bottom fluxes, but large discrepancies may exist on some others making the use of PTFs in this framework very questionable. We also observe for both approaches that uncertainties related to HCC and bottom fluxes are strongly non-linearly related to pressure heads. This is obviously not very interesting when quantifying ET fluxes with the water balance approach as a thorough estimation of bottom fluxes is mainly needed when this component is large compared to ET fluxes.

For ET fluxes estimated with HCC field determined, results show for two dry periods that the uncertainty range in terms of standard deviation between 3.82-5.97 mm with corresponding relative errors between 3.4 and 1180%. The uncertainty in ET fluxes can even be reduced to smaller values, i.e. 2.6-2.8 mm, if errors due to the integration method are assumed to be negligible. It should be stressed that the estimated total standard deviation associated to ET fluxes can be considered as very low and that a better precision is probably very difficult to obtain. Indeed, all sensitive factors contributing to the ET variance have been optimally determined, i.e. excellent calibration curves were found for both instruments, very small bottom fluxes and associated uncertainties were obtained and an appropriate integration method was selected. Nevertheless, the obtained precision prevents to use the water balance method to estimate robustly daily ET fluxes, at least under climate with relatively moderate climatic demand. On the other hand, the water balance method seems more appropriate for local estimations of ET fluxes over longer periods. Concerning the ET fluxes estimated with HCCs predicted with PTF, results show that it may introduce serious bias questioning therefore strongly the use of PTF in the framework of the water balance approach.

To conclude, we recommend investigating a priori by means of the presented methodology the minimum or at least the order of magnitude of uncertainty associated to ET fluxes that one should obtain according to the level of precision of the calibration curve, to the vertical sampling soil water content measurement strategy, to the method of integration, and to the approach used for estimating bottom fluxes. Indeed, this step, though generally neglected, remains of paramount importance to rationalise the allocation of resources for accurate ET estimates.

Appendix 1

Considering that $\widehat{\theta}_i$ and $\widehat{\theta}_j$ are soil water content measurements performed either at the same depth at days i and j, or at depths i and j the same day, the covariance between $\widehat{\theta}_i$ and $\widehat{\theta}_j$ can be expressed as:

$$\sigma(\widehat{\theta}_i, \widehat{\theta}_j) = E\left[(\widehat{\theta}_i - \theta_i)(\widehat{\theta}_j - \theta_j)\right]$$
$$E = \left[\left[(\widehat{a} - a) + \widehat{b}(\widehat{n}_i - n_i) + n_i(\widehat{b} - b) - e\right]\left[(\widehat{a} - a) + \widehat{b}(\widehat{n}_j - n_j) + n_j(\widehat{b} - b) - e\right]\right] \tag{8.21}$$

$$\begin{aligned}\sigma(\widehat{\theta}_i, \widehat{\theta}_j) &= E\left[(\widehat{a} - a)^2\right] + E\left[\widehat{b}(\widehat{a} - a)(\widehat{n}_j - n_j)\right] + n_j E\left[(\widehat{a} - a)(\widehat{b} - b)\right] - E\left[e(\widehat{a} - a)\right] \\ &+ E\left[\widehat{b}(\widehat{n}_i - n_i)(\widehat{a} - a)\right] + E\left[\widehat{b}^2(\widehat{n}_i - n_i)(\widehat{n}_j - n_j)\right] + n_j E\left[\widehat{b}(\widehat{n}_i - n_i)(\widehat{b} - b)\right] \\ &- E\left[\widehat{b}e(\widehat{n}_i - n_i)\right] + n_i E\left[(\widehat{b} - b)(\widehat{a} - a)\right] + n_i E\left[\widehat{b}(\widehat{b} - b)(\widehat{n}_j - n_j)\right] + n_i n_j E\left[(\widehat{b} - b)^2\right] \\ &- n_i E\left[e(\widehat{b} - b)\right] - E\left[e(\widehat{a} - a)\right] - E\left[e\widehat{b}(\widehat{n}_j - n_j)\right] - n_j E\left[e(\widehat{b} - b)\right] + E\left[e^2\right]\end{aligned} \tag{8.22}$$

As $E\left[\widehat{a} - a\right]$, $E\left[\widehat{b} - b\right]$, $E\left[\widehat{n}_i - n_i\right]$, $E\left[\widehat{n}_j - n_j\right]$ and as $\widehat{a}$ and $\widehat{b}$ are independent of $\widehat{n}_i$ and $\widehat{n}_j$, one can write :

$$\sigma(\widehat{\theta}_i, \widehat{\theta}_j) = \sigma^2(\widehat{a}) + (n_i + n_j)\sigma(\widehat{a}, \widehat{b}) + n_i n_j \sigma^2(\widehat{b}) + \sigma^2(e) \tag{8.23}$$

Estimating and replacing n_i, n_j with $\widehat{n}_i$, $\widehat{n}_j$, and with e equal to e_{neut} for the neutron probe, we can estimate by:

$$s(\widehat{\theta}_i, \widehat{\theta}_j) = s^2(\widehat{a}) + (\widehat{n}_i + \widehat{n}_j)s(\widehat{a}, \widehat{b}) + \widehat{n}_i \widehat{n}_j s^2(\widehat{b}) + s^2(e_{neut}) \tag{8.24}$$

Similar development for TDR leads to:

$$s(\widehat{\theta}_i, \widehat{\theta}_j) = s^2(\widehat{c}) + (\sqrt{\widehat{K}_{ai}} + \sqrt{\widehat{K}_{aj}})s(\widehat{c}, \widehat{d}) + \sqrt{\widehat{K}_{ai}}\sqrt{\widehat{K}_{aj}} s^2(\widehat{d}) + s^2(e_{TDR}) \tag{8.25}$$

Appendix 2

$$
\begin{aligned}
&\sigma(\widehat{S}_{t1}, \widehat{S}_{t2}) = E\left[(\widehat{S}_{t1} - S_{t1})(\widehat{S}_{t2} - S_{t2})\right] \\
&\quad = E\Big[\Big[200(\widehat{\theta}_{1t1} - \theta_{1t1}) + 133(\widehat{\theta}_{2t1} - \theta_{2t1}) + 333(\widehat{\theta}_{3t1} - \theta_{3t1}) + 166(\widehat{\theta}_{4t1} - \theta_{4t1}) \\
&\qquad +333(\widehat{\theta}_{5t1} - \theta_{5t1}) + 83(\widehat{\theta}_{6t1} - \theta_{6t1})\Big]\Big[200(\widehat{\theta}_{1t2} - \theta_{1t2}) + 133(\widehat{\theta}_{2t2} - \theta_{2t2}) \\
&\quad +333(\widehat{\theta}_{3t2} - \theta_{3t2}) + 166(\widehat{\theta}_{4t2} - \theta_{4t2}) + 333(\widehat{\theta}_{5t2} - \theta_{5t2}) + 83(\widehat{\theta}_{6t2} - \theta_{6t2})\Big]\Big] \qquad (8.26)
\end{aligned}
$$

As TDR soil water content measurements and neutron probe measurements are independent, we can write:

$$\sigma(\widehat{S}_{t1}, \widehat{S}_{t2}) = 200^2 + \sigma(\widehat{\theta}_{1t1}, \widehat{\theta}_{1t2}) + f^2h^2 \sum_{i=2}^{6} \sum_{j=2_{j\neq i}}^{6} \sigma(\widehat{\theta}_{it1}, \widehat{\theta}_{jt2}) \qquad (8.27)$$

which can be estimated by:

$$s(\widehat{S}_{t1}, \widehat{S}_{t2}) = 200^2 + s(\widehat{\theta}_{1t1}, \widehat{\theta}_{1t2}) + f^2h^2 \sum_{i=2}^{6} \sum_{j=2_{j\neq i}}^{6} s(\widehat{\theta}_{it1}, \widehat{\theta}_{jt2}) \qquad (8.28)$$

with f and h equal to 133, 333, 166 or 83.

Chapter 9

Sampling strategies to estimate field areal evapotranspiration fluxes with a soil water balance approach

Abstract*

In this chapter, we analyse the spatio-temporal variability of instantaneous and cumulated evapotranspiration (ET) fluxes measured during two long drying periods with a soil water balance approach on 28 measurement points located within a small maize cropped field. Then we test three sampling procedures to estimate field averaged ET and their associated uncertainty. Results of this study show that the "within-field" spatial variability of the local scale instantaneous measured ET is large with coefficients of variation ranging between 15.5 and 46.3%. The corresponding cumulated ET for the first and the second period ranges between 39.4-107.5 mm and 30.3-55.7 mm respectively. We show that this variability of ET fluxes can be related in some way to the measured spatially variable crop growth (2.55<Leaf Area Index<4.32). This one has directly an impact on the ratio between measured actual ET and ETo which generally is smaller than 1 in our field. The first sampling strategy which consists in increasing the number of sampling locations shows that, for a probability level of 95%, the number of samples needed

*adapted from Hupet, F. and M. Vanclooster, accepted for publication in *Journal of Hydrology*.

to estimate the field mean cumulated ET flux with a relative precision of 5, 10 and 20% ranges between 40 and 360, 10 and 90, and 2 and 22 respectively. The number of samples required for the estimation of "instantaneous" ET fluxes is even larger. The second sampling strategy which exploits the concept of temporal stability can only be applied for the estimation of cumulated ET. In this case the field averaged ET is estimated with a relative precision of 10% if only one representative location is selected a-priori. The third sampling strategy consists in using a covariant such as the LAI or the dry matter yield. For this case, cumulated ET equals 119 $\pm$6.1 mm and 118.5 $\pm$4.5 mm by means of the relationships existing between cumulated ET and LAI and yields respectively. The latter strategy seems very attractive but necessitates more research to investigate the robustness of the relationships with respect to different climatic and agronomic conditions and to different plant cultivars.

9.1 Introduction

The estimation of water fluxes at different spatial scales remains a challenging task in hydrology. Indeed, the scale of the hydrological measurement technique is generally much smaller than the scale at which the predictions are required. This scale issue mainly arises from the fact that hydrological processes exhibit generally a stunning degree of spatial variability [*Blöschl and Sivapalan*, 1995]. Specific upscaling and sampling strategies are therefore needed to estimate water fluxes at large scales based on a series of local measurements. This issue has been extensively studied at different scales for a range of hydrological processes such as rainfall [e.g., *Pardo-Iguzquiza*, 1998] and transpiration [e.g., *Hatton and Wu*, 1995]. For evapotranspiration (ET), the scale issue is well acknowledged at large scale [e.g., *Famiglietti and Wood*, 1995; *Mauser and Schädlich*, 1998] due to the spatial variability of the climatic demand, of the vegetation and of the soils. In most of the studies however, ET is considered as homogeneous at the field scale. The very few studies investigating "within-field" variability of evaporation, transpiration and ET fluxes showed that the spatial variability is high [e.g., *Soegaard and Boegh*, 1995; *Lewan and Jansson*, 1996]. This is not really surprising as the vegetation is generally highly variable within the fields [e.g., *Jordan et al.*, 2003] and as surface fluxes are linked in some way to the vegetation growth. In addition, ET is also driven by the variability of the soil water flow processes which is well known to be highly variable within the field [e.g., *Russo and Dagan*, 1993]. A very good knowledge of the "within-field" spatial variability of ET and its temporal dynamics is therefore of paramount importance to estimate field areal ET. This is reinforced by the fact that ET estimations are still often performed with the soil water balance approach which is characterized by a small measurement support. In addition, estimation of the spatial variability of actual evapotranspiration fluxes is crucial for the development of stochastic water transport models [*Bertuzzi et al.*, 1991]. The suspected high spatial variability of ET and the small measurement support associated to the soil water balance method requires therefore appropriate sampling strategies. Three different sampling strategies can be used for the field areal estimation of spatially independent state variables or water fluxes. The first basic strategy consists in intensifying "randomly" the spatial sampling frequency as to decrease uncertainty in the field areal ET fluxes. This strategy has been previously used and tested to investigate the number of samples required to estimate the field areal ET flux for a given probability level [e.g., *Bertuzzi et al.*, 1991]. The second sampling strategy consists in using temporally stable locations particularly representative of the field mean behaviour in terms of ET fluxes. This strategy assumes that such stable locations exist within the field and that their a-priori selection can be made. This strategy has previously been applied for the areal estimation of soil water content [e.g., *Vachaud et al.*, 1985; *Grayson and Western*, 1998], pressure head [e.g., *Van Pelt and Wierenga*, 2001] and nutrients [*Goovaerts and Chiang*, 1993]. This strategy has until now not been tested for estimating field averaged ET. The third sampling strategy consists in using a covariant (i.e. an auxiliary variable or a surrogate). This strategy assumes implicitly i) that there is a relationship between the variable of interest and the covariant; ii) that this relationship is known; and iii) that the covariant can more readily be measured than the variable of interest. This upscaling strategy has to the author's knowledge not yet been tested for the estimation of ET at the field scale. To evaluate the performance of different sampling strategies for estimating field scale ET we designed an experimental study with the following main objectives:

(1) to analyse the spatio-temporal dynamics of the ET fluxes measured on 28 sampling locations within a small agricultural cropped field during two long drying periods;

(2) to investigate and to test the three above-mentioned sampling strategies to estimate the field areal ET fluxes.

9.2 Material and methods

This chapter uses the data set collected during the 1999 field campaign, i.e. the soil water content, the pressure head, the Leaf Area Index and the dry matter yield measured on each 28 location. Unsaturated hydraulic conductivity measurements were also used to estimate fluxes at the bottom of the soil profile as well as climatic variables measured at the GERU meteorological station for the estimation of the reference evapotranspiration. For further details, the reader is referred to Chapter 2.

9.2.1 Data analysis

Spatial variability of evapotranspiration

The actual evapotranspiration fluxes were estimated on each 28 sampling location using the conservation of mass equation:

$$ET_{t_1,t_2} = \Delta S_{t_1,t_2} + q_{t_1,t_2} \tag{9.1}$$

with ET_{t_1,t_2} the estimated actual evapotranspiration fluxes between t_1 and t_2 (mm), $\Delta S_{t_1,t_2}$ the estimated difference of soil water storage between t_1 and t_2 (mm), and q_{t_1,t_2} the estimated water flux at the bottom of the profile between t_1 and t_2 (mm). Note that Eq. (9.1) is a simplified version of the full soil water balance equation as there was no irrigation and as the rainfall was very small and negligible (runoff was therefore non existent). The quantification of ET with Eq. (9.1) was performed for two long dry periods of 24 days (DOY 190-214 and DOY 232-256). We calculated ET cumulated over periods going from DOY 190 or DOY 232 to days where soil water storages were estimated. "Instantaneous" ET fluxes were estimated for periods of minimum three and maximum six days included within the two long dry periods. This results in a data set of 10 cumulated and 6 instantaneous ET fluxes for the first dry period and in 6 cumulated and instantaneous ET fluxes for the second dry period. We calculated also ET cumulated over the two dry periods. The spatial variability of ET was quantified by calculating both the standard deviation (std in mm) and the coefficient of variation (CV in %) of the 28 measured ET values. Note that in this study we considered that all the observed ET variability was explained by the spatial variations. Indeed, it has been shown in the study of *Hupet et al.* [2003] that for certain conditions which have been met in this study the uncertainty on the locally estimated ET fluxes ranges between 2.6-2.8 mm (independently of the considered time step) which is clearly smaller than the observed ET variability in our experimental field. In a preliminary step, we investigated if the estimated ET fluxes were normally distributed with the visual inspection of normal probability plots. The degree of spatial dependence was then investigated using standard geostatistical techniques [*Isaaks and Srivastava*, 1989] such as the visual examination of sample semivariograms. The sample semivariogram, $\gamma_s(h)$ at a given lag, h, is given by:

$$\gamma_s(h) = \frac{1}{2N(h)} \sum_{i,j} (ET_i - ET_j)^2 \tag{9.2}$$

with N the number of pairs of observations for a specified lag, ET_i and ET_j the estimated ET fluxes at sampling locations respectively i and j and the summation performed for all the i, j pairs of observations of the selected lag. In order to ensure a minimum number of pairs of observations within each lag, only omnidirectional semivariograms were used with a minimum and maximum lag of respectively 15 m and 58 m. This resulted in a minimum of 33 ET fluxes data pairs for each selected lag interval, except 20 and 23 pairs for the 42.5 and 45 m lags. The geostatistical analysis was done by means of a geostatistical toolbox programmed in a MATLAB^{TM} environment [*Christakos et al.*, 2001].

9.2.2 Sampling strategies

Three different sampling strategies were tested to obtain field averaged actual ET. The first strategy consists in increasing "randomly" the number of sampling locations within the field as to decrease the uncertainty on the mean averaged ET. In this framework, we used the central limit theorem to quantify the number of samples necessary to estimate the mean with a given accuracy for a given probability level:

$$n = \frac{t_\alpha^2 s^2}{d} \tag{9.3}$$

where n is the number of samples, s^2 is the estimated sample variance, t_α^2 the Student's parameter corresponding to the confidence level $(1-\alpha)$ and d the relative accuracy. Note that the use of this theorem requires normality and spatial independence of estimated ET fluxes which has previously been investigated (see section 9.2.1). The second sampling strategy consists in using the concept of temporal stability to investigate if some locations within the field are representative for the mean ET and if this representativeness is conserved during the considered period. In this context, we used two different approaches.

The first one calculates the relative difference expressed as follows:

$$\delta_{i,j} = \frac{ET_{i,j} - \bar{ET_j}}{\bar{ET_j}} \tag{9.4}$$

with $\delta_{i,j}$ the relative difference, $ET_{i,j}$ the ET flux measured at location i (1-28) during a period of length j (3-24 days) and $\bar{ET_j}$ the spatially averaged ET flux for the corresponding period. Subsequently, the relative differences were averaged over the considered period for each 28 location and ranked from the smallest to the largest. Temporal stability was investigated by visual inspection of the graphs presenting the ranked mean relative differences with their extremes. The second approach is the non-parametric method of Spearman's rank correlation coefficient [*Snedecor and Cochran*, 1967]. This coefficient is calculated as follows:

$$r_s = 1 - \frac{6\sum_{i=1}^{28}(R_{ij} - R'_{ij})^2}{n(n^2-1)} \tag{9.5}$$

with n the number of locations (i.e. 28), R_{ij} the rank of ET measured at location i during the period j and R'_{ij} the rank of ET measured on the same location during another period j'. The closer r_s is to one, the more stable the process will be with a value of one corresponding to a perfect time stability between period j and j'.

The third tested sampling strategy consists in using an auxiliary variable as covariant. In our case, the auxiliary variables can be the LAI and the dry matter yield. Note that this third sampling strategy implicitly assumes that there is a relationship between the variable of interest, i.e. ET, and the considered auxiliary variable. Therefore, we investigated in a preliminary step if any correlation existed between the measured ET, the LAI and the dry matter yield. Subsequently, these correlations were used to estimate field averaged ET. The confidence intervals of the estimated field averaged ET were derived from the confidence bands of the correlations. Note that this sampling strategy was only applied for the ET fluxes cumulated over the two considered dry periods.

9.3 Results and discussions

9.3.1 Spatio-temporal variability

Figure 9.1 shows the mean cumulated and "instantaneous" ET measured over the 28 sampling locations with their respective coefficient of variation. In Fig. 9.1a, we can observe that the mean cumulated ET for the first dry period is much larger (77.68 mm) than that of the second

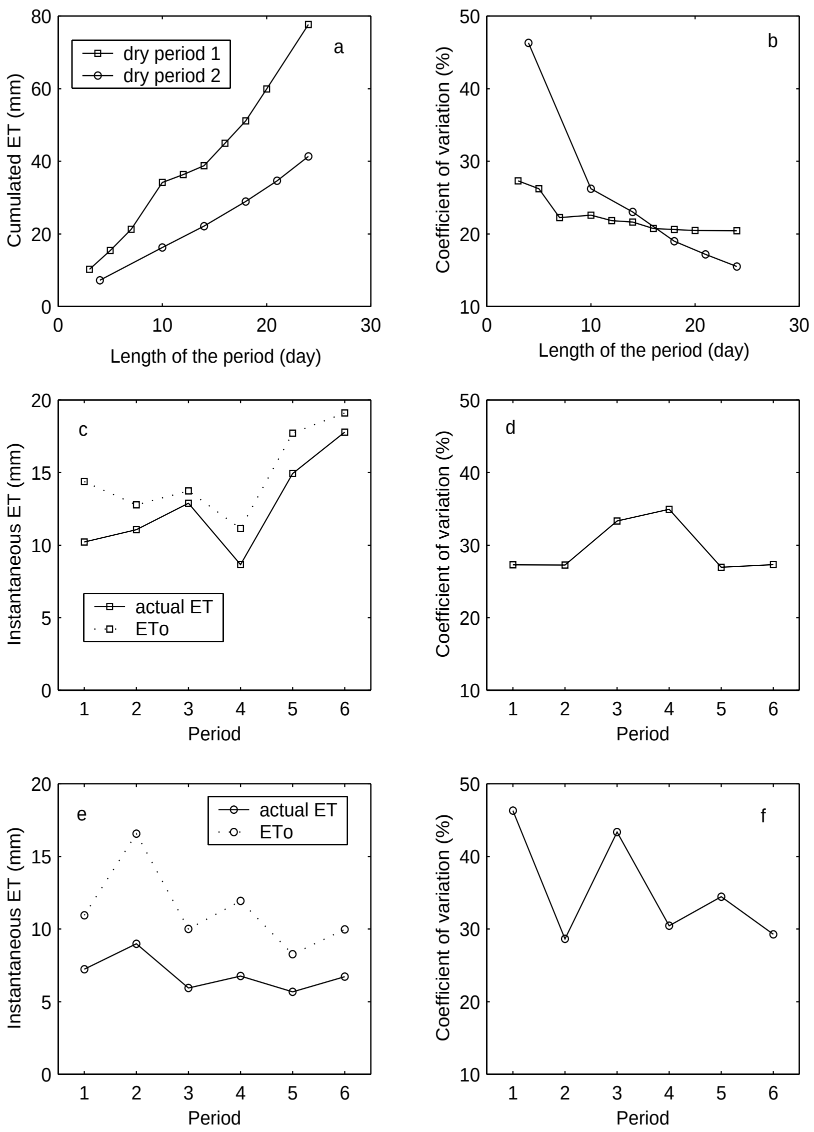

Figure 9.1. Mean cumulated (a) and instantaneous (c-e) ET measured over the 28 sampling locations with their respective coefficients of variation (b-d-f).

dry period (41.3 mm). This a direct consequence of both the smaller climatic demand, 67.7 mm for the second period instead of 96.1 mm for the first period, and the larger bulk surface resistance for maize crop as this started to become senescent at the beginning of the second considered dry period (mid-August). This relative reduction of ET can be observed in Fig. 9.1c and e where both climatic demand (ETo) and actual evapotranspiration fluxes are illustrated. Note that the X-axis in Fig. 9.1 c-d-e-f linearly represents the six considered periods though the length of these are different. The right figures (b-d-f) present the time evolution of the coefficient of variation (CV in %). For cumulated ET (Fig. 9.1b), CV progressively decrease as the length of the considered period increases with values evolving from 27.3 to 20.4% and from 46.3 to 15.5% for periods 1 and 2 respectively.

Such a decrease of the spatial variability with the increasing time scale, a characteristic feature of hydrological processes, was already observed for evapotranspiration by *Bertuzzi et al.* [1994] and for transpiration by *Jara et al.* [1998]. Note that the decrease of the CV values for cumulated periods is revealing of a certain temporal instability of the spatially measured ET (see further sampling strategy II). For instantaneous fluxes the CV values of ET measured over periods ranging from 3 to 6 days are larger and range between 26.95 and 46.3% without any significant temporal trend. These observed values of ET spatial variability are in the range of those found in other field experiments. For sap flow measurements, *Soegaard and Boegh* [1995] and *Trambouze and Voltz* [2001] found CV values ranging from 15 to 80% and from 15 to 50% within a millet field and a vineyard respectively. For evapotranspiration measured with a soil water balance approach within irrigated fields, *Raghuwanshi and Wallender* [1997] and *Villagra et al.* [1995] found CV values ranging from 13 to 46% and up to 42%. The observed ET variability within our small experimental field is therefore not very surprising but reinforces the fact that ET is a highly spatially variable process even for "apparent" homogeneous fields of small size (<1ha). The high observed ET variability also suggests implicitly that the sampling frequency has to be quite intensive in space to obtain good areal mean ET estimates (see further sampling strategy I). Beyond the pure descriptive statistical analysis of the observed ET variability, it is certainly worth to examine the factors generating such a spatial variability. A thorough study of the processes driving the observed variability is quite difficult to achieve, since the temporal resolution of the ET measurements is quite poor, and since some information about the crop and the soil are lacking or are very punctual in time. Notwithstanding this, an attempt of explanation will be given. First of all, one has to realise that for the two considered dry

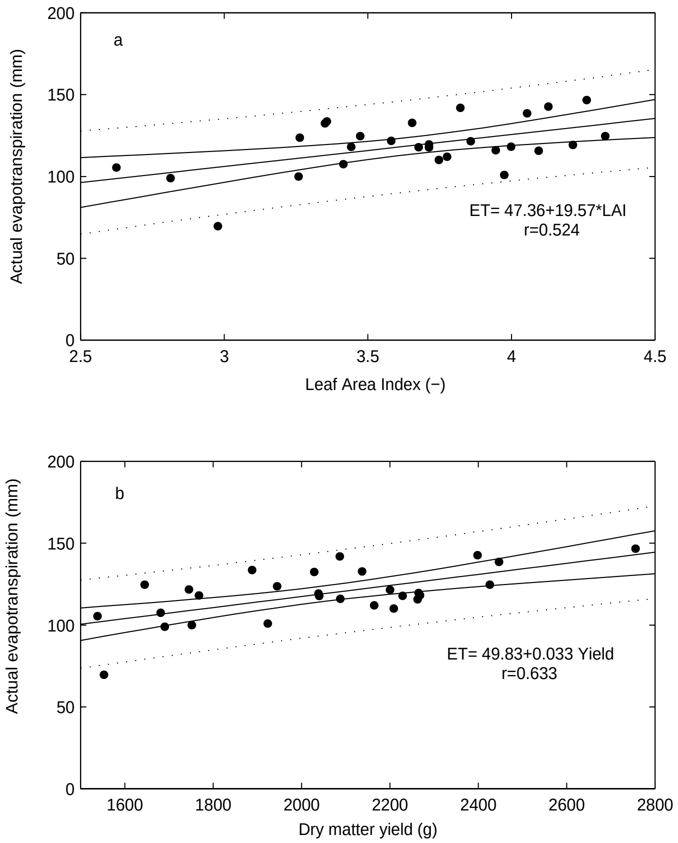

Figure 9.2. Relationships with the 95% confidence bands (continuous line) and the 95% prediction bands (dotted line) between ET cumulated over the two dry periods and both the Leaf Area Index (a) and the dry matter yield (b).

periods the maize is nearly or even completely developed. Transpiration fluxes are therefore the main contributor to ET while soil evaporation represents only a minor fraction of total ET (approximated to be less than 13% based on numerical model simulations). Consequently, the spatial variability of the soil evaporation process cannot be considered as the major driver of the observed variability of ET. This is in contrast to observations of ET variability on bare soils [e.g., *Lascano and van Bavel*, 1992; *Lewan and Jansson*, 1996]. We will therefore assume that the observed ET spatial variability is totally explained by the spatial variability of the transpiration fluxes. Further we consider that the meteorological variables, and hence the ET demand, are uniform over the whole field. This is a realistic assumption in our case given the small field size, the nearly flat topography and the sampling strategy avoiding field borders. Hence, the spatial variability of ET can only be explained by the spatial variability of the soil-plant flow process. In Table 4.1 we observe that the crop growth is quite variable with a broad range of LAI values, i.e. from 2.55 to 4.32, though the corresponding coefficient of variation is not so large (12%). Such a variability is caused by the combination of various biotic and abiotic factors such as, e.g., delay at emergence due to variability of sowing depth, genetic factors, crop management practices, variability of nutrient and water stresses, etc. As it is generally well accepted that the transpiration fluxes are closely related to the aerial crop size, we investigated if a relationship existed between ET and crop parameters for our data set. Fig. 9.2 illustrates the relationships between ET fluxes cumulated over the two dry periods and both the Leaf Area Index (Fig. 9.2a) and the dry matter yield (Fig. 9.2b). Note that such relationships were only investigated with total cumulated ET fluxes and not with "instantaneous" ET fluxes.

From Fig. 9.2a and b, we can observe that a certain relationship exists between the transpiration fluxes and the crop size and the crop weigth. The relationships are poor but significant at the 99% probability level (r=0.52 and r=0.64). The fact that the relationships are poor is not really surprising as the relationships are theoretically non-univocal due to the various factors affecting the crop growth and as they are based on ET fluxes cumulated over only 48 days (length of the total agricultural season = 171 days) and on LAI measured at mid-season. Furthermore, the number of maize plants used to estimate the LAI and the dry matter yield (10), i.e. those affecting the measured soil water content, was selected quite arbitrarily. Nevertheless, it is quite obvious from Fig. 9.2 that the spatial variability of ET has to be linked with the variable crop growth. In this context, it is worth mentioning that water stress probably played a minor role in the variable crop growth. Indeed, soil water availability was very close to its optimum between the sowing date and DOY 193 (date at which the LAI measurements were performed) confirming therefore that the observed LAI spatial variability was not caused by a water stress. Furthermore, the ratio between measured actual "instantaneous" ET and climatic demand (i.e. ETa/ETo) is nearly constant during the two considered drying periods (see Fig. 9.1c and e). Finally, the limited impact of the water stress for the encountered climatic conditions was also confirmed with different simulations performed with the WAVE model [*Vanclooster et al.*, 1996]. In Fig. 9.3, we illustrate the spatial variability of both cumulated ET for the first and the second dry period (Fig. 9.3 a and c) and ratio between actual cumulated ET and climatic demand (Fig. 9.3 b and d). Note that these figures were generated

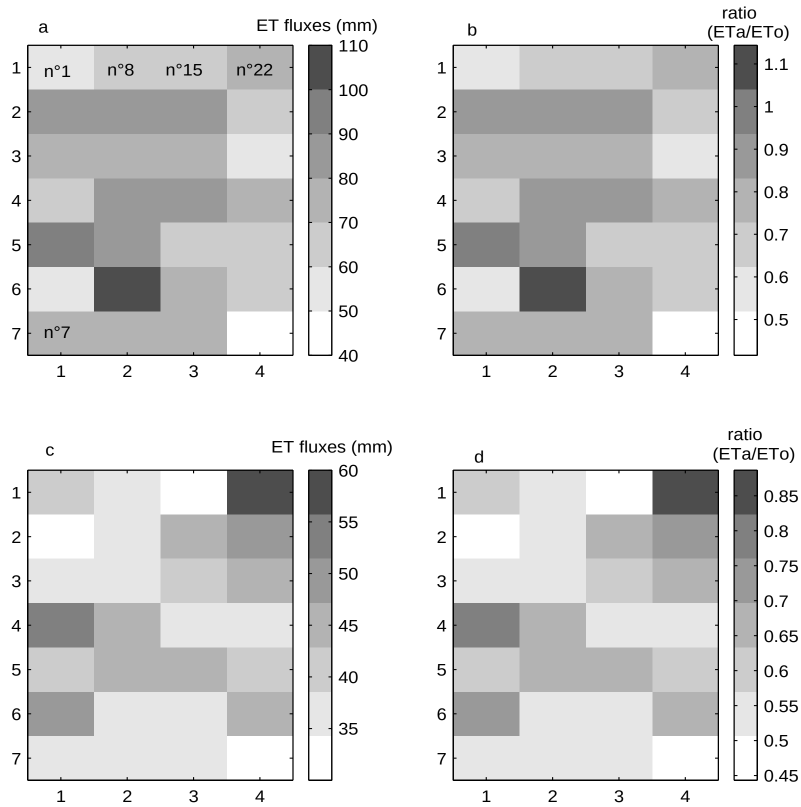

Figure 9.3. Spatial variability of both cumulated ET for the first and the second dry period (a and c) and ratio between actual cumulated ET and climatic demand (b and d).

without using any interpolation procedure as there is no spatial structure in the data (see further). Each of the 28 pixels representing a homogeneous ET value for an area of 15x15m has therefore to be considered as representative of what happens on each of the 28 sampling points, i.e. a pixel of about 0.75 x 0.75 m. On the left figures, we can observe that the range of actual ET is very large with values for the first period ranging between 39.4 and 107.5 mm and for the second period between 30.3 to 55.7 mm. Such a range of ET fluxes values was also reported by *Booltink and Epinat* [2001] for a 15 ha field integrating remote sensing information within a detailed soil-crop model. A more detailed inspection of the ET patterns presented in Fig. 9.3 a and c reveals a clear difference for some pixels between the two periods. Indeed, though some pixels present low ET values for both periods (e.g., pixel 28), some are characterised by a high ET value for the first period and a low one for the second period (e.g., pixel 13) or the inverse (e.g., pixel 24). This behaviour is obviously revealing of a certain temporal instability (see further). Concerning the ratio between the actual ET fluxes and the climatic demand (Fig. 9.3 b and d), these are logically as variable as the ET fluxes because ETo is considered as homogeneous over the whole field. On the other hand, seemingly more surprising is that a vast majority of the pixels present ratio values smaller than expected values for a maize crop under standard conditions, i.e. about 1.15 for the first period and about 0.8 for the second period [*Allen et al.*, 1998]. Standard conditions refer to crops optimally developed under excellent agronomic conditions, namely for which water and nutrients are not limiting factors and for which pest and diseases are absent. Mean ratio values derived for our field for the first and second period are respectively 0.81 and 0.62. Note that such small ratio values were also found by *Booltink and Epinat* [2001] within a winter wheat cropped field. Different factors can explain the small ratio values observed within our experimental field. Firstly, the actual soil evaporation though representing only a small fraction of the total ET fluxes was certainly smaller than the potential soil evaporation after few days as the two long considered periods were completely dry. Secondly, transpiration fluxes were probably reduced by a small water stress though the magnitude of this one has to be quite limited. Thirdly, all the soil water content measurements were performed mid-way between the maize rows which could have lead to an underestimation of the ET fluxes as we can intuitively suspect that the root length density and the root water uptake are maximum just beneath the row. Nevertheless this hypothesis, though confirmed in some way by some studies [e.g., *Coelho and Or*, 1999; *Liedgens and Richner*, 2001] may be questionable as others showed for maize that it is not necessarily valid and in addition is strongly depth and time dependent [e.g., *Tardieu*, 1988; *Bruckler et al.*, 1991]. Furthermore, some locations of our experimental field produce ratio values only a little bit smaller than the ratio expected for standard conditions leading us to consider that the third factor has only a limited impact on the smaller observed ratios. Finally, the small observed ratio values can be explained by the crop size which is less than under standard conditions (e.g., lysimeter conditions) under which the ratios between crop evapotranspiration and climatic demand are generally established [*Allen et al.*, 1998]. We estimate that this latter hypothesis is the most likely for our study. This is also consistent with the study of *Allen* [2000] who suggested to consider a reduction factor of 15% and even larger to represent the difference between field and pristine (i.e. standard) conditions. We should mention that this reduction of the potential evapotranspira-

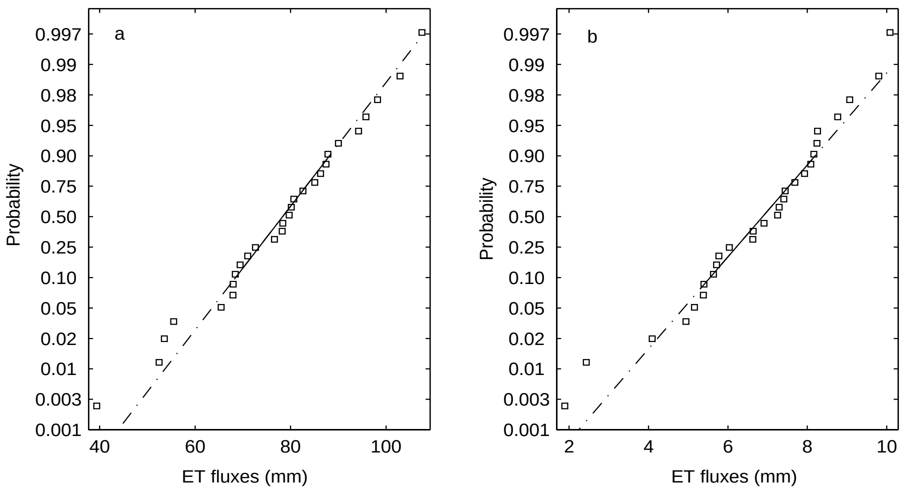

Figure 9.4. Probability plots for ET fluxes cumulated over the whole first drying period (a) and for instantaneous ET fluxes for the sixth period of the second drying period (b).

tion is generally not taken into account within detailed agro-hydrological models such as WAVE [*Vanclooster et al.*, 1996] or SWAP [*van Dam et al.*, 1997]. Indeed, the crop potential evapotranspiration is determined in these models with the two-step approach, namely by multiplying the reference evapotranspiration (ETo) with an appropriate crop coefficient (Kc) derived from standard conditions. This may lead to a clear overestimation of the evapotranspiration, since standard conditions are rarely or even never met in real agricultural fields.

Before applying the sampling strategy I, we investigated systematically for cumulated and instantaneous ET fluxes if these were normally distributed and spatially dependent. This was done by visually examining the probability plots and omni-directional sample semivariograms. Fig. 9.4 presents results obtained for ET fluxes cumulated over the whole first drying period (Fig. 9.4a) and for instantaneous ET fluxes for the sixth period of the second drying period (Fig. 9.4b). From these figures, we can observe that the ET fluxes values appeared to be closely normally distributed. Similar results (not shown) were obtained for all the other periods both for cumulated and instantaneous ET fluxes. Figure 9.5 shows sample omnidirectional semivariograms calculated for instantaneous (Fig. 9.5 a and b) and cumulated ET fluxes over the first and the second dry period (c and d). Also are presented sample semivariograms calculated for Leaf Area Index and dry matter yield (Fig. 9.5 e and f).

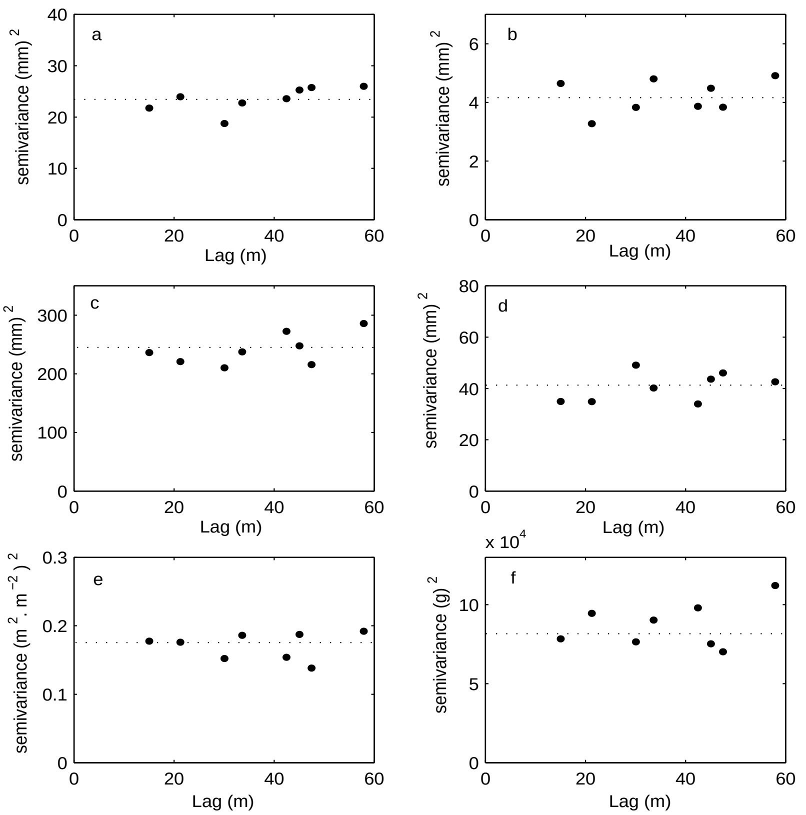

Figure 9.5. Omnidirectional semivariograms for instantaneous ET fluxes (a and b), cumulated ET fluxes over the first and the second dry period (c and d) and for Leaf Area Index and dry matter yield (e and f).

No apparent spatial structure was found for the ET fluxes, i.e. there is a pure nugget effect (Figs. 9.5 a-d) and there is even no decreasing trend in semivariance values for the smallest lags (15 m and 21.2 m). These results are consistent with the findings of *Raghuwanshi and Wallender* [1997] showing there is spatial independence between ET fluxes measured at a 10 m interval along a 265 m long irrigated furrow cropped with beans. From Fig. 5e and f, we can similarly observe that the variables associated to the crop growth, i.e. the LAI and the dry matter yield do not present any spatial dependence. This spatial independence at small distance can be explained among other things by the small sampling support (10 plants). For identical sampling supports, some studies found similar results, i.e. absence of any spatial dependence at small distance in other agroclimatic conditions [*Samra et al.*, 1992 ; *Doberman*

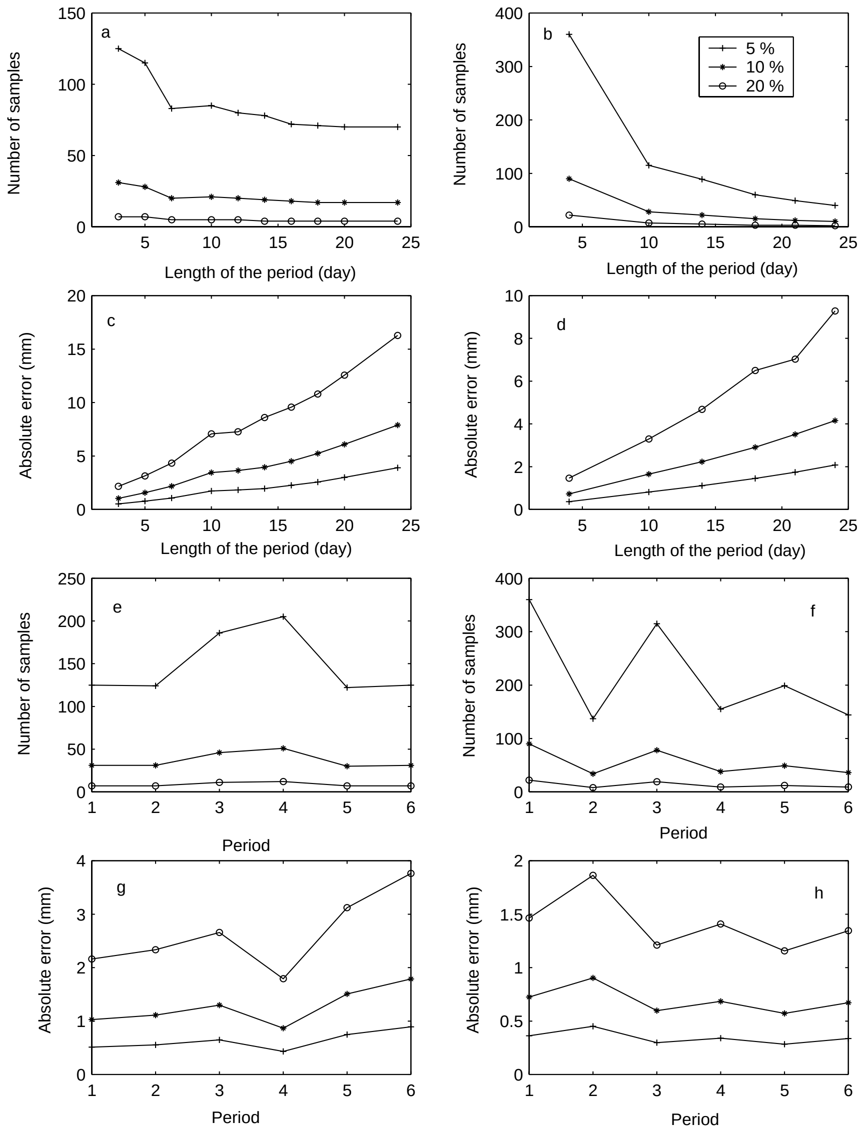

Figure 9.6. Number of sample needed to estimate the field mean ET flux with a relative precision of 5, 10 and 20%, for a probability level of 95%. Results are presented for cumulated (a-b) and instantaneous ET fluxes (Fig. 6e-f). Also are shown the absolute error of ET fluxes expressed in mm corresponding to the number of samples chosen to reach the three selected relative precision levels (c-d, g-h).

et al., 1995; *Yamagishi et al.*, 2002] whereas others found spatial dependence over much larger distances, i.e. about 60-80 m [e.g., *Miller et al.*, 1988]. As a summary, in our case normality and spatial independence of locally measured ET are met and allows therefore the application of the central limit theorem for evaluating sampling strategy I (see below).

9.3.2 Sampling strategies

Random intensification of the sampling frequency

The first sampling strategy consists in increasing "randomly" the number of sampling locations as to improve the accuracy on the field averaged ET estimates. We applied the central limit theorem as the raw data are spatially independent and normally distributed. Fig. 9.6 shows the number of sample needed to estimate the field mean ET flux with a given relative precision, i.e. 5, 10 and 20%, for a probability level of 95%. Results are presented for cumulated (Fig. 9.6 a-b) and instantaneous ET fluxes (Fig. 9.6 e-f). Also are shown the absolute error of ET fluxes expressed in mm corresponding to the number of samples chosen to reach the three selected relative precision levels (Figs. 9.6 c-d, g-h). Results presented in Fig. 9.6a-b-d-f are summarised in Table 9.1 in which are indicated minimum and maximum number of samples needed to reach the three levels of precision. We observe in Fig. 9.6 and in Table 9.1 that the number of samples needed to reach the 5% level of precision is considerably high both for cumulated and instantaneous ET fluxes with values ranging between 40 and 360. It is evident that such an intensive sampling is unrealistic and unfeasible and therefore that such a level of precision can not be reached for field ET estimates based on the soil water balance method. Note that the number of samples rapidly decreases when the length of the considered period increases which is a direct consequence of the decreasing CV for longer periods (see Fig. 9.1). Concerning the second level of relative precision (10%), the number of required samples is much smaller with values ranging between 10 and 90. It is worth mentioning that for most of the considered periods the sample number values are lower than 31. This means that the sampling strategy adopted for our experimental field, i.e. 28 replicates, allowed us to estimate the field mean actual ET fluxes with a level of precision of about 10%. This precision corresponds to absolute errors of maximum 7.5 and 4 mm for ET cumulated over the first and the second period (see Figs. 9.6 c and d) and to absolute errors ranging between 0.5 and 2 mm for instantaneous ET fluxes (see Figs. 9.6 g and h). Note that the order of magnitude of such errors can be considered as acceptable within an

Table 9.1. Summary of the number of samples (min. and max.) needed to reach a given relative precision (5-10-20%) for a probability level of 95% for cumulated and "instantaneous" ET fluxes.

	Period 1	Period 2	Period 1	Period 2
	cumulated	cumulated	"instantaneous"	"instantaneous"
5%	70-125	40-360	122-205	144-360
10%	17-31	10-90	30-51	34-90
20%	4-7	2-22	7-12	8-22

applied or even a research context but it requires however an intensive spatial sampling frequency. To reach the third level of error (relative error of 20%) it needs a much smaller number of samples namely between 4 and 22 but generally lower than 10. Nevertheless, the absolute precision corresponding to such a small number of samples is quite poor with values ranging between 9 and 15 mm for cumulated ET fluxes and between 1.3 and 3.8 mm for "instantaneous" ET fluxes (Figs. 9.6 c-d-g-h). Such a precision can only be tolerated for ET fluxes cumulated over long periods and for applications in which one is more interested in the order of magnitude of ET fluxes rather than in accurate estimates. The results of the sampling strategy I are consistent with the findings of *Bertuzzi et al.* [1994] showing for a field of similar size (0.6 ha) that about 30 sites are needed to estimate the field mean ET flux with a soil water balance approach for a relative precision of 10%. The results of *Jara et al.* [1998] estimating transpiration fluxes with sapflow within a maize cropped field are also quite coherent with our results. Indeed, they found that 18 and 11 sap flow gauges were enough to estimate respectively the daily and weekly field mean transpiration fluxes for a relative precision of 10%. It is interesting to mention that in this later study the number of samples increases considerably for shorter time intervals, e.g., 37 samples for 20-min. average estimates. On the other hand, the study of *Vandervaere et al.* [1994] presented results much more optimistic in terms of sampling requirements due to the less pronounced ET spatial variability. Indeed, for two different cropped fields, only 6 and 8 sampling locations were sufficient to estimate the mean ET with an absolute error of 0.42 and 0.48 mm.

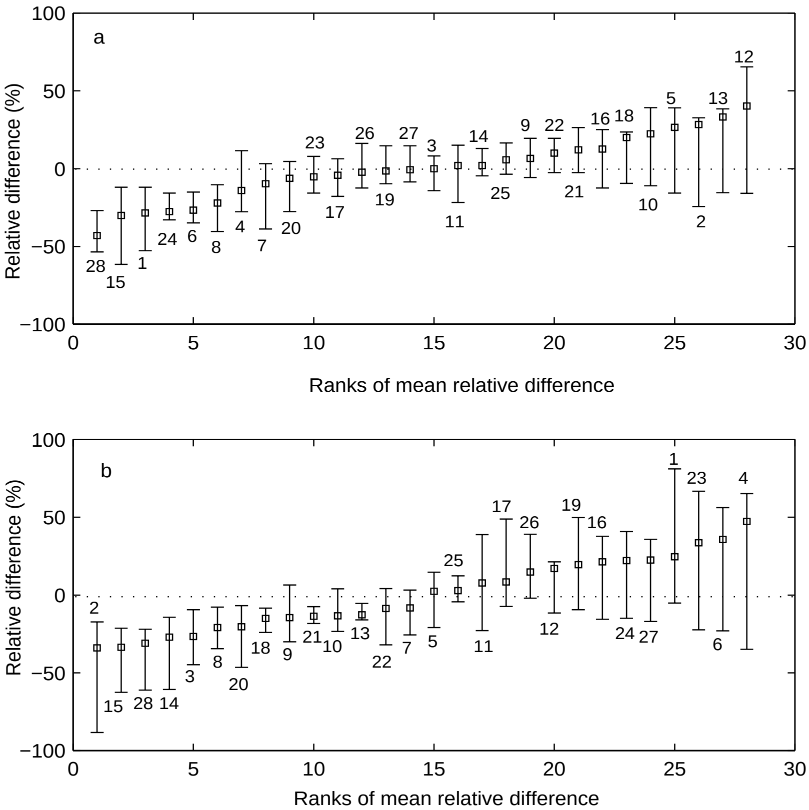

Figure 9.7. Ranked mean relative differences of cumulated ET for the first (a) and the second dry period (b). Means are represented by blocks, and the extremes by vertical bars.

Use of temporally stable sampling locations

The second sampling strategy consists in using some sampling locations representative of the field mean ET fluxes. Therefore, the first step is to investigate if such temporally stable locations exist within the field. For that purpose, we firstly performed a visual inspection of the graphs presenting the ranked mean relative differences with their extremes. Note that in previous studies dealing with the time stability concept, this kind of graph was presented with standard deviations of the relative differences [see e.g., *Vachaud et al.*, 1985 ; *Van Pelt and Wierenga* , 2001]. In our case, we chose rather to present extremes instead of standard deviations as the number of replicates was quite low, i.e. 6 or 10, and as the statistical distributions were in general very different of a normal distribution. Fig. 9.7 a and b presents results obtained for cumulated

ET for respectively the first and the second drying period. For the first drying period, we can observe that the temporal stability is quite high with a range of variation between the extremes of the relative differences of about 25 to 30%. Some sampling locations are obviously less stable (e.g., n°12) but others are much more. For example, sampling locations n°24, 6, 23, 3, 14 and 25 are temporally very stable as they present a small range between the minimum and the maximum value of their relative differences. Among these stable locations, locations n°14 and 25 are particularly well representative of the field mean behaviour in terms of ET fluxes. In this context, the a priori selection of for instance sampling locations n°14 or n°25 would have allow to estimate the mean cumulated fluxes with a relative precision of about 10%. Note that a similar precision requires between 17 and 31 samples with a random sampling strategy (see Table 9.1). It should be stressed that the selection of the time-stable sampling locations n°14 and n°25 was made a-posteriori, namely after the experimental field campaign and the data analysis was made. It is evident that this a-posteriori reasoning is not really interesting to reduce the experimental efforts for the estimation of field averaged ET. Hence, we look for a procedure to estimate time-stable locations a-priori. By assuming that the ET is related to the LAI, a strategy would consist to use the LAI as a covariant. Therefore, we investigate if the time-stable locations, i.e. those very representative of the field mean ET fluxes (n°14 and 25), are characterised by a LAI close to the field mean LAI. The field areal LAI is 3.66 and the LAI for sampling locations n°14 and 25 are respectively 3.77 and 3.67. Although these results are limited to one data set and to one period, this suggests that the LAI could be used as a covariant to select a priori representative sampling locations. However, one has to realise that other additional sampling locations also present LAI values close to the field mean LAI. These additional sampling locations are also close to the field mean ET fluxes, except locations n°8 and 10. These observations and the aforementioned reasoning suggest therefore that the selection and the use of some locations (e.g., 2 or 3) with a LAI representative of the field mean LAI could lead to accurate field areal ET flux estimates. For the second drying period, Fig. 9.7b shows that there is a certain temporal stability though less pronounced than that observed during the first drying period. It is very striking to notice that sampling location n°25 is again very temporally stable and very representative of field mean ET fluxes. On the other hand, some sampling locations present a very contrasted behaviour between the two drying periods. This is now particularly well illustrated in Fig. 9.7b for sampling locations 4 and 24, i.e. those underestimating field areal ET fluxes during the first period and

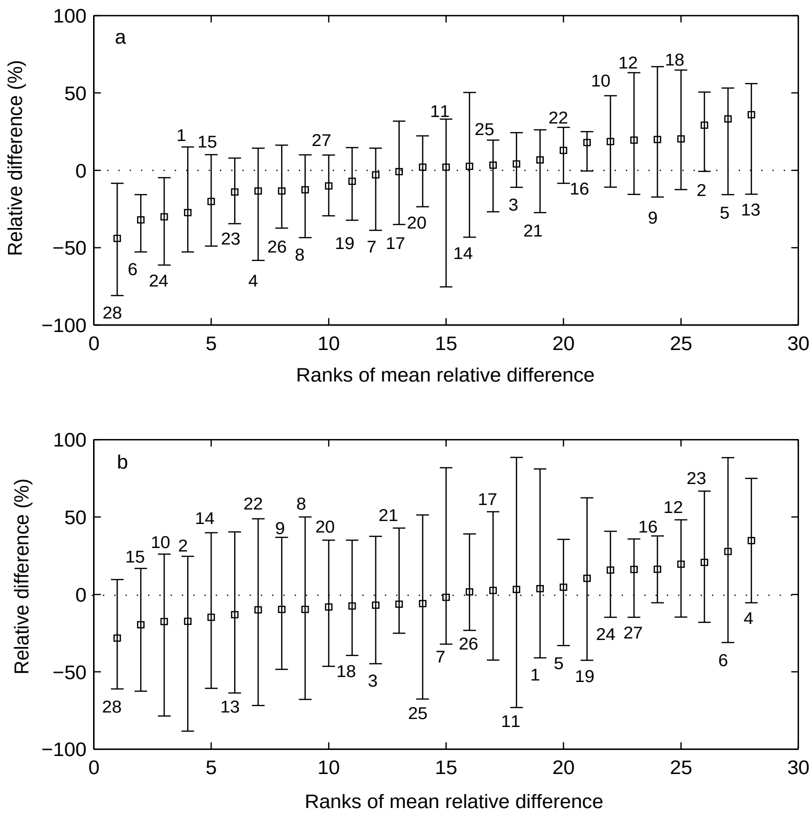

Figure 9.8. Ranked mean relative differences of instantaneous ET for the first (a) and the second dry period (b). Means are represented by blocks, and the extremes by vertical bars.

overestimating them during the second period, and for sampling location n°2 presenting an inverse behaviour. In addition, sampling location n°14 previously selected as temporally stable and representative of the mean ET fluxes for the first period is now much less stable and generally underestimates the mean ET fluxes. This fact obviously questions the usefulness of the aforementioned strategy for the selection of temporally stable and representative locations. Figure 9.8 a and b shows results obtained for the temporal stability of instantaneous ET. These results are markedly different than those obtained for cumulated fluxes. Indeed, instantaneous ET is temporally unstable, especially for the second drying period. For this period, the range between minimum and maximum values of the relative differences is very large, i.e. 60% and in some cases more. Such high ranges exclude the use of the concept of time stability

Table 9.2. Matrix of Spearman's rank correlation coefficients for cumulated ET fluxes for the first drying period.

	09-12/07	09-16/07	09-21/07	09-25/07	09/07-02/08
09-12/07	1				
09-16/07	0.76	1			
09-21/07	0.67	0.82	1		
09-25/07	0.74	0.87	0.97	1	
09/07-02/08	0.55	0.72	0.94	0.91	1

for the estimation of field averaged instantaneous ET. Furthermore, we can again observe that some locations are very unstable between Fig. 9.8 a and b, for example n°6 and n°24. The observed temporal instability for instantaneous ET for our experimental field is perfectly in agreement with the findings of *Raghuwanshi and Wallender* [1997]. Note that for our case, the pronounced temporal stability observed for the cumulated ET, compared to the instantaneous ET, is partially explained by the fact itself that the fluxes are cumulated, namely that ET flux cumulated over e.g. the 09/07-02/08 period contains ET flux cumulated over the 09/07-25/07 period. The content of Figs. 9.7 and 9.8 can also be expressed under a more quantitative and statistical form with the matrix of the rank correlation coefficients calculated with Eq. (9.4). Tables 9.2 and 9.3 give those matrix for cumulated and instantaneous ET fluxes respectively for the first drying period. All the values presented in Table 9.2 are highly significant (for n=28, the critical Rs-value is 0.47 at the 0.01 probability level [*Sokal and Rohlf*, 1995]) confirming therefore that time stability in the ranks of the locations in terms of cumulated ET fluxes can be assumed. On the other hand, rank correlation coefficients presented in Table 9.3 are much smaller. Although some of these correlation coefficients are not statistically significant (see * in Table 9.3), they indicate a quite well pronounced temporal instability for instantaneous ET fluxes. Note that similar results were obtained both for cumulated and instantaneous ET fluxes for the second drying period (not shown).

Use of a covariant

Before using the LAI or the dry matter yield as covariant, one has to investigate if any relationship exists between these variables and the actual evapotranspiration fluxes. The analysis in section 9.3.1. showed that a certain relationship exists between the ET fluxes cumulated over

Table 9.3. Matrix of Spearman's rank correlation coefficients for "instantaneous" ET fluxes for the first drying period. Values marked with * are not significant at the 99% probability level.

	P1	P2	P3	P4	P5	P6
P1(09-12/07)	1					
P2(12-16/07)	0.34*	1				
P3(16-19/07)	0.55	0.24*	1			
P4(21-25/07)	0.48	0.36*	0.38*	1		
P5(25-29/07)	0.31*	0.3*	0.66	0.03*	1	
P6(29/07-02/08)	0.14*	0.45*	0.58	0.36*	0.51	1

the two periods of interest and the LAI measured on the 12^{nd} of July and the dry matter yield measured on the 17^{th} of September. Figs. 9.2 show the relationships with the 95% confidence bands (continuous line) and the 95% prediction bands (dotted line) for respectively the LAI (Fig. 9.2a) and the dry matter yield (Fig. 9.2b). Note that for the application of this "sampling" strategy, two conditions are implicitly required. The first condition is the knowledge of the relationship between the variable of interest and the covariant and the associated uncertainties (derived from the regression analysis). In this study, we will make use of the relationship derived from our experimental site (see Figs. 9.2a and b) but in practice there is no limitation to use relationships found in the literature as far as these are broadly applicable. The second condition is the knowledge of the mean value or even the spatial distribution of the covariant for the considered area. For our field, the mean LAI and dry matter yield values are 3.66 and 2041 g/10 plants respectively. Using the relationships presented in Figs. 9.2, the estimated field averaged ET is equal to 119 $\pm$6.1 mm (LAI as covariant) and equal to 118.5 $\pm$ 4.5 mm (dry matter yield as covariant) at a probability level of 95%. The two field averaged ET estimates are very similar with further quite similar narrow confidence intervals. This suggests therefore that the proposed sampling strategy can be used to estimate field areal ET flux at least for long periods, e.g., for the whole agricultural season. This requires however to use valid relationships predetermined for such long periods. Note that the presented sampling strategy allows additionally to distribute spatially the ET fluxes at the condition that the information about the covariant is spatially distributed. The within-field spatial variability of the LAI and crop yield can be derived from remote sensing [*Booltink and Epinat*, 2001] and from sensors placed on harvesting machines combined with global positioning systems such as the systems typically used in precision agriculture [*Joernsgaard and Halmoe*, 2003]. In our case however, we did not perform this exercise since the uncertainties associated to the point ET predictions would have been very large (see prediction bands in Figs. 9.2). Nevertheless, the use of better defined relationships could allow to use this approach to derive accurate maps of "within-field" spatial variability of ET fluxes.

9.4 Conclusions

In this chapter, we have analysed the spatio-temporal variability of actual evapotranspiration (ET) within a small agricultural field and investigated the usefulness and the efficiency of three different sampling strategies to estimate the field averaged ET flux.

The spatio-temporal analysis showed that the evapotranspiration process is highly variable within the field with CV values ranging between 15.5 and 46.3% for cumulated ET and between 26.95 and 46.3% for instantaneous ET fluxes. The observed spatial variability systematically decreases with the increase of the length of the considered period. In terms of absolute spatial variability of cumulated ET, the values range between 39.4 and 107.5 mm for the first drying period and between 30.3 and 55.7 mm for the second drying period. The reasons of this variability were investigated by relating ET cumulated over the two dry periods with crop growth parameters, i.e. the LAI and the dry matter yield. The established relationships are not very well defined but statistically significant allowing us to argue that the spatial variability of the ET can mainly be explained by the spatially variable crop growth. Furthermore, this spatially variable crop growth explains that the ratio between the measured actual ET and the reference evapotranspiration is systematically smaller than the ratios suggested for standard conditions [see *Allen et al.*, 1998]. These findings strongly questions the pertinence of using ratios derived from standard conditions (i.e. crop coefficients) for the modelling of ET fluxes with agro-hydrological models. Indeed, the aim of those models is to simulate water fluxes for field conditions for which standard conditions are rarely or even never met. We suggest therefore before using agro-hydrological models in a predictive mode to adjust the crop coefficients according to the variable crop growth (e.g., see procedures proposed in the FAO n°56 bulletin) as to improve the estimation of simulated water fluxes. For agro-hydrological models using directly the Penman-Monteith formulation for ET estimation, it should be feasible to adjust the surface and the aerodynamic resistances according to spatially variable Leaf Area Index and crop heigth.

Prior to the use of sampling strategy I, we showed that the cumulated and the instantaneous ET fluxes were spatially independent and normally distributed. By applying the central limit theorem, we estimated that to reach a relative precision of 5% at a probability level of 95% for the estimation of the field averaged ET, it requires between 70 and 360 samples. Such an intensive sampling is clearly unrealistic leading therefore to the conclusion that such a level of precision can not be reached for field ET estimates based on the soil water balance method. For a relative precision level of 10%, the number of required samples is much smaller with values ranging between 10 and 90. Furthermore, for all the considered periods apart from five the sample number values are lower than 31. This means that the sampling strategy adopted for our experimental field, i.e. 28 replicates, allowed us to estimate the field mean actual ET fluxes with a level of precision of about 10%. For the 20% relative precision level, the number of samples varies between 4 and 22.

For the use of the sampling strategy II, we showed for cumulated ET fluxes that the sampling locations were in general temporally stable. It was also shown that some location were very representative of the field averaged cumulated ET. The use of only one representative location (e.g., n°14) selected a-priori allows to estimate the field areal ET flux with a relative precision of 10%. However, we believe that the procedure to select an appropriate a-priori location needs further research. Furthermore, there is some instability of ET between the two considered periods showing that the representative locations for the first period are not necessarily those for the second period. In contrary to cumulated ET, instantaneous ET is temporally very unstable precluding the use of the concept of time stability for the estimation of field areal instantaneous ET flux. We further showed that significant positive relationships exist between the cumulated ET, the LAI and the dry matter yield. The use of these relationships produced very similar cumulated ET estimates, namely 119 $\pm$6.1 mm and 118.5 $\pm$4.5 mm respectively when the LAI and the yield are used as covariant.

To conclude, our study showed that the evapotranspiration process is spatially extremely variable even within small fields. This spatial variability requires therefore an efficient sampling strategy for the estimation of field averaged ET with a soil water balance approach. The use of the "random" sampling strategy requires a quite large number of samples to reach an acceptable level of error compared to the strategy based on the use of temporally stable locations. Nevertheless, the accuracy of this later strategy strongly depends on the selected sampling locations which obviously comprises a certain risk. Finally, the sampling strategy using a covariant seems very attractive as the information about the crop size is generally much easily available and further is generally spatially distributed. This strategy assumes yet a good knowledge of the relationships between the ET fluxes and the covariants. In this framework, more in depth research is needed to investigate the robustness of these relationships with respect to different climatic and agronomic conditions and to different plant cultivars.

Chapter 10

Micro-variability of hydrological processes at the maize row scale: implications for soil water content measurements and evapotranspiration estimates

Abstract*

In this chapter, we analyze the micro-variability of the hydrological processes (i.e. rainfall redistribution, root water uptake and evapotranspiration) at the maize row scale during a long drying period. Then, we study the impact of the variability of these processes on the spatio-temporal dynamics of the soil water content and on the sampling strategies to estimate soil water content and evapotranspiration at the maize row scale. Results of our study firstly show that the rainfall reaching the ground under the maize canopy is very variable with coefficients of variation ranging between 77.87 and 188.7%. Some locations receive up to 4.47 more water than the incident rainfall. The estimated root water uptake (RWU) is also extremely variable laterally within the maize rows with CV values ranging between 13.9 and 137%. Well-defined cyclical patterns of RWU due to the row layout are observed at some depths. Throughout the long drying period, maximum RWU progressively moves downwards and towards the middle of the row. Evapotranspiration (ET) is less vari-

*adapted from Hupet, F., and M. Vanclooster, submitted to *Journal of Hydrology*.

able across the rows with CV values ranging between 11.95 and 29.07%. Cyclical patterns are also observed except at the end of the considered period. Concerning the spatio-temporal dynamics of the soil water content, this one is clearly influenced by the maize row layout, with the progressive appearance of a fingered pattern within the rows due to the spatially variable RWU. The maximum difference of soil water content measured within a maize row is important and range between 0.046 and 0.079 $cm^3\ cm^{-3}$. In absolute terms, coefficients of variation for soil water content range between 1.05 and 12.1%. For the soil water content and ET estimates at the maize row scale, we show that the location of soil water content sensors is critical. The use of "central" sampling locations in the middle of the row leads to estimate the mean row scale soil water content and ET with a maximum error of 0.022 $cm^3\ cm^{-3}$ and 0.47 mm d^{-1} respectively. More research is needed to generalize the results obtained in this study for other climatic conditions and for other soil water content measurement techniques.

10.1 Introduction

The transport of water through the soil is often much more complex than is assumed and formulated in traditional models [*Philip*, 1991; *Hillel*, 1993]. One of the main simplifications in simulation models is that the processes are represented in one dimension [e.g. *Vanclooster et al.*, 1996; *Van Dam et al.*, 1997]. For modelling water fluxes within the soil-plant-atmosphere system, one considers explicitly that the root water uptake is uniform around the plant and that the rainfall reaching the ground under the canopy is equally distributed at the soil surface. In reality, the processes are spatially variable due to the crop canopy architecture inducing redistribution of the incident rainfall into stemflow and throughfall [e.g. *Bui and Box*, 1992], and due to the three-dimensional configuration of the root system inducing spatially variable root water uptake [e.g. *Green and Clothier*, 1999]. For forested ecosystems and orchards, issues related to the micro-variability of the hydrological processes have long been recognized and quite extensively studied [e.g. *Rambal et al.*, 1984; *Bouten et al.*, 1992; *Green and Clothier*, 1995; *Andreu et al.*, 1997]. Comparatively less attention has been paid to the study of the micro-variability of the processes for agricultural crops, although the recent appearance of multi-dimensional soil-plant-atmosphere models [e.g. *Coelho and Or*, 1996; *Vrugt et al.*, 2001] strongly stimulates the investigation of the variability at such spatial scale. For agricultural crops, the small scale variability of the hydrological processes has mainly been studied for row crops (e.g.

soybean and maize) as it is implicitly assumed that micro-variability is the highest for such crops. The spatially variable hydrological processes likely to be encountered within a row crop include the soil evaporation, the root water uptake and the rainfall redistribution. Few authors have examined the magnitude of the variability focusing generally on only one process, e.g. the rainfall redistribution [*Parkin and Codling*, 1990], or by observing the spatio-temporal dynamics of a state variable, e.g. the soil water content, resulting of the complex interactions of all the variable processes [*Timlin et al.*, 2001]. For maize, the impact of the canopy on the rainfall partitioning into stemflow and throughfall was studied by *Quinn and Laflen* [1983], *Van Elewijck* [1989], *Parkin and Codling* [1990], *Bui and Bow* [1992], *Paltineanu and Starr* [2000] and *Bussière et al.* [2002]. All these studies have shown that the maize canopy has an important effect on the rainfall redistribution and that some locations under the canopy may receive very large amount of water under the form of stemflow or throughfall while other locations may receive much less. The results of these studies were derived from measurements of rainfall reaching the ground under the canopy except in the study of *Paltineanu and Starr* [2000] where the soil water content dynamics was simultaneously measured. Some studies also put forward the variability of the rainfall reaching the soil surface by only measuring the temporal dynamics of the soil water content within the maize rows [e.g. *van Wesenbeeck and Kachanoski*, 1988; *van Wesenbeeck et al.*, 1988; *Dekker and Ritsema*, 1997; *Michot et al.*, 2003]. Concerning the micro-variability of the root water uptake within the maize rows, *van Wesenbeeck and Kachanoski* [1988] and *Van Wesenbeeck et al.* [1988] clearly showed that for the surface layer (0-20 cm) this one is maximum in the row and very variable between the rows. Laboratory and field experiments also put forward that the root water uptake of maize is spatially variable both laterally and vertically and that the root water uptake can be influenced by external factors such as irrigation [e.g. *Coelho and Or*, 1999; *Michot et al.*, 2003]. All the above-mentioned studies showed that the micro-variability of the processes varies significantly in time as it is strongly dependent on the crop growth stage. A better understanding of the micro-variability of the processes occurring within a maize crop and its time dependence is of primary importance. It should allow the optimization of sampling strategies for measuring soil water content and evapotranspiration with a soil water balance at the maize row scale. Furthermore, it constitutes an essential step for improving the multi-dimensional modeling (2-D or 3-D) of the soil water transport within the soil-maize-atmosphere system.

Our study has to be situated within this context. The general purpose is to investigate the micro-variability of the hydrological processes at the maize row scale using a comprehensive field data set measured within two maize rows. The specific objectives are the following:

(1) To analyse the micro-variability of the rainfall redistribution, of the root water uptake and of the evapotranspiration at the maize row scale;

(2) To study the spatio-temporal dynamics of the soil water content and to probe the role of the different hydrological processes on the soil water content dynamics; and

(3) To investigate the optimum sampling strategy for estimating soil water content and evapotranspiration at the maize row scale.

10.2 Material and methods

This chapter is based on the data set collected during the 2003 agricultural season. The data set consists in soil water content measurements performed with a neutron probe in 14 access tubes installed perpendicularly to 3 maize rows (i.e. within two interrows) and in throughfall measurements. The measurements were performed during the very dry and hot period from the 3^{rd} of June to the 28^{th} of August. The reader is referred to Chapter 2 for more detailed information about the experimental setup. In this chapter, we firstly analyse the spatio-temporal variability of the hydrological processes at the maize row scale. In a first step, we investigate the variability of the rainfall redistribution below the maize canopy using throughfall measurements performed after 7 significant rainfalls in 52 small plastic boxes placed within two maize interrows. These measurements are combined with incident rainfall measurements performed with a rain gauge located 100 m away from the experimental field in order to determine the transmission ratios (rainfall at the soil surface to incident rainfall). As explained in Chapter 2, throughfall was not measured in the row itself as the small plastic boxes were placed 1.5 cm away on each side of the maize stems (see Fig. 2.4 bottom right). Consequently, the stemflow was not directly measured. Alternatively, we estimate this component with the following equation:

$$S_f = R_{out}\,3897 - R_{in}\,3731 - I_c\,3897 \tag{10.1}$$

where S_f is the stemflow (cm^3); R_{out} (cm) and R_{in} (cm) are the measured incident rainfall and the mean throughfall respectively; and I_c is the crop interception (cm) fixed at 0.25 cm [*Boons-Prins et al.*, 1993]. The coefficient 3731 corresponds to the total surface of the 52 small boxes. R_{out} is multiplied in Eq. (10.1) by 3897 (i.e. 3731+166) as the surface over which throughfall is not measured is equal to 166 cm^2. This surface is used to convert values of stemflow expressed in cm^3 into mm. It is worth mentioning that we use in this study the "stemflow" term to express both the rainfall reaching the ground by flowing along the maize stems (i.e. the stemflow itself) and the rainfall reaching the ground between the maize stems of a same row. In second step, we investigate the spatio-temporal dynamics of the root water uptake in the rows and in the interrows. Root water uptake for a given period and for a certain depth is quantified using soil water content measurements performed at this depth at the beginning and at the end of the considered period assuming no vertical or lateral soil water fluxes. This approach considers that the whole soil water depletion is due to the root water uptake. The methodology is particularly well adapted for dry periods during which root water uptake is larger than soil water fluxes [*Musters et al.*, 2000; *Hupet et al.*, 2002]. Such conditions are met in our study and the root water uptake is quantified as follows:

$$RWU_{t_1,t_2} = \theta_{t_1} - \theta_{t_2} \tag{10.2}$$

where RWU_{t_1,t_2} is the root water uptake at a certain depth occurring between t_1 and t_2 ; and θ_{t_1} and θ_{t_2} are the soil water content measured for the given depth at t_1 and t_2 respectively. The RWU in Eq. (10.2) is expressed in L^3 L^{-3} T^{-1} but is generally divided by the length of the considered period in order to produce daily root water uptake values (expressed in cm^3 cm^{-3} d^{-1} or simply in d^{-1}). In a third step, we analyse the spatio-temporal dynamics of the evapotranspiration (ET). ET is quantified for each of the 14 sampling locations using the following simplified water balance equation:

$$ET_{t_1,t_2} = 300(\theta_{t_1-25} - \theta_{t_2-25}) + 100\sum_{i=35}^{65}(\theta_{t_1-i} - \theta_{t_2-i}) \tag{10.3}$$

where ET_{t_1,t_2} is the evapotranspiration (mm) estimated between t_1 and t_2; and θ_{t_1-i} and θ_{t_2-i} the soil water content (cm^3 cm^{-3}) measured at depth i at t_1 and t_2 respectively. This simplified equation is assumed to be valid as it is only applied during dry periods without any significant rainfall and during which soil water fluxes at the bottom of the soil profile (70 cm) are likely to be very small due the low hydraulic conductivity values associated to the low soil water content measured at this depth. Note that in Eq. (10.3), we assume implicitly (as for the root water uptake) that there are no lateral soil water fluxes, i.e. that all the soil water depletion measured on a sampling location is representative of the soil evaporation and the vertically integrated root water uptake of this location. After studying the micro-variability of the hydrological processes, we analyse the soil water content patterns focusing on the impact of the above-mentioned hydrological processes on the temporal dynamics of the soil water content. We also investigate the relationships existing between mean soil water content and both standard deviation and coefficient of variation. For these relationships, mean soil water content and standard deviation are calculated for the two maize rows together and for each one separately. Then, we investigate for each depth (i.e. 25, 35, 45, 55 and 65 cm) and each day (i.e. 22 days) the optimum sampling locations within each maize row to estimate the mean soil water content of the maize row. We systematically calculate the deviations between the locally measured soil water content and the mean value of the maize row. Finally, we determine optimum sampling locations for estimating ET at the maize row scale. Optimum sampling locations within the two considered rows are determined for 3 long drying periods, for 8 sub-periods and for the whole season. As for soil water content, we quantify across the maize row the deviations between the mean row scale ET and ET of each sampling location.

10.3 Results and discussions

Climate encountered during the 2003 summer was characterised by very high temperatures and by a very low rainfall amount. The considered period, i.e. from the 3^{rd} of June (DOY 154) to the 28^{th} of August (DOY 240), coincided with the long drought period which affected most of the Western Europe's countries during July and August 2003. Fig. 10.1a presents the time evolution of the climatic demand (ETo) for the considered period characterized by a mean and a maximum ETo of 5.19 mm d^{-1} and 7.26 mm d^{-1} respectively. The mean temperature for July and August is 19.3 °C and 21.2 °C respectively with maximum values of 33.4 °C and 36.4 °C. The total amount of rainfall between the 3^{rd} of June and the 28^{th} of August is 94.8 mm distributed in only 4 significant rainfalls. The effect of such climatic conditions is obviously well pronounced on the time evolution of the soil water content presented in Fig. 10.1b. For the first depth (25 cm), the mean soil water content decreases from 0.337 to 0.157 cm^3 cm^{-3} with only a very small increase after DOY 204 due to the rainfall. The rainfall encountered during the considered period has no impact on the soil water content of deeper depths, decreasing therefore in a monotonous way from the beginning to the end of the 2003 field campaign. In absolute terms and for all depths confounded, minimum and maximum soil water content values are 0.132

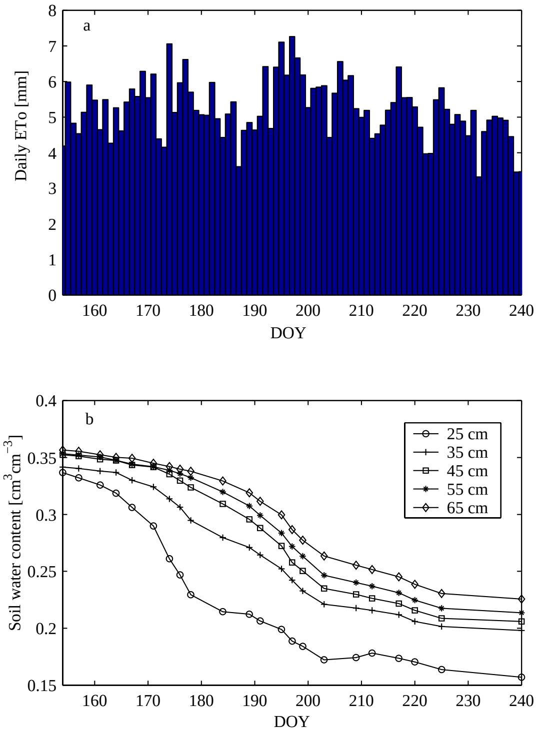

Figure 10.1. Temporal evolution of the daily evaporating demand (ETo) encountered during the 2003 field campaign (a) and of the mean soil water content measured at 25, 35, 45, 55 and 65 cm depth (b).

and 0.366 cm^3 cm^{-3}, which corresponds to almost the whole range of soil water content that can be observed for the medium-fine textured soil under consideration. Soil water content values presented in Fig. 10.1b are the average for each depth for the 14 different sampling locations but a very similar behaviour is observed if the two investigated rows are treated separately (results not shown).

The micro-variability of the rainfall distribution below the maize canopy is analysed for seven different rainy events. Table 10.1 firstly presents the rainfall values measured outside of the maize cropped field (called hereafter incident rainfall or rain out) for the seven events three of which are really significant (i.e. DOY 181, 209 and 211). The mean values of the measured throughfall are also presented. Both types of measurements are expressed in mm. It is remarkable that the throughfall values are systematically much smaller than the incident rainfall values. The difference between these two components includes both the maize

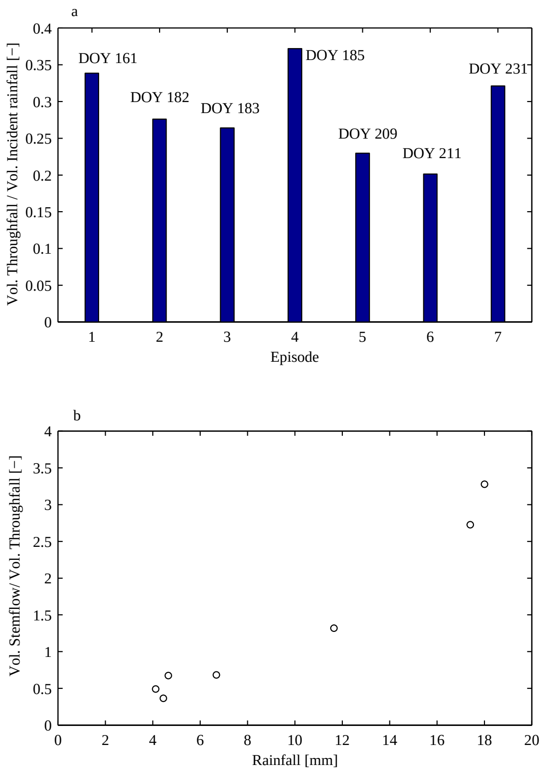

Figure 10.2. Ratios between measured throughfall and incident rainfall for the 7 considered rainy events (a) and relationship between the rainfall and the ratio between stemflow and throughfall (b).

interception and the stemflow. This latter was calculated with Eq. (10.1) for each rainy event considering an interception of 2.5 mm. The ratios between stemflow, throughfall and incident rainfall in terms of volume of water are presented in the second part of Table 10.1. The ratios between the mean throughfall and the incident rainfall are quite small and vary in a narrow range between 20.12 and 33.86%. Fig. 10.2a illustrates the time evolution of these ratios. In Fig. 10.2a, we can observe that there is no true temporal trend probably due to the fact that the maize crop is fully covering the soil ($2.5<LAI<3.6$) during the 7 considered rainy events. For the last rainy event (DOY 231), the measured throughfall is yet larger than that of the two previous ones which could be explained by the leaves bending increasingly downward due to the maize senescence.

Table 10.1. Values of measured incident rainfall, mean values of measured throughfall, and mean and maximum ratios between the three components. Also presented are the coefficients of variation of the rainfall reaching the ground below the maize canopy.

	DOY 181	DOY 182	DOY 183	DOY 185	DOY 209	DOY 211	DOY 231
Mean incident rainfall (mm)	11.65	4.65	4.12	6.68	17.4	18	4.45
Mean throughfall (mm)	4.12	1.34	1.14	2.59	4.17	3.78	1.49
Vol. throughall/Vol. incident rainfall (%)	33.86	27.59	26.4	37.15	22.97	20.12	32.11
Vol. stemflow/Vol. incident rainfall (%)	44.67	18.64	12.91	25.39	62.65	65.98	11.70
Vol. stemflow/Vol. throughfall (%)	131	67.5	48.9	68.3	272.7	327.9	36.4
Max. ratio throughfall/rainfall out (%)	98	93	114	352	143	75	301
Max. ratio (throughfall+ stemflow)/rainfall out (%)	303	126	114	352	425	447	301
CV throughfall (%)	73.6	79.8	71.7	130.4	101.7	73.05	145.5
CV throughfall+stemflow (%)	133.5	94.8	77.87	115.87	179.9	188.7	121

The small values obtained for these ratios mean that the preferential stemflow component is large. Ratios between estimated stemflow and measured incident rainfall are larger and much more variable with values ranging between 12.91 and 65.98%. These ratios are similar to those obtained for a maize crop by *Haynes* [1940], *Quinn and Laflen* [1983], *Parkin and Codling* [1990], and *Bussière et al.* [2002] with values of 22%, from 16 to 49%, from 19 to 49% and of 70% respectively. Table 10.1 shows that the ratios between the collected throughfall volume and the estimated stemflow volume are still larger and much more variable with values ranging between 36.4 and 327.9%. The relationship between these ratios and the incident rainfall amount is illustrated in Fig. 10.2b. This figure shows that the proportion of stemflow considerably increases with the incident rainfall amount meaning that long rainy events will produce comparatively more stemflow than small rainfall events. The obtained relationship is quite surprisingly inverse to that found by *Paltineanu and Starr* [2002]. Note however that the relationship between stemflow and throughfall depends on many additional variables such as rainfall intensity, duration of rainfall, foliar ground cover, size and orientation of leaves, and development of canopy. The effect of all these factors combined with the relatively small number of considered rainy events (i.e. 7) can explain such a difference between the two identified relationships. Table 10.1 also shows maximum ratios between the rainfall below the maize canopy (with and without stemflow) and the incident rainfall. We can observe that some locations under the maize canopy receive up to 3.52 more water than the incident rainfall, and up to 4.47 more if stemflow is taken into account. For DOY 183, 185 and 231, maximum ratios are similar meaning that maximum ratios are not obtained under the form of stemflow. The results obtained are coherent with the ratios presented by *Bussière et al.* [2002] ranging between 0.05 and 3 for throughfall. Considering stemflow, these authors obtained maximum ratios of 35 which are clearly much higher than those obtained in our study. However, the results of *Bussière et al.* [2002] were obtained for one isolated maize plant which is likely to strongly influence the results. The micro-variability of throughfall is illustrated in Fig. 10.3 for 5 different rainy events. Left graphs (a-c-e-g-i) show the micro-variability only considering the measured throughfall while right graphs (b-d-f-h-j) show the micro-variability of both measured throughfall and estimated stemflow. These graphs firstly show that the micro-variability is huge and that this one still increases if stemflow is considered (see right graphs). Secondly, we can clearly observe for each rainy event some well defined patterns of higher rainfall intensity in the middle of the rows. Such patterns are visible for the two considered rows. High intensities of throughfall are also

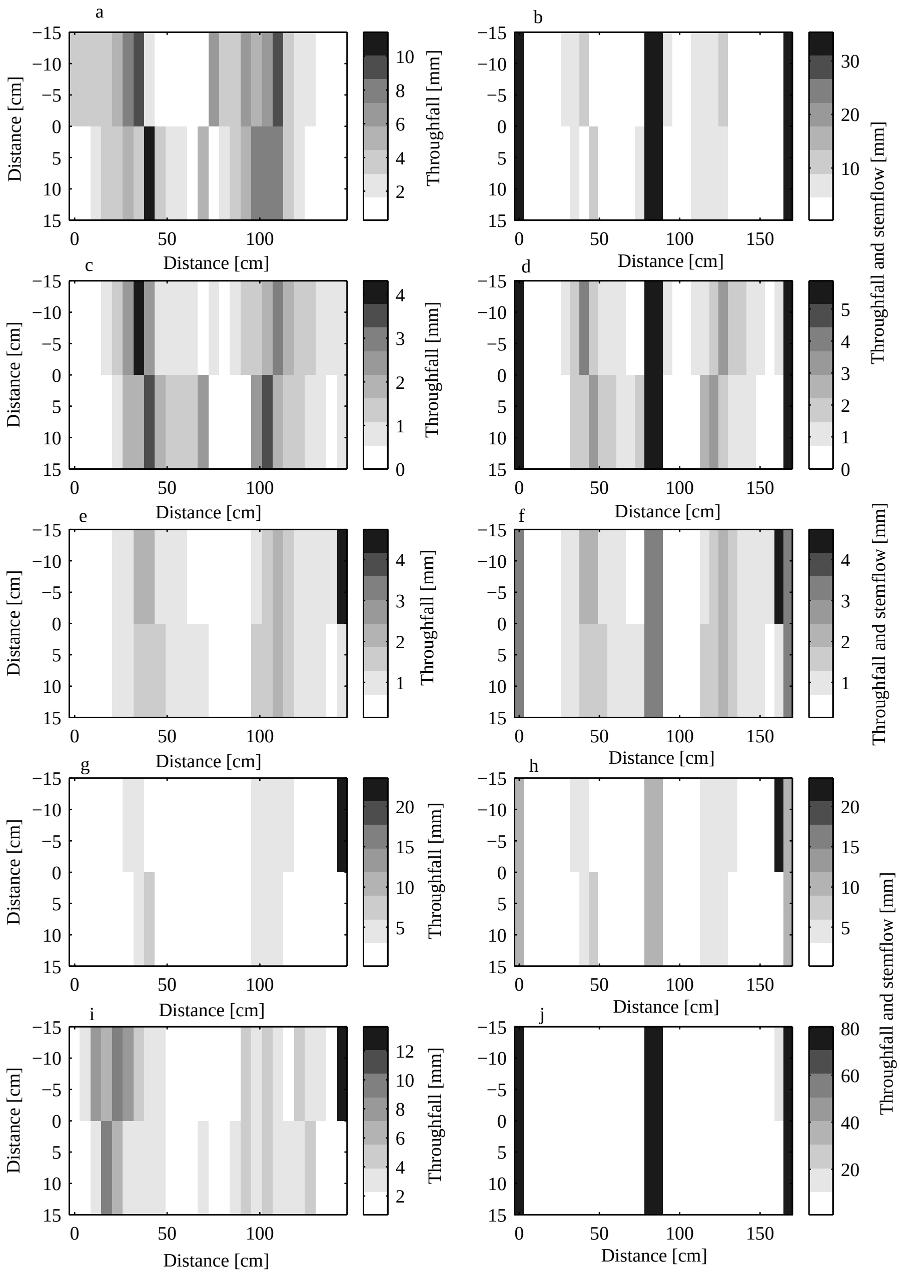

Figure 10.3. Spatial variability of the throughfall measured for 5 different rainy events, i.e. on DOY 181 (a), 182 (c), 183 (e), 209 (g), and 231 (i). Right graphs (b-d-f-h-j) show the corresponding patterns considering the estimated stemflow.

observed very close to the rows (Fig. 10.3e-g-i), which is due to a certain part of the stemflow collected with the installed plastic boxes. Such high values are observed in the same plastic box on DOY 183 (e), DOY 185 (g) and 231 (i) revealing a certain time stability of the rainfall redistribution process. Right graphs (b-d-f-h-j) show that stemflow clearly dominates the patterns if it is taken into account. The micro-variability of the rainfall under the maize canopy is quantified by calculating coefficients of variation (CV expressed in %) that are displayed in the last two lines of Table 10.1. The CV values range between 73.6 and 145.5% for the case where only throughfall is considered and between 77.87 and 188.7% for the case where both stemflow and throughfall are considered. The observed spatial variability of the rainfall redistribution is positively correlated to the rainfall amount, with CV values ranging from 77.87% for the smallest rainfall (i.e. 4.12 mm) to 188% for the largest (i.e. 18 mm). It is obvious that the observed spatial variability of the rainfall under the maize canopy is likely to influence the spatio-temporal dynamics of the soil water content, especially near the soil surface. The impact of the rainfall redistribution under a maize canopy on the soil water content dynamics has been elucidated by *van Wesenbeeck and Kachanoski* [1988], *van Wesenbeeck et al.* [1988], *Dekker and Ritsema* [1997] and *Paltineanu and Starr* [2000]. All these studies show the effect of the large amount of stemflow on the soil water content dynamics measured in the maize row. Yet, soil water content variability at the maize row scale is also controlled by additional processes such as the soil water redistribution, the soil evaporation and the root water uptake which also strongly vary spatially. The observed spatio-temporal dynamics of the soil water content will therefore depend on the relative importance of these different processes.

The micro-variability of the root water uptake (RWU) is investigated for three long dry periods (hereafter called P_1, P_2 and P_3) without any significant rainfall, i.e. from the 10^{th} to the 27^{th} of June (DOY 161-178, rainfall=9.1 mm), from the 3^{rd} to the 22^{nd} of July (DOY 184-203, rainfall=1.1 mm), and from the 5^{th} to the 28^{th} of August (DOY 217-240, rainfall= 4.4 mm). In order to study more thoroughly the temporal dynamics of the RWU, P_1 and P_2 are subdivided into three shorter periods (hereafter called P_{1a-b-c} and P_{2a-b-c}) and P_3 in two shorter periods (hereafter called P_{3a-b}). The climatic conditions encountered during all these periods are optimum to study the RWU as the rainfall is very low and the climatic demand is very high. Furthermore, the three periods are well contrasted in terms of maize development. During P_1 (i.e. in June), the maize crop is actively growing and is not fully covering the soil (LAI=2.5 on DOY 165). During P_2 (i.e. in July), the maize reaches

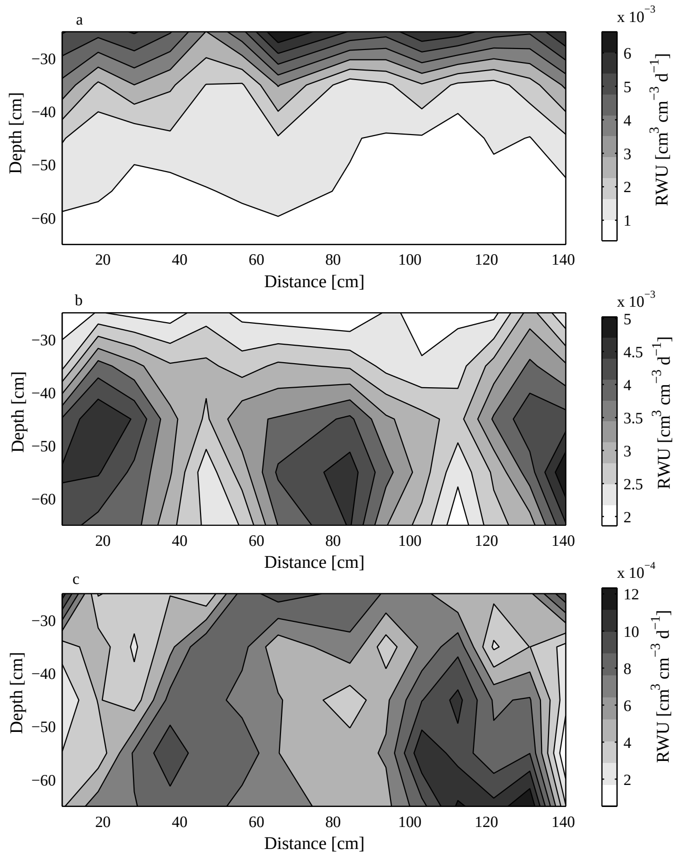

Figure 10.4. Two-dimensional maps of daily RWU estimated for P_1 (from DOY 161 to 178), for P_2 (from DOY 184-203) and for P_3 (DOY 217-240) illustrated in Fig. 10.4a, b and c respectively.

the maximum development (LAI=3.6) while during P_3 (i.e. in August) the crop becomes progressively senescent with a LAI of 2.6 on DOY 231. The RWU is estimated with Eq. (10.2) for P_1, P_2 and P_3 and for the 8 sub-periods. In order to make easier comparisons between periods of different lengths, the RWU is systematically converted into daily values (i.e. expressed in d^{-1}). The estimated RWU is systematically illustrated for each period in Figs. 10.4 and 10.5. Fig. 10.4 shows the RWU patterns estimated for P_1 (a), P_2 (b) and P_3 (c). Fig. 10.5 shows the lateral variability of the RWU for the same three periods for certain depths (a, c and e) and the RWU averaged for each depth for the considered sub-periods (b, d and f).

For the first drying period (DOY 161-178), Fig. 10.4a clearly shows that the RWU is mainly limited to the superficial soil layer, with 80% of the RWU occurring above 45 cm depth and almost all above 55 cm depth. The superficial RWU is obviously related to the maize root system mainly developed at the surface at this time of the season. In terms of lateral variability, Fig. 10.4a shows that the RWU is the highest under the maize rows which produces quite well defined RWU patterns corresponding to the maize rows layout. Note that the impact of the row layout is still visible at 50 cm depth. The RWU lateral variability estimated for P_1 is clearly illustrated in Fig. 10.5a for the 25, 55 and 65 cm depths. Fig. 10.5a shows that the RWU at 25 cm depth is very laterally variable with a minimum and a maximum daily RWU of 0.00345 d^{-1} and 0.00745 d^{-1} respectively. Besides the maximum RWU observed under the rows, we can also see a small increase of the RWU in the middle of the two considered interrows. This small increase can be explained by the fact that the RWU estimated at the soil surface also include the soil evaporation which is likely to be maximum in the middle of the maize rows due to the not completely covering maize canopy. The true (unknown) RWU patterns for the surface layers are therefore biased in some way by the soil evaporation. Fig. 10.5b illustrates the mean RWU estimated for each depth and for the three considered sub-periods, i.e. P_{1a} (DOY 161-167), P_{1b} (DOY 167-174), and P_{1c} (DOY 174-178). The mean RWU profiles seem to progressively adopt an exponential shape. In terms of absolute values, the RWU increases from the first to the third period for nearly all the considered depths. The increase of RWU can probably be explained by the daily ETo increasing from the first to the third period with values of 5.07, 5.62 and 6.09 mm for P_{1a}, P_{1b}, and P_{1c} respectively. These observations clearly reinforce the assumption stating that the magnitude of the RWU at a certain depth depends on the climatic demand. It is worth mentioning that this concept of RWU variable according to the climatic demand validates the RWU model proposed by *Feddes et al.* [1978] and invalidates the model by *Hoogland et al.* [1981]. Indeed, this latter considers for a non growing root system that the RWU is constant and independent of the climatic demand for a certain depth. The increase of the RWU at a certain depth observed in Fig. 10.5b could also be explained by the root growth although we do not have any root observations to support this assumption. It is also likely that both effects combined, i.e. the increase of ETo and the root dynamics, govern the temporal dynamics of the RWU.

For the second drying period (DOY 184-203), Fig. 10.4b shows that the maize RWU is very limited and rather uniform at 25 cm depth. The small RWU values can be explained by the low soil water contents observed at this depth during P_2 (from 0.2 to 0.17 $cm^3\ cm^{-3}$) corresponding

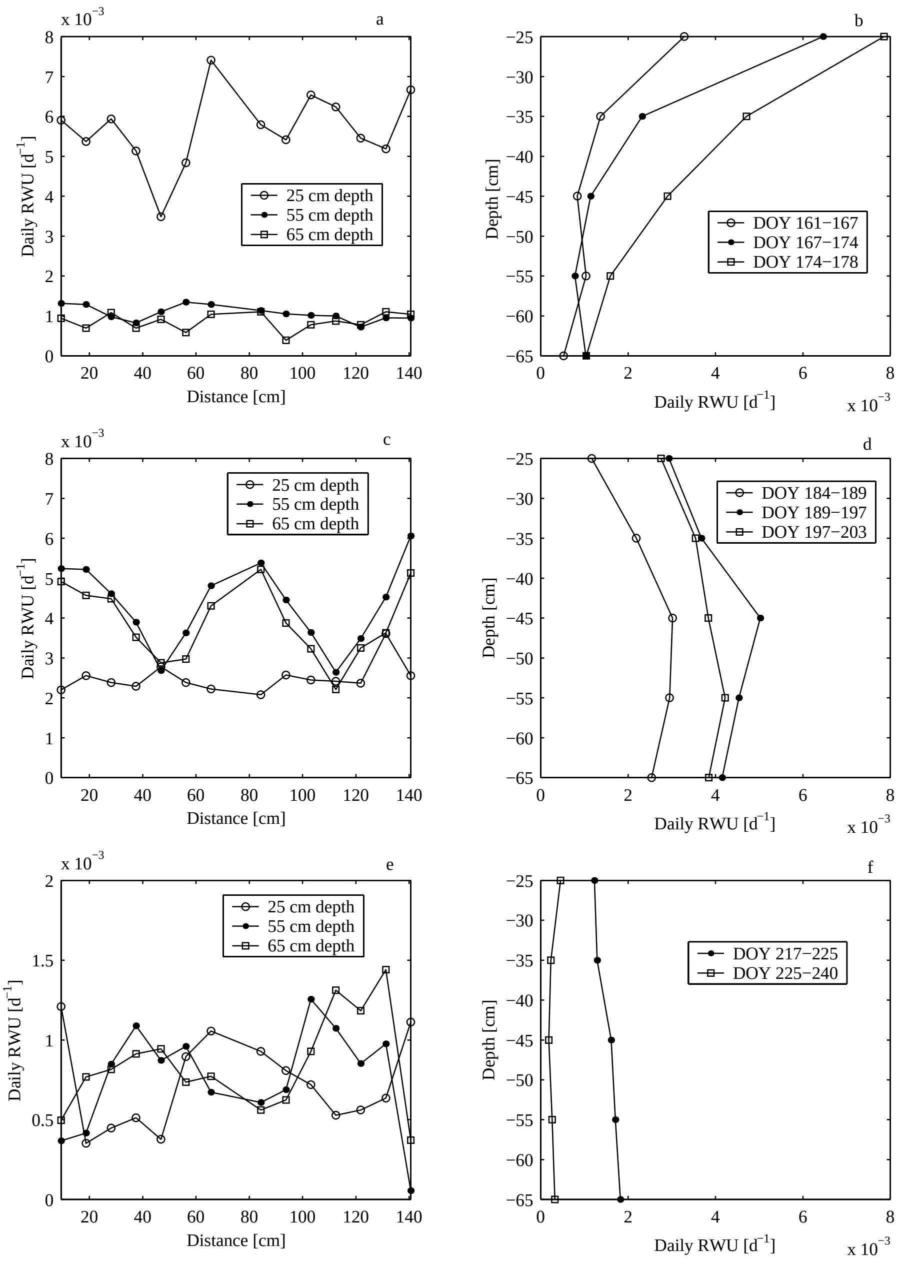

Figure 10.5. Spatial variability of daily RWU estimated at 25, 55 and 65 cm depth for P_1 (a), P_2 (c) and P_3 (e). Right graphs show the mean RWU estimated for 3 sub-periods of P_1 and P_2 (b and d) and for 2 sub-periods of P_3 (f).

to very low soil pressure head values (<-4000 cm) at which the maize RWU is very likely to be reduced. On the other hand, the RWU is much higher at deeper depths, i.e. between 45 and 65 cm depth, and is maximum under and close to the maize rows producing very well organized RWU patterns. This effect of the rows on the deep RWU is also very well illustrated in Fig. 5c showing the cyclical RWU observed at 55 and 65 cm depth. The RWU values are about 0.005 d^{-1} under the row and about 0.003 d^{-1} between the rows. These cyclical RWU patterns are clearly related to the configuration of the maize root system which does not reach the middle of the row. Indeed, soil water content measured at 55 and 65 cm depth at the start of P_2 is very uniform through the 14 sampling locations meaning that preferential RWU only occur under or close to the rows due to a higher root activity. In Fig. 10.5d, we can observe that the RWU profiles observed during P_2 are more uniform than during P_1, with only a slight peak of RWU at 45 cm depth. As for P_1, the magnitude of the RWU is related to that of the climatic demand. Minimum RWU values are observed for P_{2a} (DOY 184-189, mean ETo=4.71 mm d^{-1}) and maximum RWU values for P_{2b} (DOY 189-197) and P_{2c} (DOY 197-203) with a mean ETo of 6.15 and 6.13 mm d^{-1} respectively. The small decrease of RWU at 45 cm depth could be explained by a water stress occurring at this depth during P_2.

For the third drying period (DOY 217-240), Fig. 10.4c shows that the RWU patterns are a little bit less organized than for P_1 and P_2 although having two characteristic features. Firstly, the RWU at the soil surface only occurs just below the maize row. Secondly, areas of high RWU in deeper depths coincide with areas of low RWU occurring during P_2 (compare Fig. 10.4b with 10.4c). These particular RWU patterns can be explained either by the growth of the maize root system allowing the extraction of the "less available" soil water located in the middle of the rows or by lateral water fluxes allowing the redistribution of the soil water and thereby the uptake of this water by roots located under the rows. The importance of this latter assumption could be tested by using a two-dimensional Soil-Plant-Atmosphere model such as HYDRUS-2D [*Simunek et al.*, 1998] although the root dynamics is not explicitly taken into account in this model. In Fig. 10.4c, we can also see that the RWU is maximum at the deepest investigated depth, i.e. at 65 cm. This observation allows us to suspect that RWU occurs at deeper depths than those investigated which is very likely to occur due to the dryness of the considered period (Ratio ETo/rainfall=5.42). Fig. 10.5e also illustrates the non uniform RWU lateral distribution at 55 and 65 cm depths. In Fig. 10.5f, we can see that the RWU is now very limited (X-scale is similar to that of Fig. 10.5b and d) and vertically uniform although the

Table 10.2. Coefficients of variation of ET calculated for the three long dry periods (a) and for 8 different selected dry sub-periods (b).

a

	P_1	P_2	P_3
CV (%)	12.29	12.76	11.95

b

	P_{1a}	P_{1b}	P_{1c}	P_{2a}	P_{2b}	P_{2c}	P_{3a}	P_{3b}
CV (%)	19.72	19.54	14.35	29.07	15.90	16.64	22.56	17.10

climatic demand is still high with daily ETo values of 5.19 mm and 4.97 mm for P_{3a} and P_{3b} respectively. For all the considered periods, maximum values of the mean RWU averaged for the 14 sampling locations are equal to 0.00785 d^{-1} and 0.004835 d^{-1} for the 25 and 55 cm depths respectively. These values are quite similar to those obtained by *Hupet et al.* [2002], i.e. 0.00875 d^{-1} and 0.0058 d^{-1} for 25 and 50 cm depths respectively. In terms of lateral variability, the RWU process can be considered as highly variable with CV ranging between 13.9 and 137% for the 8 different investigated periods. The effect of this laterally highly variable RWU process, strongly conditioned by the maize row layout, is very likely to influence the spatio-temporal dynamics of the soil water content at the maize row scale. Note, however, that the influence is reciprocal as there is a clear feedback between the soil water content and the laterally variable RWU. Such feedbacks were put forward by e.g. *Coelho and Or* [1999] for a drip irrigated maize crop.

The micro-variability of the evapotranspiration (i.e. the RWU integrated from the surface down to 65 cm depth) is analysed by estimating the evapotranspiration (ET) with Eq. (10.3) for each of the 14 sampling locations (hereafter called SL). This is performed for P_1, P_2 and P_3, and for the 8 different sub-periods previously considered. Fig. 10.6 illustrates the observed micro-variability of ET for P_1, P_2 and P_3 (Fig. 10.6a, b and c respectively), and the 8 sub-periods (Fig. 10.6 d, e, f, g, h, i, j, k). The corresponding coefficients are presented in Tables 2a and 2b. Fig. 10.6a shows that the micro-variability of ET calculated from DOY 161 to 178 presents a quite well defined cyclical behaviour. The maximum values of ET are systematically observed in the rows (SL n°1, 7 and 14). These results are not surprising as ET is calculated as the vertical integration of the RWU which also presents a cyclical behaviour (see Fig. 10.4a). We can observe in Fig. 10.6a that the minimum values of ET are observed on each side of the maize rows (i.e. SL n°5, 6, 8, 9, 12 and 13) with a small increase just in the middle of the interrows (i.e. SL n°3, 10 and 11). As explained previously for the RWU, such an increase is probably due to the soil evaporation component. Across the 14 sampling locations, ET values range between 42.94 and 60.07 mm with a mean value of 48.05 mm. For the second drying period (P_2, DOY 184-203), Fig. 10.6b shows that the ET lateral variability also presents a cyclical behaviour. A slight difference with P_1 is that the maximum ET values are no longer observed in the maize rows but just beside the rows (i.e. SL n°2, 3, 8 and 13). This small shift of the ET peaks can be explained by the RWU progressively moving laterally across the maize growing season due to the growth of the root system and to the decrease of the available soil water under the maize rows. During P_2, ET values range between 31.9 and 49.5 mm with a mean value of 41.05 mm. Note that the magnitude between the minimum and maximum ET values is very similar to that obtained for the first period, i.e. about 17 mm. Fig. 10.6c shows that the ET lateral variability observed during the third period (DOY 217-240) is much less organized and does no longer present the typical cyclical behaviour observed for P_1 and P_2. Yet, it is remarkable that the minimum ET values estimated during P_3 correspond to the maximum values observed during P2 and vice versa (see SL n°2-3 and 10-11). This observation can be explained by a high RWU during P_2 in some areas of the soil profile forcing the roots to extract soil water during P_3 from zones where it is still available. Note that as stated previously, it is very likely that the RWU occur deeper than 65 cm depth during P_3 which could clearly bias the patterns of ET estimated during P_3. In terms of absolute values, ET values quantified for P_3 range between 12.16 and 18.38 mm with a mean value of 16.06 mm. Bottom figures of Fig. 10.6 (c to k) illustrate the lateral variability of ET for the 8 sub-periods. These figures show that for shorter periods, the ET patterns are a little bit less well organized although maximum ET values are still observed in the rows (d, e, f and g).

In terms of ET spatial variability, Tables 2a and b summarize the coefficients of variation obtained (CV in %). For the three long drying periods (see Table 2a), CV are very uniform and quite small with values ranging between 11.95 and 12.76%. For the 8 shorter considered periods (see Table 2b), CV are larger and more variable with values ranging between 14.35 to 29.07%. Such an increase of the ET spatial variability with the decreasing time scale, a characteristic feature of hydrological processes, has previously been put forward by *Bertuzzi et al.* [1994] and *Hupet and Vanclooster* [2003, submitted]. In these two latter studies,

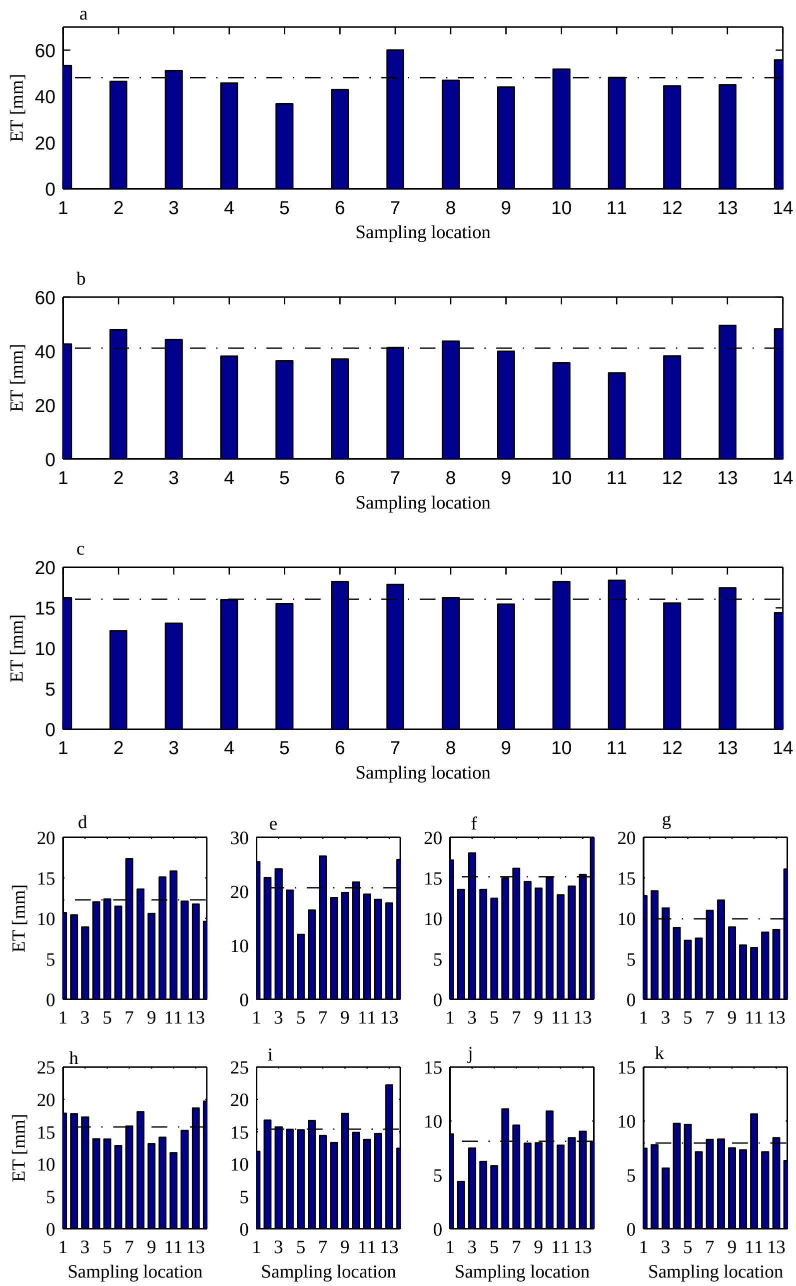

Figure 10.6. Spatial variability of ET estimated on each of the 14 sampling locations for P_1 (a), P_2 (b) and P_3 (c). Bottom graphs show the observed spatial variability of ET for the 8 considered sub-periods, i.e. for P_{1a} (d), P_{1b} (e), P_{1c} (f), P_{2a} (g), P_{2b} (h), P_{2c} (i), P_{3a} (j) and P_{3b} (k). The mean ET value is indicated in each graph with a dotted line.

the spatial variability of ET was yet investigated at the field scale and not at the maize row scale. It is worth noting that the lateral variability of ET across the rows ($11.95<CV<29.07\%$) is much smaller than the variability of RWU ($13.9<CV<137\%$) which is a direct consequence of the larger "measurement" support of ET compared to that of the RWU. The observed evolution of the variability of the hydrological processes occurring at the maize row scale is very illustrative of the dependence of the processes on the considered spatio-temporal scale, with the decrease of the variability for the increase of the time and measurement scales.

The spatio-temporal variability of the soil water content is illustrated in Fig. 10.7 for each depth separately. Fig. 10.7a displays the daily rainfall while Figs. 10.7b, c, d, e and f show the soil water content patterns measured at 25, 35, 45, 55 and 65 cm depth respectively. In these figures, we can see that the rainfall does not influence the soil water content dynamics. This is due to the limited rainfall amount, to the soil water content measurement instrument, and to the measurements performed from only 25 cm depth and further generally one or two days after the main rainfall events. It is obvious that measuring soil water content from 0 to 5 cm with kopecky rings or TDR just after a rainy event would allow the observation of the impact of the stemflow and the throughfall variability on the soil water content dynamics. This effect was observed e.g. by *van Wesenbeeck and Kachanoski* [1988] with TDR sensors vertically installed from 0 to 20 cm depth and by *Paltineanu and Starr* [2000] with capacitance sensors horizontally placed from 10 to 50 cm depth. Fig. 10.7b clearly shows the effect of the maize row layout on the temporal dynamics of the soil water content with the progressive appearance of a fingered pattern within the rows. It is remarkable that this fingered pattern can be observed at each investigated depth but with a time lag corresponding to the progressively deeper RWU. The observed "continuous" fingered patterns are also revealing of a certain time stability of the soil water content dynamics. In a more general way, our results suggest that the effect of the vegetation on the within-field variability of the soil water content can be twofold, i.e. local due to the layout of the vegetation (e.g. in rows such as presented in this study) and non-local due to the variable crop growth within fields [*Hupet and Vanclooster*, 2002].

Figure 10.8 presents two-dimensional maps of the soil water content measured within the maize rows at 10 different dates. In Fig. 10.8a and b (DOY 154-161), the soil water content patterns are not well organized and the impact of the maize row layout is not yet visible as maize is quite small at that time (i.e. early June). From Fig. 10.8c (DOY 171) to Fig. 10.8j (DOY 240), we can observe the appearance of well defined soil water content patterns due to the spatially variable RWU within

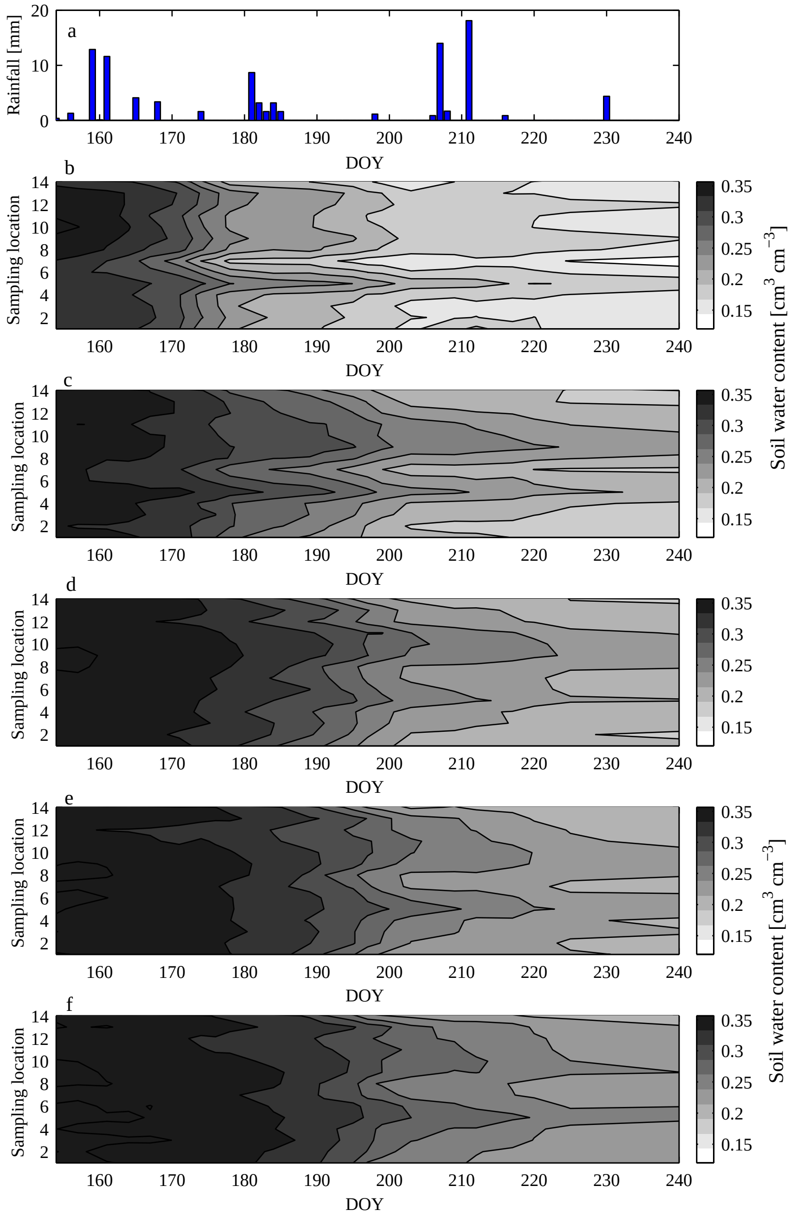

Figure 10.7. Spatio-temporal patterns of soil water content measured at 25 cm (b), 35 cm (c), 45 (d), 55 (e) and 65 cm depth (f). The soil water content scale is identical for all of these graphs. Fig. 10.7a shows the rainfall encountered during the considered period.

Table 10.3. Absolute maximum differences of soil water content (cm^3 cm^{-3}) observed within the maize rows for the whole considered period (DOY 154-240).

	Maize row 1	Maize row 2
25 cm	0.079	0.047
35 cm	0.060	0.062
45 cm	0.048	0.068
55 cm	0.052	0.054
65 cm	0.046	0.058

the maize rows. The variable RWU clearly drives the soil water content dynamics under the encountered dry climatic conditions. Note that the scale of soil water content is not similar across the subplots of Fig. 10.8. From Fig. 10.8g to 10.8i, it also appears that the soil water is not equally available across the maize interrow for a given depth (e.g. at 45 and 55 cm) due to the configuration of the maize root system. Indeed, at the end of the considered period, the soil water content in the middle of the rows is still higher than in the rows. These observations obviously raise numerous questions, such as "Where do we have to measure soil water content for irrigation scheduling of a row crop?, Is it really relevant to use the mean soil water content measured at a certain depth to activate the irrigation?", or in a modelling framework "How can we consider such a 2-D variability within 1-D agro-hydrological models?". All these questions undoubtedly need more in depth research.

Table 3 shows the absolute maximum differences of soil water content observed during the season within the maize rows. The differences are large and range between 0.046 and 0.079 cm^3 cm^{-3}. The maximum differences are observed close to the soil surface for the first row and a little bit deeper (35 and 45 cm depth) for the second row. These differences implicitly mean that the sampling of the soil water content at the maize row scale is not at all straightforward. Compared to our results, *Dekker and Ritsema* [1997] obtained much larger differences for the soil water content measured within three maize rows with values ranging between 0.1 and 0.3 cm^3 cm^{-3} for some days. Yet, the sampling was performed closer to the soil surface with 100 cm^3 soil cores and soil water repellency was an additional factor generating spatial variability. Before investigating the optimum sampling strategy for measuring soil water content and ET at the maize row-scale, we analyze the relationships existing between the mean soil water content and the standard deviation and the coefficient of variation. Indeed, a good knowledge of these relationships

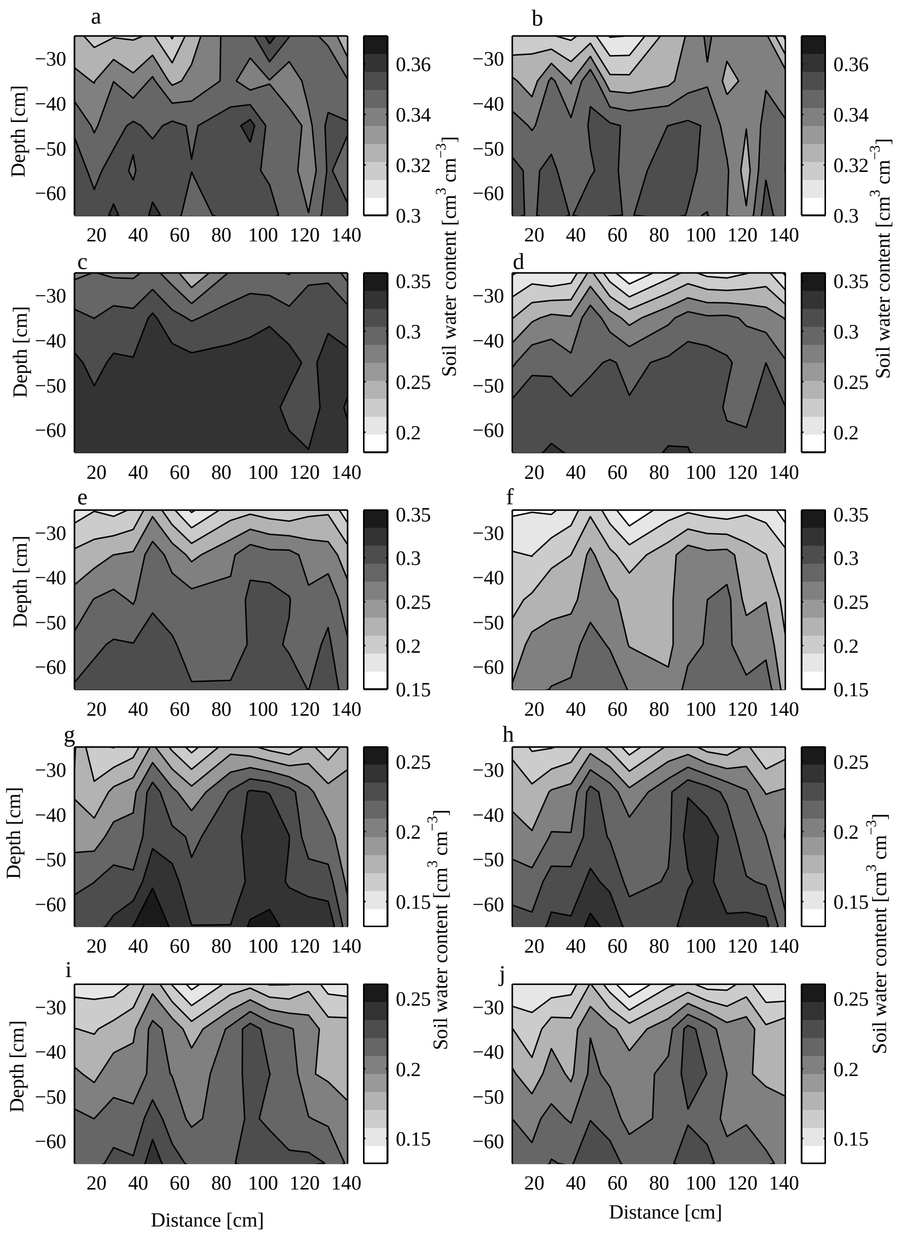

Figure 10.8. Two-dimensional maps of soil water content measured on DOY 154 (a), 161 (b), 171 (c), 184 (d), 191 (e), 199 (f), 212 (g), 217 (h), 225 (i), and 240 (j). The soil water content scale is different across these graphs.

is very important for optimising sampling [e.g. *Hupet and Vanclooster*, 2002]. The existence of any relationship is investigated considering all the 14 sampling locations together (i.e. the two considered rows simultaneously) and each row separately. Fig. 10.9a presents the relationship between the mean soil water content values and the corresponding standard deviations (circles represent the behaviour of the two rows and dots and crosses each one taken separately). The relationship presents some scattering although this one shows a characteristic trend where the spatial variability is minimal at low and high mean soil water content. This trend is well marked for the two rows treated together or separately. The obtained relationship exactly corresponds to the conceptual relationship presented by *Western et al.* [2003] and to the relationship found gathering soil water data from 13 study areas around the world [*Western et al.*, 2003]. It is worth noting that all these latter studies derived the relationship investigating spatial variability at a much larger scale, i.e. at the field or the catchment scale. The relationship obtained in our study at the maize row scale would tend to demonstrate that the conceptual relationship presented by *Western et al.* [2003] is scale independent. The magnitude of the spatial variability obtained in our study is yet much smaller with standard deviation of maximum 0.024, i.e. a variance of 5.76 $(\%v/v)^2$, compared to values of maximum 50 $(\%v/v)^2$ in the data set gathered by *Western et al.* [2003]. The magnitude of the spatial variability obviously depends on the considered scale and is intuitively assumed to be smaller at the maize row scale than at the field or at the catchment scale. *Hupet and Vanclooster* [2002] obtained for the same experimental field a negative correlation between the soil water content and the variability but the mean soil water content values were systematically larger than 0.215 cm^3 cm^{-3}. In this study, Fig. 10.9a shows that the spatial variability only decreases from soil water content values of about 0.25 cm^3 cm^{-3} meaning that a similar relationship would probably have been obtained by *Hupet and Vanclooster* [2002] if the whole range of soil water content would have been explored. *Van Weseenbeeck and Kachanoski* [1988] also obtained a negative correlation between soil water content and variance for the soil water content measured under a maize crop. Yet, in this latter study, the decrease of the variability beyond some "threshold" soil water content values was not observed. We can see in Fig. 10.9a that the relationship obtained between the mean and the standard deviation presents some scattering. Yet, if each depth is treated separately, the relationships become extremely well defined and very continuous. Figs. 10.9c to f illustrate few examples for the 45 (c-e) and the 65 cm depths (d-f) for the two rows together (c-d) and one of the two rows (e-f). Beyond the pure descriptive analysis of the

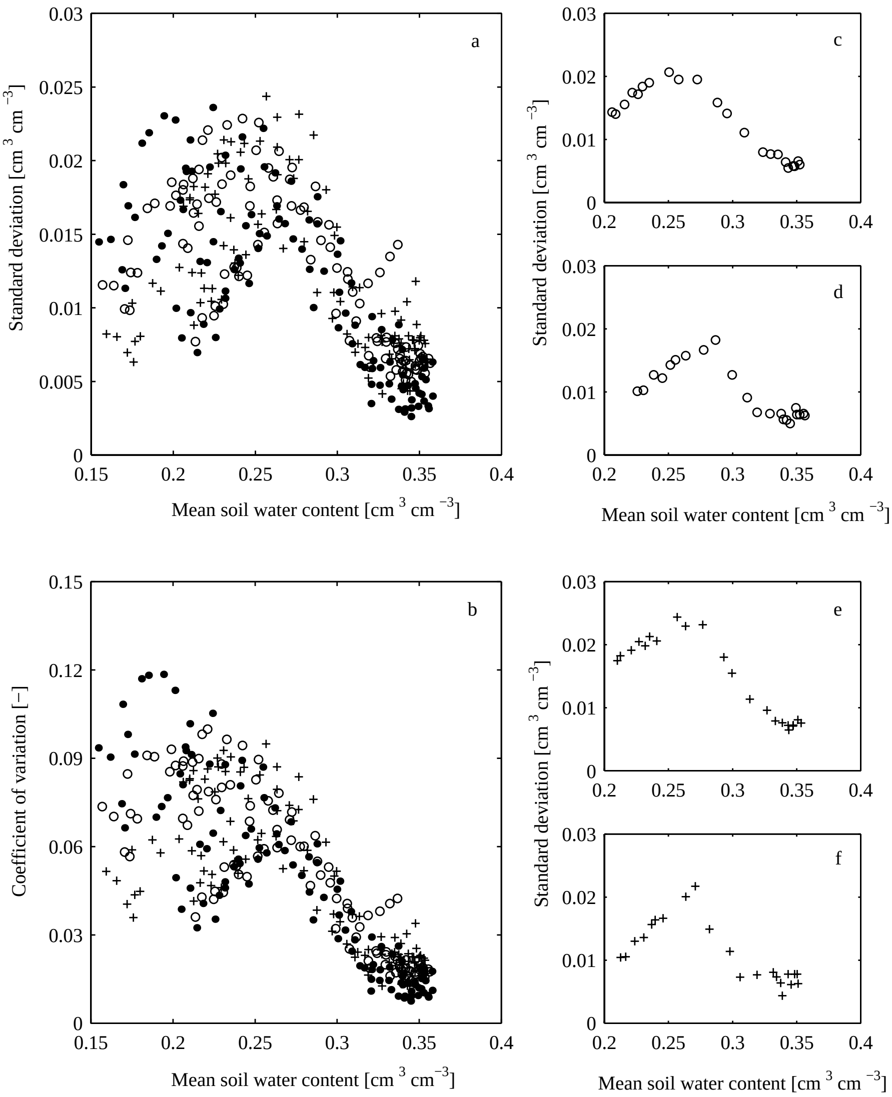

Figure 10.9. Relationship between mean soil water content and standard deviation (a) and coefficient of variation (b) for all depths confounded. Right graphs show the relationship obtained for 45 (c-e) and 65 (d-f) cm depth, considering the two rows together (c-d) or only one row (e-f).

Table 10.4. Mean values of the daily absolute difference between mean soil water content of the row and the soil water content measured on each sampling location, i.e. SL n°1 to 7 for row 1 and SL n°8 to 14 for row 2. Values are given for each investigated depth for the two considered rows and are expressed in $cm^3\ cm^{-3}$.

Maize row 1	SL 1	SL 2	SL 3	SL 4	SL 5	SL 6	SL 7
25 cm	0.0062	0.0058	0.0065	0.0028	0.0266	0.0044	0.0235
35 cm	0.0123	0.0123	0.0043	0.0015	0.0257	0.0099	0.0088
45 cm	0.011	0.0094	0.0026	0.0041	0.0105	0.009	0.0038
55 cm	0.0088	0.0047	0.0027	0.003	0.01	0.00577	0.0059
65 cm	0.0085	0.0068	0.0038	0.00255	0.011	0.0063	0.0065
Maize row 2	SL 8	SL 9	SL 10	SL 11	SL 12	SL 13	SL 14
25 cm	0.0036	0.0073	0.0042	0.0037	0.0073	0.0082	0.0179
35 cm	0.0033	0.0153	0.009	0.0088	0.0042	0.0124	0.0178
45 cm	0.0054	0.015	0.0138	0.009	0.011	0.006	0.0195
55 cm	0.008	0.0087	0.0083	0.0064	0.00755	0.0052	0.013
65 cm	0.0071	0.0086	0.0069	0.0064	0.0068	0.00625	0.0165

shape of the obtained relationship, it is certainly worth to examine the factors generating such a relationship for a given depth. For instance at 35 cm depth, the soil water content is quite homogenous at the start of the season (i.e. DOY 154, Fig. 10.8a). From DOY 184 to 212 (see Fig. 8d to 8g), the mean soil water content progressively decreases due to the RWU. During the same period, the soil water content variability markedly increases as the RWU occurs preferentially under the row compared to the middle of the interrow where RWU is negligible. After DOY 212 (see Figs. 10.8h, i and j), RWU moves laterally within the interrow to extract water from still wet areas. From that time, the soil water content variability starts to decrease while the mean soil water content continues to decrease due to the RWU. The example given for the 35 cm depth is also valid for other depths and put forward that the RWU combined in some way with the root growth dynamics allows explaining the typical relationship obtained between the standard deviation and the mean soil water content. Finally, Fig. 10.9b shows the relationship between the mean soil water content and the coefficients of variation. This relationship obviously presents a similar behavior to that obtained between the mean and the standard deviation. In absolute terms, CV values range between 1.05 and 12.1% which is clearly smaller than the variability obtained for RWU and ET.

The soil water content variability observed at the maize row scale means that obtaining a soil water content value representative of the mean row behaviour is not straightforward. Table 10.4 summarizes for each depth and for the two considered maize rows the mean values of the daily absolute difference between the mean soil water content of the maize row and the soil water content of each sampling location (from n°1 to 7 and from n°8 to 14 for row 1 and 2 respectively). For maize row 1, the minimum differences are found for the sampling locations n°3 and 4 situated just in the middle of the interrow. The other sampling locations also produce quite small differences except sampling locations n°5 and 7 for which the large differences are observed. Maize row 2 displays a dissimilar behaviour with minimum differences obtained for sampling locations n°8 (close to the maize row) and n°13. For this maize row, all sampling locations produce yet acceptable results except sampling location n°14. It is noteworthy that the two sampling locations closely situated to the maize crop (i.e. SL n°8 and 14 at about 9.5 cm of the maize stems) produce very different mean daily differences. From Table 10.4, it is therefore not straightforward to draw conclusions concerning the optimal sampling location of a soil water content sensor to estimate mean soil water content at the maize row scale. Indeed, for row 1 the optimum locations seem to be rather in the middle of the interrow while for row 2 there are no really optimal locations. Nevertheless, sampling location n°11 situated in the middle of the row gives quite satisfactory results though not the best.

In order to derive some general recommendations about the optimum location of soil water content sensor within a maize row, we investigate whether the central sampling locations are better than the extreme ones. Figure 10 shows the temporal evolution of the differences between the mean soil water content of the maize row and the soil water content of the individual sampling locations. Results are presented for row 1 (a-b) and row 2 (c-d) for the central sampling locations situated between the rows (i.e. n°4 and 11 for row 1 and 2 respectively) and for the extreme sampling locations situated close to the rows (i.e. n°1 and 7 and n°8 and 14 for row 1 and 2 respectively). We can observe in Fig. 10.10a and c that the central sampling locations produce very good estimates of the mean soil water content of the maize rows at 25 cm depth with errors ranging between -0.0069 and +0.0059 cm^3 cm^{-3} and -0.0082 and +0.01 cm^3 cm^{-3} for row 1 and 2 respectively. Similar good results are obtained for all the depths for SL n°4. For SL n°11 results obtained for other depths are generally similar, although less satisfactory at 35 and 45 cm depth with maximum errors up to 0.022 cm^3 cm^{-3}. On the other hand, results obtained for the extreme sampling locations are poorer. One of the two systematically produces quite good results (i.e. SL n°1

Table 10.5. Errors between mean ET estimated at the maize row scale and ET estimated for each sampling location (n°1 to 14) for P_1, P_2 and P_3 and for the three together. All the values are expressed in mm. Negative values correspond to an underestimation of ET while positive values to an overestimation. Best estimators are indicated in bold.

maize row 1	SL 1	SL 2	SL 3	SL 4	SL 5	SL 6	SL 7
P_1	5.26	-1.61	3.05	-2.03	-11.23	-5.14	11.97
P_2	1.49	6.84	3.16	-2.99	-4.66	-4.02	0.17
P_3	0.65	-3.42	-2.5	0.41	-0.07	2.65	2.28
$P_1+P_2+P_3$	7.41	**1.8**	**3.71**	**-4.87**	-15.97	-6.51	14.43
Maize row 2	SL 8	SL 9	SL 10	SL 11	SL 12	SL 13	SL 14
P_1	-1.12	-3.98	3.78	0.13	-3.5	-3.03	7.72
P_2	2.64	-1.11	-5.29	-9.09	-2.82	8.49	7.19
P_3	-0.28	-1.08	1.7	1.84	-0.96	0.93	-2.14
$P_1+P_2+P_3$	**1.23**	-6.17	**0.19**	-7.12	-7.29	6.93	12.77

and 8) while the other ones (n°7 and 14) give larger errors up to 0.042 $cm^3\ cm^{-3}$. The results of this study tend to demonstrate that the sampling of the soil water content at the maize row scale seems to be more appropriate in the middle of the interrow (though SL n°5 produces poor results) than just in the rows. However, it is worth reminding that these results are obtained for very specific climatic conditions (i.e. extremely dry). Other results could be obtained in different climatic conditions (e.g. more humid where infiltration of both stemflow and throughfall could be the dominant hydrological process). Furthermore, it is very likely that the results obtained are dependent on the soil water content measurement technique used and on the fact that soil water content was not measured close to the soil surface. The impact of the variability of the hydrological processes on the estimation of ET with a soil water balance at the maize row scale is presented in Table 10.5. This table shows the differences (expressed in mm) between ET measured on each sampling location and the mean ET value of the maize row. Results are presented for the three dry periods (P_1, P_2 and P_3), for the whole season and for the two maize rows considered separately. During P_1, the use of an access tube closely located to the maize rows tends to overestimate ET (e.g. n°1, 7 and 14) while the use of a central one tends to underestimate ET (n°4, 5 and 12). This is obviously a consequence of the RWU patterns presented in Fig. 10.5a. During P_2, sampling locations where the overestimation occurs slightly shift towards the middle of the

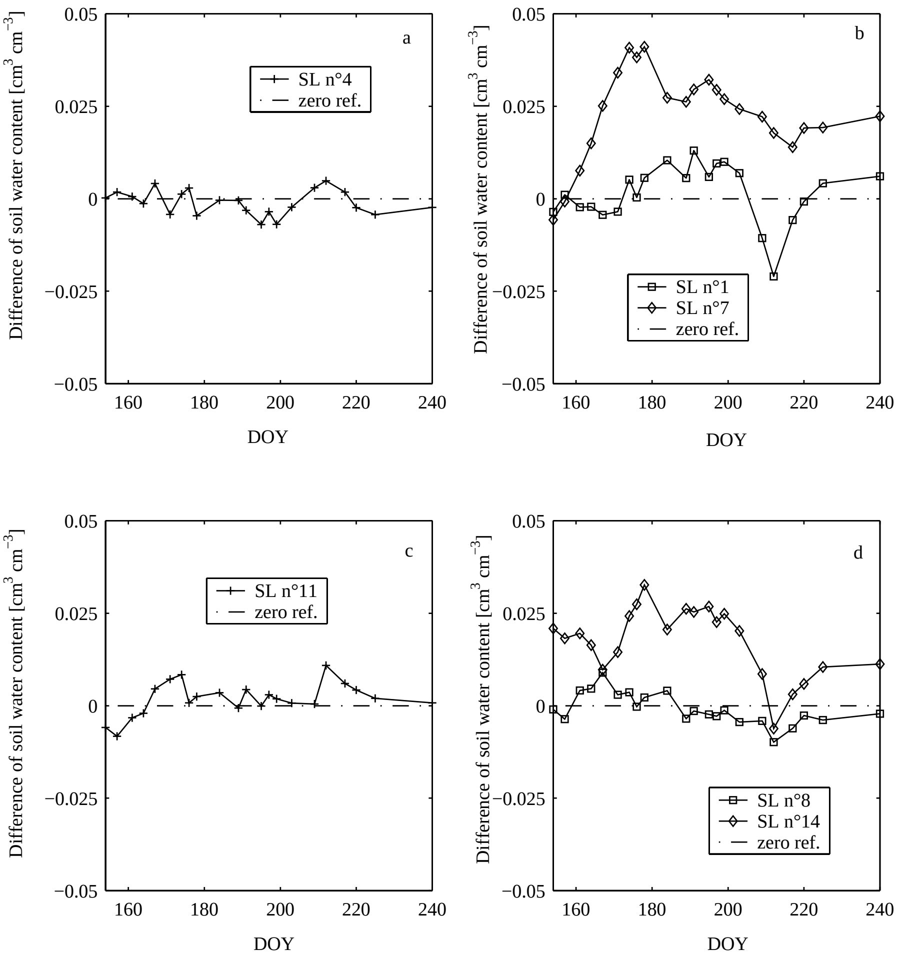

Figure 10.10. Temporal evolution of the deviation between the mean soil water content estimated at the maize row scale and the soil water content estimated on each sampling location (SL). Results obtained for the "central" SL of row 1 and 2 (i.e. n°4 and 11) and for the "extreme" SL of row 1 and 2 (n°1, 7, 8 and 14) are presented in Fig. 10.10a and c, and b and d respectively.

interrow (e.g. SL n°2 and 13), which is a consequence of the shifting RWU. This also clearly illustrated in Fig. 10.6b. During P_3, there is no specific trend in the errors obtained in ET due to the sampling location. The errors in ET tend to progressively decrease with maximum values of 11.97, 9.09 and 3.42 mm for P_1, P_2 and P_3 respectively. Concerning the errors in ET estimated for the whole period, these ones are limited (i.e. <8mm in absolute values) except for few specific sampling locations (n°5, 7, and 14).

Concerning the optimum sampling location of an access tube to estimate ET at the maize row scale, there is no miracle solution as the optimum location progressively shifts across the interrow during the season. Yet, as stated for the estimation of the soil water content, the use of measurements performed very close to the row does not seem very judicious. On the contrary, using one access tube situated in the middle of the interrow seems more attractive in the vast majority of the cases (except in fact SL n°5). The results obtained in Table 10.5 confirm that the study of *Hupet and Vanclooster* [2003, submitted] is not biased or at least to a very limited extent. Indeed, *Hupet and Vanclooster* [2003, submitted] estimate ET on 28 different locations with only one access tube located just in the middle of the interrow on each location, which can obviously be criticised. From Table 10.5, we can see that the generated errors using the central sampling locations (i.e. SL n°4 or n°11) are smaller than 9.09 mm (in absolute values) for all the considered periods confounded. Finally, it is worth noting that errors obtained both for soil water content and ET at the maize row scale were analysed in this study taking systematically each sampling location separately. Better results should be obtained considering some specific combinations of sampling locations, e.g. one located in the middle of the interrow and the other close to the row. That could lead to decrease the errors as the overestimations observed during certain periods on some sampling locations could be compensated by underestimations on other ones and vice versa.

10.4 Conclusions

In this chapter, we investigate the micro-variability of the hydrological processes at the maize row scale during a long dry and hot period focusing on the rainfall redistribution under the maize canopy, on the root water uptake (RWU) and on the evapotranspiration (ET). Then, we study the impact of the variability of these processes on the spatio-temporal dynamics of the soil water content and on the sampling strategies to adopt to estimate the soil water content and the evapotranspiration at the maize row scale.

Concerning the micro-variability of the rainfall distribution under the maize canopy, we show for 7 different rainy events that the measured throughfall represents maximum 33.86% of the incident rainfall. On the other hand, the estimated stemflow is larger and represents up to 65.98% of the incident rainfall. The micro-variability of the rainfall reaching the ground is huge as some locations under the maize canopy receive up to 3.52 more water than the incident rainfall, and up to 4.47 more if stemflow is taken into account. In terms of coefficients of variation, values range between 77.87 and 188.7% for the case where both stemflow and throughfall are considered.

Concerning the root water uptake (RWU), we observe a high micro-variability within the maize rows with CV values ranging between 13.9 and 137% for all the considered periods. During the first long dry period (June), the RWU is mainly located in the first 45 cm of the soil profile and is clearly maximum in the maize rows. During the second dry period (July), the RWU occurs mainly between 45 and 65 cm depth with the maximum extraction under or close to the rows generating a very cyclical RWU patterns. For the first and the second periods, the magnitude of the RWU at a certain depth clearly depends on the climatic demand. For the third period (August), the RWU preferentially occurs in areas located in the middle of the rows where soil water is still available.

Compared to RWU, the micro-variability of evapotranspiration (ET) across the maize rows is less variable with CV values ranging between 11.95 and 29.07%. We observe that during the first period the patterns of ET measured across the maize rows presents a quite well defined cyclical behaviour, with maximum ET values observed in the rows. During the second period, ET patterns still present the cyclical behaviour but with a slight shift of the ET peaks. For the third period, the ET patterns are not well organized but the minimum ET values correspond to the maximum values observed during the second period and vice versa.

Concerning the spatio-temporal dynamics of the soil water content, this one is clearly influenced by the maize row layout, with the progressive appearance of a fingered pattern within the rows due to the spatially variable RWU. The temporal dynamics of this latter allows us to explain the relationship found between the mean soil water content and the standard deviation. The variability is minimal at high soil water content, then increases progressively with the decreasing soil water content, and finally decreases beyond some "threshold" soil water content value (about 0.25 cm^3 cm^{-3}). The maximum difference of soil water content measured within a maize row is important and range between 0.046 and 0.079 cm^3 cm^{-3}. In absolute terms, coefficients of variation for soil water content range between 1.05 and 12.1%.

Finally, we investigate the impact of the spatio-temporal variability of the hydrological processes on the sampling strategies to adopt for the soil water content and ET estimates at the maize row scale. For the soil water content, the placement of the soil water content sensor in the middle of the row seems more judicious than in the row. Using such "central" sampling locations leads to estimate the mean row scale soil water content with a maximum error of 0.022 cm^3 cm^{-3}. For the ET estimates, the use of the central sampling locations seems also to provide satisfactory results allowing the estimation of the ET at the maize row scale with a maximum error of 0.47 mm d^{-1} for all the considered periods confounded. In a more general way, our study suggests that the above-mentionned twofold effect of the vegetation conditions the sampling strategies to adopt for the estimation of soil water content, root water uptake and evapotranspiration at the field scale. Within this context, a two-stage upscaling procedure seems appropriate with in a first stage the scaling of punctual measurements to the maize row scale, and then in a second stage the scaling of these values to the field scale.

We conclude by giving some recommendations for future research in the framework of the study of the variability of the hydrological processes for row crops. Firstly, it must be noted that the results obtained in this study depend on the climatic conditions encountered and on the soil water measurement instrument used. We recommend therefore investigating the spatio-temporal variability of the processes in other climates with other measurement techniques such as horizontally installed TDR probes. Such a configuration should allow investigating more thoroughly the temporal dynamics of some processes such as the infiltration and the redistribution of stemflow and throughfall. Secondly, we stress on the importance of conducting studies that simultaneously consider the different components of the system in order to improve the understanding of the physical processes generating the soil water content variability at the row scale. Finally, within a modelling framework, future investigations should tackle specific issues related to the typical bi-dimensionality observed in row crops, such as e.g.: "Is it feasible to model a 2-D Soil-Plant system with a 1-D agro-hydrological model? How can effective parameters (e.g. RWU parameters) and effective inputs (e.g. rainfall reaching the ground) at the row scale be defined for 1-D agro-hydrological models? Is it possible to disaggregate results obtained with a 1-D model (e.g. soil water content) to produce 2-D spatial variability?".

Chapter 11

Summary, conclusions and perspectives

The accurate estimation of field-scale evapotranspiration (ET) and the quantification of the associated uncertainties still remain a very tricky task. Within a hydrological and agronomical framework, two different approaches can be used to obtain field scale ET estimates, i.e. the agro-hydrological modelling and the soil water balance approach. In case of agro-hydrological modelling, field-scale ET estimations are not straightforward and generally uncertain as (i) driving forces are prone to errors, (ii) time series of observed data (e.g. soil water content) used for the calibration process may be not representative of the mean field behaviour, and (iii) some model parameters are very difficult to estimate at the field scale and further generally highly spatially variable. For the soil water balance approach, field-scale ET estimations are not straightforward and generally uncertain as (i) local ET measurements are prone to errors due e.g. to uncertainties in soil water content measurements and in estimated bottom soil water fluxes, and (ii) within-field variability of ET is likely to be high and its complete capture is difficult to achieve. The research developed within this thesis has to be situated within this context. The topic of this work was formulated under the form of the following basic question "Which strategies may be adopted to obtain accurate estimates of the field scale ET and how can we quantify associated uncertainties with these estimates?" To tackle this very broad question, different specific issues have been identified and thoroughly investigated through Chapter 3 to 10 (see Fig. 1.1). We present hereafter the main research results for the agro-hydrological modelling and the soil water balance approach. Then, all the results are summarized in general conclusions. Finally, we present some perspectives of future research.

11.1 Summary of the results

11.1.1 Agro-hydrological modelling

Uncertainties in driving forces

In this study, we have investigated uncertainty associated to driving forces, and more specifically to the reference evapotranspiration (ETo), caused by the temporal sampling frequency of climatic variables (see Chapter 3). The results show that the solar radiation and the wind speed are the most sensitive variables to bias induced by inadequate temporal sampling frequency. Daily errors of 5.1 MJ m^{-2} d^{-1} or 41.05% for the solar radiation, and 0.45 m s^{-1} or 18% for the wind speed may be obtained if these variables are hourly sampled. The sensitivity analysis illustrates further that ETo estimates are particularly sensitive to the maximum and the dry temperature. By combining the sensitivity analysis with the errors due to inappropriate temporal sampling, solar radiation and maximum temperature are identified as the two climatic variables that have the most pronounced influence on the estimation of the daily ETo. A non-intensive hourly temporal sampling schedule of all meteorological variables may induce errors on daily ETo as high as -0.76 mm d^{-1} or 27%. Fortunately, the errors generated on the estimation of the long term integrated ETo are clearly lower (3.8%).

Field and maize row scale estimation of soil water content

The accurate estimation of soil water content is of primary importance as it is generally the only "easily" measurable state variable that can be used to calibrate agro-hydrological models. In this study, we have investigated issues related to the soil water content estimates at two different scales, i.e. the field (see Chapter 4) and the maize row (see Chapter 10). At the field scale, results of our study firstly show that the vegetation growth, and subsequently the evapotranspiration and the root water uptake play a non-negligible role in the temporal dynamics of the observed soil water content patterns. Considering that the spatial variability is due to the root water uptake variability, variable vegetation growth could explain spatial variance of 6.2 to 6.7 (%vol/vol)^2 for the superficial layers. In absolute terms, coefficients of variation of soil water content range between 3.8 and 15%. Secondly, we show for the adopted sampling scheme and for the superficial layers that the observed spatial structure was non-existent. Thirdly, we put forward that a negative correlation exists between the spatial variability and the mean soil water content. Finally, we show that to estimate the mean field soil water content with an absolute error of 2.5% (v/v) for a probability level of 95%, the number of samples varies between 1 and 12 according to the depth and the time. For an error of 1.5%, the number of samples increases to a maximum of 33. At the maize row scale, we firstly show that the spatio-temporal dynamics of the soil water content is strongly influenced by the maize row layout, with the progressive appearance of a fingered pattern within the rows due to the vertically and laterally variable root water uptake. The maximum difference of soil water content measured within a maize row is important and range between 0.046 and 0.079 $cm^3\ cm^{-3}$. In absolute terms, coefficients of variation for soil water content range between 1.05 and 12.1%. Secondly, we put forward that the temporal dynamics of the root water uptake allows us to explain the relationship between the mean soil water content and the variability. This one is minimum at high soil water content, then increases progressively with the decreasing soil water content, and finally decreases beyond some "threshold" soil water content value (about 0.25 $cm^3\ cm^{-3}$). Finally, we show for the estimation of the soil water content at the maize row scale that it seems more adapted to place the soil water content sensor in the middle of the row than in the row. The use of such central locations leads to estimate the mean row scale soil water content with a maximum error of 0.022 $cm^3\ cm^{-3}$.

Impact of the spatial variability of the soil hydraulic parameters

Spatial variability of soil hydraulic properties is likely to impact field-scale estimations of transpiration and crop yield as soil hydraulic properties are key parameters governing the soil water movement. In this study we have studied this impact performing a thorough sensitivity analysis, and combining measurements of soil hydraulic properties with numerical agro-hydrological simulations for three contrasted climatic scenarios (see Chapter 5). The results firstly show that the sensitivity of transpiration and crop yield differs according to the hydraulic parameters (sensitivity is maximum to θ_s and n) and is more pronounced for drier climatic conditions. Second, the numerical simulations with the soil independent stress factors demonstrate that the impact of the within-field variability of the soil hydraulic properties on the simulated transpiration and crop yield can be very large. The generated spatial variability increases systematically with the dryness of the climate, with coefficients of variation increasing from 7 to 14.6% and from 6.7 to 16% for the actual transpiration and the crop yield respectively. In a subsequent analysis, all agro-hydrological simulations are rerun considering that the water stress parameters are spatially variable and soil dependent. The results obtained with the adjusted water stress parameters are quite different though the generated spatial variability still increases for drier conditions. The different results obtained show that the use of an agro-hydrological simulation model in a stochastic mode for a vegetated surface requires an accurate estimation of the water stress parameters which should further be considered as soil dependent. Finally, we show that the simultaneous estimation of the water stress and the soil hydraulic parameters can not be robustly performed using measurements of transpiration and dry matter yield alone. Alternative strategies for the specification of reliable water stress parameters are therefore needed.

Field and maize row scale estimation of root water uptake parameters

The specification of root water uptake parameters (RWUP) constitutes an unavoidable stage before we can apply an agro-hydrological model to estimate evapotranspiration. In this study, two different approaches have been tested and used to estimate RWUP. The first one uses a simplified water balance (see Chapter 6 and 10) while the second uses an inverse modelling procedure (see Chapter 6 and 7). Results obtained using the simplified water balance show that the root water uptake measured within the field is quite variable. Coefficients of variation range from 22 to 34% for the two considered macroscopic RWUP A and B respectively. Next, numerical experiments show that the use of this approach during a dry period gives quite good estimates of the A and B parameters. Though very simple, this approach is robust. In a subsequent analysis, we investigate the micro-variability of the RWU within the maize rows using the simplified water balance. The results show that the RWU is very laterally and vertically variable with coefficients of variation ranging between 13.9 and 137%. Measured RWU patterns tend to support the RWU model by *Feddes et al.* [1978] as RWU at a certain depth is variable according to the climatic demand. We also show that the temporal dynamics of RWU is much more complex than is assumed in 1-D model considering "non-dynamic" RWU. Finally, the results put forward that the accurate estimation of RWU at the maize row scale is not straightforward and that the set-up of the soil water content sensors within the rows is likely to strongly influence the RWU estimates. The feasibility of using an inverse procedure to derive RWUP is tested numerically. Using the RWU model by *Hoogland et al.* [1981], we show for differently textured soils that the soil water content dynamics is quite insensitive to RWUP, at least compared to soil hydraulic parameters. Then, we show by visual inspection of 2-D response surfaces that the RWUP are very unstable with respect to small uncertainties on the soil hydraulic parameters. Finally, we show by visual inspection of scatter plots that non-unique parameter sets may be expected if RWUP are simultaneously optimized with soil hydraulic parameters. The results obtained in this part of the study, though not derived from full model inversions, tend to emphasize that a robust estimation of RWUP during a dry period is unlikely to be achieved by means of a full soil water balance inversion. In a subsequent analysis, we test for three differently textured soils the feasibility of the estimation of RWUP using the RWU model by *Feddes et al.* [1978]. This one shows that the soil water content dynamics is relatively insensitive to RWUP and that the sensitivity depends on the texture of the considered soil. For the medium-fine textured soil, the sensitivity is particularly low due to a "compensating effect", i.e., vertical unsaturated water flows overshadowing in some way the RWU. In a second step, we analyze the well-posedness of the solution when only RWUP are optimized. For this case, the inverse problem is clearly ill-posed except for the estimation of the rooting depth parameter for the coarse and the very-fine textured soils. In a third step, we address the case where RWUP are estimated simultaneously with additional parameters of the system. For this case, our study show that the inverse problem is well-posed for the coarse and the very-fine textured soils allowing the estimation of both RWUP of interest at the condition that a powerful global optimization algorithm is used. In opposite, the estimation of RWUP is unfeasible for the medium-fine textured soil. These results show that the inverse modeling approach can be applied to derive RWUP for some soils (coarse and very-fine textured) and that the feasibility is strongly improved if the RWUP are simultaneously optimized with additional parameters.

11.1.2 Soil water balance

Uncertainty in a local scale evapotranspiration estimate

The measurement support of a soil water balance based ET estimate is very limited, i.e. at most few dm^2. A good knowledge of the uncertainties in a local ET estimate is needed to quantify the within-field variability of ET and to scale the local measurements to the field scale. In this study, the quantification of the uncertainties was performed using an error propagation analysis and two different methods to estimate bottom soil water fluxes. For estimated ET with in-situ estimated hydraulic conductivity curve (HCC) results show that the uncertainty range in terms of standard deviation between 3.82 and 5.97 mm and between 2.6

and 2.8 mm if errors due to the integration method are considered as negligible. A better precision is probably very difficult to obtain as all sensitive factors contributing to the ET variance have been determined in a consistent and optimal way. Results of this study also show that the uncertainties in estimated HCC with pedotransfer functions (PTF's) may results in large uncertainties in estimated ET, questioning thereby the use of PTF's in characterising the field water balance.

Field and maize row scale estimation of evapotranspiration

In this study, we have investigated the spatio-temporal variability of evapotranspiration (ET) at two different scales, i.e. the field (see Chapter 9) and the maize row (see Chapter 10) and the sampling strategies to adopt to obtain accurate field ET estimates. At the field scale, our results firstly show that the "within-field" variability of the local scale instantaneous measured ET is large with coefficients of variation ranging between 15.5 and 46.3%. The corresponding cumulated ET for the two considered periods ranges between 39.4-107.5 mm and 30.3-55.7 mm. We show that this variability of ET fluxes can be related in some way to the measured spatially variable crop growth ($2.2 < \text{Leaf Area Index} < 4.6$). This one has directly an impact on the ratio between measured actual ET and ETo which generally is smaller than 1 in our field. The first sampling strategy which consists in increasing the number of sampling locations shows that, for a probability level of 95%, the number of samples needed to estimate the field mean cumulated ET flux with a relative precision of 5, 10 and 20% ranges between 40 and 360, 10 and 90, and 2 and 22 respectively. The second sampling strategy which exploits the concept of temporal stability show that the field averaged ET can be estimated with a relative precision of 10% if only one representative location is selected a-priori. The third sampling strategy consists in using a covariant such as the LAI or the dry matter yield. For this case, cumulated ET equals 119 mm $\pm$ 6.1 mm and 118.5 mm $\pm$ 4.5mm by means of the relationships existing between cumulated ET and LAI and yields respectively. In a subsequent analysis, we study the spatio-temporal dynamics of ET at the maize row scale. Coefficients of variation of ET estimated at this scale range between 11.95 and 29.07%. The results show that the patterns of ET estimated across the rows are time dependent. During the first considered dry period, the patterns of ET present a quite well defined cyclical behaviour, with maximum ET values observed in the rows. During the second dry period, the ET patterns still present the cyclical behaviour but with a slight shift of the ET peaks. For the third dry period, the ET patterns are not well organized but the minimum ET values correspond to the maximum values observed during the second period and vice versa. With regard to the sampling strategy to adopt for estimating ET at the maize row scale, the use of a central location i.e. in the middle of the row seems to provide satisfactory results with errors smaller than 0.47 mm d^{-1} in absolute values for all the periods confounded.

11.2 General conclusions

The results of this work clearly put forward that the use of an agro-hydrological model to obtain accurate field scale ET estimates, and more generally the different components of the water balance, remains very difficult. Indeed, we firstly show that characterization of the driving forces may be uncertain if a poor sampling frequency is adopted. The uncertainties are not negligible as the ET estimates are particularly sensitive to the driving forces. Second, we show that the accurate estimation of the time series of the soil water content (generally used to calibrate the model) is very tricky to achieve at the field scale. As a matter of fact, soil water content is highly variable both in time and space. For soil water content, our study clearly puts forward that two different scales have to be considered for a maize cropped field: the maize row and the field. At the maize row scale, variability of the soil water content (max. CV=12%) is due to the laterally variable RWU and the rainfall redistribution. At the field scale, we show that the crop size, and subsequently ET and RWU play a non-negligible role in the spatio-temporal dynamics of soil water content (max. CV=15%). This study shows therefore for a small maize cropped field that the effect of the vegetation on the soil water content dynamics can be twofold, i.e. local and non-local. This twofold effect obviously conditions the sampling strategies to adopt for the estimation of soil water content at the field scale. Within this context, a two-stage up scaling procedure seems appropriate with in a first stage the scaling of punctual soil water content measurements to the maize row scale, and then in a second stage the scaling of these values to the field scale. Note that the field scale soil water content variability is quite similar to the variability observed at the maize row scale. Although the results obtained at the field scale may be biased due to the sampling location of the soil water content sensors, one may suspect that the two types of the observed soil water content variability are different. In that case, the field scale variability of the soil water content is likely to be larger than that observed. Third, we show that the impact of the within-field variability of the soil hydraulic properties on the transpiration and the crop yield can be very large and is further dependent on the dryness of the climate. The incomplete capture of the within-field variability of the soil hydraulic properties is therefore likely to bias the field-scale ET estimates. The results also point out that the impact of the variability on the simulated transpiration and crop yield is strongly dependent on the selected water stress parameterization. The proposed alternative procedure to adjust the water stress parameters according to the spatially variable soil properties seems attractive. Indeed, the simultaneous estimation of the water stress and the soil hydraulic parameters can not be robustly performed using measurements of transpiration and dry matter yield alone. These latter results obviously constitute a serious limitation for the large-scale estimation of effective soil hydraulic parameters inverting ET fluxes remote sensed over vegetated surfaces. Four, we show that the estimation of the RWUP at the field-scale is not straightforward. Indeed, RWUP can be estimated locally using a simplified water balance but the observed spatial variability of the RWUP is very large, both at the field and at the maize row scale with coefficients of variation of maximum 34 and 137% respectively. The estimated RWU show further a pronounced temporal dynamic behaviour, much more complex than is assumed in 1-D models considering "non-dynamic" RWU. The study also point out that an inverse procedure can be used to estimate RWUP provided that a powerful global optimization algorithm is used, that the soil under consideration is not too hydraulically conductive, and that the fixed soil hydraulic parameters are not too biased.

The results of this study also elucidate that the estimation of ET at the field-scale by means of a soil water balance approach remains very tricky and quite uncertain. Indeed, we show that the accuracy in a local ET estimate can be poor in some circumstances (e.g. if PTF's are used to estimate bottom fluxes) and that a precision better than 2.6-2.8 mm (in terms of standard deviation) is very difficult to obtain. Then, the results of our study show that the upscaling of the punctual ET values to the field-scale is difficult to achieve due to the high spatial variability of ET. Our study show that the spatial variability of ET, as that of soil water content and of RWU, can be encountered both at the field and at the maize row scale with coefficients of variation of maximum 46.3% and 29.07% respectively. At the maize row scale, the spatial variability of ET is due to the laterally variable RWU and presents in some cases a typical cyclical pattern. We show that the set-up of the measurement instrument within the rows is very important to obtain accurate maize row scale estimates of ET. At the field scale, we show that the spatial variability of ET can be related to the measured spatially variable crop growth. The estimated ratios between actual ET and ETo, generally smaller than 1, strongly questions the use of crop coefficients derived from standard conditions to predict the field behaviour. To capture the within-field variability of ET, we show that both the use of temporally stable locations and the use of a covariant (e.g. LAI) are attractive strategies. In a more general way, the results of our study suggest that the estimation of field scale ET for a row crop by means of the soil water balance must be performed in two stages. In first stage, ET must be estimated at the maize row scale to capture the RWU laterally variable within the rows. In a second stage, these values have to be up scaled to the field using one of the proposed strategies.

11.3 Perspectives of future research

At the end of this work, different issues related to the basic question defined in Chapter 1 still remain unsolved. Furthermore, numerous additional questions have been raised through this thesis. We summarize hereafter the main research topics which should be tackled in the near future in order to improve the field scale modelling of water fluxes, and in particular the estimation of evapotranspiration.

Impact of the vegetation on the soil water content

Our study put forward that the vegetation can have a twofold effect, i.e. local and non-local, on the spatio-temporal dynamics of the soil water content at the field scale. More research is yet needed to understand more thoroughly these effects both at the row scale and at the field scale. At the row scale, we suggest using small permanently installed TDR probes to progress in the understanding of the laterally variable hydrological processes. To quantify the rainfall redistribution under the canopy and to investigate whether some lateral water fluxes occur at the soil surface we recommend sampling soil water content with a high spatio-temporal frequency. Although micro-variability of soil water content is most likely to occur within row crops, we recommend studying the magnitude of this one for other crops. This is particularly important as the micro-variability makes much more complex the field scale estimation of near-surface soil water content. As the accurate estimation of this one is a primary importance, e.g. in case of ground truthing for remote sensing applications, the selection of some specific crops could probably improve the accuracy of the field scale soil water content estimates. At the field scale, we suggest investigating more in detail the effect of the spatially variable vegetation growth on the soil water content patterns. In this context, we recommend selecting a crop for which micro-variability effects of the crop on the soil water content are implicitly assumed to be minimum (e.g. wheat). We should stress that the study of the effects of the vegetation on the soil water content is of primary importance as the soil water content patterns are likely to strongly influence some hydrological processes such as the runoff production. Furthermore, highlighting the effects of the vegetation on the soil water content patterns could also allow explaining the poor performances of terrain indices [see *Western et al.*, 1999a].

Modelling of water fluxes within a row crop

Our study shows that the hydrological processes, i.e. mainly the root water uptake and the rainfall redistribution, are highly laterally variable within the rows of a maize crop. These results may question therefore strongly the use of a one-dimensional soil-plant-atmosphere model for such a complex system. In this framework, two different issues need more in depth research. With regard to the modelling of water fluxes with a 1-D model, the issue is clearly to derive effective parameters for the maize row, as far as these ones exist. This could be tested numerically using an appropriate 2-D model. In any case, the estimation of effective soil and plant parameters must be performed by fitting time series of a measured state variable, e.g. the soil water content, representing at best the mean maize row behaviour. Note that if one is only interested in the modelling of ET, it is likely that the use of a 1-D model may suffice. Yet, the correct modelling of all the components of the system, and more particularly the runoff, with a 1-D model is probably much trickier due to the high spatial variability of both near-surface soil water content and rainfall reaching the ground. For the modelling of water fluxes within a maize crop by means of a 2-D model, other issues must be considered. Calibration issues may arise as the parameters estimation must be performed using time series of two-dimensional maps of measured state variables, which obviously requires a heavy experimental set-up only conceivable within a research context. Issues related to the parameter estimation process itself (e.g. non-uniqueness) are also likely to occur as the number of parameters strongly increases in a 2-D model compare with a 1-D model. Finally, the use of a 2-D model requires the specification of two-dimensional boundary conditions such as e.g. the rainfall reaching the ground under the canopy which is far from being easy if that is not measured. All these topics clearly need more research, both from an experimental point of view to improve the characterization of the variability, and from a modelling point of view to investigate the derivation of effective parameters or to test the robustness of parameter estimation techniques.

Specification of crop parameters in agro-hydrological models

The results of our study show that vegetation exhibits much more complexity than is generally assumed in agro-hydrological models. As a matter of fact, the crop growth is spatially variable within the field due to many factors. Such a variable crop growth can unfortunately not be simulated with agro-hydrological models although it is very likely to impact the crop parameters, i.e. the Leaf Area Index (LAI) and the crop coefficient. We recommend therefore investigating and developing specific procedures to adjust the "reference" crop coefficients derived from standard conditions to field conditions for which crop growth is systematically more limited. This is of primary importance as ET estimates are particularly sensitive to the crop coefficient parameterization. Within this context, the use of remote sensing could be very valuable to derive spatially variable inputs (e.g. LAI) which could then be used to adjust the crop coefficients. Alternatively, the use of more physical concepts of the ET process within agro-hydrological models should allow the direct incorporation of both measured LAI and height of the crop. Additionally, it should be also interesting to analyze the temporal stability of within-field patterns of crop growth through different years. In case of stability, that could help the selection of sampling locations for the estimation of field scale ET using the soil water balance approach. Concerning the underground parts of the crop, our study shows that the root water uptake (RWU) is much more dynamic in time that is assumed in agro-hydrological model. Although the full temporal dynamics of the RWU can not be easily incorporated within agro-hydrological models, it is certainly worth continuing to quantify RWU, e.g. using the robust simplified water balance method, to make progress both in the concepts and the parameterization of the RWU used by agro-hydrological models. To conclude, we state, and this work clearly points out this fact, that the study of the micro-variability, i.e. that existing at the maize row scale is very relevant and of primary importance to improve the field scale water fluxes estimates. Quite surprisingly, this constitutes the analogue of the recommendation made by *Michaud and Shuttleworth* [1997], which has largely motivated the setup of our research, stating that quantification of fine-scale heterogeneity remains a clear and high priority to improve ET estimations at a regional scale.

Concurrently to those three research topics, an issue that also should be tackled concerns what can be formulated under the form of the following question "Which level of accuracy is needed?". Indeed, although each chapter of this thesis addresses the interdependent issues of uncertainty, accuracy and spatio-temporal variability, the topic of the "accuracy requirement" has not been directly addressed. Yet, it is obvious that beyond the pure academic exercise consisting to make the quest for accuracy, there is a real need to define the requirements of accuracy. Indeed, the requirement of accuracy is inherent to any research project, applied or more fundamental, although it is generally not explicitly defined. The topic of the accuracy is in some cases straightforward to address. Yet, in other cases it is much more complicated as that requires to combine some physical aspects of the considered system (e.g. hydrological processes) with socio-economical aspects or even with cost-gain analysis. As a matter of fact, any accuracy has a certain cost. Consequently, the challenge will often consist to find the best compromise between additional gain generated by a better accuracy and additional costs needed to reach a better accuracy. Within this framework, the research developed within this thesis must be considered as a preliminary and basic step allowing to rigorously investigate the issue of the accuracy requirement.

References

Abrisqueta, J.M., A. Ruiz, and J.A. Franco, Water balance of Apricot trees (*Prunus Armeniaca* L. cv. Bulida) under drip irrigation, *Agricultural Water Management, 50*, 211-227, 2001.

Al-Ghobari, H.M., Estimation of reference evapotranspiration for indent southern region of Saudi Arabia, *Irrigation Science, 19*, 81-86, 2000.

Allen, R.G., M.E. Jensen, J.L. Wright, and R.D. Burman, Operationnal estimates of reference evapotranspiration, *Agronomy Journal, 81*, 650-662, 1989.

Allen, R.G., M. Smith, A. Perrier, and L.S. Pereira, An update for the definition of reference evapotranspiration, *ICID Bulletin, 43*, 1-34, 1994a.

Allen, R.G., M. Smith, L.S. Pereira, and A. Perrier, An update for the calculation of reference evapotranspiration, *ICID Bulletin, 43*, 35-92, 1994b.

Allen, R.G., L.S. Pereira, D. Raes, and M. Smith, *Crop evapotranspiration Guidelines for computing crop water requirements*, FAO Irrigation and Drainage paper n°56, FAO, Rome, 1998.

Allen, R.G., Using the FAO-56 dual crop coefficient method over an irrigated region as part of an evapotranspiration intercomparison study, *Journal of Hydrology, 229*, 27-41, 2000.

Allmaras, R.R., W.W. Nelson, and W.B. Voorhees, Soybean and corn rooting in SW Minnesota : I. Water uptake sink, *Soil Science Society of America Proceedings, 39*, 764-777, 1975.

Andreu, L., J.W. Hopmans, and L.J. Schwankl, Spatial and temporal distribution of soil water balance for a drip-irrigated almond-tree, *Agricultural and Water Management, 35*, 123-146, 1997.

Assouline, S., A model for soil relative hydraulic conductivity based on the water retention characteristic curve, *Water Resources Research, 37*, 265-271, 2001.

Baldocchi, D.D., B.B. Hicks, and T.P. Meyers, Measuring biosphere-atmosphere exchanges of biologically related gases with micrometeorological methods, *Ecology, 69*, 1331-1340, 1998.

Bastiaanssen, W.G.M., SEBAL-based sensible and latent heat fluxes in the irrigated Gediz Basin, Turkey, *Journal of Hydrology, 229*, 87-100, 2000.

Batchelor, C.H., The accuracy of evapotranspiration estimated with the FAO modified Penman equation, *Irrigation Science, 5*, 223-233, 1984.

Batchelor, W.D., B. Basso, and J. O. Paz, Examples of strategies to analyze spatial and temporal yield variability using crop models, *European Journal of Agronomy, 18*, 141-158, 2002.

Bell, K.R., B.J. Blanchard, T.J. Schmugge, and M.W. Witczak, Analysis of surface soil moisture variations within large-field sites, *Water Resources Research, 16*, 796-810, 1980

Belmans, C.J, J.G. Wesseling, and R.A. Feddes, Simulation model of the water balance of a cropped soil: SWATRE, *Journal of Hydrology, 63*, 271-286, 1983.

Bertuzzi, P., L. Bruckler, and A. Chanzy, Sampling strategies for soil water content to estimate evapotranspiration, *Irrigation Science, 14*, 105-115, 1994.

Beven, K., A sensitivity analysis of the Penman-Monteith actual evapotranspiration estimates, *Journal of Hydrology, 44*, 169-190, 1979.

Beven, K.J., *Rainfall - Runoff Modeling - The Primer*, 360 pp., Wiley, Chichester, 2001.

Bierkens, M.F.P, P.A. Finke, and P. de Willingen, *Upscaling and downscaling methods for environmental research*, 204 pp., Developments in Plant and Soil Sciences 88, Kluwer Academic, 2000.

Blöschl, G., and M. Sivapalan, Scale issues in hydrological modelling - a review, *Hydrological Processes, 9*, 251-290, 1995.

Booltink, H.W.G., and V. Epinat, Using remote sensing data to improve simulation modeling for precision agriculture, in *Proceedings of the Fifth International Conference on Precision Agriculture*, Minnesota, USA, 2001.

Boons-Prins, E.R., G.H.J. de Koning, C.A. van Diepen, and F.W.T. Penning de Vries, Crop specific simulation parameters for yield forecasting across the European Community, Simulation Rep. 32, CABO-DLO, Wageningen, The Netherlands, 1993.

Boote, K.J., J.W. Jones, and N.B. Pikering, Potential uses and limitations of crop models, *Agronomy Journal,* , 704-716, 1996.

Bouten, W., T.J. Heimovaara, and A. Tiktak, Spatial patterns of throughfall and soil water dynamics in a Douglas fir stand, *Water Resources Research, 28*, 3227-3233, 1992.

Braud, I., R. Haverkamp, J.L. Arrue and M.V Lopez, Spatial variability of soil surface properties and consequences for the annual and monthly water balance of a semiarid environment (EFEDA Experiment), *Journal of Hydrometeorology, 62*, 121-136, 2003.

Brooks, R.H., and A.T. Corey, Hydraulic properties of porous media, Hydrology paper 3, 27 pp., Colorado State University, Fort Collins, 1964.

Bruckler, L., F. Lafolie, and F. Tardieu, Modeling root water potential and soil-root water transport: II. Field comparisons, *Soil Science Society of America Journal, 57*, 372-381., 1991

Brunel, J-P, G.R. Walker, and A.K. Kennett-Smith, Field validation of isotopic procedures for determining sources of water used by plants in a semi-arid environment, *Journal of Hydrology, 167*, 351-368, 1995.

Brunt, D., *Physical and dynamical meteorology*, 428 pp., 2^{nd} edition. Univ. Press, Cambridge, 1952.

Bui, E., and J.E. Box Jr, Stemflow, Rain throughfall, and erosion under canopies of corn and sorghum, *Soil Science Society of America Journal, 56*, 242-247, 1992.

Bussière, F., F. Solmon, and A. Fouéré, Implementation and evaluation of DROP, a model for the simulation of rainfall distribution below plants described in 3D, *Agronomie, 22*, 93-103.

Canadell, J., R.B. Jackson, J.R. Ehleringer, H.A. Mooney, O.E. Sala, and E.D. Schulze, Maximum rooting depth of vegetation types at the global scale, *Oecologica, 108*, 583-595, 1996.

Carnahan, B., H.A. Luther, and J.O. Wilkes, *Applied numerical methods*, 604 pp., John Wiley and Sons, New York, 1969.

Carrera, J., and S.P. Neuman, Estimation of aquifer parameters under transient and steady state conditions, 2, Uniqueness, stability, and solution algorithm, *Water Resources Research, 22*, 211-227, 1986.

Chahine, M.T., The hydrological cycle and its influence on climate, *Nature, 359*, 373-380, 1992.

Charpentier, M.A., and P. Groffman, Soil moisture variability within remote sensing pixels, *Journal of Geophysical Research, 97*, 18987-18995, 1992.

Christakos, G., P. Bogaert, and M.L. Serre, *Temporal GIS*, 217 pp., Springer-Verlag, New York, NY, 2001.

Clausnitzer, V., J.W. Hopmans, and J.L. Starr, Parameter uncertainty analysis of common infiltration models, *Soil Science Society of America Journal, 62*, 1477-1487, 1998.

Coelho, F.E., and D. Or, A parametric model for two-dimensional water uptake intensity by corn roots under drip irrigation, *Soil Science Society of America Journal, 60*, 1039-1049, 1996.

Coelho, E.F., and D. Or, Root distribution and water uptake patterns of corn under surface and subsurface drip irrigation, *Plant and Soil, 206*, 123-136, 1999.

Coleman, G., and D. Decoursey, Sensitivity and model variance analysis applied to some evaporation and evapotranspiration models, *Water Resources Research, 12*, 873-879, 1976.

Crave, A., and C. Gascuel-Odoux, The influence of topography on time and space distribution of soil surface water content, *Hydrological Processes, 11*, 203-210, 1997.

Dagan, G., and E. Bresler, Unsaturated flow in spatially variable fields, 1, Derivation of models of infiltration and redistribution, *Water Resources Research, 19*, 413-420.

Dagan, G., and E. Bresler, Variability of yield of an irrigated crop and its causes 3. Numerical simulation and field results, *Water Resources Research, 24*, 395-401, 1983.

Dane, J.H., R.B. Reed, and J.W. Hopmans, Estimating soil parameters and sample size by bootstrapping, *Soil Science Society of America Journal, 50*, 283-287, 1986.

Dane, J.H, and G.C. Topp, *Methods of soil analysis, Part 4 Physical Methods*, SSSA Book series, Madison, Wisconsin, USA, 2002.

Denmead, O.T., F.X. Dunin, S.C. Wong, and E.A.N. Greenwood, Measuring water use efficiency of eucalyptus trees with chambers and micrometeorological techniques, *Journal of Hydrology, 150*, 649-664, 1993.

Dekker, L.W., and C. Ritsema, Effect of maize canopy and water repellency on moisture patterns in a Dutch black plaggen soil, *Plant and Soil, 195*, 339-350, 1997.

Dickinson, R.E., A. Henderson-Sellers, and P.J. Kennedy, Biosphere Atmosphere Transfer Scheme (BATS) Version 1e as coupled to the NCAR Community Climate Model, NCAR Technical Note, NCAR /TN-387 + STR, 1993.

Diels, J., A validation procedure accounting for model input uncertainty: methodology and application to the SWATRER model, Ph.D. thesis, 173 pp., Leuven, 1994.

Dirksen C., and S. Dasberg, Improved calibration of time domain reflectometry soil water content measurements, *Soil Science Society of America Journal, 57*, 660-667, 1993.

Dirksen C., *Soil Physics Measurements*, 154 pp., Catena Verlag, 1999.

Doherty, J., L. Brebber, and P. Whyte, *PEST, Model independent parameter estimation*, 140 pp., Australian Centre for Tropical Freshwater Research, James Cooke University, Townsville, Australia, 1995.

Dobermann, A., M. Pampolino, and H-U. Neue, Spatial and temporal variability of transplanted rice at the field scale, *Agronomy Journal, 87*, 712-720, 1995.

Dolman, A.J., A.J. Hall, M.L. Kavvas, T. Oki, and J.W. Pomeroy (ed.), *Soil-Vegetation-Atmosphere transfer schemes and large scale hydrological models*, IAHS, Publication n°270, 2001.

Doorenbos, J., and W.O. Pruitt, *Crop water requirements*, 156 pp., FAO Irrigation and Drainage Paper n°24, Rome, 1977.

Doorenbos, J., and A.H. Kassam, *Réponse des rendements à l'eau*, 235 pp., FAO Irrigation and Drainage Paper n°33, Rome, 1987.

Droogers, P., Estimating actual evapotranspiration using a detailed agro-hydrological model, *Journal of Hydrology, 229*, 50-58, 2000.

Duan, Q.S., S. Sorooshian, and V.K. Gupta, Effective and efficient global optimization for conceptual rainfall-runoff models, *Water Resources Research, 28*, 1015-1031, 1992.

Ducoudré, N., K. Laval, and A. Perrier, SECHIBA, a new set of parameterizations of the hydrologic exchanges at the land/atmosphere interface within the LMD atmospheric general circulation model, *Journal of Climate, 6*, 248-273, 1993.

Dudal, R., Etude morphologique et génétique d'une séquence de sols sur limon loessique, *Agricultura, I*, 119-163, 1953.

Dupriez, G.L., and R. Sneyers, Précipitations: les normales du réseau pluviométrique belge, Institut Royal Météorologique de Belgique, Publications série A, n°101, 1982.

D'Urso, G. and A. Santini, A remote sensing and modeling integrated approach for the management of irrigation distribution systems, in *Proceedings of the International conference Evapotranspiration and irrigation Scheduling*, edited by C.R. Camp, E.J. Sadler and R.E. Yoder, pp. 435-441, San Antonio, Texas, 1996.

Elhers, W., A.P. Hamblin, D. Tennant, and R.R. van der Ploeg, Root systems parameters determining water uptake of field crops, *Irrigation Science, 12*, 115-124, 1991.

Famiglietti, J.S., and E.F. Wood, Effects of spatial variability and scale on areally averaged evapotranspiration, *Water Resources Research, 31*, 699-712, 1995.

Famiglietti, J.S., J.W. Rudnicki, and M. Rodell, Variability in surface moisture content along a hillslope transect: Rattlesnake Hill, Texas, *Journal of Hydrology, 210*, 259-281, 1998.

Famiglietti, J.S., J.A. Devereaux, C.A. Laymon, T. Tsegaye, P.R. Houser, T.J. Jackson, S.T. Graham, M. Rodell, and P.J. van Oevelen, Ground-based investigation of soil moisture variability within remote sensing footprints during the Southern Great Plains 1997 (SGP97) Hydrology Experiment, *Water Resources Research, 35*, 1839-1851, 1999.

Feddes, R.A., E. Bresler, and S.P. Neuman, Field test of a modified numerical model for root water uptake by root systems, *Water Resources Research, 10*, 1199-1206, 1974.

Feddes, R.A., P.J. Kowalik, and H. Zaradny, *Simulation of field water use and crop yield*, 189 pp., Simulation Monographs, Pudoc. Wageningen, 1978.

Finsterle, S., and K. Pruess, Solving the estimation-identification problem in two-phase modeling, *Water Resources Research*, 31, 913-924, 1995.

Franks, S.W., K.J. Beven, P.F. Quinn, and I.R. Wright, On the sensitivity of soil-vegetation-atmosphere transfer (SVAT) schemes : equifinality and the problem of robust calibration, *Agricultural and Forest Meteorology, 86*, 63-75, 1997.

Gardner, W., Some steady state solutions of the unsaturated moisture flow equation with application to evaporation from a water table, *Soil Science, 85*, 228-232, 1958.

Gardner, W.R., Modeling water uptake by roots, *Irrigation Science, 12*, 109-114, 1991.

Gellens-Meulenberghs, F., and D. Gellens, L'évapotranspiration potentielle en Belgique: variabilité spatiale et temporelle, Institut Royal Météorologique de Belgique, Publication série A, n°130, 1992.

Georgakakos, K.P., and O.W. Baumer, Measurement and utilization of on-site soil moisture data, *Journal of Hydrology, 184*, 131-152, 1996.

Girardin, P., *Ecophysiologie du maïs*, 325 pp., AGPM, Pau, 1999.

Goovaerts, P. and C. Chiang, Temporal persistence of spatial patterns of mineralizable nitrogen and selected soil properties, *Soil Science Society of America Journal, 57*, 372-381, 1993.

Graedel, T.E. and P.J. Crutzen, *Atmosphere, Climate, and Change*, 196 pp., Scientific American Library, New York, USA, 1997.

Grayson, R.B., A.W. Western, H.S. Chiew, and G. Blöschl, Preferred states in spatial soil moisture patterns: local and nonlocal controls, *Water Resources Research, 33*, 2897-2908, 1997.

Grayson, R.B., and A.W. Western, Towards areal estimation of soil water content from point measurements: time and space stability of mean response, *Journal of Hydrology, 207*, 68-82, 1998.

Green, S.R., and B.E. Clothier, Root water uptake by kiwifruit vines following partial wetting of the root zone, *Plant and Soil, 173*, 317-328, 1995.

Green, S.R., and B.E. Clothier, The root zone dynamics of water uptake by a mature apple tree, *Plant and Soil, 206*, 61-77, 1999.

Gupta, V.K., and S. Sorooshian, Uniqueness and observability of conceptual rainfall-runoff model parameters. The percolation of process examined, *Water Resources Research, 19*, 269-276, 1985.

Gupta, H.V., S. Sorooshian, and P.O. Yapo, Toward improved calibration of hydrologic models: multiple and noncommensurable measures of information, *Water Resources Research, 34*, 751-763, 1998.

Hatton, T., and H. Wu, Scaling theory to extrapolate individual tree water use to stand water use, *Hydrological Processes, 9*, 527-540, 1995.

Haverkamp, R., M. Vauclin, and G. Vachaud, Error analysis in estimating soil water content from neutron probe measurements: 1. Local standpoint, *Soil Science, 137*, 78-90, 1984.

Hawley, M., T. Jackson, and R. McCuen, Surface soil moisture variation on small agricultural watersheds, *Journal of Hydrology, 62*, 179-200, 1983.

Haynes, J.L., Ground rainfall under vegetative canopy of crops, *Journal of American Society of Agronomy, 32*, 176-184, 1940.

Henninger, D.L., G.W. Petersen, and E.T. Engman, Surface soil moisture within a watershed-variations, factors influencing, and relationship to surface runoff, *Soil Science Society of America Journal, 40*, 773-776, 1976.

Herkelrath W.N., S.P. Hamburg, and F. Murphy, Automatic, real-time monitoring of soil water content in a remote field area with time domain reflectometry, *Water Resources Research, 27*, 857-864, 1991.

Hillel, D., Science and the crises of the environment, *Geoderma, 60*, 377-382, 1993.

Hills, R.C., and S.G. Reynolds, Illustrations of soil moisture variability in selected areas and plots of different sizes, *Journal of Hydrology, 8*, 27-47, 1969.

Homaee, M., Root water uptake under non-uniform transient salinity and water stress, Ph.D. thesis, 169 pp., Agric. Univ. Wageningen, Wageningen, 1999.

Hoogland, J.C., R.A. Feddes, and C. Belmans, Root water uptake model depending on soil water pressure head and maximum extraction rate, *Acta Horticulturae, 119*, 123-131, 1981.

Hopmans, J.W., and J. Simunek, Review of inverse estimation of soil hydraulic properties, in *Proceedings of the International Workshop on Characterization and Measurements of the Hydraulic properties of Unsaturated Porous Media*, edited by M.Th. van Genuchten, F.J. Leij, and L. Wu, pp. 643-660, Univ. of Calif., Riverside, 1999.

Howell T., J. Tolk, A. Schneider, and S. Evett, Evapotranspiration, yield and water use efficiency of corn hybrids differing in maturity, *Agronomy Journal, 90*, 3-9, 1998.

Huisman, J.A., C. Sperl, W. Bouten and J.M. Verstraten, Soil water content measurements at different scales: accuracy of time domain reflectometry and ground-penetrating radar, *Journal of Hydrology, 245*, 48-58, 2001.

Hupet, F., and M. Vanclooster, Effect of the sampling frequency of meteorological variables on the estimation of the reference evapotranspiration, *Journal of Hydrology, 243*, 192-204, 2001.

Hupet, F., and M. Vanclooster, Intraseasonal dynamics of soil moisture variability within a small agricultural maize cropped field, *Journal of Hydrology, 261*, 86-101, 2002.

Hupet, F., S. Lambot, M. Javaux, and M. Vanclooster, On the identification of macroscopic root water uptake parameters from soil water content observations, *Water Resources Research, 38*, doi :10.1029 /2001WR001556, 2002.

Hupet, F., P. Bogaert, and M. Vanclooster, Quantifying the local scale uncertainty of estimated actual evapotranspiration, accepted for publication in *Hydrological Processes*, September 2003.

Hupet, F., and M. Vanclooster, Sampling strategies to estimate field areal evapotranspiration fluxes with a soil water balance approach, submitted to *Journal of Hydrology*, June 2003.

Huyer, W., and A. Neumaier, Global Optimization by Multilevel Coordinate Search, *Journal of Global Optimization, 14*, 331-355, 1999.

Isaaks, E.H., and R.M. Srivastava, *An introduction to Applied Geostatistics*, 561 pp., Oxford University Press, New York, 1989.

Itier, B., and Y. Brunet, Recent developments and present trends in evaporation research : a partial survey, in *Proceedings of the International conference Evapotranspiration and irrigation Scheduling*, edited by C.R. Camp, E.J. Sadler and R.E. Yoder, pp. 1-20, San Antonio, Texas, 1996.

Jacques D., Analysis of water and solute transport at the field scale, Ph.D. thesis, 255 pp., Univ. of Leuven, Leuven, 2000.

Janssen, P.H.M., and P.S.C. Heuberger, Calibration of process-oriented models, *Ecological Modelling, 83*, 55-66, 1995.

Jara, J., C. Stockle, and J. Kjelgaard, Measurement of evapotranspiration and its components in a corn (*Zea Mays* L.) field, *Agricultural and Forest Meteorology, 92*, 131-145, 1998.

Jarvis, N.J., The MACRO model (Version 3.1). Technical description and sample simulations, 51 pp., Reports and Dissertation 19, Department of Soil Science, Swedish University of Agricultural Sciences, Uppsala, Sweden, 1994.

Jensen, M.E., R.D. Burman, and R.G. Allen, *Evapotranspiration and irrigation water requirements*, 332 pp., ASCE Manuals and Reports on Engineering Practice, n° 70, 1990.

Jhorar, R.K., Estimation of effective soil hydraulic parameters for water management studies in semi-arid zones, Integral use of modelling, remote sensing and parameter estimation, Ph.D. thesis, 158pp, Wageningen, 2002.

Jhorar R., W. Bastiaanssen, R. Feddes, and J.C. van Dam, Inversely estimating soil hydraulic functions using evapotranspiration fluxes, *Journal of Hydrology, 258*, 198-213, 2002.

Joernsgaard, B., and S. Halmoe, Intra-field variation over crops and years, *European Journal of Agronomy, 19*, 23-33, 2003.

Jones, C.A., and J.R. Kiniry (ed.), CERES-Maize: a simulation model of maize growth and development, Texas A and M Univ. Press, College Station, 1986.

Jordan, C., Z. Shi, J.S. Bailey, and A.J. Higgins, Sampling strategies for mapping "within-field" variability in the dry matter yield and mineral nutrient status of forage grass crops in cool temperate climes, *Precision Agriculture, 4*, 69-86.

Katerji N., F.A. Daudet, and C. Valancogne, Contribution des réserves profondes du sol au bilan hydrique des cultures. Détermination et importance, *Agronomie, 4*, 779-787, 1984.

Kim, C.P., J.N. Stricker, and R.A. Feddes, Impact of soil heterogeneity on the water budget of the unsaturated zone, *Water Resources Research, 33*, 991-999, 1997.

Kite, G.W., and P. Droogers, Comparing evapotranspiration estimates from satellites, hydrological models and field data, *Journal of Hydrology, 229*, 3-18, 2000.

Klute, A. (ed.), *Methods of soil analysis, part 1, Physical and Mineralogical Methods*, Agronomy Monograph 9, 2nd ed., American Society of Agronomy, Madison IV, 1986.

Kool, J.B., J.C. Parker, and M.Th. van Genuchten, Determining soil hydraulic properties from one-step outflow experiments by parameter estimation: I. Theory and numerical studies, *Soil Science Society of America Journal, 49*, 1348-1354, 1985.

Kool, J.B., and J.C. Parker, Analysis of the inverse problem for transient unsaturated flow, *Water Resources Research, 24*, 817-830, 1988.

Lambot, S., M. Javaux, F. Hupet, and M. Vanclooster, A global multilevel coordinate search procedure for estimating the unsaturated soil hydraulic properties, *Water Resources Research, 38*, doi :10.1029 /2001WR001224, 2002.

Lascano, R.J., and C.H.M. Van Bavel, Simulation and measurement of evaporation of a bare soil, *Soil Science Society of America Journal, 50*, 1127-1132, 1986.

Lascano R., R. Baumhardt, S. Hicks, S. Evett, and J. Heilman, Daily measurement and calculation of crop water use, in *Proceedings of the International conference Evapotranspiration and irrigation Scheduling*, edited by C.R. Camp, E.J. Sadler and R.E. Yoder, pp. 225-230, San Antonio, Texas, 1996.

Ledieu J., P. De Ridder, P. De Clerck, and S. Dautrebande, A method for measuring soil water content by time-domain reflectometry, *Journal of Hydrology, 88*, 319-328, 1986.

Leuning R., A.G. Condon, F.X. Dunin, S. Zegelin, and OT Denmead, Rainfall interception and evaporation from soil below a wheat canopy, *Agricultural and Forest Meteorology, 67*, 221-238, 1994.

Lewan, E., and P. Jansson, 1996, Implications of spatial variability of soil physical properties for simulation of evaporation at the field scale, *Water Resources Research, 32*, 2067-2074.

Liedgens, M., and W. Richner, Minirhizotron observations of the spatial distribution of the maize root system, *Agronomy Journal, 93*, 1097-1104, 2001.

Lindsey, D., and R. Farnsworth, Sources of solar radiation estimates and their effect on daily potential evaporation for use in streamflow modeling, *Journal of Hydrology, 201*, 348-366, 1997.

Loague, K., Soil water content at R-5. Part 1. Spatial and temporal variability, *Journal of Hydrology, 139*, 233-251, 1992.

Loague, K., and P.C. Kyriakidis, Spatial and temporal variability in the R-5 infiltration data set: Déjà vu and rainfall-runoff simulations, *Water Resources Research, 32*, 2883-2895, 1997.

Logdson and Jaynes, Spatial variability of hydraulic conductivity in a cultivated field at different times, *Soil Science Society of America Journal, 60*, 703-709, 1996.

Malcorps, H., Observations climatologiques octobre 1999 - Partie I, Institut Royal Météorologique, bulletin mensuel, 1999.

Mallants D., Mohanty B.P., D. Jacques, and J. Feyen, Spatial variability of hydraulic properties in a multi-layered soil profile, *Soil Science, 161*, 167-181, 1995.

Mallants, D., D. Jacques, M. Vanclooster, J. Diels, and J. Feyen, A stochastic approach to simulate water flow in a macroporous soil, *Geoderma, 70*, 299-324, 1996.

Mallants, D., Water flow and solute transport in a heterogeneous soil profile, Ph.D. thesis, 316 pp., Univ. of Leuven, Leuven, 1996.

Mallants, D., B.P. Mohanty, A. Vervoort, and J. Feyen, Spatial analysis of saturated hydraulic conductivity in a soil with macropores, *Soil Technology, 10*, 115-131, 1997.

Mauser, W., and S. Schädlich, Modelling the spatial distribution of evapotranspiration on different scales using remote sensing data, *Journal of Hydrology*, 212-213, 250-267, 1998.

McCuen, R.H., A sensitivity and error analysis of procedures used for estimating evapotranspiration, *Water Resources Bulletin, 10*, 486-498, 1974.

McVicar, T.R., and D.L.B. Jupp, Estimating one-time-of-day meteorological data from standard daily data as inputs to thermal remote sensing based energy balance models, *Agricultural and Forest Meteorology, 96*, 219-238, 1999.

Meijninger, W.M.L., and H.A.R. De Bruin, The sensible heat fluxes over irrigated areas in western Turkey determined with a large aperture scintillometer, *Journal of Hydrology, 229*, 42-49, 2000.

Meiresonne, L., N. Nadezhdin, J. Cermak, J. Van Slycken, and R. Ceulemans, Sap flow and simulated transpiration from a polplar stand in Flanders (Belgium), *Agricultural and Forest Meteorology, 96*, 165-179, 1999.

Merz, B., and E.J. Plate, An analysis of the effects of spatial variability of soil and soil moisture on runoff, *Water Resources Research, 33*, 2909-2922, 1997.

Meyer, S., K. Hubbard, and D. Wilhite, Estimating potential evapotranspiration : the effect of random and systematic errors, *Agricultural and Forest Meteorology, 46*, 285-296, 1989.

Michaud, J.D., and W.J. Shuttleworth, Executive summary of the Tucson Aggregation Workshop, *Journal of Hydrology, 190*, 176-181, 1997.

Michot, D., Y. Benderitter, A. Dorigny, B. Nicoullaud, D. King, and A. Tabbagh, Spatial and temporal monitoring of soil water content with an irrigated corn crop cover using surface electrical resistivity tomography, *Water Resources Research, 39*, 5, 1138, doi:10.1029/2002 WR001581, 2003.

Miller, M.P., M.J. Singer, and D.R. Nielsen, Spatial variability of wheat yield and soil properties on complex hills, *Soil Science Society of America Journal, 52*, 1133-1141, 1988.

Mohanty, B.P., M.D. Ankeny, R. Horton, and R.S. Kanwar, Spatial-analysis of hydraulic conductivity measured using disc infiltrometers, *Water Resources Research, 30*, 2489-2498, 1994.

Mohanty, B.P., J.S. Famiglietti, and T.H. Skaggs, Evolution of soil moisture spatial structure in a mixed vegetation pixel during the

Southern Great Plains 1997 (SGP97) Hydrology Experiment, *Water Resources Research, 36*, 3675-3687, 2000.

Mohanty, B.P., T.H. Skaggs, and J.S. Famiglietti, Analysis and mapping of field-scale soil moisture variability using high-resolution, ground-based data during the Southern Great Plains 1997 (SGP97) Hydrology Experiment, *Water Resources Research, 36*, 1023-1031, 2000b.

Molz, F.J, Models of water transport in the soil-plant system: a review, *Water Resources Research, 17*, 1245-1260, 1981.

Moore, I.D., G.J. Burch, and D.H. Mackenzie, Topographic effects on the distribution of surface soil water and the location of ephemeral gullies, *Transactions of the ASAE, 31*, 1098-1107, 1988.

Mualem, Y., A new model for predicting the hydraulic conductivity of unsaturated porous media, *Water Resources Research, 12*, 513-522, 1976.

Musters, P.A.D., and W. Bouten, Assessing rooting depths of an Austrian pine stand by inverse modeling soil water content maps, *Water Resources Research, 35*, 3041-3048, 1999.

Musters, P.A.D., and W. Bouten, A method for identifying optimum strategies of measuring soil water contents for calibrating a root water uptake model, *Journal of Hydrology, 227*, 273-286, 2000.

Musters P.A.D., W. Bouten, and J.M. Verstraten, Potentials and limitations of modeling vertical distributions of root water uptake of an Austrian pine forest on a sandy soil, *Hydrological Processes, 14*, 103-115, 2000.

Nimah, M.N., and R.J. Hanks, Model for estimating soil, water, plant and atmospheric interrelations, *Soil Science Society of America Journal, 37*, 522-527, 1973.

Nyberg, L., Spatial variability of soil water content in the covered catchment at Gardsjön, Sweden, *Hydrological Processes, 10*, 89-103, 1996.

NRC, National Research Council, *Opportunities in the Hydrological Sciences*, 348 pp., National Academy Press, Washington, DC., 1991.

Or, D., B. Fisher, R. Hubsher, and J. Wraith, WinTDR 98 v4.0-Users Guide-Utah State University - Plants, Soils, and Biometeorology - Logan, Utah, 1998.

Otegui, M.E., F.H. Andrade, and E.E. Suero, Growth, water use, and kernel abortion of maize subjected to drought at silking, *Field Crops Research, 40*, 87-94, 1995.

Otegui, M.E., R.A. Ruiz, and D. Petruzzi, Modeling hybrid and sowing date effects on potential grain yield of maize in a humid temperate region, *Field Crop Research, 47*, 167-174, 1996.

Ould Mohamed S., P. Bertuzzi, A. Bruand, L. Raison, and L. Bruckler, Field evaluation and error analysis of soil water content measurement using the capacitance probe method, *Soil Science Society of American Journal, 61*, 399-408, 1997.

Paltineanu, I.C., and J.L. Starr, Preferential water flow through corn canopy and soil water dynamics across rows, *Soil Science Society of America Journal, 64*, 44-54, 2000.

Pardo-Iguzquiza, E., Optimal selection of number and location of rainfall gauges for areal estimation using geostatistics and simulated annealing, *Journal of Hydrology, 210*, 206-220, 1998.

Parkin, T.B., and E.E. Codling, Rainfall distribution under a corn canopy: implications for managing agrochemicals, *Agronomy Journal, 82*, 1166-1169, 1990.

Paz, J.O., W.D. Batchelor, T.S. Colvin, S.D. Logsdon, T.C. Kaspar, and D.L. Karlen, Analysis of water stress effects causing spatial yield variability in soybeans, *Transactions of ASAE, 41*, 1527-1534, 1998.

Paz, J.O., W.D. Batchelor, G.L. Tylka, R.G. Hartzler, A modeling approach to quantify the effects of spatial soybean yield limiting factotrs, Transactions of the ASAE, 5, 1329-1334, 2001.

Peirera, L.S., R.A. Feddes, J.R. Gilley, and B. Lesaffre, *Sustainability of irrigated agriculture*, 631 pp., Kluwer Academic Publishers, 1994.

Penning de Vries, F.W.T., D.M. Jansen, H.F.M. ten Berge, and A. Bakema, Simulation of ecophysiological processes of growth in several annual crops, Pudoc, Wageningen, The Netherlands, 271 pp., 1989.

Poss R., Transferts de l'eau et des minéraux dans les terres de Barre du Togo. Conséquences agronomiques, Ph.D. thesis, Université Paris VI, Paris, 1991.

Prasad, R., A linear root water uptake model, *Journal of Hydrology, 99*, 297-306, 1988.

Press, W.H., S.A. Teukolsky, W.T. Vetterling, and B.P. Flannery, Numerical Recipes in C., 2^{nd} ed., Cambridge Univ. Press, Cambridge, England, 1992.

Qui, G.Y., T. Yano, and K. Momii, An improved methodology to measure evaporation from bare soil based on comparison of surface temperature with a dry soil surface, *Journal of Hydrology, 210*, 93-105, 1998.

Quinn, N.W., and J.M. Laflen, Characteristics of raindrop throughfall under corn canopy, *Transactions of the ASAE, 26*, 1445-1450, 1983.

Raats, P.A.C., Steady flows of water and salt in uniform soil profiles with plant roots, *Soil Science Society of America Proceedings, 38*, 717-722, 1974.

Raghuwanshi, N.S. and W.W. Wallender, Field-measured evapotranspiration as a stochastic process, *Agricultural Water management, 32*, 111-129, 197.

Rambal, S., M. Ibrahim, and M. Rapp, Variabilité spatiale des variations du stock d'au du sol sous forêt, application à l'optimisation d'un dispositif de mesure du bilan hydrique, *Catena, 11*, 177-186, 1984.

Rana, G., and N. Katerji, A measurement based sensitivity analysis of the Penman-Monteith actual evapotranspiration model for crops of different height and in contrasting water status, *Theoretical and Applied Climatology, 60*, 141-149, 1998.

Rana G, and N. Katerji, Measurement and estimation of actual evapotranspiration in the field under Mediterranean climate: a review, *European Journal of Agronomy, 13*, 125-153, 2000.

Rasiah, V., G. Carlson, and R. Kohl, Assessment of functions and parameter estimation methods in root water uptake simulation, *Soil Science Society of America Journal, 56*, 1267-1271, 1992.

Rawls, W.J., D.L. Brakensiek, and N. Miller, Green-Ampt infiltration parameters from soils data, *Journal of Hydraulic engineering, 109*, 62-70, 1983.

Refsgaard, J.C., and J. Knudsen, Operational validation and intercomparison of different types of hydrological models, *Water Resources Research, 32*, 2189-2202, 1996.

Reid, I., The influence of slope orientation upon the soil moisture regime, and its hydrogeomorphological significance, *Journal of Hydrology, 19*, 309-321, 1973.

Reynolds, S.G., The gravimetric method of soil moisture determination, Part III: an examination of factors influencing soil moisture variability, *Journal of Hydrology, 11*, 288-300, 1970.

Reynolds, W.D., D.E. Elrick, E.G., Youngs, A. Amoozegar, H.W.G., Booltink, and J. Bouma, Saturated and field-saturated water flow parameters, in *Methods of soil analysis, Part 4 Physical Methods*, edited by J.H. Dane, and G.C. Topp, SSSA Book series, Madison, Wisconsin, USA, 2002.

Ritchie, J.T., T.A. Howell, W.S. Meyer, and J.L. Wright, Sources of biased errors in evaluating evapotranspiration equations, in *Proceedings of the International conference Evapotranspiration and irrigation Scheduling*, edited by C.R. Camp, E.J. Sadler and R.E. Yoder, pp. 147-157, San Antonio, Texas, 1996.

Ritter, A., Hupet, F., Munoz-Carpena, R., Vanclooster, M., and S. Lambot, Using inverse methods for estimating soil hydraulic properties from field data as an alternative to direct methods, *Agricultural Water Management, 59*, 77-96, 2003.

Robinson, M., and T.J. Dean, Measurement of near surface soil water content using a capacitance probe, *Hydrological Processes, 7*, 77-86, 1993.

Rolston, D.E., J.W. Biggar, and H.I. Nightingale, Temporal persistence of spatial soil-water patterns under trickle irrigation, *Irrigation Science, 12*, 181-186, 1991.

Romano, N., and A. Santini, Determining soil hydraulic functions from evaporation experiments by a parameter estimation approach: experimental verifications and numerical studies, *Water Resources Research, 35*, 3343-3359, 1999.

Ruget, F., R. Bonhomme, and M. Chartier, Estimation simple de la surface foliaire de plantes de maïs en croissance, *Agronomie, 16*, 553-562, 1996.

Russo, D., E. Bresler, U. Shani, and J.C. Parker, Analyses of infiltration events in relation to determining soil hydraulic properties by inverse problem methodology, *Water Resources Research, 27*, 1361-1373, 1991.

Russo, D., and G. Dagan, *Water flow and solute transport in soils*, 304 pp., Advanced series in agricultural sciences, Springer Verlag, 1993.

Samra, J.S., R.K. Rajput, and V. Katyal, Structured heterogeneity of soil pH and grain yield of rice and wheat growth in a sodic soil, *Agronomy Journal, 84*, 877-881, 1992.

Saxton, K., Sensitivity analyses of the combination evapotranspiration equation, *Agricultural and Forest Meteorology*, 15, 343-353, 1975.

Schaap M., F. Leij, M. Th. Van Genuchten, Rosetta: a computer program for estimating soil hydraulic parameters with hierarchical pedotransfer functions, Journal of Hydrology, 251, 163-176, 2001.

Selim, H.M., and I.K. Iskandar, Nitrogen behaviour in a land treatment of wastewater: a simplified model, in State of knowledge in Land treatment of wastewater, pp. 171-179, edited by Cold Regions Research and Engineering Laboratory, Hanover, New Hampshire, 1978.

Sellers, P.J., D.A. Randall, G.J. Collatz, J.A. Berry, C.B. Field, D.A. Dazlich, C. Zhang, G.D. Collelo, and L. Bounoua, A revised land surface parameterization (SiB2) for atmospheric GCMs.1. Model formulation, *Journal of Climate, 9*, 676-689.

Shapiro, S.S., and M.B. Wilk, An analysis of variance test for normality, *Biometrika, 52*, 591-611, 1965.

Shouse, P.J., W.B. Russel, D.S. Burden, H.M. Selim, J.B. Sisson, and M.Th. van Genuchten, Spatial variability of soil water retention functions in a silt loam soil, *Soil Science, 159*, 1-12.

Shuttleworth, W.J., and J.S. Wallace, Evaporation from sparse crops - an energy combination theory, *Quarterly Journal of the Royal Meteorological Society, 111*, 839-855, 1985.

Si, B.C., and R.G. Kachanoski, Estimating soil hydraulic properties during constant flux infiltration: Inverse procedures, *Soil Science Society of America Journal, 64*, 439-449, 2000.

Simunek, J., and M. Th. van Genuchten, Estimating unsaturated soil hydraulic properties from tension disc infiltrometer data by numerical inversion, *Water Resources Research, 32*, 2683-2696, 1996.

Simunek, J., O. Wendroth, and M. Th. van Genuchten, Parameter estimation analysis of the evaporation method for determining soil hydraulic properties, *Soil Science Society of America Journal, 62*, 894-905, 1998.

Simunek, J., M. Sejna, and M. Th. van Genuchten, *The Hydrus-1D software package for simulating the one-dimensional movment of water, heat, and multiple solutes in variably-saturated media, Version 2.0.*, 202 pp., Rep. IGWMC-TPS-70, Int. Ground Water Model. Cent., Colo. Sch. of Mines, Golden, 1998a.

Sinclair D.F., and J. Williams, Components of variance involved in estimating soil water content and water content change using a neutron moisture meter, *Australian Journal of Soil Research, 17*, 237-247, 1979.

Snedecor, G.W., and W.G. Cochran, *Statistical methods*, 593 pp., 3^{rd} edition, The Iowa State University Press, Ames, IA, 1967.

Soegaard, H. and E. Boegh, Estimation of evapotranspiration from a millet crop in the Sahel combining sap flow, leaf area index and eddy correlation technique, *Journal of Hydrology, 166*, 265-282, 1995.

Sokal, R.R, and F.J. Rohlf, *Biometry: the principles and practice of statistics in biological research*, third edition, 887 pp., W.H. Freeman and Co., New York.

Soppe, R.W.O., and J.E. Ayars, Characterizing groundwater use by sapflower using weighing lysimeters, *Agricultural Water Management*, 60, 59-71, 2003.

Spitters, C.J.T., H. van Keulen, and D.W.G. van Kraalingen, A simple and universal crop growth simulator: SUCROS87, in Simulation and systems management in crop protection, edited by R. Rabbinge, S.A. Ward, and H.H. van Laar, Simulation Monographs, Pudoc, Wageningen, The Netherlands, pp. 147-181, 1995.

St'astna, M., and Z. Zalud, Sensitivity analysis of soil hydrologic parameters for two crop growth simulation models, *Soil and Tillage Research, 50*, 305-318, 1999.

Tardieu, F., Analysis of the spatial variability of maize root density, *Plant and Soil, 107*, 259-266, 1988.

The MathWorks, MATLAB, version 5.3, MathWorks, Natick, Mass., 1999.

Thompson, E.S., Computation of solar radiation from sky cover, *Water Resources Research, 12*, 859-865, 1976.

Timlin, D., Y. Pachepsky, and V. R. Reddy, Soil water dynamics in row and interrow positions in soybean (*Glycine max* L.), *Plant and Soil, 237*, 25-35, 2001.

Tiktak A., D.S. De Nie, J.D. Pineros Garcet, A. Jones and M. Vanclooster, Assessing the pesticide leaching risk at the pan European level: the EuroPEARL approach., Journal of Hydrology, In press.

Topp G.C., J.L. Davis, and A.P. Annan, Electromagnetic determination of soil water content: measurements in coaxial transmission lines, *Water Resources Research, 16*, 574-582, 1980.

Trambouze, W., and M. Voltz, Measurement and modelling of the transpiration of a Mediterranean vineyard, *Agricultural and Forest Meteorology, 107*, 153-166, 2001.

Ulaby, F.T., P.C. Dubois and J. van Zyl, Radar mapping of surface soil moisture, *Journal of Hydrology, 184*, 57-84, 1996.

Vachaud, G., A. Passerat de Silans, P. Balabanis, and M. Vauclin, Temporal stability of spatially measured soil water probability density function, *Soil Science Society of America Journal, 49*, 822-828, 1985.

Vachaud, G., and T. Chen, Sensitivity of computed values of water balance and nitrate leaching to within soil class variability of transport parameters, *Journal of Hydrology, 264*, 87-100, 2002.

Vanclooster, M., P. Viaene, K. Christiaens, and S. Ducheyne, *WAVE : a mathematical model for simulating water and agrochemicals in the soil and vadose environment, Reference and user's manual (release 2.1)*, Institute for Land and Water Management, Katholieke Universiteit Leuven, Leuven, Belgium, 1996.

Vanclooster, M., M. Javaux, F. Hupet, S. Lambot, A. Rochdi, J.D. Piñeros-Garcet and C. Bielders, Effective approaches for modelling chemical transport in soils supporting soil management at the larger scale, in *Sustainable land management - environmental protection. A soil physical approach*, edited by M. Pagliai and R. Jones, Advances in geo-ecology, 2002.

van Dam, J.C., J.N.M. Stricker, and P. Droogers, Inverse method to determine soil hydraulic functions from multi step outflow experiments, *Soil Science Society of America Journal, 58*, 647-652, 1994.

Van Dam, J.C., J. Huygen, J.G. Wesseling, R.A. Feddes, P. Kabat, P.E.V. van Walsum, P. Groenendijk, and C.A. van Diepen, *Theory* *of SWAP version 2.0. Simulation of water flow, solute transport and plant growth in the Soil-Water-Atmosphere-Plant environment*, 167 pp., Report 71, Department Water Resources, Wageningen University, Technical Document 45, Alterra, Wageningen, The Netherlands, 1997.

van Dam, J.C., and R.A. Feddes, Numerical simulation of infiltration, evaporation and shallow groundwater levels with the Richards equation, *Journal of Hydrology, 233*, 72-85, 2000.

Van den Broek, B.J., and P. Kabat, SAWCROP: dynamic simulation model of soil water and crop yield applied to potatoes, In 'Modeling and parameterization of the Soil-Plant-Atmosphere System, A comparison of potato growth models', P. Kabat, B. Marshall, B.j. van den Broek, J. Vos and H. van Keulen (Eds.), Wageningen Press, p. 299-334, 1995.

Vanderborght, J., R. Kasteel, M. Ciocanaru, M. Herbst, H. Vereecken, M. Javaux, and M. Vanclooster, Analytical solutions of non-linear flow and transport equations to test numerical models for simulating flow and transport in unsaturated soils, First Workshop on Mathematical modelling of environmental problems, Bucarest, June 2002.

Vandervaere JP., M. Vauclin, R. Haverkamp, and R.H. Cuenca, Error analysis in estimating soil water balance of irrigated fields during the EFEDA experiment : 1. Local standpoint, *Journal of Hydrology, 156*, 351-370, 1994.

Vandervaere JP., M. Vauclin, R. Haverkamp, and R.H. Cuenca, Error analysis in estimating soil water balance of irrigated fields during the EFEDA experiment : 2. Spatial standpoint, *Journal of Hydrology, 156*, 371-388, 1994.

Van Elewijck, L., Stemflow on maize: a stemflow equation and the influence of rainfall intensity on stemflow amount, *Soil Technology, 2*, 41-48, 1989.

Van Genuchten, M. Th., A closed-form equation for predicting the hydraulic conductivity of unsaturated soils, *Soil Science Society of America Journal, 44*, 892-898, 1980.

Van Pelt, R.S., and P.J. Wierenga, Temporal stability of spatially measured soil matric potential probability density function, *Soil Science Society of America Journal, 65*, 668-677, 2001.

Van Weesenbeck, I.J., and R.G. Kachanoski, Spatial and temporal distribution of soil water in the tilled layer under a corn crop, *Soil Science Society of America Journal, 52*, 363-368, 1988.

Van Weesenbeck, I.J., R.G. Kachanoski, and D.E. Rolston, Temporal persistence of spatial patterns of soil water content in the tilled layer under a corn crop, *Soil Science Society of America Journal, 52*, 934-941, 1988.

Vauclin, M., R. Haverkamp, and G. Vachaud, Error analysis in estimating soil water content from neutron probe measurements: 2. Spatial standpoint. *Soil Science, 137*, 141-148, 1984.

Villagra, M.M., O.O.S. Bacchi, R.L. Tuon, and K. Reichardt, Difficulties of estimating evapotranspiration from the water balance equation, *Agricultural and Forest Meteorology, 72*, 317-325, 1995.

Vogeler, I., S. Green, D. Scotter, and B. Clothier, Measuring and modeling the transport and root uptake of chemicals in the unsaturated zone, *Plant and Soil, 231*, 161-174, 2001.

Vrugt, J.A., M.T. van Wijk, J.W. Hopmans, and J. Simunek, One-, two-, and three-dimensional root water uptake functions for transient modeling, *Water Resources Research, 37*, 2457-2470, 2001a.

Vrugt, J.A., J.W. Hopmans, and J. Simunek, Calibration of a two-dimensional root water uptake model, *Soil Science Society of America Journal, 65*, 1027-1037, 2001b.

Wesseling, J.G. Meerjarige simulaties van grondwaterontrekking voor verschillende bodemprofielen, groundwatertrappen en gewassen met het model SWATRE, Report 152, Winand Staring Centre, Wageningen, 1991.

Western, A.W., G. Blöschl, and R.B. Grayson, Geostatistical characterisation of soil moisture patterns in the Tarrawarra catchment, *Journal of Hydrology, 205*, 20-37, 1998.

Western, A.W., and G. Blöschl, On the spatial scaling of soil moisture, *Journal of Hydrology, 205*, 20-37, 1999.

Western, A.W., R.B. Grayson, G. Blöschl, G.R. Willgoose, and T.A. McMahon, Observed spatial organization of soil moisture and its relation to terrain indices, *Water Resources Research, 35*, 797-810, 1999a.

Western, A.W., R.B. Grayson, and T.R. Green, The Tarrawarra project: high resolution spatial measurement, modelling and analysis of soil moisture and hydrological response, *Hydrological Processes, 13*, 633-652, 1999b.

Western, A.W., R.B. Grayson, G. Blöschl, and D.J. Wilson, Spatial variability of soil moisture and its implications for scaling, in *Scaling Methods in soil physics*, edited by Y. Pachepsky, D.E. Radcliffe, and H. M. Selim, CRC Press, 2003.

Whisler, F.D., A.D. Klute, and R.J. Millington, Analysis of steady state evapotranspiration from a soil column, *Soil Science Society of America Proceedings, 32*, 167-174, 1968.

Wilson K., P. Hanson, P. Mulholland, D. Baldocchi, and S. Wullschleger, A comparison of methods for determining forest evapotranspiration and its component: sap-flow, soil water budget, eddy covariance and catchment water balance, *Agricultural and Forest Meteorology, 106*, 153-168, 2001.

Wooding, R.A., Steady state infiltration from large shallow circular pond, *Water Resources Research, 4*, 1259-1273, 1968.

Wösten, J.H.M., A. Lilly, A. Nemes, and C. Le Bas, Using existing soil data to derive hydraulic parameters for simulation models in environmental studies and in land use planning, DLO Winand Staring Centre, Report 157, Wageningen, the Netherlands, 1998.

Wright, J.L., Crop coefficients for estimates of daily crop evapotranspiration. Irrig. Scheduling for Water and Energy Conserv. in the 80's. Am. Soc. Agric. Engr.(Dec), pp. 18-26, 1981.

Wright, J.L., New evapotranspiration crop coefficients, *Journal of Irrigation and Drainage Division*, ASCE, 108 (IR2), 57-74, 1982.

Yamagishi, J., T. Nakamoto, and W. Richner, Stability of spatial variability of wheat and maize biomass in a small field managed under two contrasting tillage systems over 3 years, *Field Crops Research*, In Press, 2002.

Zhu, J., and B.P. Mohanty, Upscaling of hydraulic properties of heterogeneous soils, in *Scaling methods in soil physics* edited by Y. Pachepsky, D. Radcliffe, and H. Magdi Selim, CRC Press, 2003.

Zuo, Q. and R. Zang, Estimating root-water-uptake using an inverse method, *Soil Science, 167*, 561-571, 2002.

List of publications

1. **Hupet, F.**, and M. Vanclooster, Effect of the sampling frequency of meteorological data on the estimation of the reference evapotranspiration, *Journal of Hydrology*, 243, 192-204, 2001.
2. **Hupet, F.**, and M. Vanclooster, Intraseasonal dynamics of soil moisture variability within a small maize cropped field, *Journal of Hydrology*, 261, 86-101, 2002.
3. Lambot, S., M. Javaux, **F. Hupet**, and M. Vanclooster, A global multilevel coordinate search procedure for estimating the unsaturated soil hydraulic properties, *Water Resources Research*, 38(11), doi:10.1029/2001WR001224, 2002.
4. **Hupet, F.**, S. Lambot, M. Javaux, and M. Vanclooster, On the identification of macroscopic root water uptake parameters from soil water content observations, *Water Resources Research*, 38(12), 1300, doi:10.1029/2001WR001556, 2002.
5. Ritter, A., **F. Hupet**, R. Munoz-Carpena, M. Vanclooster, and S. Lambot, Using inverse methods for estimating soil hydraulic properties from field data as an alternative to direct methods, *Agricultural Water Management*, 59, 77-96, 2003.
6. **Hupet, F.**, S. Lambot, R.A. Feddes, J.C. van Dam, and M. Vanclooster, Estimation of root water uptake parameters by inverse modeling with soil water content data, *Water Resources Research*, 39(11), 1312, doi:10.1029/2003WR00 2046, 2003.
7. **Hupet F.**, and M. Vanclooster, Comment on " Water flux estimates from a Belgian Scots pine stand: a comparison of different approaches " L. Meiresonne, D. A. Sampson, A. S. Kowalski, I. A. Janssens, N. Nadezhdina, J. Cermák, J. Van Slycken and R. Ceulemans, 2003, Journal of Hydrology, 230-252 (*Journal of Hydrology*, in press).
8. **Hupet, F.**, P. Bogaert, and M. Vanclooster, Quantifying the local scale uncertainty of estimated actual evapotranspiration (accepted for publication in *Hydrological Processes*).
9. **Hupet, F.**, and M. Vanclooster, Sampling strategies to estimate field areal ET fluxes with a soil water balance approach (accepted for publication in *Journal of Hydrology*).
10. Lambot, S., **F. Hupet**, M. Javaux, and M. Vanclooster, Laboratory application of the GMCS-NMS based inverse modeling approach to estimate subsurface water transfer parameters (resubmitted to *Water Resources Research*).
11. **Hupet, F.**, and M. Vanclooster, Micro-variability of hydrological processes at the maize row scale: implications for soil moisture and evapotranspiration estimates (submitted to *Journal of Hydrology*).
12. **Hupet, F.**, J.C. van Dam, and M. Vanclooster, Impact of within-field variability of soil hydraulic properties on transpiration and crop yields: a numerical study (to be submitted to *Agricultural and Forest Meteorology*).

About the author

François Hupet was born in Brussels, Belgium, on July 10^{th}, 1973. He is the second of a four children family. During his secondary studies at the Collège Cardinal Mercier (Braine-l'Alleud), he has been progressively fond of all kind of problems related to the Environment which led him to start Agricultural Engineer studies. From 1991 to 1996, he studied Agronomy (agricultural engineer section) in Louvain-la-neuve at the Université catholique de Louvain (UCL). During his studies, he spent one month in the fish breeding exploitation of the William's Lake in Québec and two months in the southeast of Morocco (Drâa valley) within the framework of his Master's Thesis. This latter dealt with the management procedures of a small irrigated area, and more specifically with the development of a GIS tool allowing the monitoring of the irrigation channels network. After graduation, he worked for two years on a project supported by the Walloon Region aiming at improving the irrigation scheduling of potatoes in Belgium and wheat in Morocco using infrared thermometry. Within this context, he stayed several times in the southeast of Morocco. In October 1998, he started a Ph. D thesis devoted to the estimation of the within-field variability of the hydrological processes with an emphasis on the evapotranspiration fluxes. During the period 1998-2003, he shortly stayed at the ICIA of Tenerife to work on the modelling of the water transport in irrigated banana plantations; he also stayed four months in the Sub-Department of Water Resources in Wageningen (The Netherlands) to study the inverse modelling of the root water uptake parameters. His main scientific interest focuses on the estimation of the water transport within the soil-plant-atmosphere system and the variability of this system at the field-scale. More specific topics of interest include the spatio-temporal dynamics of the soil moisture at different scales and the estimation of the root water uptake by plants. Besides his interest for scientific research, he is passionately fond of birdwatching since he was 10 years old; he is a fervent adept of trekking in mountains and cross-country skiing in Scandinavian countries. He is married and has a son.

From early February 2004 onwards, he will work as a postdoctoral scientist at the HortResearch Center (New Zealand) in the laboratory of Dr. B.E. Clothier to study the multidimensional root water uptake by grape vines.